VIBRATION, BUCKLING AND POSTBUCKLING OF LAMINATED COMPOSITES WITH DELAMINATIONS

by

Jaehong Lee

Dissertation submitted to the Faculty of the

Virginia Polytechnic Institute and State University

in partial fulfillment of the requirements for the degree of

Doctor of Philosophy

in

Engineering Mechanics

APPROVED:

O. Hayden Griffin, Co-Chairman

Zafer Gürdal, Co-Chairman

J. N. Reddy

Eric R. Johnson

Dean T. Mook

May, 1992

Blacksburg, Virginia

c.2

LD
5655
V856
1992
L43
c.2

VIBRATION, BUCKLING AND POSTBUCKLING OF LAMINATED COMPOSITES WITH DELAMINATIONS

by

Jaehong Lee

O. Hayden Griffin, Co-Chairman

Zafer Gürdal, Co-Chairman

Engineering Mechanics

(ABSTRACT)

Free vibration, buckling and postbuckling analyses of laminated composite plates with multiple delaminations are presented. A finite element method based on a layer-wise laminated composite plate theory is developed to formulate the problem. Geometric nonlinearity in the sense of von Kármán and the imperfection in the plate in the form of initial global deflection and initial delamination openings are included. A simple contact algorithm which precludes the physically inadmissible overlapping between delaminated surfaces is proposed and incorporated in the analysis. A sublaminate concept is adopted in the analysis to reduce the computational efforts, and found to be efficient.

Numerical results are obtained for through-the-width, circular and rectangular delaminations addressing the effects of the number of delaminations, their lengths and through-the-thickness and axial locations on the critical buckling load and buckling mode shapes as well as free vibration frequency and modes. Postbuckling responses are investigated with respect to different magnitudes and directions of initial imperfections. The effects of material anisotropy and contact condition between delaminated surfaces are also considered. It is found that the proposed approach is very efficient and powerful for solving the above mentioned problems.

DEDICATION

I wish to dedicate this work
to my loving wife, Myoungwha.

Acknowledgements

I would like to express my sincere appreciation to my advisors, Profs. O. Hayden Griffin and Zafer Gürdal for their guidance, support, assistance and encouragement during the course of this work. I am also grateful to Profs. J. N. Reddy and Eric R. Johnson for their helpful comments and Prof. Dean T. Mook for being an advisory committee member. Thanks are also due to Prof. Raymond H. Plaut for his invaluable and helpful discussion. Their standards improved this dissertation.

Most of the work was supported by Virginia Institute for Material Systems. The support is gratefully acknowledged. I am also sincerely grateful to my parents in Korea for their continuous concern, encouragement and support.

Last but not least, I would like to express my deepest appreciation to my wife and best friend, Myoungwha, for her love, patience, and the many sacrifices she has made during this endeavor. Without her presence, this work would have never been possible.

Table of Contents

INTRODUCTION 1

LITERATURE REVIEW 5

2.1 Computational Modelling of Laminated Composite Plates 6

2.2 Delamination Buckling, Vibration and Postbuckling 9

2.2.1 Through-the-Width Delaminations 9

2.2.1.1 Buckling and Postbuckling of Delaminated Composites 9

2.2.1.2 Vibration of Delaminated Composites 14

2.2.2 Embedded Delaminations 15

BUCKLING AND VIBRATION ANALYSIS 21

3.1 Axisymmetric Model 22

3.1.1 Kinematics 22

3.1.2 Variational Formulation 27

3.1.3 Equations of Motion 30

3.1.4 Constitutive Equations 31

3.1.5 Finite Element Model 33

3.2 Two-Dimensional Model 35

3.2.1 Kinematics 35

3.2.2 Variational Formulation 38

3.2.3 Equations of Motion 41

3.2.4 Constitutive Equations 42

3.2.5 Finite Element Model 43

3.3 Numerical Procedure 46
3.3.1 Eigenvalue Problem 46
3.3.2 Investigations of contact conditions 46

POSTBUCKLING ANALYSIS 49
4.1 Axisymmetric Model 50
4.1.1 Kinematics 50
4.1.2 Variational Formulation 53
4.1.3 Equilibrium Equations 55
4.1.4 Constitutive Equations 57
4.1.5 Finite Element Model 58
4.2 Two-Dimensional Model 61
4.2.1 Kinematics 61
4.2.2 Variational Formulation 64
4.2.3 Equilibrium Equations 66
4.2.4 Constitutive Equations 68
4.2.5 Finite Element Model 69
4.3 Numerical Procedure 71
4.3.1 Newton-Raphson Method 71
4.3.2 Investigations of Contact Conditions 72

VERIFICATIONS OF THE PRESENT APPROACH 76
5.1 Buckling and Postbuckling Analyses 77
5.1.1 Through-the-Width Delaminations 77
5.1.2 Embedded Delaminations 88
5.1.2.1 Axisymmetric Circular Delaminations 88
5.1.2.2 Two-Dimensional Delaminations 95
5.2 Free Vibration Analysis 102

5.2.1 Through-the-Width Delaminations 102

5.2.1.1 Isotropic Clamped Beam 102

5.2.1.2 Composite Cantilever Beam 106

5.2.2 Embedded Delamination 107

BUCKLING AND POSTBUCKLING FOR THROUGH-THE-WIDTH DELAMINATIONS 111

6.1 Single Delamination 112

6.1.1 The Effects of Initial Imperfections and Contact Condition 112

6.1.2 The Effects of Location and Length of Delamination 127

6.1.3 The Effect of Anisotropy 131

6.2 Multiple Delaminations 140

6.2.1 Two and Three Delaminations 140

6.2.2 Seven Delaminations 162

6.3 Layer-Wise Model vs. Sublaminate Model 170

6.3.1 Buckling Response of Delaminated Composites 170

6.3.2 Postbuckling Analysis of Multiply Delaminated Composites 172

SUMMARY AND CONCLUSIONS 188

REFERENCES 193

LAMINATE STIFFNESSES 203

STIFFNESS, GEOMETRIC STIFFNESS AND MASS MATRICES 207

DIRECT AND TANGENT STIFFNESS MATRICES 212

Vita **219**

List of Illustrations

Figure 1. Conventional modelling of through-the-width delamination 12

Figure 2. Penny-shaped delamination in a circular plate 16

Figure 3. Geometry of an axisymmetric problem with delaminations 23

Figure 4. Configuration of kinematics for a circular plate 24

Figure 5. Description of displacements for layer-wise and sublaminate theories . . 25

Figure 6. Geometry of a rectangular plate with delaminations 36

Figure 7. Configuration of kinematics for a rectangular plate 37

Figure 8. Geometry of the initially deflected circular plate element with delaminations 51

Figure 9. Geometry of the initially deflected rectangular plate element with delaminations 63

Figure 10. Contact procedure 74

Figure 11. Flowchart for postbuckling analysis 75

Figure 12. Description of the through-the-width delaminations and the finite element model 78

Figure 13. Geometry of a clamped beam-plate containing a through-the-width delamination at midplane 80

Figure 14. Three possible buckling mode shapes for a composite containing a delamination at midplane 81

Figure 15. Buckling load vs. delamination length for a composite containing a delamination at midplane with $h/l = 1/400$ 84

Figure 16. Buckling load vs. delamination length for a composite containing a delamination at midplane with $h/l = 1/10$ 85

Figure 17. Load-end shortening curve for a composite containing a delamination ($\bar{a} = 0.4$) at midplane 87

Figure 18. Geometry of a circular plate containing a concentric penny-shaped delamination at midplane 89

Figure 19. Buckling loads vs. delamination radius for a circular plate containing a single midplane penny-shaped delamination with h/R = 1/500 90

Figure 20. Buckling loads vs. delamination radius for a circular plate containing a single midplane penny-shaped delamination with h/R = 1/10 91

Figure 21. Buckling loads vs. delamination radius for a circular plate containing three equidistant uniform, penny-shaped delaminations 94

Figure 22. Geometry of a clamped circular plate containing three equidistant penny-shaped delaminations with $\bar{a}_1 = 0.4$, $\bar{a}_2 = 0.3$, $\bar{a}_3 = 0.2$ 95

Figure 23. Load-deflection curve for a circular plate containing three equidistant penny-shaped delaminations with $\bar{a}_1 = 0.4$, $\bar{a}_2 = 0.3$, $\bar{a}_3 = 0.2$ 96

Figure 24. Geometry of a square plate containing a single square delamination and the finite element mesh 98

Figure 25. Buckling loads vs. delamination size for a square orthotropic plate under uniaxial and biaxial compressive loads 99

Figure 26. Boundary conditions of the simply-supported quarter-plate model for one half-wave and two half-waves in the loading direction 100

Figure 27. Buckling loads vs. lamination angle for undelaminated and delaminated angle-ply composite plates 101

Figure 28. Vibration mode change during the period of the motion for a clamped beam with $\bar{t} = 0.2$, $\bar{a} = 0.3$ 103

Figure 29. Natural vibration mode shape for a clamped beam with $\bar{t} = 0.2$, $\bar{a} = 0.6$ 104

Figure 30. Geometry of a composite cantilever beam containing two delaminations 107

Figure 31. Natural frequencies vs. fiber angle for $[0/\theta]_S$ composites containing one and two delaminations with $\bar{a}_1 = \bar{a}_2 = 0.5$ 108

Figure 32. Natural frequencies vs. delamination radius for a circular plate containing a single midplane penny-shaped delamination 110

Figure 33. Geometry of a composite containing single through-the-width delamination 113

Figure 34. Buckling mode shape for $\bar{a} = 0.3$ and $\bar{t} = 0.2$ 114

Figure 35. Load-deflection curve of a delaminated composite ($\bar{a} = 0.3$ and $\bar{t} = 0.2$) with imperfection of buckling mode shape 117

Figure 36. Load-deflection curve of a delaminated composite ($\bar{a} = 0.3$ and $\bar{t} = 0.2$) with imperfection of $w_o = 0.001$. 118

Figure 37. Load-deflection curve of a delaminated composite ($\bar{a}$ = 0.3 and $\bar{t}$ = 0.2) with imperfection of w_o = 0.025. 119

Figure 38. Load-deflection curve of a delaminated composite ($\bar{a}$ = 0.3 and $\bar{t}$ = 0.2) with imperfection of w_o = 0.035. 120

Figure 39. Load-deflection curve of a delaminated composite ($\bar{a}$ = 0.3 and $\bar{t}$ = 0.2) with imperfection of w_o = 0.04. 121

Figure 40. Load-deflection curve of a delaminated composite ($\bar{a}$ = 0.3 and $\bar{t}$ = 0.2) with imperfection of w_o = 0.1 (without contact condition) 122

Figure 41. Load-deflection curve of a delaminated composite ($\bar{a}$ = 0.3 and $\bar{t}$ = 0.2) with imperfection of w_o = 0.1 (with contact condition) 123

Figure 42. Load-deflection curve of a delaminated composite ($\bar{a}$ = 0.3 and $\bar{t}$ = 0.2) with imperfection of w_o = -0.001 124

Figure 43. Load-deflection curve of a delaminated composite ($\bar{a}$ = 0.3 and $\bar{t}$ = 0.2) with imperfection of w_o = -0.1 125

Figure 44. Load-end shortening curve of a delaminated composite ($\bar{a}$ = 0.3 and $\bar{t}$ = 0.2) for various initial imperfections. 126

Figure 45. Effect of axial location of a delamination at midplane for $\bar{a}$ = 0.2 . . . 128

Figure 46. Effect of axial location of a delamination at midplane for $\bar{a}$ = 0.4 . . . 129

Figure 47. Effect of axial location of a delamination at midplane for $\bar{a}$ = 0.6 . . . 130

Figure 48. Load-deflection curve of a delaminated composite with $\bar{a}$ = 0.3 for various through-the-thickness location of delaminations ($\bar{t}$) 132

Figure 49. Load-deflection curve of a delaminated composite with $\bar{a}$ = 0.5 for various through-the-thickness location of delaminations ($\bar{t}$) 133

Figure 50. Load-deflection curve of a delaminated composite with $\bar{a}$ = 0.9 for various through-the-thickness location of delaminations ($\bar{t}$) 134

Figure 51. Geometry of simply-supported cross-ply laminates containing a delamination between 3rd and 4th layers. 135

Figure 52. Load-deflection curve of a simply-supported [0/90/90//0] laminate with a delamination 137

Figure 53. Load-deflection curve of a simply-supported [90/0/0//90] laminate with a delamination 138

Figure 54. Load-deflection curve of a simply-supported [90/0/0//0] laminate with a delamination 139

Figure 55. Geometry of two and three symmetrically located delaminations with respect to midplane 141

Figure 56. Buckling load vs. delamination lengths for a composite containing two delaminations for $\bar{t} = 0.25$ with and without contact condition 143

Figure 57. Buckling load vs. delamination lengths for a composite containing three delaminations for $\bar{t} = 0.25$ with and without contact condition 144

Figure 58. Buckling load vs. delamination lengths for a composite containing two delaminations for $\bar{t} = 0.5$ with and without contact condition 145

Figure 59. Buckling load vs. delamination lengths for a composite containing three delaminations for $\bar{t} = 0.5$ with and without contact condition 146

Figure 60. Buckling load vs. delamination lengths for a composite containing two delaminations for $\bar{t} = 0.75$ with and without contact condition 147

Figure 61. Buckling load vs. delamination lengths for a composite containing three delaminations for $\bar{t} = 0.75$ with and without contact condition 148

Figure 62. Buckling loads and mode shapes for two and three delaminations with $\bar{t} = 0.25$ 151

Figure 63. Buckling loads and mode shapes for two and three delaminations with $\bar{t} = 0.5$ 152

Figure 64. Buckling loads and mode shapes for two and three delaminations with $\bar{t} = 0.75$ 153

Figure 65. Load-deflection curve for a composite containing two delaminations for $\bar{t} = 0.25$ with imperfection of first symmetric buckling mode 154

Figure 66. Load-deflection curve for a composite containing two delaminations for $\bar{t} = 0.25$ with imperfection of second symmetric buckling mode 155

Figure 67. Load-end shortening curve for a composite containing two delaminations for $\bar{t} = 0.25$ with various initial imperfections 156

Figure 68. Load-deflection curve for a composite containing three delaminations for $\bar{t} = 0.25$ with imperfection of first symmetric buckling mode 157

Figure 69. Load-deflection curve for a composite containing three delaminations for $\bar{t} = 0.25$ with imperfection of second symmetric buckling mode . . . 158

Figure 70. Load-end shortening curve for a composite containing three delaminations for $\bar{t} = 0.25$ with various initial imperfections 159

Figure 71. Load-deflection curve for a composite containing two delaminations for $\bar{t} = 0.5$ with imperfection of first symmetric buckling mode 160

Figure 72. Load-deflection curve for a composite containing two delaminations for $\bar{t} = 0.5$ with imperfection of second symmetric buckling mode 161

Figure 73. Load-end shortening curve for a composite containing two delaminations for $\bar{t} = 0.5$ with various initial imperfections 163

Figure 74. Load-end shortening curve for a composite containing three delaminations for $\bar{t} = 0.5$ with various initial imperfections 164

Figure 75. Load-end shortening curve for a composite containing two delaminations for $\bar{t} = 0.75$ with various initial imperfections 165

Figure 76. Load-end shortening curve for a composite containing three delaminations for $\bar{t} = 0.75$ with various initial imperfections 166

Figure 77. Geometry for composites containing one, triangular and full uniform delaminations 168

Figure 78. Buckling load vs. delamination lengths for composites containing one, triangular , and full uniform delaminations. 169

Figure 79. Geometry of an 8-layered quasi-isotropic composite containing two delaminations 173

Figure 80. Load-deflection curve for a $[0/\pm 45/90]_s$ composite with $\bar{a}_1 = 0.3$, $\bar{a}_2 = 0.3$ 176

Figure 81. Load-deflection curve for a $[0/\pm 45/90]_s$ composite with $\bar{a}_1 = 0.4$, $\bar{a}_2 = 0.2$ 177

Figure 82. Load-deflection curve for a $[0/\pm 45/90]_s$ composite with $\bar{a}_1 = 0.2$, $\bar{a}_2 = 0.4$ 178

Figure 83. Load-deflection curve for a $[0/90/\pm 45]_s$ composite with $\bar{a}_1 = 0.3$, $\bar{a}_2 = 0.3$ 179

Figure 84. Load-deflection curve for a $[0/90/\pm 45]_s$ composite with $\bar{a}_1 = 0.4$, $\bar{a}_2 = 0.2$ 180

Figure 85. Load-deflection curve for a $[0/90/\pm 45]_s$ composite with $\bar{a}_1 = 0.2$, $\bar{a}_2 = 0.4$ 181

Figure 86. Load-deflection curve for a $[45/90/-45/0]_s$ composite with $\bar{a}_1 = 0.3$, $\bar{a}_2 = 0.3$ 182

Figure 87. Load-deflection curve for a $[45/90/-45/0]_s$ composite with $\bar{a}_1 = 0.4$, $\bar{a}_2 = 0.2$ 183

Figure 88. Load-deflection curve for a $[45/90/-45/0]_s$ composite with $\bar{a}_1 = 0.2$, $\bar{a}_2 = 0.4$ 184

Figure 89. Load-deflection curve for a $[0]_8$ composite with $\bar{a}_1 = 0.3$, $\bar{a}_2 = 0.3$ 185

Figure 90. Load-deflection curve for a $[0]_8$ composite with $\bar{a}_1 = 0.4$, $\bar{a}_2 = 0.2$ 186

Figure 91. Load-deflection curve for a $[0]_8$ composite with $\bar{a}_1 = 0.2$, $\bar{a}_2 = 0.4$ 187

List of Tables

Table 1. Comparison of nondimensional buckling loads for various length of a midplane delamination 82

Table 2. Comparison of postbuckling solution for a penny-shaped delamination at midplane of a circular plate 93

Table 3. Natural frequencies of a clamped beam with a midplan delamination 105

Table 4. Natural frequencies of a clamped beam with t/h=0.2 105

Table 5. Comparison between the layer-wise and sublaminate theories for buckling loads of a $[0/90/45/-45]_s$ laminate with a midplane delamination 171

Chapter I

INTRODUCTION

Fiber-reinforced composite materials have been increasingly used over the past few decades in a variety of structures that require high ratio of stiffness and strength to weight. The ability to tailor the directionally dependent properties of laminated fiber-reinforced composites by bonding together with various fiber orientations offers additional advantages over the use of conventional engineering materials.

While composite materials enjoy these advantages, they are also prone to a wide range of defects and damage which may significantly reduce their structural integrity. Among various types of damage modes that are likely to occur in laminated composites during service, a matrix-dominated interlaminar cracking or *delamination* is the one that is the most commonly observed and sometimes unavoidably incurred in practical situations. Delamination may develop as a result of manufacturing defects such as incomplete wetting and entrapped air pockets between layers, or as a result of certain in-service factors, such as low velocity impact by foreign objects, for instance, dropped tools or bird strikes. While such impact damage can cause a number of delaminations [1] , a small surface indentation is the only external indication since the delaminations are

cracks in the interior of the laminate. Thus, this type of damage is often called *barely visible impact damage* (BVID) [2], which is not readily identified by visual inspection. Such delamination damage is known to cause a degradation of overall stiffness and strength.

In particular, delamination damage can result in a substantial loss of compressive load-carrying capacity of a laminate through local instability and stress concentration in the vicinity of a delamination. Once an initially symmetric laminate contains delaminations, it behaves locally as a set of sublaminates which are generally unsymmetric, and therefore, exhibit bending-extension coupling. These behaviors cause a stress redistribution and may cause the sets of sublaminates to buckle. Under increased load, the delamination may propagate as a result of excessive crack tip stresses. Consequently, this *delamination buckling* and growth lead to global structural compression failure at loads well below the design level of an undamaged laminate.

Delaminations are also known to cause a change in vibration characteristics. The delaminated sublaminate generally exhibits new vibration modes and frequencies that depend on the size and location of the delamination. Thus, provided that the natural frequencies and mode shapes are known for a composite containing delaminations, the presence of invisible delamination can be detected, and their size and location can be estimated.

Understanding of delamination behavior is, therefore, a subject of vital importance in view of the intended widespread use of laminated composite materials in many engineering applications. In principle, a full three-dimensional analysis is necessary in order to model general configurations of delaminations in composite laminates. While three-dimensional finite element analysis gives accurate results with sufficiently refined meshes, it is computationally very intensive requiring large amounts of computer storage and running time. For that reason, in many cases, a one-dimensional beam-plate model for

a through-the-width delamination, or a *thin-film* model, where the delaminated layer is assumed to be so thin compared to the base laminate that the behavior of the layer does not affect the deformation of the base plate, have been used by many researchers. These analytical models, however, are inadequate for general configurations of delaminations, such as anisotropy of composite, varying location of delamination, general two-dimensional embedded delamination, or multiple delaminations. For these more general problems, a two-dimensional *layer-wise* model, in which each layer of a composite is separately modelled, is preferred because it offers accurate results with significantly reduced computational cost compared to a full three-dimensional model. Despite of efficiency and accuracy of the layer-wise theory, it still has a shortcoming in that the number of dependent variables is a function of the number of layers. This, in turn, suggests a *sublaminate* approach in which each sublaminate created by delaminations is modelled as an equivalent, single, homogeneous layer. In the sublaminate approach, multiple delaminations can easily be modelled employing the Heaviside unit step function in displacement fields as in the layer-wise theory, and the number of dependent variables depends only on the number of delaminations. As will be described in the next chapter, no model exists for predicting buckling loads, natural frequencies and postbuckling response of anisotropic laminates with single or multiple general shaped delaminations such as through-the-width, circular, rectangular or elliptical shapes.

Therefore, the main objective of this dissertation is to develop a displacement based, layer-wise finite element model based on Reddy's theory [3] and to extend it to the sublaminate finite element model capable of addressing general problems of delamination in a laminated composite plate. More specifically, five major objectives are identified:

1. Determination of buckling loads and buckling mode shapes for laminated composites containing single and multiple delaminations with arbitrary configuration.

2. Determination of natural frequencies and vibration mode shapes for laminated composites containing delaminations.
3. Analysis of the postbuckling response of laminated composites containing multiple delaminations with respect to initial imperfection of the composites.
4. Investigation of the effects of the contact between delaminated surfaces and anisotropy on the vibration, buckling and postbuckling problems.
5. Comparison between layer-wise and sublaminate theories as well as with previously available results.

With these introductory remarks, the following chapters constitute the dissertation. A state-of-the-art survey on the various aspects of literature pertaining to the present study is provided in Chapter II. The computational modelling of laminated composite plate and the vibration, buckling and postbuckling of delaminated composites are reviewed separately. Chapter III addresses a theoretical formulation for vibration and buckling problems of circular and rectangular plates with delaminations. Chapter IV describes the issue of postbuckling behavior of delaminated composites. The theoretical solution procedure is addressed by applying a contact condition. Verifications of the present study are made in Chapter V for vibration, buckling and postbuckling problems of through-the-width and embedded delaminations. Numerical results and discussions are provided in Chapter VI for buckling and postbuckling analyses of through-the-width delaminations. Chapter VII provides brief summary and concluding remarks with recommendation for future research.

Chapter II

LITERATURE REVIEW

In this chapter, a review of previous studies relevant to the present subject is given. For convenience, the section is divided into two parts involving computational modelling of laminated composite plates, and buckling, vibration and postbuckling of delaminated composites.

2.1 Computational Modelling of Laminated Composite Plates

Modelling of laminated plates has been mostly done using classical lamination theory (CLT), which is a straightforward extension of the Kirchhoff assumptions. This theory is adequate for many engineering problems. However, CLT cannot account for the transverse shear deformation that is significant for moderately thick composite plates. Thus, for such plates, the inclusion of transverse shear effects is necessary.

Since the development of first-order shear deformable plate theory (FSDT) which allows linear variation of in-plane displacements in the thickness direction (Yang, Norris and Stavsky [4] and Whitney [5]), numerous refined plate theories have been proposed. Among them, polynomial based higher order shear deformable plate theories (HSDT) were developed by Whitney and Sun [6], Lo, Christensen and Wu [7], and Reddy [8]. Detailed reviews of this topic may be found in [9-12].

All the theories discussed above, including CLT, FSDT, and HSDT can be grouped as equivalent single-layer two-dimensional theories [9]. In general, single-layer laminate theories give satisfactory results for global behavior (e.g. deflections, stresses, buckling loads, and natural frequencies); however, they are inadequate in modelling localized effects such as delaminations. For these localized effects, layer-wise modelling of laminated composite plates seems to be necessary.

In layer-wise modelling, the transverse variation of the displacement fields is represented by piecewise polynomial functions. Early efforts in layer-wise modelling of laminated composites are due to Pryor and Barker [13], Srinivas [14], Mau [15] and Seide [16]. Spilker [17] proposed hybrid stress plate bending element using layer-wise approach. Chaudhuri [18] developed a displacement based layer-wise, two dimensional triangular element which has $2N + 3$ degree of freedom at each node for an N-layered plate

To improve the in-plane response of laminated plates, a layer-wise theory based on Reissner's mixed variational principle [19] was presented by Toledano and Murakami [20]. The theory assumed piecewise continuous in-plane displacement variations to satisfy continuity of interlaminar stresses. The transverse variation of the displacements is constant through the thickness. Thus, the interlaminar shear strains are constant within each layer. DiSciuva [21,22] proposed a model which allows a piecewise linear variation of the in-plane displacements, and a constant for the transverse component through the thickness of laminates. The number of independent variables was reduced from $2N + 3$ to 5 by applying continuity conditions of the transverse shear stresses at each layer interface for an N-layer laminate. Cho et al. [23] modeled laminated plates using a higher-order theory for each layer. Although the results obtained in that work were very accurate, the theory required $11N$ unknowns for an N-layer laminate and was thus inefficient for multilayered plates.

Reddy [3] proposed a generalized model which allows layer-wise representation of in-plane displacement using linear combinations of the thickness coordinate and undetermined functions of position within each layer. Reddy and Barbero [24] developed a finite element model based on the model by Reddy [3] with linear approximation of the in-plane displacements through the thickness of each layer, and extended that model to geometric nonlinear theory [25]. Epstein and Huttelmaier [26] developed a finite element model including linear variation of transverse displacements. Barboni and Gaudenzi [27] reduced a quasi-three-dimensional finite element to a one-dimensional layer-wise model including the transverse normal strain to analyze free edge effects in laminates. Robbins and Reddy [28] extended Reddy's theory [3], including transverse normal strain. Lee and Liu [29] proposed an analytical model using a Hermite cubic interpolation function in the thickness direction in order to satisfy the continuity of interlaminar shear stresses. The number of independent variables in that formulation is $5N$.

Three-dimensional finite element models based on the layer-wise concept have also been developed by many researchers including Owen and Li [30,31], and Wanthal and Yang [32]. A detailed review of three-dimensional modelling of composite laminates can be found in Griffin [33].

All the previously discussed layer-wise theories have successfully predicted not only the global response but also local effects, such as free edge effects [27]. However, since the number of unknowns depends on the number of layers, these theories are intractable as the number of layers becomes even moderately large. Thus, there is still a need to develop laminated plate theories which can model delaminations with a tractable number of dependent variables.

In this point of view, the proposed sublaminate theory, which models sublaminates created by delaminations as an equivalent single-layer and allows linear variation of in-plane displacements through the thickness of each sublaminate, seems to be a compromise between accuracy and computational costs for delamination problem in composite laminates.

2.2 Delamination Buckling, Vibration and Postbuckling

In general, delaminations can be grouped as through-the-width delaminations and embedded delaminations. In the following, previous research on each type of delamination is reviewed.

2.2.1 Through-the-Width Delaminations

2.2.1.1 Buckling and Postbuckling of Delaminated Composites

Chai, Babcock, and Knauss [34] may have been the first investigators to study buckling and postbuckling of a plate containing a through-the-width delamination. They presented a one-dimensional analytical model to assess the compressive strength of a delaminated composite employing a Griffith-type fracture criterion. Simitses and his collaborators [35-37] investigated delamination buckling and growth in simply-supported and clamped composite plates using a one-dimensional beam-plate theory. The effects of delamination position, length, and laminate thickness on the buckling loads and delamination growth were studied. Bolotin et al. [38] investigated the bifurcation problem for several equidistant delaminations of equal lengths. He has shown that the buckling mode for that problem is antisymmetric.

Sheinman, Bass and Ishai [39] extended the work of Simitses et al. [35] to include the effect of bending-extension coupling on the stability of a delaminated composite using a finite difference model. The effect of bending-extension coupling on postbuckling re-

sponse was investigated by Yin [40] for both mid-plane delamination and thin-film delamination. Sheinman and Souffer [41] investigated the effects of bending-extension coupling and initial imperfection on the postbuckling behavior of a composite beam with various delamination geometries. It was found that the coupling effect significantly reduces the buckling load and increases the postbuckling deformations, and the global postbuckling deformation was shown to be very sensitive to the initial imperfections. However, the postbuckling analysis for some initial imperfection in that work exhibits physically inadmissible deformed shape due to neglecting contact condition between delaminated sublaminates.

Moshaiov and Marshall [42] predicted buckling loads for a random short fiber composite using a Rayleigh-Ritz method. Somers et al. [43] developed an analytical model to investigate the buckling and postbuckling behavior of a sandwich beam with a delamination. Tracy and Pardoen [44] studied higher order buckling loads and mode shapes of a composite containing a midplane delamination. The effect of axial location of delamination on the buckling load was also studied. The delamination opening was suppressed to zero in order to prevent overlapping of delaminated surfaces in that work.

Most of the above mentioned literature employed classical beam theory which does not account for shear deformations for each portion of sublaminates. In general, however, especially for a short delamination, the sublaminates created by delamination may become moderately thick, and shear deformation is not negligible any more.

Effects of transverse shear deformation were studied by Kardomateas and Schmueser [45] using a perturbation expansion method and Kardomateas [46] by improving the model used in [34] on delamination buckling and growth in composite laminates. They found that these shear effects precipitate the possibility of crack growth because of the extra energy from the transverse forces. More recently, Chen [47] proposed a shear deformation theory using variational energy principle and extended his

work to unsymmetric laminates [48] having a thin-film delamination. He found that the magnitude of the transverse shear effect depends on the delamination location and size.

Modelling the interply matrix as an elastic foundation, Vizzini and Lagace [49] investigated buckling behavior of a delaminated composite beam. Anastasiad and Simitses [50] improved the model by Simitses [35] to include springs between sublaminates to simulate the matrix layer. A strong spring distribution was shown to be a stabilizing effect for delamination buckling. Kardomateas [51] also studied the effect of an elastic foundation on the buckling and postbuckling response. It was reported that the delamination growth may occur sooner for a large foundation modulus.

Shear buckling and postbuckling behavior of a composite laminate with a delamination were investigated by Suemasu [52] by employing a no-penetration condition of delaminated surface. The shear behavior of delaminated composites was found to be a combination of both local and global buckling modes. It was also reported that the postbuckling deformation is sensitive to initial imperfections of the composite. Madenzi [53] solved the mixed boundary value problem to obtain an analytical solution of delamination buckling and growth. He showed that delamination growth may occur prior to buckling by means of crack propagation at the points of stress concentrations. However, the analytic model in that study was shown to be unsuitable for thin delaminated layer.

Most of the works cited above employed either thin-film models [34,40,45,48,49,51] or analytical models with four divided regions [34-37,39,41-44,46-48,50,52] created by delamination in a composite laminate (Figure 1). In those analytical beam-plate models, boundary and continuity conditions were applied for all edges and interfaces of the regions, respectively, to formulate the problem.

It also appears that the boundary conditions were assumed to be either simply-supported or clamped in the beam-plate model. Moreover, it is extremely difficult to

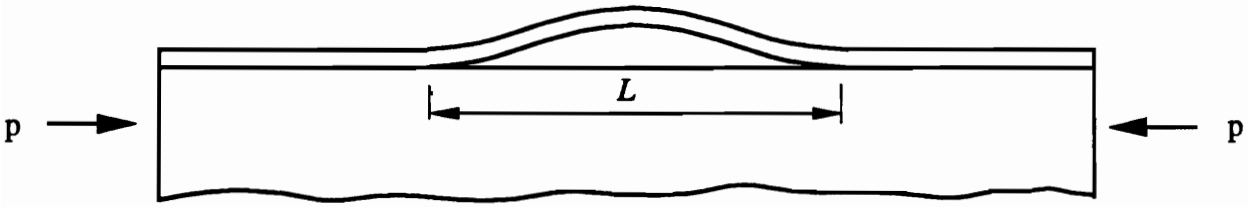

Thin-film Model

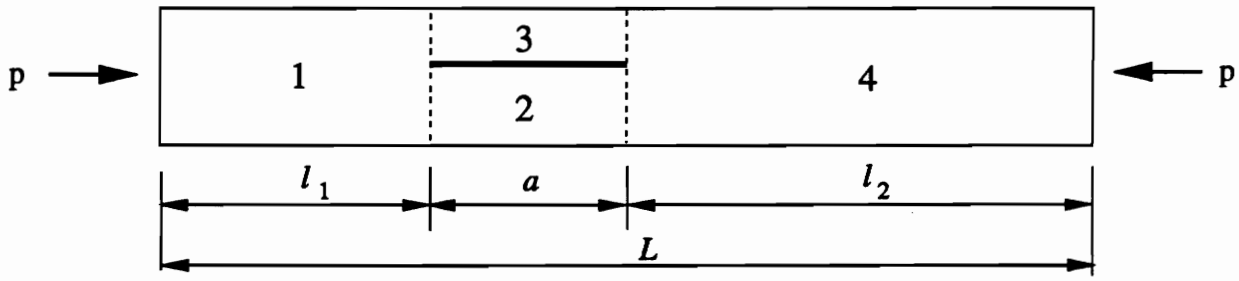

Beam-plate Model

Figure 1. Conventional modelling of through-the-width delamination

employ these analytical methods, including the model in [53], if there is more than one delamination with arbitrary boundary conditions or if loading is dynamic. For these more general configurations, finite element analysis is often employed. For example, plane-elasticity finite element models were applied by Whitcomb [54], Wang et al. [55,56], Williams et al. [57], and Shaw and Tsai [58], and three-dimensional finite elements were applied by Chaouk et al. [59] and Jones et al. [60] to study buckling and postbuckling of composites with a through-the-width delamination. However, two- and even three-dimensional finite element models make the analysis complicated, with a considerable computational cost because a very fine mesh must be used near the delamination crack tip. In this regard, Kapania and Wolfe [61] developed a one-dimensional finite element model based on the model suggested by Simitses et al. [35] and extended this model to the case of two delaminations in a subsequent paper [62]. However, their model is limited to isotropic materials and one or two delaminations.

Most of the literature on delamination buckling and growth in composite laminates deals with a single delamination and only a few [55,56,62] consider two or at most three through-the-width delaminations. In actual situations, however, when composite laminates are subjected to impact, a number of delaminations with a very complicated configuration may occur. Therefore, there is a great need to have an analytical capability that can be applied to general multiple delaminations with a complex geometry.

Recently, Kutlu and Chang [63] proposed an analytical model to simulate the compression response of laminated composites containing multiple delaminations. They found that the multiple delaminations can reduce the load-carrying capacity more than a single delamination does. Breivik [64] investigated the compressive behavior of multiply delaminated quasi-isotropic composite beams both experimentally and numerically. It was found that the beam containing short multiple through-the-width delaminations

failed antisymmetrically, while the beam containing long delaminations failed symmetrically.

Most recently, the buckling loads and corresponding mode shapes of a laminated composite containing multiple delaminations were systematically studied using a layer-wise approach by Lee et al. [65]. They found that the antisymmetric buckling mode is dominant for a composite laminate having short multiple delaminations as experimentally shown by Breivik [64]. It was also shown that the buckling mode shapes for a midplane delaminated composite depend on the slenderness of the laminate.

2.2.1.2 Vibration of Delaminated Composites

Relatively little research has been done to determine the change in vibration characteristics of composites with through-the-width delaminations. Ramkumar et al. [66] investigated free vibration frequencies of a cantilever beam with a delamination using the shear deformable beam theory. But, their results demonstrated poor agreement with experimental results. They attributed this discrepancy to the contact between delaminated layers. However, this explanation may be questionable in view of the subsequent results of Wang et al. [67], who proposed an analytical model based on classical beam theory by including the effect of the coupling between flexural and longitudinal motion of the delaminated layers. By including the coupling, the calculated results showed good agreement with experiment, implying that the discrepancy in Ramkumar et al. [66] was mainly due to the neglecting of coupling effect. Yin and Jane [68], and Chen and Goggin [69] studied vibrations of a delaminated beam with respect to buckled reference states based on classical beam theory and shear deformable beam theory, respectively. The effects of higher order frequencies and mode shapes were studied by Tracy and Pardoen [70]. In their analyses, a delamination was assumed to remain closed during the motion.

Shen and Grady [71] developed an analytical model which can predict vibration frequencies and modes of delaminated beams. They found that the coupling between longitudinal vibration and transverse vibration has significant effects on the modes of vibration, and the natural frequencies and mode shapes are affected by the size and location of delamination.

In all the previous studies involved in vibration analysis of delaminated composite, the basic assumption is that a delamination always remains either opened or closed during the whole period of the motion. In actual situations, however, a delamination may breathe (open and close) during the motion of composites. In the present analysis, an attempt to include the interaction between opening and closing vibration modes of delamination states will be made.

It also appears that analytical studies concerning the vibration frequencies of composite containing more than one delamination have not yet been treated in the open literature.

2.2.2 Embedded Delaminations

Axisymmetric models have often been applied for a problem with a concentric penny-shaped delamination in a circular plate under compressive load uniformly distributed in the circumferential direction (Figure 2) because it can be treated as one-dimensional problem without the need for solution of formidable and complicated two-dimensional counterparts. Axisymmetric buckling and growth of a thin circular delamination in a plate was first studied by Kachanov [72] on the basis of a linear postbuckling solution.

Bottega and Maewal [73] developed an analytical model based on asymptotic analysis of postbuckling behavior for a symmetric two-layer isotropic circular plate. It was

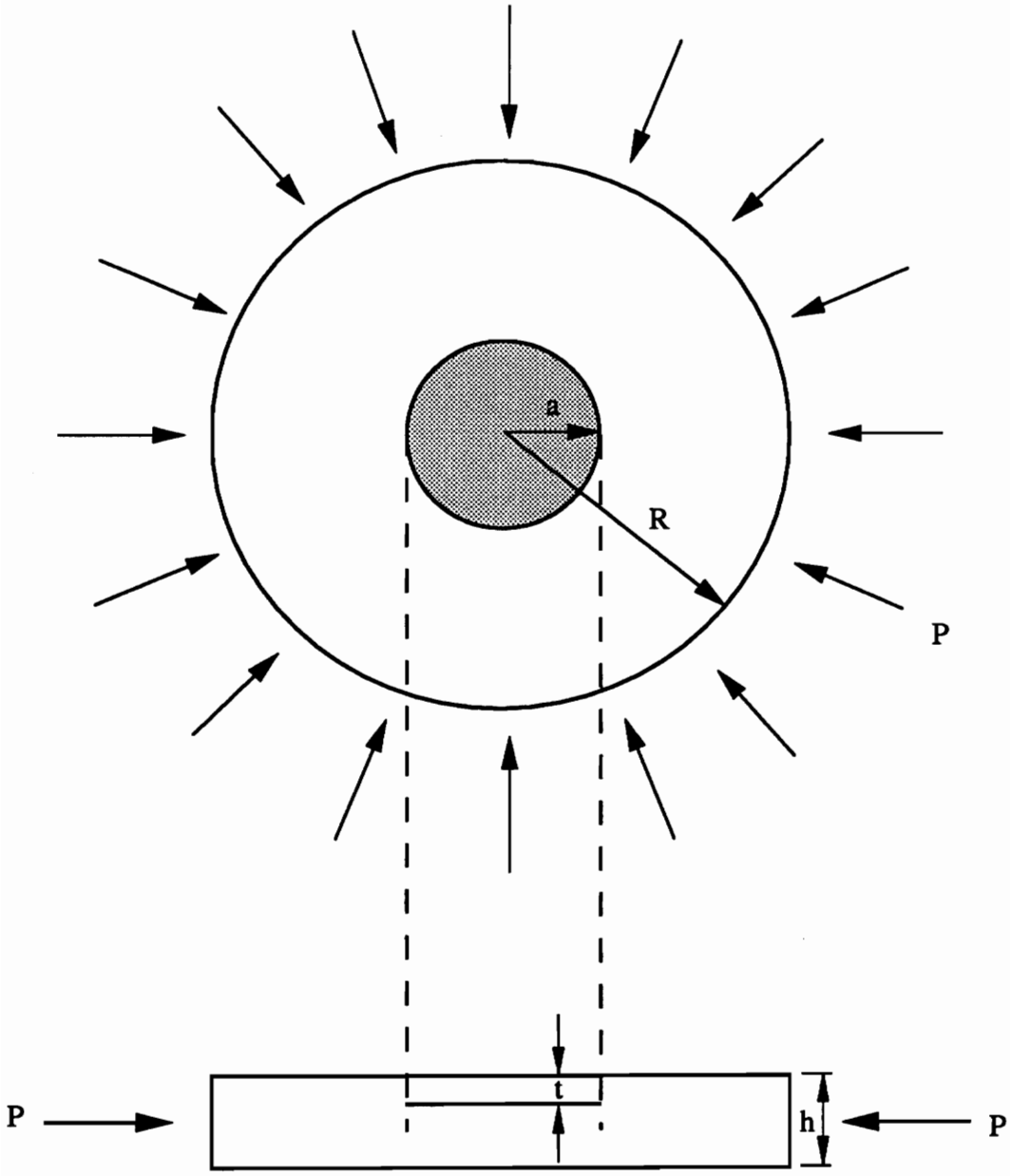

Figure 2. Penny-shaped delamination in a circular plate

found that delamination growth based on a Griffith-type fracture criterion may occur following delamination buckling provided that sufficient bending energy is produced at the delamination crack front. In a subsequent paper [74], they extended the analysis in [73] to include the dynamics of the delamination growth process resulting from buckling of the delamination.

Yin [75] investigated postbuckling behavior for an isotropic circular plate containing thin-film or midplane delamination employing von Kármán's nonlinear plate equations. Yin and Fei [76] determined the critical buckling load of an isotropic circular plate with concentric delamination for various delamination geometries under uniform circumferential loading. They also improved Yin's work [75] by including the deformation of the base plate for postbuckling analysis of a delaminated circular plate in a subsequent paper [77].

Partridge et al. [78] used a two-dimensional axisymmetric finite element model for delaminated isotropic circular plates to obtain strain energy release rate. Bruno and Grimaldi [79] studied both through-the-width and circular delaminations for symmetric two layer plates. They developed analytical and finite element models based on the von Kármán thin plate theory in conjunction with the unilateral contact approach [80] in which delamination is modeled by means of elastic foundation.

Larsson [81] proposed a model which includes a hole at the center and polar orthotropy using nonlinear thin plate theory. He investigated the geometric threshold where the thin film approximation is applicable. Larsson [82] also investigated the effects of multiple delaminations for various combinations of geometry and material parameters. It was reported that the contact effect between delaminated layers is no longer negligible for some cases of multiple delaminations.

A general shaped two-dimensional embedded delamination configuration has also been studied by several researchers. Among them, Konish and Johnson [83], and

Ashizawa [84] analyzed rectangular shape delaminations. Chai and Babcock [85] developed a model for an orthotropic plate containing near-the-surface (thin-film) delamination. They employed a polynomial series expansion for the displacement field incorporating three out-of-plane and two in-plane displacement terms in Rayleigh-Ritz method for clamped elliptical plate. Kassapoglou [86] improved Chai and Babcock's work [85] by extending the number of polynomial terms in displacement fields and by including bending-stretching coupling effects. A perturbation method was adopted in that analysis. Kassapoglou and Hammer [87] studied the effect of delamination in a laminate under combined loads and the effect of aspect ratio of plates on delamination buckling load. Shivakumar and Whitcomb [88] used Rayleigh-Ritz and finite element approaches to determine buckling strains of elliptical delaminations in quasi-isotropic composites. They showed that the direction of the delaminating sublaminate that has the lowest buckling strain correlates with the direction of delamination growth. Flanagan [89] also employed a similar model as proposed by Chai and Babcock [85] to correlate with post-impact test data. It was shown that damage tolerance may be improved by placing the 0 degree plies far from the surface. Transverse shear deformation, thermal loads, and contact effects for delaminated elliptical plate were investigated by Peck and Springer [90] based on a higher-order laminated plate theory in conjunction with the Rayleigh-Ritz method as proposed by Chai and Babcock [85]. Cairns et al. [91] correlated analytical and experimental results for an elliptical thin-film delamination. The analysis in that work was also based on the model in [85].

Yin and Jane [92] studied the buckling and postbuckling behavior of elliptic plates. They used polynomial series expansions with as many as 56 terms in the displacement fields to obtain accurate solutions by the Rayleigh-Ritz method. The bifurcation strain and the postbuckling solutions of cross-ply and angle-ply elliptical sublaminates were obtained in a companion paper [93]. Chai [94] also employed a polynomial series ex-

pansion of up to 77 displacement terms. In a companion paper [95], the buckling and postbuckling behavior of an elliptical delaminated layer were investigated considering contact effect. Chai found that employing a contact condition between the delaminated layer and base plate may lead to an increase in the boundary stress, which in turn, changes each component of strain energy release rate.

It appears that all the literature cited above concerning two-dimensional delaminations [83-95] employed a unique case of near-the-surface delamination (thin-film assumption), so that the deformation of the base plate was totally neglected. In this regard, Davidson [96] proposed a Rayleigh-Ritz based analytical model considering base plate deformation for buckling load and compression failure behavior. He also extended this model to the multiple delamination problem [97]. But, the postbuckling analysis and delamination growth process were not studied in [96,97].

Steinmetz et al. [98] proposed a model which is a two-dimensional version of the model by Simitses et al. [35]. They calculated buckling loads for composites with rectangular, circular and elliptical delamination by using Rayleigh-Ritz and finite element methods. Cochelin and Potier-Ferry [99] improved the analytical model in Steinmetz et al. [98] by employing shear deformable plate theory for each part of the plate. Postbuckling solutions were obtained for circular and elliptical delaminations, and the strain energy release rate was computed along the delamination front using a J-integral concept for their model. They reported that the Griffith-type delamination propagation criterion is not appropriate, and more realistic propagation laws should be developed for delamination growth. Mukherjee et al. [100] developed a model based on Seide's layer-wise theory [16] to obtain buckling loads and mode shapes for an embedded delamination by applying the finite element method in conjunction with asymptotic expansion.

It is noted that the three recent papers [98-100] cited above dealt with an embedded delamination buckling and postbuckling with no thin-film assumption. All three models

are, however, obviously limited to the single delamination problem. More recently, Barbero and Reddy [101] developed a layer-wise laminated plate theory which is capable of modelling multiple delaminations in composites. They obtained strain energy release rates for through-the-width, square, and circular delaminations. However, all the problems considered in that work were limited to single thin-film delamination cases, and bifurcation analysis was not undertaken.

On the other hand, a fully nonlinear three-dimensional finite element model was developed by Whitcomb [102] based on three-dimensional nonlinear elasticity for delamination problem. He obtained each component of strain energy release rate using the virtual crack closure method [103] for postbuckled embedded elliptical delamination. In a subsequent paper [104] , a thin-film plate model, which has been adopted by many investigators, was compared to full 3-D, and thin film 3-D finite element model.

Although three-dimensional finite element models predict delamination behavior quite well, the computational cost is significantly high, especially for postbuckling analysis. It is also found that significantly higher order Rayleigh-Ritz approximation may be necessary in order to obtain accurate postbuckling solutions as addressed by Yin and Jane [92]. Thus, Rayleigh-Ritz method is likely to be as computationally cost intensive as three-dimensional finite element analysis. In addition, for multiple delaminations, three-dimensional finite element analysis may become more inefficient due to the mesh refinement needed at the each delamination crack tip.

As far as author's knowledge, no attempts have been made in the open literature on the vibration of a laminated composite containing embedded delaminations.

Chapter III

BUCKLING AND VIBRATION ANALYSIS

In this chapter, a mathematical model is developed for the analysis of buckling and free vibration of composite plates with delaminations.

A finite element method based on the layer-wise and sublaminate theories is developed to formulate the problem. First, an axisymmetric model is proposed for penny-shaped concentric delaminations in circular plates. And then, a two-dimensional model is developed for rectangular plates containing arbitrary shapes of delaminations.

Two techniques for the contact condition of delaminated surfaces are proposed in order to prevent physically inadmissible eigenmodes.

3.1 Axisymmetric Model

3.1.1 Kinematics

An N-layer fiber-reinforced composite circular plate of radius R containing multiple delaminations is considered. A cylindrical coordinate system (r, θ, z) is introduced in such a way that the center of the plate coincides with the origin of the coordinate system (Figure 3).

As a result of axisymmetry, the displacements in a cylindrical coordinate system have the form:

$$U_r(r, \theta, z) = U_r(r, z)\,, \tag{3.1}$$

$$U_\theta(r, \theta, z) = 0\,, \tag{3.2}$$

$$U_z(r, \theta, z) = U_z(r, z)\,. \tag{3.3}$$

To model the multiple delaminations, the assumed displacement field is supplemented with unit step functions which allow discontinuities in the displacement field as suggested by Barbero and Reddy [101]. The resulting displacements U_r and U_z at a generic point r,z in the laminate and time t are assumed to be of the form (Figure 4):

$$U_r(r,z,t) = u_r(r,t) + \phi^j(z)\, u_r^j(r,t) + \delta^i(z)\, \bar{u}_r^i(r,t)\,, \tag{3.4}$$

$$U_z(r,z,t) = u_z(r,t) + \delta^i(z)\, \bar{u}_z^i(r,t)\,, \tag{3.5}$$

here i and j indices range from 1 to D and 1 to M, respectively, where D is the number of delaminations, and M is the number of equivalent single-layers (i.e. number of layers for layer-wise model and number of sublaminates for sublaminate model) (Figure 5). Repeated superscript denotes summation convention.

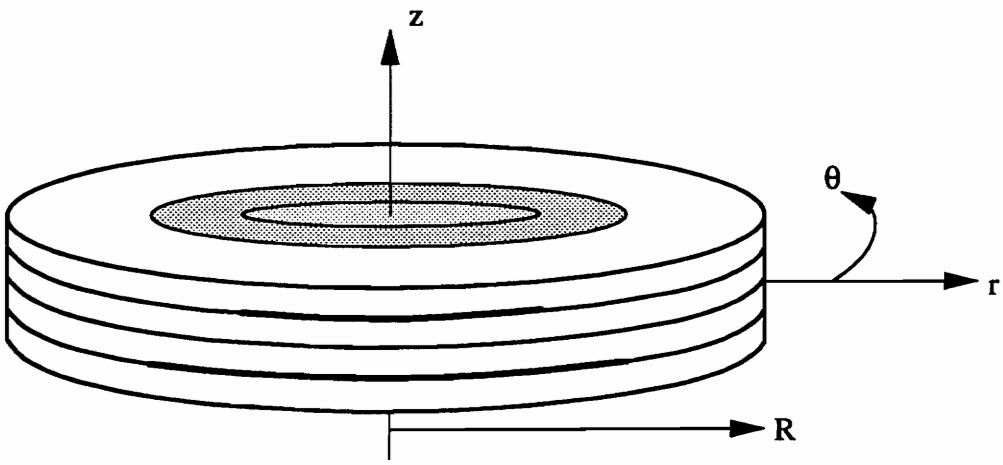

Figure 3. Geometry of an axisymmetric problem with delaminations

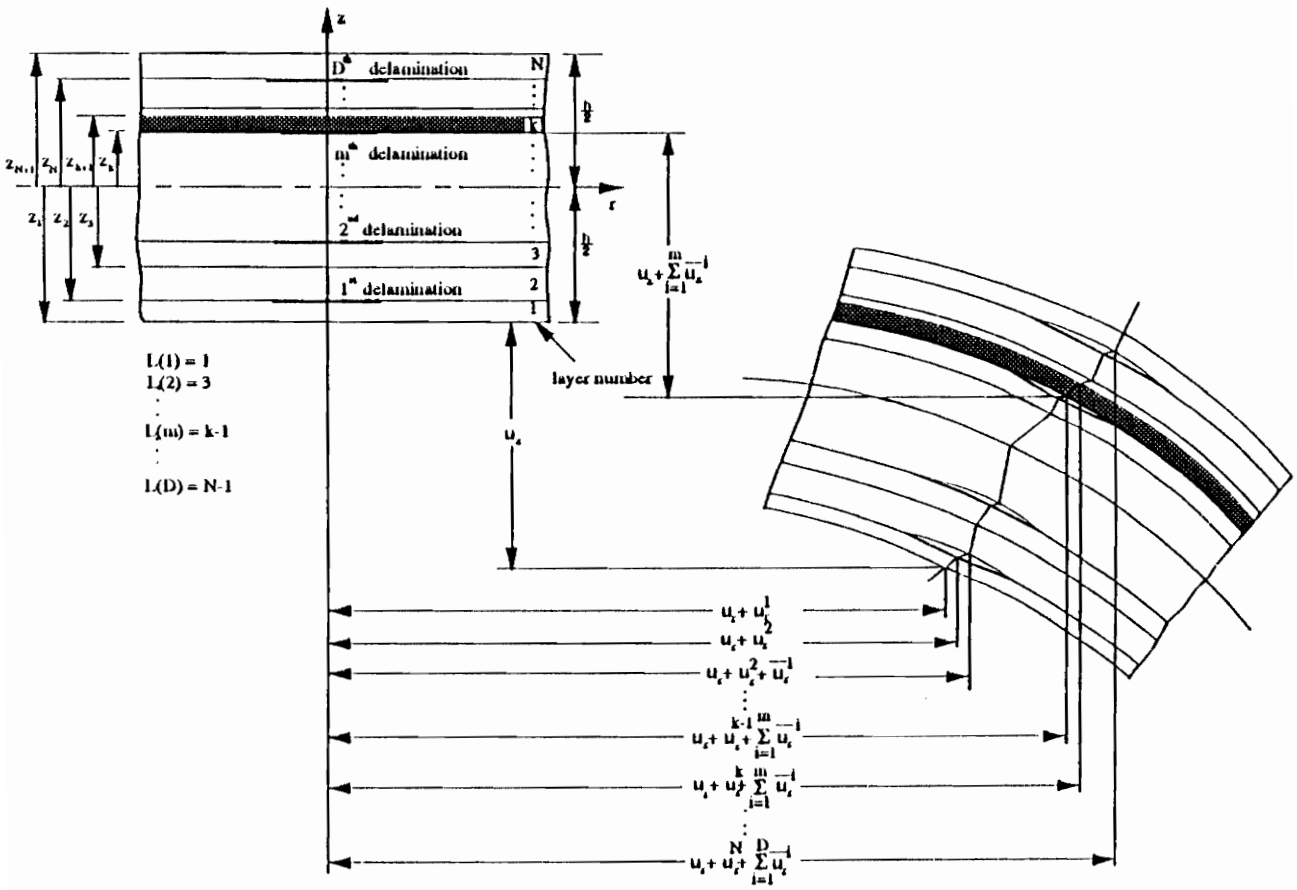

Figure 4. Configuration of kinematics for a circular plate

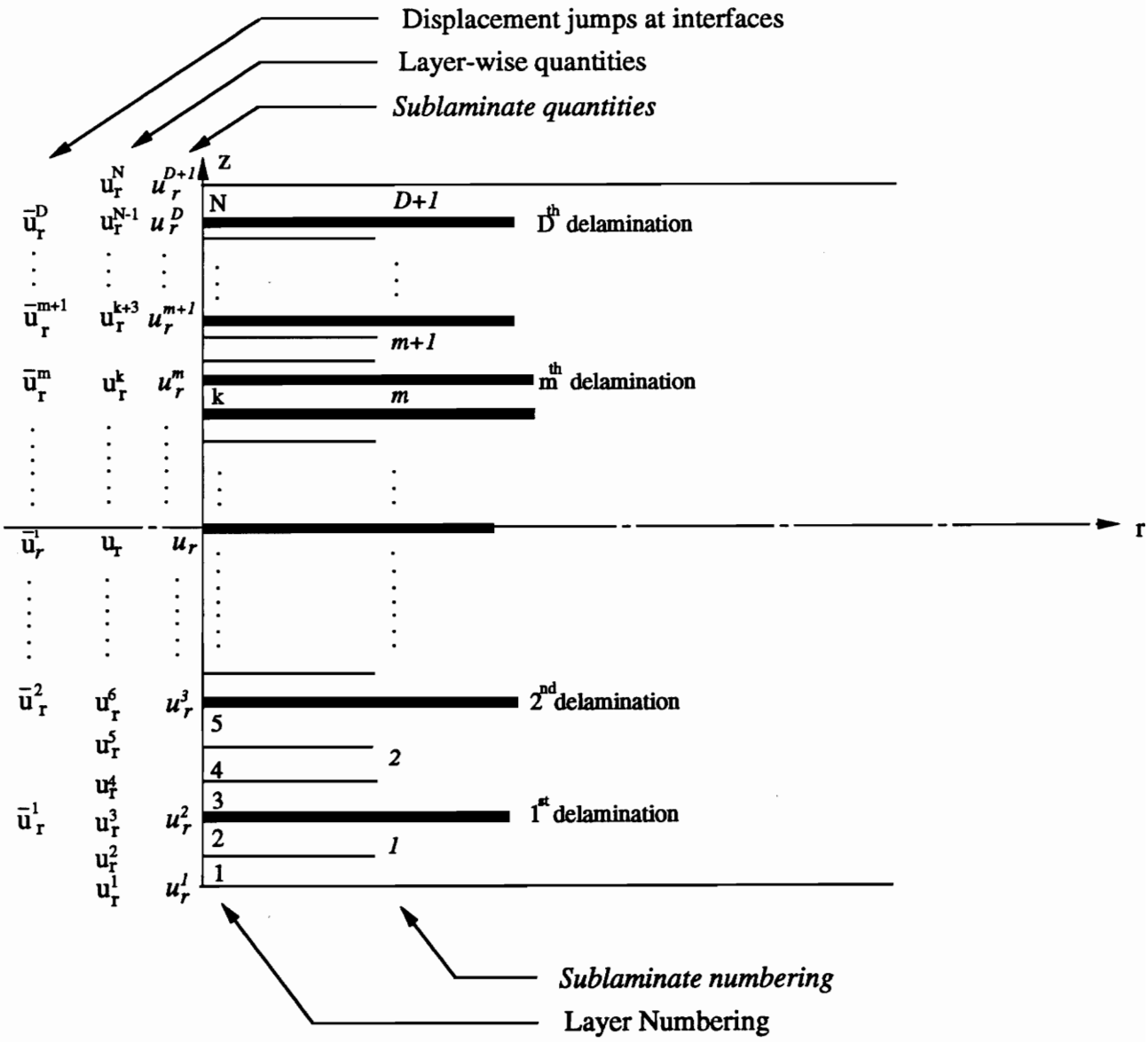

Figure 5. Description of displacements for layer-wise and sublaminate theories

The terms u_r and u_z are the displacements of a point $(r,0,t)$ on the reference surface of the laminate, u_r^j are nodal values of the displacements in the r direction of each equivalent single-layer, and $\bar{u}_r^i$ and $\bar{u}_z^i$ represent possible jumps in the slipping and opening displacements respectively at $L(i)$-th delaminated interface. $L(i)$-th denotes the location of interface where i-th delamination lies (Figure 4). $\phi^j(z)$ is a linear Lagrangian interpolation function through the thickness of the laminate. The step function $\delta^i(z)$ can be represented as Heaviside unit step function,

$$\delta^i(z) = H(z - z_{L(i)}). \tag{3.6}$$

It should be noted here that the theoretical modelling of layer-wise and sublaminate approaches are basically the same. The only difference between two approaches will be the constitutive relationship. The displacement fields for both theories are schematically illustrated in Figure 5.

It follows that $\gamma_{\theta z} = \gamma_{r\theta} = 0$ due to axisymmetry, and the remaining nonzero components of strain tensor associated with the small-displacement theory of elasticity are independent of θ and given by

$$\varepsilon_{rr} = \varepsilon_{rr}^o + \phi^j \varepsilon_{rr}^j + \delta^i \bar{\varepsilon}_{rr}^i , \tag{3.7}$$

$$\varepsilon_{\theta\theta} = \varepsilon_{\theta\theta}^o + \phi^j \varepsilon_{\theta\theta}^j + \delta^i \bar{\varepsilon}_{\theta\theta}^i , \tag{3.8}$$

$$\gamma_{rz} = \gamma_{rz}^o + \phi_{,z}^j \gamma_{rz}^j + \delta^i \bar{\gamma}_{rz}^i , \tag{3.9}$$

where

$$\varepsilon_{rr}^o = u_{r,r} , \qquad \varepsilon_{rr}^j = u_{r,r}^j , \qquad \bar{\varepsilon}_{rr}^i = \bar{u}_{r,r}^i , \tag{3.10}$$

$$\varepsilon_{\theta\theta}^o = \frac{u_r}{r} , \qquad \varepsilon_{\theta\theta}^j = \frac{u_r^j}{r} , \qquad \bar{\varepsilon}_{\theta\theta}^i = \frac{\bar{u}_r^i}{r} , \tag{3.11}$$

$$\gamma_{rz}^o = u_{z,r} , \qquad \gamma_{rz}^j = u_r^j , \qquad \bar{\gamma}_{rz}^i = \bar{u}_{z,r}^i . \tag{3.12}$$

It should be mentioned here that the derivative of step function, $\delta^{i}(z)$, with respect to z is Dirac delta function. However, owing to the characteristics of Dirac delta function, the strain component containing Dirac delta function is vanishing in the variational formulation, and thus, neglected hereafter.

3.1.2 Variational Formulation

The total potential energy of the system can be stated, in its buckled shape neglecting surface tractions and body forces, as [105]

$$\Pi = U + V, \tag{3.13}$$

where U is the strain energy

$$U = \frac{1}{2}\int_V (\sigma_{rr}\,\varepsilon_{rr} + \sigma_{\theta\theta}\,\varepsilon_{\theta\theta} + \sigma_{rz}\,\gamma_{rz})dV\,, \tag{3.14}$$

and V is the potential of inplane loads due to transverse deflection

$$V = \frac{1}{2}\int_\Omega N^o_{rr}\,(U_{z,r})^2 d\Omega\,, \tag{3.15}$$

where V is the volume of the plate and Ω is the reference plane of the plate.

The kinetic energy of the system is given by

$$T = \frac{1}{2}\int_V \rho(\dot{U}_r^2 + \dot{U}_z^2)dV\,. \tag{3.16}$$

In order to derive equations of motion, Hamilton's principle is used

$$\delta\int_{t_1}^{t_2}(T-\Pi)dt=0\ . \tag{3.17}$$

Substituting Eqs. (3.13) through (3.16) into Eq. (3.17), and integrating through the thickness of the laminate, the variational form of the present theory can be obtained:

$$\begin{aligned}
0=&-\int_{t_1}^{t_2}\int_{\Omega}\Big[N_{rr}\delta u_{r,r}+\frac{1}{r}N_{\theta\theta}\delta u_r+Q_{rz}\delta u_{z,r}+N^j_{rr}\delta u^j_{r,r}+\frac{1}{r}N^j_{\theta\theta}\delta u^j_r+Q^j_{rz}\delta u^j_r\\
&+\overline{N}^i_{rr}\delta\overline{u}^i_{r,r}+\frac{1}{r}\overline{N}^i_{\theta\theta}\delta\overline{u}^i_r+\overline{Q}^i_{rz}\delta\overline{u}^i_{z,r}\\
&+N^o_{rr}u_{z,r}\delta u_{z,r}+\overline{N}^{io}_{rr}\left(u_{z,r}\delta\overline{u}^i_{z,r}+\overline{u}^i_{z,r}\delta u_{z,r}\right)+\frac{1}{2}\overline{N}^{iso}_{rr}\left(\overline{u}^i_{z,r}\delta\overline{u}^s_{z,r}+\overline{u}^s_{z,r}\delta\overline{u}^i_{z,r}\right)\Big]rdrd\theta dt\\
&+\int_{t_1}^{t_2}\int_{\Omega}\Big[I^o(\dot{u}_r\delta\dot{u}_r+\dot{u}_z\delta\dot{u}_z)+I^j\left(\dot{u}_r\delta\dot{u}^j_r+\dot{u}^j_r\delta\dot{u}_r\right)\\
&+\overline{I}^i\left(\dot{u}_r\delta\dot{\overline{u}}^i_r+\dot{\overline{u}}^i_r\delta\dot{u}_r+\dot{u}_z\delta\dot{\overline{u}}^i_z+\dot{\overline{u}}^i_z\delta\dot{u}_z\right)\\
&+I^{jk}\dot{u}^j_r\delta\dot{u}^k_r+\widetilde{I}^{ij}\left(\dot{u}^j_r\delta\dot{\overline{u}}^i_r+\dot{\overline{u}}^i_r\delta\dot{u}^j_r\right)+\overline{I}^{is}\left(\dot{\overline{u}}^i_r\delta\dot{\overline{u}}^s_r+\dot{\overline{u}}^s_r\delta\dot{\overline{u}}^i_r\right)\Big]rdrd\theta dt\ ,
\end{aligned} \tag{3.18}$$

where the indices i,s range from 1 to D, and j,k range from 1 to M. The stress resultants are defined as:

$$[N_{rr},\ N^j_{rr},\ \overline{N}^i_{rr}]=\int_{-\frac{h}{2}}^{\frac{h}{2}}\sigma_{rr}\,[1,\ \phi^j,\ \delta^i]dz, \tag{3.19}$$

$$[N_{\theta\theta},\ N^j_{\theta\theta},\ \overline{N}^i_{\theta\theta}]=\int_{-\frac{h}{2}}^{\frac{h}{2}}\sigma_{\theta\theta}\,[1,\ \phi^j,\ \delta^i]dz, \tag{3.20}$$

$$[Q_{rz},\ Q^j_{rz},\ \overline{Q}^i_{rz}]=\int_{-\frac{h}{2}}^{\frac{h}{2}}\sigma_{rz}\,[1,\ \frac{d\phi^j}{dz},\ \delta^i]dz, \tag{3.21}$$

and inertia coefficients are defined as:

$$[I^o,\ I^j,\ \bar{I}^i] = \int_{-\frac{h}{2}}^{\frac{h}{2}} \rho\,[1,\ \phi^j,\ \delta^i]dz, \tag{3.22}$$

$$[I^{jk},\ \tilde{I}^{ij},\ \bar{I}^{is}] = \int_{-\frac{h}{2}}^{\frac{h}{2}} \rho\,[\phi^j\phi^k,\ \delta^i\phi^j,\ \delta^i\delta^s]dz, \tag{3.23}$$

and ρ is the material density. In Eq. (3.18), N^o_{rr}, $\overline{N}^{io}_{rr}$, $\overline{N}^{iso}_{rr}$ are the constant in-plane edge loads defined respectively by the following:

$$N^o_{rr} = -\lambda n\,, \tag{3.24}$$

$$\overline{N}^{io}_{rr} = -\lambda n^i\,, \tag{3.25}$$

$$\overline{N}^{iso}_{rr} = -\lambda n^{is}\,, \tag{3.26}$$

where λ is a buckling load parameter, n is the specified value of the compressive in-plane force, and n^i and n^{is} are newly-introduced layer-wise variables given as

$$n^i = \frac{\sum_{k=1}^{N}\int_{z_k}^{z_{k+1}} \delta^i dz}{\sum_{k=1}^{N}\int_{z_k}^{z_{k+1}} dz}\, n\,, \tag{3.27}$$

$$n^{is} = \frac{\sum_{k=1}^{N}\int_{z_k}^{z_{k+1}} \delta^i\delta^s dz}{\sum_{k=1}^{N}\int_{z_k}^{z_{k+1}} dz}\, n\,. \tag{3.28}$$

3.1.3 Equations of Motion

The Euler-Lagrange equations of motion of the present theory can be derived by integrating the derivatives of the varied quantities by parts to transfer differentiation from the displacements to the stress resultants and collecting the coefficients of δu_r, δu_z, δu_r^j, $\delta \overline{u}_r^i$, $\delta \overline{u}_z^i$:

$$\frac{1}{r}(rN_{rr})_{,r} - \frac{N_{\theta\theta}}{r} = I^o \ddot{u}_r + I^j \ddot{u}_r^j + \overline{I}^i \ddot{\overline{u}}_r^i \ , \tag{3.29}$$

$$\frac{1}{r}(rQ_{rz})_{,r} + \frac{N_{rr}^o}{r}(ru_{z,r})_{,r} + \frac{\overline{N}_{rr}^{io}}{r}\left(r\overline{u}_{z,r}^i\right)_{,r} = I^o \ddot{u}_z + \overline{I}^i \ddot{\overline{u}}_z^i \ , \tag{3.30}$$

$$\frac{1}{r}\left(rN_{rr}^j\right)_{,r} - \frac{N_{\theta\theta}^j}{r} - Q_{rz}^j = I^j \ddot{u}_r + I^{jk} \ddot{u}_r^k + \widetilde{I}^{ij} \ddot{\overline{u}}_r^i \ , \tag{3.31}$$

$$\frac{1}{r}\left(r\overline{N}_{rr}^i\right)_{,r} - \frac{\overline{N}_{\theta\theta}^i}{r} = \overline{I}^i \ddot{u}_r + \widetilde{I}^{ij} \ddot{u}_r^j + \overline{I}^{is} \ddot{\overline{u}}_r^s \ , \tag{3.32}$$

$$\frac{1}{r}\left(r\overline{Q}_{rz}^i\right)_{,r} + \frac{\overline{N}_{rr}^{io}}{r}(ru_{z,r})_{,r} + \frac{\overline{N}_{rr}^{iso}}{r}\left(r\overline{u}_{z,r}^s\right)_{,r} = \overline{I}^i \ddot{u}_z + \overline{I}^{is} \ddot{\overline{u}}_z^s \ , \tag{3.33}$$

where $i,s = 1, \ldots, D$ and $j,k = 1, \ldots, M$.

The equations of motion consist of $(2 + M + 2D)$ differential equations in $(2 + M + 2D)$ variables $(u_r, u_z, u_r^j, \overline{u}_r^i, \overline{u}_z^i)$. The first two equations (Eqs. (3.29) and (3.30)) are involved in the in-plane and out-of-plane actions at the reference plane, respectively. The third sets of equations (Eq. (3.31)) are from the layer-wise theory, and the last two sets of equations (Eqs. (3.32) and (3.33)) are involved in the in-plane and out-of-plane actions of sublaminates due to the delaminations, respectively.

The essential and natural boundary conditions are of the form:

essential	natural	
u_r	N_{rr}	(3.34)
u_z	Q_{rz}	(3.35)
u_r^j	N_{rr}^j	(3.36)
$\overline{u}_r^i$	$\overline{N}_{rr}^i$	(3.37)
$\overline{u}_z^i$	$\overline{Q}_{rz}^i$	(3.38)

3.1.4 Constitutive Equations

The constitutive equations of a *k-th* orthotropic lamina in the laminate co-ordinate system are given by [106]

$$\begin{bmatrix} \sigma_{rr} \\ \sigma_{\theta\theta} \\ \sigma_{rz} \end{bmatrix}^{(k)} = \begin{bmatrix} \overline{Q}_{1111} & \overline{Q}_{1122} & 0 \\ \overline{Q}_{1122} & \overline{Q}_{2222} & 0 \\ 0 & 0 & \overline{Q}_{1313} \end{bmatrix}^{(k)} \begin{bmatrix} \varepsilon_{rr} \\ \varepsilon_{\theta\theta} \\ \gamma_{rz} \end{bmatrix}^{(k)} \tag{3.39}$$

where $[\overline{Q}]^{(k)}$ denote the transformed reduced stiffness matrix of the *k-th* layer.

Substitution of Eq. (3.39) into Eqs. (3.19) - (3.21) gives the constitutive equations of the laminate:

$$\begin{bmatrix} N_{rr} \\ N_{\theta\theta} \\ N_{rr}^{k} \\ N_{\theta\theta}^{k} \\ \overline{N}_{rr}^{s} \\ \overline{N}_{\theta\theta}^{s} \end{bmatrix} = \begin{bmatrix} A_{1111} A_{1122} B_{1111}^{j} B_{1122}^{j} E_{1111}^{i} E_{1122}^{i} \\ A_{1122} A_{2222} B_{1122}^{j} B_{2222}^{j} E_{1122}^{i} E_{2222}^{i} \\ B_{1111}^{k} B_{1122}^{k} D_{1111}^{jk} D_{1122}^{jk} F_{1111}^{ik} F_{1122}^{ik} \\ B_{1122}^{k} B_{2222}^{k} D_{1122}^{jk} D_{2222}^{jk} F_{1122}^{ik} F_{2222}^{ik} \\ E_{1111}^{s} E_{1122}^{s} F_{1111}^{sj} F_{1122}^{sj} E_{1111}^{is} E_{1122}^{is} \\ E_{1122}^{s} E_{2222}^{s} F_{1122}^{sj} F_{2222}^{sj} E_{1122}^{is} E_{2222}^{is} \end{bmatrix} \begin{bmatrix} \varepsilon_{rr}^{o} \\ \varepsilon_{\theta\theta}^{o} \\ \varepsilon_{rr}^{j} \\ \varepsilon_{\theta\theta}^{j} \\ \overline{\varepsilon}_{rr}^{i} \\ \overline{\varepsilon}_{\theta\theta}^{i} \end{bmatrix}, \tag{3.40}$$

$$\begin{bmatrix} Q_{rz} \\ Q_{rz}^{k} \\ \overline{Q}_{rz}^{s} \end{bmatrix} = \begin{bmatrix} A_{1313} B_{1313}^{j} E_{1313}^{i} \\ B_{1313}^{k} D_{1313}^{jk} F_{1313}^{ik} \\ E_{1313}^{s} F_{1313}^{sj} E_{1313}^{is} \end{bmatrix} \begin{bmatrix} \gamma_{rz}^{o} \\ \gamma_{rz}^{j} \\ \overline{\gamma}_{rz}^{i} \end{bmatrix}, \tag{3.41}$$

where A_{1111}, B_{1111}^{j}, *etc.* are the stiffnesses of the laminate and given by

$$\left(A_{\alpha\alpha\beta\beta}, B_{\alpha\alpha\beta\beta}^{j}, E_{\alpha\alpha\beta\beta}^{i}\right) = \sum_{k=1}^{N} \int_{z_k}^{z_{k+1}} \overline{Q}_{\alpha\alpha\beta\beta}^{(k)} \left(1, \phi^{j}, \delta^{i}\right) dz \ , \tag{3.42}$$

$$\left(A_{1313}, B_{1313}^{j}, E_{1313}^{i}\right) = \sum_{k=1}^{N} \int_{z_k}^{z_{k+1}} \overline{Q}_{1313}^{(k)} \left(1, \phi_{,z}^{j}, \delta^{i}\right) dz \ , \tag{3.43}$$

$$\left(D_{\alpha\alpha\beta\beta}^{jk}, F_{\alpha\alpha\beta\beta}^{ik}, E_{\alpha\alpha\beta\beta}^{is}\right) = \sum_{k=1}^{N} \int_{z_k}^{z_{k+1}} \overline{Q}_{\alpha\alpha\beta\beta}^{(k)} \left(\phi^{j}\phi^{k}, \delta^{i}\phi^{k}, \delta^{i}\delta^{s}\right) dz \ , \tag{3.44}$$

$$\left(D_{1313}^{jk}, F_{1313}^{ik}, E_{1313}^{is}\right) = \sum_{k=1}^{N} \int_{z_k}^{z_{k+1}} \overline{Q}_{1313}^{(k)} \left(\phi^{j}\phi^{k}, \delta^{i}\phi_{,z}^{k}, \delta^{i}\delta^{s}\right) dz \ . \tag{3.45}$$

It is noted that the difference between layer-wise and sublaminate theories occurs only in the constitutive equation, and the explicit form of laminate stiffnesses for each theory is presented in Appendix A.

3.1.5 Finite Element Model

The equations of motion obtained are highly coupled, and analytical solutions are intractable even for very simple problems. Thus, the finite element method is used to obtain numerical solutions of the present theory.

The generalized displacements $(u_r, u_z, u_r^j, \bar{u}_r^i, \bar{u}_z^i)$ are expressed over each element as a linear combination of the one-dimensional Lagrangian interpolation function ψ_l associated with node l and the nodal values $(u_r)_l, (u_z)_l, (u_r^j)_l, (\bar{u}_r^i)_l, (\bar{u}_z^i)_l$ [107]:

$$
\begin{aligned}
u_r &= \sum_{l=1}^{n} (u_r)_l \psi_l \ , \\
u_z &= \sum_{l=1}^{n} (u_z)_l \psi_l \ , \\
u_r^j &= \sum_{l=1}^{n} (u_r^j)_l \psi_l \ , \\
\bar{u}_r^i &= \sum_{l=1}^{n} (\bar{u}_r^i)_l \psi_l \ , \\
\bar{u}_z^i &= \sum_{l=1}^{n} (\bar{u}_z^i)_l \psi_l \ ,
\end{aligned}
\tag{3.46}
$$

where n is the number of nodes in a typical finite element.

Substituting these expressions into the weak statement in Eq. (3.18), the finite element model of a typical element can be obtained as

$$
([K] - \lambda [G])\{\Delta\} = \{0\} \ , \tag{3.47}
$$

where $[K]$ is the element stiffness matrix,

$$
[K] = \begin{bmatrix}
[{}^{11}K] & [\ 0\ ] & [{}^{13}K^{k}] & [{}^{14}K^{s}] & [\ 0\ ] \\
 & [{}^{22}K] & [{}^{23}K^{k}] & [\ 0\ ] & [{}^{25}K^{s}] \\
 & & [{}^{33}K^{lk}] & [{}^{34}K^{ls}] & [{}^{35}K^{ls}] \\
 & & & [{}^{44}K^{ns}] & [\ 0\ ] \\
sym. & & & & [{}^{55}K^{ns}]
\end{bmatrix} \tag{3.48}
$$

and $[G]$ is the element geometric stiffness matrix in the case of buckling,

$$
[G] = \begin{bmatrix}
[\ 0\ ] & [\ 0\ ] & [\ 0\ ] & [\ 0\ ] & [\ 0\ ] \\
 & [{}^{22}G] & [\ 0\ ] & [\ 0\ ] & [{}^{25}G^{s}] \\
 & & [\ 0\ ] & [\ 0\ ] & [\ 0\ ] \\
 & & & [\ 0\ ] & [\ 0\ ] \\
sym. & & & & [{}^{55}G^{ns}]
\end{bmatrix} \tag{3.49}
$$

and the element mass matrix in the case of free vibration,

$$
[G] = \begin{bmatrix}
[{}^{11}G] & [\ 0\ ] & [{}^{13}G^{k}] & [{}^{14}G^{s}] & [\ 0\ ] \\
 & [{}^{22}G] & [\ 0\ ] & [\ 0\ ] & [{}^{25}G^{s}] \\
 & & [{}^{33}G^{lk}] & [{}^{34}G^{ls}] & [\ 0\ ] \\
 & & & [{}^{44}G^{ns}] & [\ 0\ ] \\
sym. & & & & [{}^{55}G^{ns}]
\end{bmatrix}. \tag{3.50}
$$

The explicit forms of $[K]$ and $[G]$ are presented in Appendix B. In Eq. (3.47), λ refers to a buckling coefficient or frequency parameter and $\{\Delta\}$ is the eigenvector of nodal displacements corresponding to an eigenvalue

$$
\{\Delta\} = \left\{\{u_r\}\ \{u_z\}\ \{u_r^k\}\ \{\bar{u}_r^s\}\ \{\bar{u}_z^s\}\right\}^{\mathrm{T}}. \tag{3.51}
$$

It is noted that the reduced integration scheme is used to calculate the stiffness coefficients associated with transverse shear terms (i.e., coefficients in $[K]$ containing A_{1313}, B^{j}_{1313}, D^{jk}_{1313}, E^{j}_{1313}, F^{jk}_{1313}, and E^{jk}_{1313}).

3.2 Two-Dimensional Model

3.2.1 Kinematics

An N-layer fiber-reinforced composite plate containing multiple delaminations is considered. (Figure 6). To model the multiple delaminations, the assumed displacement field is supplemented with unit step functions which allow discontinuities in the displacement field.

The resulting displacements U_α and U_3 at a generic point x_1, x_2, x_3 in the laminate and time t are assumed to be of the form:

$$U_\alpha(x_\beta,x_3,t) = u_\alpha(x_\beta,t) + \phi^j(x_3)\, u^j_\alpha(x_\beta,t) + \delta^i(x_3)\, \bar{u}^i_\alpha(x_\beta,t) \ , \tag{3.52}$$
$$U_3(x_\beta,x_3,t) = u_3(x_\beta,t) + \delta^i(x_3)\, \bar{u}^i_3(x_\beta,t) \ .$$

The usual Cartesian indicial notation is employed where Latin and Greek subscripts are assumed to have values from 1 to 3 and 1 to 2, respectively. Superscript i and j range from 1 to D and 1 to M, where D is the number of delaminations, and M is the number of equivalent single-layers. Repeated indices imply the summation convention and $()_{,i}$ is used to denote partial derivative with respect to x_i.

The terms u_α and u_3 are the displacements of a point $(x_1, x_2, 0, t)$ on the reference surface of the laminate, u^j_α are nodal values of the displacements in the x_α direction of each equivalent single-layer, and $\bar{u}^i_\alpha$ and $\bar{u}^i_3$ represent possible jumps in the slipping and opening displacements respectively at $L(i)$-th delaminated interface. $L(i)$-th denotes the location of interface where i-th delamination lies (Figure 7). $\phi^j(x_3)$ and $\delta^i(x_3)$ denote a

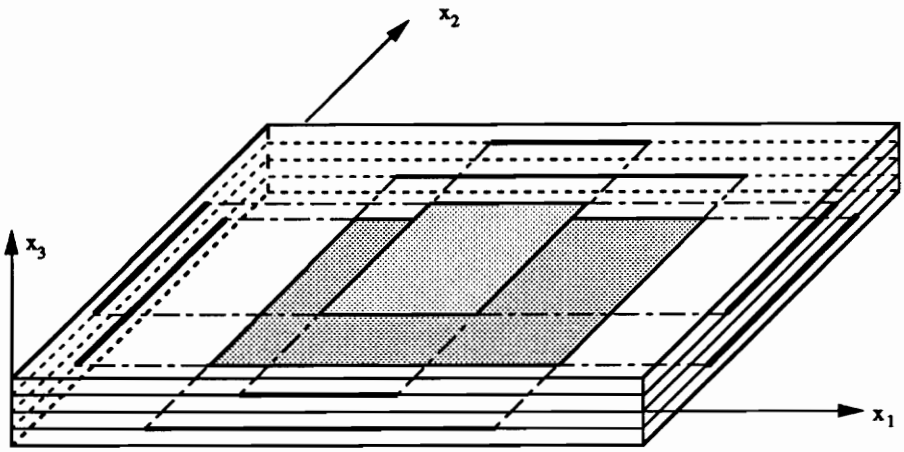

Figure 6. Geometry of a rectangular plate with delaminations

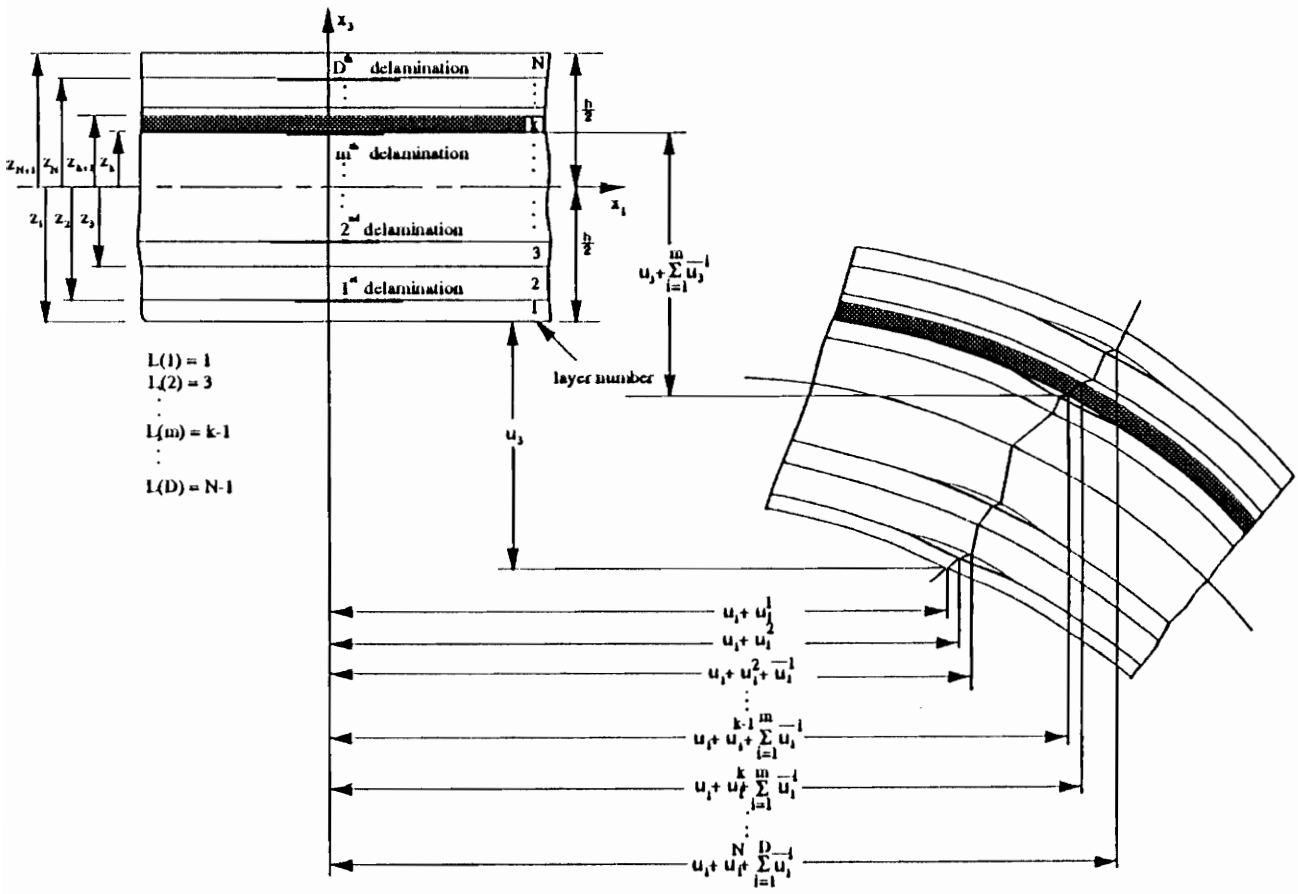

Figure 7. Configuration of kinematics for a rectangular plate

linear Lagrangian interpolation function through the thickness of the laminate and unit step function, respectively.

The strain tensor associated with the small-displacement theory of elasticity are given by

$$\varepsilon_{\alpha\beta} = \overset{o}{\varepsilon}_{\alpha\beta} + \phi^j \overset{j}{\varepsilon}_{\alpha\beta} + \delta^i \overset{\bar{i}}{\varepsilon}_{\alpha\beta} , \tag{3.53}$$

$$\gamma_{\alpha 3} = \overset{o}{\gamma}_{\alpha 3} + \phi^j_{,3} \overset{j}{\gamma}_{\alpha 3} + \delta^i \overset{\bar{i}}{\gamma}_{\alpha 3} , \tag{3.54}$$

where

$$\overset{o}{\varepsilon}_{\alpha\beta} = \frac{1}{2}(u_{\alpha,\beta} + u_{\beta,\alpha}) ,$$

$$\overset{j}{\varepsilon}_{\alpha\beta} = \frac{1}{2}\left(\overset{j}{u}_{\alpha,\beta} + \overset{j}{u}_{\beta,\alpha}\right) , \tag{3.55}$$

$$\overset{\bar{i}}{\varepsilon}_{\alpha\beta} = \frac{1}{2}\left(\overset{\bar{i}}{u}_{\alpha,\beta} + \overset{\bar{i}}{u}_{\beta,\alpha}\right) ,$$

$$\overset{o}{\gamma}_{\alpha 3} = u_{3,\alpha}, \qquad \overset{j}{\gamma}_{\alpha 3} = \overset{j}{u}_{\alpha}, \qquad \overset{\bar{i}}{\gamma}_{\alpha 3} = \overset{\bar{i}}{u}_{3,\alpha} . \tag{3.56}$$

3.2.2 Variational Formulation

The total potential energy of the system can be stated, in its buckled shape, as

$$\Pi = U + V, \tag{3.57}$$

where U is the strain energy

$$U = \frac{1}{2}\int_V (\sigma_{\alpha\beta}\varepsilon_{\alpha\beta} + \sigma_{\alpha 3}\gamma_{\alpha 3}) dV , \tag{3.58}$$

and V is the potential of inplane loads due to transverse deflection

$$V = \frac{1}{2}\int_{\Omega} N^{o}_{\alpha\beta} U_{3,\alpha} U_{3,\beta} d\Omega \,. \tag{3.59}$$

The kinetic energy is

$$T = \frac{1}{2}\int_{V} \rho(\dot{U}^2_{\alpha} + \dot{U}^2_3) dV \,. \tag{3.60}$$

Hamilton's principle can be stated as

$$\delta\int_{t_1}^{t_2} (T - \Pi) dt = 0 \,. \tag{3.61}$$

Substituting Eqs. (3.57) through (3.60) into Eq. (3.61), the following weak statement is obtained:

$$\begin{aligned} 0 = &-\int_{t_1}^{t_2}\int_{\Omega} \Big[N_{\alpha\beta}\delta u_{\alpha,\beta} + N^{j}_{\alpha\beta}\delta u^{j}_{\alpha,\beta} + \overline{N}^{i}_{\alpha\beta}\delta \overline{u}^{i}_{\alpha,\beta} + Q_{\alpha 3}\delta u_{3,\alpha} + Q^{j}_{\alpha 3}\delta u^{j}_{\alpha} + \overline{Q}^{i}_{\alpha 3}\delta \overline{u}^{i}_{3,\alpha} \\ &+ N^{o}_{\alpha\beta} u_{3,\alpha}\delta u_{3,\beta} + \overline{N}^{io}_{\alpha\beta}\big(\overline{u}^{i}_{3,\alpha}\delta u_{3,\beta} + u_{3,\alpha}\delta \overline{u}^{i}_{3,\beta}\big) + \overline{N}^{iso}_{\alpha\beta}\overline{u}^{i}_{3,\alpha}\delta \overline{u}^{s}_{3,\beta}\Big] dx_1 dx_2 dt \\ &+ \int_{t_1}^{t_2}\int_{\Omega} \Big[I^{o}(\dot{u}_{\alpha}\delta\dot{u}_{\alpha} + \dot{u}_3\delta\dot{u}_3) + I^{j}\big(\dot{u}_{\alpha}\delta\dot{u}^{j}_{\alpha} + \dot{u}^{j}_{\alpha}\delta\dot{u}_{\alpha}\big) \\ &\quad + \overline{I}^{i}\big(\dot{u}_{\alpha}\delta\dot{\overline{u}}^{i}_{\alpha} + \dot{\overline{u}}^{i}_{\alpha}\delta\dot{u}_{\alpha} + \dot{u}_3\delta\dot{\overline{u}}^{i}_3 + \dot{\overline{u}}^{i}_3\delta\dot{u}_3\big) \\ &\quad + I^{jk}\dot{u}^{j}_{\alpha}\delta\dot{u}^{k}_{\alpha} + \tilde{I}^{ij}\big(\dot{u}^{j}_{\alpha}\delta\dot{\overline{u}}^{i}_{\alpha} + \dot{\overline{u}}^{i}_{\alpha}\delta\dot{u}^{j}_{\alpha}\big) + \overline{I}^{is}\big(\dot{\overline{u}}^{i}_{\alpha}\delta\dot{\overline{u}}^{s}_{\alpha} + \dot{\overline{u}}^{s}_{\alpha}\delta\dot{\overline{u}}^{i}_{\alpha}\big)\Big] dx_1 dx_2 dt \,, \end{aligned} \tag{3.62}$$

where $j, k = 1, \ldots, M$ and $i, s = 1, \ldots, D$. The stress resultants are

$$[N_{\alpha\beta},\ N^{j}_{\alpha\beta},\ \overline{N}^{i}_{\alpha\beta}] = \int_{-\frac{h}{2}}^{\frac{h}{2}} \sigma_{\alpha\beta}\,[1,\ \phi^{j},\ \delta^{i}] dx_3, \tag{3.63}$$

$$[Q_{\alpha 3},\ Q^{j}_{\alpha 3},\ \overline{Q}^{l}_{\alpha 3}] = \int_{-\frac{h}{2}}^{\frac{h}{2}} \sigma_{\alpha 3}\,[1,\ \phi^{j}_{,3},\ \delta^{l}]dx_3. \tag{3.64}$$

The inertia coefficients are the same as in Eqs. (3.22) and (3.23). In Eq. (3.62), $N^{o}_{\alpha\beta}$, $\overline{N}^{io}_{\alpha\beta}$, $\overline{N}^{iso}_{\alpha\beta}$ are the constant in-plane edge loads defined respectively by the following:

$$N^{o}_{\alpha\beta} = -\lambda n_{\alpha\beta}\,, \tag{3.65}$$

$$\overline{N}^{io}_{\alpha\beta} = -\lambda n^{l}_{\alpha\beta}\,, \tag{3.66}$$

$$\overline{N}^{iso}_{\alpha\beta} = -\lambda n^{ls}_{\alpha\beta}\,, \tag{3.67}$$

where λ is a buckling load parameter, $n_{\alpha\beta}$ is the specified value of the compressive or shear in-plane force, and $n^{l}_{\alpha\beta}$ and $n^{ls}_{\alpha\beta}$ are newly-introduced layer-wise variables given as

$$n^{l}_{\alpha\beta} = \frac{\sum_{k=1}^{N}\int_{z_k}^{z_{k+1}} \delta^{l} dx_3}{\sum_{k=1}^{N}\int_{z_k}^{z_{k+1}} dx_3}\, n_{\alpha\beta}, \tag{3.68}$$

$$n^{ls}_{\alpha\beta} = \frac{\sum_{k=1}^{N}\int_{z_k}^{z_{k+1}} \delta^{l}\delta^{s} dx_3}{\sum_{k=1}^{N}\int_{z_k}^{z_{k+1}} dx_3}\, n_{\alpha\beta}\,. \tag{3.69}$$

3.2.3 Equations of Motion

The Euler-Lagrange equations of motion of the present theory can be derived by integrating the derivatives of the varied quantities by parts and collecting the coefficients of δu_α, δu_3, δu^j_α, $\delta \overline{u}^i_\alpha$, $\delta \overline{u}^i_3$:

$$N_{\alpha\beta,\alpha} = I^o \ddot{u}_\beta + I^j \ddot{u}^j_\beta + \overline{I}^i \ddot{\overline{u}}^i_\beta \ , \tag{3.70}$$

$$Q_{\alpha 3,\alpha} + N^o_{\alpha\beta} u_{3,\alpha\beta} + \overline{N}^{io}_{\alpha\beta} \overline{u}^i_{3,\alpha\beta} = I^o \ddot{u}_3 + \overline{I}^i \ddot{\overline{u}}^i_3 \ , \tag{3.71}$$

$$N^j_{\alpha\beta,\alpha} - Q^j_{\beta 3} = I^j \ddot{u}_\beta + I^{jk} \ddot{u}^k_\beta + \widetilde{I}^{ij} \ddot{\overline{u}}^i_\beta \ , \tag{3.72}$$

$$\overline{N}^i_{\alpha\beta,\alpha} = \overline{I}^i \ddot{u}_\beta + \widetilde{I}^{ij} \ddot{u}^j_\beta + \overline{I}^{ir} \ddot{\overline{u}}^r_\beta \ , \tag{3.73}$$

$$\overline{Q}^i_{\alpha 3,\alpha} + \overline{N}^{io}_{\alpha\beta} u_{3,\alpha\beta} + \overline{N}^{iro}_{\alpha\beta} \overline{u}^r_{3,\alpha\beta} = \overline{I}^i \ddot{u}_3 + \overline{I}^{ir} \ddot{\overline{u}}^r_3 \ , \tag{3.74}$$

where $i, r = 1, \ldots, D$ and $j, k = 1, \ldots, M$.

The equations of motion consist of $(3 + 2M + 3D)$ differential equations in $(3 + 2M + 3D)$ variables $(u_\alpha, u_3, u^j_\alpha, \overline{u}^i_\alpha, \overline{u}^i_3)$. The first two sets of equations (Eqs. (3.70) and (3.71)) are involved in the in-plane and out-of-plane actions at reference plane, respectively. The third sets of equations (Eq. (3.72)) are from the layer-wise theory, and the last two sets of equations (Eqs. (3.73) and (3.74)) are involved in the in-plane and out-of-plane actions of sublaminates due to the delaminations, respectively.

The essential and natural boundary conditions are of the form:

essential natural

$$u_\alpha \qquad N_{\alpha\beta}n_\beta \tag{3.75}$$

$$u_3 \qquad Q_{\beta 3}n_\beta \tag{3.76}$$

$$u_\alpha^j \qquad N_{\alpha\beta}^j n_\beta \tag{3.77}$$

$$\bar{u}_\alpha^i \qquad \overline{N}_{\alpha\beta}^i n_\beta \tag{3.78}$$

$$\bar{u}_3^i \qquad \overline{Q}_{\beta 3}^i n_\beta \tag{3.79}$$

where n_β is a unit normal vector in β direction.

3.2.4 Constitutive Equations

The constitutive equations of a *k-th* orthotropic lamina in the laminate co-ordinate system are given by

$$\sigma_{\alpha\beta}^{(k)} = \overline{Q}_{\alpha\beta\gamma\omega}^{(k)} \varepsilon_{\gamma\omega}^{(k)} \ , \tag{3.80}$$

$$\sigma_{\alpha 3}^{(k)} = \overline{Q}_{\alpha 3\beta 3}^{(k)} \gamma_{\beta 3}^{(k)} \ , \tag{3.81}$$

where $[\overline{Q}]^{(k)}$ denote the transformed reduced stiffness matrix of the *k-th* layer.

Substitution of Eqs. (3.81) and (3.82) into Eqs. (3.63) and (3.64) gives the constitutive equations of the laminate:

$$\begin{bmatrix} N_{\alpha\beta} \\ N_{\alpha\beta}^j \\ \overline{N}_{\alpha\beta}^i \end{bmatrix} = \begin{bmatrix} A_{\alpha\beta\gamma\omega} & B_{\alpha\beta\gamma\omega}^k & E_{\alpha\beta\gamma\omega}^s \\ B_{\alpha\beta\gamma\omega}^j & D_{\alpha\beta\gamma\omega}^{jk} & F_{\alpha\beta\gamma\omega}^{sj} \\ E_{\alpha\beta\gamma\omega}^i & F_{\alpha\beta\gamma\omega}^{ik} & E_{\alpha\beta\gamma\omega}^{is} \end{bmatrix} \begin{bmatrix} \varepsilon_{\gamma\omega} \\ \varepsilon_{\gamma\omega}^k \\ \bar{\varepsilon}_{\gamma\omega}^s \end{bmatrix} , \tag{3.82}$$

$$\begin{bmatrix} Q_{\alpha 3} \\ Q^j_{\alpha 3} \\ \overline{Q}^i_{\alpha 3} \end{bmatrix} = \begin{bmatrix} A_{\alpha 3\beta 3} & B^k_{\alpha 3\beta 3} & E^s_{\alpha 3\beta 3} \\ B^j_{\alpha 3\beta 3} & D^{jk}_{\alpha 3\beta 3} & F^{sj}_{\alpha 3\beta 3} \\ E^i_{\alpha 3\beta 3} & F^{ik}_{\alpha 3\beta 3} & E^{is}_{\alpha 3\beta 3} \end{bmatrix} \begin{bmatrix} \overset{o}{\gamma}_{\beta 3} \\ \overset{k}{\gamma}_{\beta 3} \\ \overset{s}{\gamma}_{\beta 3} \end{bmatrix} , \tag{3.83}$$

where $A_{\alpha\beta\gamma\omega}$, $B^j_{\alpha\beta\gamma\omega}$, *etc.* are the stiffnesses of the laminate given by

$$\left(A_{\alpha\beta\gamma\omega}, B^j_{\alpha\beta\gamma\omega}, E^i_{\alpha\beta\gamma\omega}\right) = \sum_{k=1}^{N} \int_{z_k}^{z_{k+1}} \overline{Q}^{(k)}_{\alpha\beta\gamma\omega}\left(1, \phi^j, \delta^i\right) dx_3 \ , \tag{3.84}$$

$$\left(A_{\alpha 3\beta 3}, B^j_{\alpha 3\beta 3}, E^i_{\alpha 3\beta 3}\right) = \sum_{k=1}^{N} \int_{z_k}^{z_{k+1}} \overline{Q}^{(k)}_{\alpha 3\beta 3}\left(1, \phi^j_{,3}, \delta^i\right) dx_3 \ , \tag{3.85}$$

$$\left(D^{jk}_{\alpha\beta\gamma\omega}, F^{ik}_{\alpha\beta\gamma\omega}, E^{is}_{\alpha\beta\gamma\omega}\right) = \sum_{k=1}^{N} \int_{z_k}^{z_{k+1}} \overline{Q}^{(k)}_{\alpha\beta\gamma\omega}\left(\phi^j\phi^k, \delta^i\phi^k, \delta^i\delta^s\right) dx_3 \ , \tag{3.86}$$

$$\left(D^{jk}_{\alpha 3\beta 3}, F^{ik}_{\alpha 3\beta 3}, E^{is}_{\alpha 3\beta 3}\right) = \sum_{k=1}^{N} \int_{z_k}^{z_{k+1}} \overline{Q}^{(k)}_{\alpha 3\beta 3}\left(\phi^j\phi^k, \delta^i\phi^k_{,3}, \delta^i\delta^s\right) dx_3 \ . \tag{3.87}$$

The explicit forms of stiffnesses for layer-wise and sublaminate theory are given in Appendix A.

3.2.5 Finite Element Model

The generalized displacements (u_α, u_3, u^j_α, $\overline{u}^i_\alpha$, $\overline{u}^i_3$) are expressed over each element as a linear combination of the one-dimensional Lagrangian interpolation function ψ_l associated with node l and the nodal values $(u_\alpha)_l, (u_3)_l, (u^j_\alpha)_l, (\overline{u}^i_\alpha)_l, (\overline{u}^i_3)_l$:

$$
\begin{aligned}
u_\alpha &= \sum_{l=1}^{n} (u_\alpha)_l \psi_l \ , \\
u_3 &= \sum_{l=1}^{n} (u_3)_l \psi_l \ , \\
u_\alpha^j &= \sum_{l=1}^{n} (u_\alpha^j)_l \psi_l \ , \\
\bar{u}_\alpha^i &= \sum_{l=1}^{n} (\bar{u}_\alpha^i)_l \psi_l \ , \\
\bar{u}_3^i &= \sum_{l=1}^{n} (\bar{u}_3^i)_l \psi_l \ ,
\end{aligned}
\tag{3.88}
$$

where n is the number of nodes in a typical finite element.

Substituting these expressions into the weak statement in Eq. (3.62), the finite element model of a typical element can be obtained as

$$
([K] - \lambda [G])\{\Delta\} = \{0\} \ , \tag{3.89}
$$

where $[K]$ is the element stiffness matrix,

$$
[K] = \begin{bmatrix}
[{}^{\alpha\beta}K] & [\ 0\ ] & [{}^{\alpha(\beta+3)}K^k] & [{}^{\alpha(\beta+5)}K^s] & [\ 0\ ] \\
 & [{}^{33}K] & [{}^{3(\beta+3)}K^k] & [\ 0\ ] & [{}^{38}K^s] \\
 & & [{}^{(\alpha+3)(\beta+3)}K^{lk}] & [{}^{(\alpha+3)(\beta+5)}K^{ls}] & [{}^{(\alpha+3)8}K^{ls}] \\
 & & & [{}^{(\alpha+5)(\beta+5)}K^{ns}] & [\ 0\ ] \\
sym. & & & & [{}^{88}K^{ns}]
\end{bmatrix}
\tag{3.90}
$$

and $[G]$ is the element geometric stiffness matrix in the case of buckling,

$$
[G] = \begin{bmatrix}
[\ 0\ ] & [\ 0\ ] & [\ 0\ ] & [\ 0\ ] & [\ 0\ ] \\
 & [{}^{33}G] & [\ 0\ ] & [\ 0\ ] & [{}^{38}G^s] \\
 & & [\ 0\ ] & [\ 0\ ] & [\ 0\ ] \\
 & & & [\ 0\ ] & [\ 0\ ] \\
sym. & & & & [{}^{88}G^{ns}]
\end{bmatrix}
\tag{3.91}
$$

and the element mass matrix in the case of free vibration,

$$[G] = \begin{bmatrix} [{}^{\alpha\beta}G] & [\ 0\ ] & [{}^{\alpha(\beta+3)}G^{k}] & [{}^{\alpha(\beta+5)}G^{s}] & [\ 0\ ] \\ & [{}^{33}G] & [\ 0\ ] & [\ 0\ ] & [{}^{3(\beta+5)}G^{s}] \\ & & [{}^{(\alpha+3)(\beta+3)}G^{lk}] & [{}^{(\alpha+3)(\beta+5)}G^{ls}] & [\ 0\ ] \\ & & & [{}^{(\alpha+5)(\beta+5)}G^{ns}] & [\ 0\ ] \\ sym. & & & & [{}^{88}G^{ns}] \end{bmatrix}. \tag{3.92}$$

The explicit forms of $[K]$ and $[G]$ are presented in Appendix B. In Eq. (3.89), λ refers to a buckling coefficient or frequency parameter and $\{\Delta\}$ is the eigenvector of nodal displacements corresponding to an eigenvalue

$$\{\Delta\} = \left\{\{u_\alpha\}\ \{u_3\}\ \{u_\alpha^k\}\ \{\bar{u}_\alpha^s\}\ \{\bar{u}_3^s\}\right\}^{\mathrm{T}}. \tag{3.93}$$

It is noted that the reduced integration scheme is used to calculate the stiffness coefficients associated with transverse shear terms (i.e., coefficients in $[K]$ containing $A_{\alpha 3\beta 3}$, $B^{j}_{\alpha 3\beta 3}$, $D^{jk}_{\alpha 3\beta 3}$, $E^{i}_{\alpha 3\beta 3}$, $F^{ik}_{\alpha 3\beta 3}$, and $E^{is}_{\alpha 3\beta 3}$)

This completes the derivation of layer-wise and sublaminate finite element model.

3.3 Numerical Procedure

3.3.1 Eigenvalue Problem

The matrix equation of Eq. (3.89) represents generalized eigenvalue problem. For buckling analysis, it may be observed that the geometric stiffness matrix $[G]$ is not necessarily positive definite. As the stiffness matrix $[K]$ is positive definite, the reciprocal of the system is solved

$$|[G] - \lambda^{*}[K]| = 0 \tag{3.94}$$

where $\lambda^{*} = \frac{1}{\lambda}$.

Consequently, the positive eigenvalues $\lambda_1 < \lambda_2 < \lambda_3 < \cdots$ correspond to the eigenvalues $\lambda_1^{*} > \lambda_2^{*} > \lambda_3^{*} > \cdots$.

In the case of free vibration problem, the eigenproblem in Eq. (3.89) can be solved directly because the mass matrix $[G]$ is always positive definite.

3.3.2 Investigations of contact conditions

In the analysis methodology described in the previous section, the buckling modes calculated from the model are not necessarily physically admissible.

For a single delamination, the mode shape corresponding to the lowest eigenvalue usually exhibits one half-wave, which indicates that the eigenvector components associated with $\bar{u}_3^{i}$ (the opening displacements across the delamination) do not change their sign through the whole range of a delamination. Consequently, the lowest eigenvalue

is always physically admissible as long as the mode shape is one wave for a single delamination. However, if the first mode shape exhibits two or more half-waves, or if there is more than one delamination, the eigenvector associated with $\bar{u}_3^i$ experiences a sign change with respect to the independent variable. That is, sublaminates may overlap each other at the same time.

In order to preclude these nonphysical buckling modes, a no-penetration condition should be imposed on the problem. Physically, all the values of $\bar{u}_3^i$ should be nonnegative for admissible mode shape. However, because the sign of a eigenvector is interchangible, mathematically, contact condition implies that all the components of the eigenvector associated with $\bar{u}_3^i$ should be either nonnegative or nonpositive.

In the present study, two kinds of contact analysis are developed which are based on the following assumptions:

1. The contact is frictionless ($\bar{u}_\alpha$ is not specified).
2. Each sublaminate is assumed to be rigid in the thickness direction, hence, the thickness variations of sublaminates are neglected.

Two methods are as follows:

Method I

1. Solve the Eq. (3.89) in the ordinary way and find the smallest eigenvalue which has an admissible eigenmode.
2. Specify essential boundary conditions $\bar{u}_3^i$ for i^{th} delamination and repeat 1.
3. repeat 2 until opening of all delaminations are specified, $\sum_{i=1}^{D} \bar{u}_3^i = 0$
4. Compare the eigenvalues for all above cases, and choose the smallest one.

Strictly speaking, the total number of cases considered is 2^D for a composite having D number of delaminations. However, by investigating the configuration of delaminations, the solution can be obtained in much fewer trials than 2^D. Another method is similar to that of Suemasu [52], and illustrated as follows:

Method 2

1. Solve the Eq. (3.89) in the ordinary way.
2. Identify the point of maximum overlap and specify essential boundary condition $\overline{u}_3^i = 0$ at that node.
3. Rerun the problem with modified boundary condition.
4. Repeat procedure 2 and 3 until all overlaps disappear.

More detailed explanation of Method 2 will be given in Chapter IV. It is assumed that each delamination is either close or open for whole range of debonding in Method 1. On the other hand, Method 2 explains point-wise delamination opening.

Consequently, combination of these two methodologies will be used and compared in this study.

Chapter IV

POSTBUCKLING ANALYSIS

A buckling load in a delaminated composite is, in many cases, significantly lower than the final failure load in the postbuckling regime. Furthermore, there may be a bending-extension coupling in debonded sublaminates even for an initially symmetric laminate so that the bifurcation analysis may not be appropriate, Therefore, in order to describe the damage process until final failure, the postbuckling analysis must be considered.

In this chapter, a finite element model with von Kármán nonlinearity is developed to analyze postbuckling response of delaminated composites. Imperfections in the plates in the form of initial global out-of-plane deflection and initial delamination openings are included. A technique for contact condition between delaminated sublaminates is also developed and incorporated in the postbuckling analysis.

4.1 Axisymmetric Model

4.1.1 Kinematics

An N-layer fiber-reinforced circular composite plate containing multiple delaminations is reconsidered here. (Figure 3). The assumed displacement field is supplemented with unit step functions to model delaminations. The resulting displacements U_r and U_z at a generic point r,z in the laminate are assumed to be of the following form due to the axisymmetric assumption:

$$U_r(r,z) = u_r(r) + \phi^j(z)\, u_r^j(r) + \delta^i(z)\, \overline{u}_r^i(r)\,, \tag{4.1}$$

$$U_z(r,z) = u_z(r) + \delta^i(z)\, \overline{u}_r^i(r)\,, \tag{4.2}$$

where i and j indices range from 1 to D and 1 to M, respectively. Repeated superscripts denote summation convention.

The terms u_r and u_z are the displacements of a point $(r,0)$ on the reference surface of the laminate, u_r^j are nodal values of the displacements in the r direction of each equivalent single-layer, and $\overline{u}_r^i$ and $\overline{u}_z^i$ represent possible jumps in the slipping and opening displacements respectively at $L(i)$-th delaminated interface. $L(i)$-th denotes the location of interface where i-th delamination lies (Figure 4). $\phi^j(z)$ and $\delta^i(z)$ are linear Lagrangian interpolation function through the thickness of the laminate, and unit step function, respectively.

Following the procedure in Chia [108], the nonlinear strain tensor with initial curvature of plate in the sense of von Kármán nonlinearity is derived.

Consider a volume element $hrdrd\theta$ from an initially deflected plate and let the vertical distance of an arbitrary point from the reference surface be $z(r)$ (Figure 8).

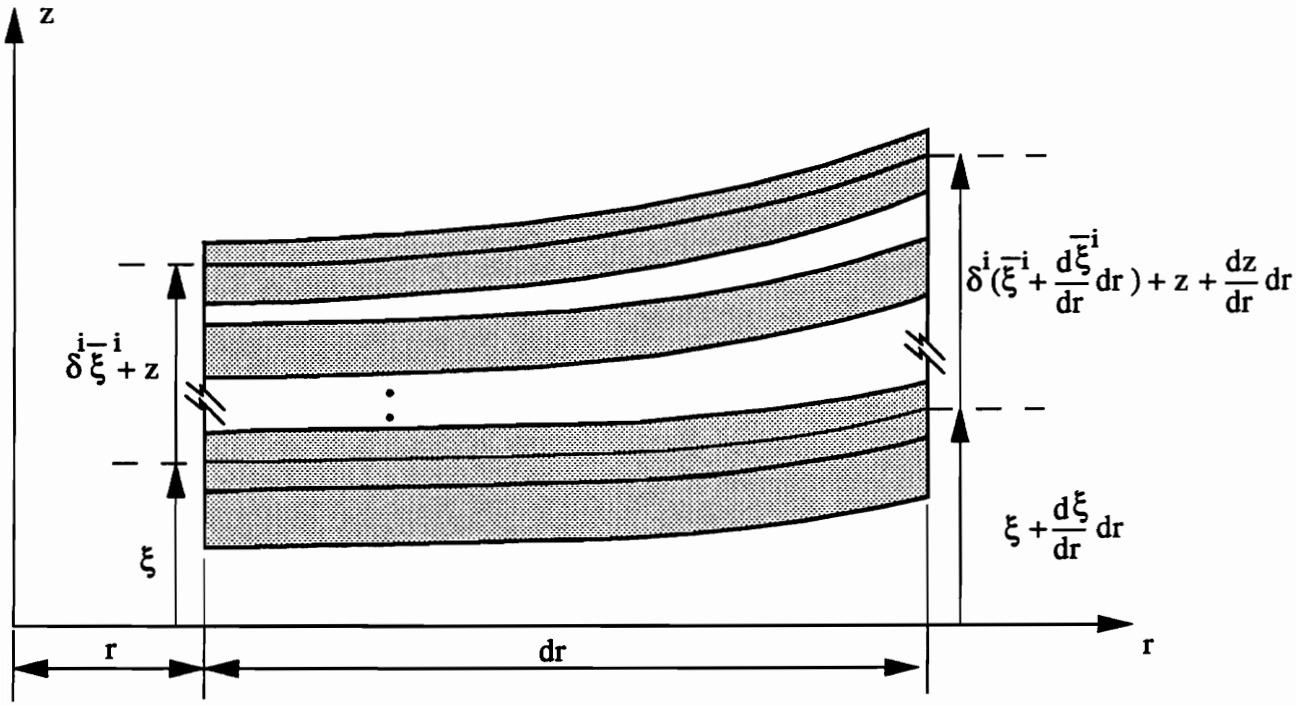

Figure 8. Geometry of the initially deflected circular plate element with delaminations

Defining $\xi(r)$ and $\bar{\xi}^i(r)$ as a globally deflected shape of a plate and a shape of an initial opening of an each delamination, respectively, the position vector of the point in the undeformed state can be written as

$$\vec{r}_o = r\cos\theta\vec{e}_1 + r\sin\theta\vec{e}_2 + \left(\xi + \delta^i\bar{\xi}^i + z\right)\vec{e}_3 \ , \tag{4.3}$$

where $\vec{e}_1$,$\vec{e}_2$ and $\vec{e}_3$ are unit vectors along x_1,x_2 and x_3 axis.

By virtue of axisymmetric deformation ($U_\theta = 0$), the position vector in the deformed state is written as

$$\vec{r} = (r + U_r)\cos\theta\vec{e}_1 + (r + U_r)\sin\theta\vec{e}_2 + \left(\xi + \delta^i\bar{\xi}^i + z + U_z\right)\vec{e}_3 \ . \tag{4.4}$$

From Eq. (4.3), the length squared of the line segment on the undeformed surfaces is given by

$$\begin{aligned} ds_o^2 &= d\vec{r}_o \bullet d\vec{r}_o \\ &= \left[1 + \left(\xi + \delta^i\bar{\xi}^i + z\right)_{,r}^2\right]dr^2 + r^2 d\theta^2 + dz^2 + 2\left(\xi + \delta^i\bar{\xi}^i + z\right)_{,r} drdz \ . \end{aligned} \tag{4.5}$$

From Eq. (4.4), the square of the length of the line segment on deformed state is given by

$$\begin{aligned} ds^2 &= d\vec{r} \bullet d\vec{r} \\ &= \left[\left\{1 + \left(u_r + \phi^j u_r^j + \delta^i\bar{u}_r^i\right)_{,r}\right\}^2 + \left\{\xi + \delta^i\bar{\xi}^i + z + u_z + \delta^i\bar{u}_z^i\right\}_{,r}^2\right]dr^2 \\ &+ \left[1 + \frac{1}{r}\left(u_r + \phi^j u_r^j + \delta^i\bar{u}_r^i\right)\right]^2 r^2 d\theta^2 \\ &+ \left[1 + \phi^j_{,z}u_r^j\phi^k_{,z}u_r^k\right]dz^2 \\ &+ 2\left[\left\{1 + \left(u_r + \phi^j u_r^j + \delta^i\bar{u}_r^i\right)_{,r}\right\}\phi^k_{,z}u_r^k + \left\{\xi + \delta^i\bar{\xi}^i + z + u_z + \delta^i\bar{u}_z^i\right\}_{,r}\right]drdz. \end{aligned} \tag{4.6}$$

Neglecting the quadratic terms involved in the radial displacements u_r, u_r^j and $\bar{u}_r^i$ according to von Kármán assumption, the difference between ds^2 and ds_o^2, which is the measure of strain, yields

$$ds^2 - ds_o^2 = 2\left(\varepsilon_{rr}dr^2 + \varepsilon_{\theta\theta}r^2d\theta^2 + \gamma_{rz}drdz\right) , \tag{4.7}$$

where ε_{rr}, $\varepsilon_{\theta\theta}$ and , γ_{rz} are the nonlinear strains given by

$$\varepsilon_{rr} = \varepsilon_{rr}^o + \phi^j\varepsilon_{rr}^j + \delta^i\bar{\varepsilon}_{rr}^i + \delta^i\delta^s\bar{\varepsilon}_{rr}^{is} , \tag{4.8}$$

$$\varepsilon_{\theta\theta} = \varepsilon_{\theta\theta}^o + \phi^j\varepsilon_{\theta\theta}^j + \delta^i\bar{\varepsilon}_{\theta\theta}^i , \tag{4.9}$$

$$\gamma_{rz} = \gamma_{rz}^o + \phi_{,z}^j\gamma_{rz}^j + \delta^i\bar{\gamma}_{rz}^i , \tag{4.10}$$

where

$$\varepsilon_{rr}^o = u_{r,r} + \frac{1}{2}u_{z,r}(u_z + 2\,\xi)_{,r} , \tag{4.11}$$

$$\varepsilon_{rr}^j = u_{r,r}^j , \tag{4.12}$$

$$\bar{\varepsilon}_{rr}^i = \bar{u}_{r,r}^i + \frac{1}{2}u_{z,r}(\bar{u}_z^i + 2\bar{\xi}^i)_{,r} + \frac{1}{2}\bar{u}_{z,r}^i(u_z + 2\xi)_{,r} , \tag{4.13}$$

$$\bar{\varepsilon}_{rr}^{is} = \frac{1}{4}\bar{u}_{z,r}^i(\bar{u}_z^s + 2\bar{\xi}^s)_{,r} + \frac{1}{4}\bar{u}_{z,r}^s(\bar{u}_z^i + 2\bar{\xi}^i)_{,r} , \tag{4.14}$$

$$\varepsilon_{\theta\theta}^o = \frac{u_r}{r} , \quad \varepsilon_{\theta\theta}^j = \frac{u_r^j}{r} , \quad \bar{\varepsilon}_{\theta\theta}^i = \frac{\bar{u}_r^i}{r} , \tag{4.15}$$

$$\gamma_{rz}^o = u_{z,r}, \quad \gamma_{rz}^j = u_r^j, \quad \bar{\gamma}_{rz}^i = \bar{u}_{r,r}^i . \tag{4.16}$$

4.1.2 Variational Formulation

In order to derive governing equilibrium equation of the present theory, the principle of virtual displacements is used [105]:

$$0 = \int_V (\sigma_{rr}\delta\varepsilon_{rr} + \sigma_{\theta\theta}\delta\varepsilon_{\theta\theta} + \sigma_{rz}\delta\gamma_{rz} - f_r\delta U_r - f_z\delta U_z)dV - \oint_S (\hat{t}_r\delta U_r + \hat{t}_z\delta U_z)dS \ , \tag{4.17}$$

where $\hat{t}_r$ and $\hat{t}_z$ are the specified radial and vertical components of surface traction forces, and f_r and f_z are the body forces acting in the radial and vertical direction, respectively. In Eq. (4.17), V is the volume of the plate and S is the boundary of V on which the tractions are specified.

Substituting Eqs. (4.8), (4.9) and (4.10) into Eq. (4.17) and defining specified traction resultants as

$$\left(\hat{N}_r, \hat{N}_r^j, \hat{\overline{N}}_r^i\right) = \int_{z_k}^{z_{k+1}} \hat{t}_r\left(1, \phi^j, \delta^i\right)dz \ , \tag{4.18}$$

$$\left(\hat{Q}_z, \hat{\overline{Q}}_z^i\right) = \int_{z_k}^{z_{k+1}} \hat{t}_z\left(1, \delta^i\right)dz, \tag{4.19}$$

Eq. (4.17) takes the form in the absence of body forces after integrating through the thickness

$$\begin{aligned} 0 = \int_\Omega \Big[& N_{rr}\{\delta u_{r,r} + \delta u_{z,r}(u_z + \xi)_{,r}\} + \frac{1}{r} N_{\theta\theta}\delta u + Q_{rz}\delta u_{z,r} \\ & + N_{rr}^j\delta u_{r,r}^j + \frac{1}{r} N_{\theta\theta}^j\delta u_r^j + Q_{rz}^j\delta u_r^j \\ & + \overline{N}_{rr}^i\{\delta\overline{u}_{r,r}^i + \delta u_{z,r}(\overline{u}_z^i + \overline{\xi}^i)_{,r} + \delta\overline{u}_{z,r}^i(u_z + \xi)_{,r}\} + \frac{1}{r}\overline{N}_{\theta\theta}^i\delta\overline{u}_r^i + \overline{Q}_{rz}^i\delta\overline{u}_{z,r}^i \\ & + \frac{1}{2}\overline{N}_{rr}^{is}\{\delta\overline{u}_{z,r}^i(\overline{u}_z^s + \overline{\xi}^s)_{,r} + \delta\overline{u}_{z,r}^s(\overline{u}_z^i + \overline{\xi}^i)_{,r}\}\Big] r dr d\theta \end{aligned} \tag{4.20}$$

$$- \int_\Omega p\delta(u_z + \delta^i\overline{u}_z^i) r dr d\theta$$

$$-\int_{\Gamma_1} \hat{N}_r \delta u_r r d\theta - \int_{\Gamma_2} \hat{Q}_z \delta u_z r d\theta - \int_{\Gamma_3} \hat{N}_r^j \delta u_r^j r d\theta - \int_{\Gamma_4} \hat{\overline{N}}_r^i \delta \overline{u}_r^i r d\theta - \int_{\Gamma_5} \hat{\overline{Q}}_z^i \delta \overline{u}_z^i r d\theta \ ,$$

where p is a specified distributed transverse load and $\Gamma_1, \Gamma_2, \Gamma_3, \Gamma_4, \Gamma_5$ are the portions of the boundary of the reference surface Ω on which $\hat{N}_r, \hat{Q}_z, \hat{N}_r^j, \hat{\overline{N}}_r^i, \hat{\overline{Q}}_z^i$, respectively, are specified. In Eq. (4.20), $\overline{N}_{rr}^{is}$ are stress resultants, coming from the nonlinear strain tensor $\overline{\varepsilon}_{rr}^{is}$, defined as

$$\overline{N}_{rr}^{is} = \int_{-\frac{h}{2}}^{\frac{h}{2}} \sigma_{rr} \delta^i \delta^s \, dz \ . \tag{4.21}$$

The other stress resultants $N_{rr}, N_{\theta\theta}, N_{rr}^j, N_{\theta\theta}^j, \overline{N}_{rr}^i, \overline{N}_{\theta\theta}^i, Q_{rz}, Q_{rz}^j$, and $\overline{Q}_{rz}^i$ are given in Eqs. (3.19) - (3.21).

4.1.3 Equilibrium Equations

The equilibrium equations of the present theory can be derived by integrating the derivatives of the varied quantities by parts and collecting the coefficients of $\delta u_r, \delta u_z, \delta u_r^j, \delta \overline{u}_r^i, \delta \overline{u}_z^i$:

$$\frac{1}{r}(rN_{rr})_{,r} - \frac{N_{\theta\theta}}{r} = 0 \ , \tag{4.22}$$

$$\frac{1}{r}(rQ_{rz})_{,r} + \frac{1}{r}\left[rN_{rr}(u_{z,r} + \xi_{,r})\right]_{,r} + \frac{1}{r}\left[r\overline{N}_{rr}^i(\overline{u}_{z,r}^i + \overline{\xi}_{,r}^i)\right]_{,r} = 0 \ , \tag{4.23}$$

$$\frac{1}{r}\left(rN_{rr}^j\right)_{,r} - \frac{N_{\theta\theta}^j}{r} - Q_{rz}^j = 0 \ , \tag{4.24}$$

$$\frac{1}{r}\left(r\overline{N}^i_{rr}\right)_{,r} - \frac{\overline{N}^i_{\theta\theta}}{r} = 0 \ , \tag{4.25}$$

$$\frac{1}{r}\left(r\overline{Q}^i_{rz}\right)_{,r} + \frac{1}{r}\left[r\overline{N}^i_{rr}(u_{z,r} + \xi_{,r})\right]_{,r} + \frac{1}{r}\left[r\overline{N}^{is}_{rr}(\overline{u}^s_{z,r} + \overline{\xi}^s_{,r})\right]_{,r} = 0 \, . \tag{4.26}$$

The equilibrium equations consist of $(2 + M + 2D)$ differential equations in $(2 + M + 2D)$ variables $(u_r, u_z, u^j_r, \overline{u}^i_r, \overline{u}^i_z)$. The geometric nonlinearity is involved only with Eqs. (4.23) and (4.26), which represent the out-of-plane action of the laminate and the sublaminates. The other equations (Eqs. (4.22), (4,24) and (4.25)) are of the same forms as the linear equations given in Eqs. (3.29), (3.31) and (3.32) without inertia terms.

The natural boundary conditions are of the form:

$$\delta u_r: \quad N_r - \hat{N}_r = 0 \qquad \text{on } \Gamma_1 \tag{4.27}$$

$$\delta u_z: \quad Q_z - \hat{Q}_z = 0 \qquad \text{on } \Gamma_2 \tag{4.28}$$

$$\delta u^j_r: \quad N^j_r - \hat{N}^j_r = 0 \qquad \text{on } \Gamma_3 \tag{4.29}$$

$$\delta \overline{u}^i_r: \quad \overline{N}^i_r - \hat{\overline{N}}^i_r = 0 \qquad \text{on } \Gamma_4 \tag{4.30}$$

$$\delta \overline{u}^i_z: \quad \overline{Q}^i_z - \hat{\overline{Q}}^i_z = 0 \qquad \text{on } \Gamma_5 \tag{4.31}$$

where

$$N_r = N_{rr} n_r \ , \tag{4.32}$$

$$Q_z = \left[N_{rr}(u_z + \xi)_{,r} + \overline{N}^i_{rr}\left(\overline{u}^i_z + \overline{\xi}^i\right)_{,r} + Q_{rz}\right] n_r \ , \tag{4.33}$$

$$N^j_r = N^j_{rr} n_r \ , \tag{4.34}$$

$$\overline{N}^i_r = \overline{N}^i_{rr} n_r \ , \tag{4.35}$$

$$\overline{Q}^i_z = \left[\overline{N}^i_{rr}(u_z + \xi)_{,r} + \overline{N}^{is}_{rr}(\overline{u}^s_z + \overline{\xi}^s)_{,r} + \overline{Q}^i_{rz}\right] n_r \ . \tag{4.36}$$

Recall that Γ_1 through Γ_5 complement the total boundary Γ in such a way that essential boundary conditions are specified:

$$u_r = \hat{u}_r \qquad \text{on } \Gamma - \Gamma_1 \tag{4.37}$$

$$u_z = \hat{u}_z \qquad \text{on } \Gamma - \Gamma_2 \tag{4.38}$$

$$u_r^j = \hat{u}_r^j \qquad \text{on } \Gamma - \Gamma_3 \tag{4.39}$$

$$\bar{u}_r^i = \hat{\bar{u}}_r^i \qquad \text{on } \Gamma - \Gamma_4 \tag{4.40}$$

$$\bar{u}_z^i = \hat{\bar{u}}_z^i \qquad \text{on } \Gamma - \Gamma_5 \,. \tag{4.41}$$

4.1.4 Constitutive Equations

Because of the additional stress resultants, $\overline{N}_{rr}^{su}$, in the geometric nonlinear formulation, the constitutive equations become different from the linear version.

The constitutive equations of a *k-th* orthotropic lamina in the laminate co-ordinate system are given by

$$\begin{bmatrix} \sigma_{rr} \\ \sigma_{\theta\theta} \\ \sigma_{rz} \end{bmatrix}^{(k)} = \begin{bmatrix} \overline{Q}_{1111} & \overline{Q}_{1122} & 0 \\ \overline{Q}_{1122} & \overline{Q}_{2222} & 0 \\ 0 & 0 & \overline{Q}_{1313} \end{bmatrix}^{(k)} \begin{bmatrix} \varepsilon_{rr} \\ \varepsilon_{\theta\theta} \\ \gamma_{rz} \end{bmatrix}^{(k)} \tag{4.42}$$

where $[\overline{Q}]^{(k)}$ denote the transformed reduced stiffness matrix of the *k-th* layer.

Substitution of Eq. (4.42) into Eqs. (3.19) - (3.21) and (4.21) gives the constitutive equations of the laminate:

$$
\begin{bmatrix} N_{rr} \\ N_{\theta\theta} \\ N_{rr}^{k} \\ N_{\theta\theta}^{k} \\ \overline{N}_{rr}^{s} \\ \overline{N}_{\theta\theta}^{s} \\ \overline{N}_{rr}^{su} \end{bmatrix}
=
\begin{bmatrix}
A_{1111} & A_{1122} & B_{1111}^{j} & B_{1122}^{j} & E_{1111}^{i} & E_{1122}^{i} & E_{1111}^{ir} \\
A_{1122} & A_{2222} & B_{1122}^{j} & B_{2222}^{j} & E_{1122}^{i} & E_{2222}^{i} & E_{1122}^{ir} \\
B_{1111}^{k} & B_{1122}^{k} & D_{1111}^{jk} & D_{1122}^{jk} & F_{1111}^{ik} & F_{1122}^{ik} & F_{1111}^{irk} \\
B_{1122}^{k} & B_{2222}^{k} & D_{1122}^{jk} & D_{2222}^{jk} & F_{1122}^{ik} & F_{2222}^{ik} & F_{1122}^{irk} \\
E_{1111}^{s} & E_{1122}^{s} & F_{1111}^{sj} & F_{1122}^{sj} & E_{1111}^{is} & E_{1122}^{is} & E_{1111}^{irs} \\
E_{1122}^{s} & E_{2222}^{s} & F_{1122}^{sj} & F_{2222}^{sj} & E_{1122}^{is} & E_{2222}^{is} & E_{1122}^{irs} \\
E_{1111}^{su} & E_{1122}^{su} & F_{1111}^{suj} & F_{1122}^{suj} & E_{1111}^{isu} & E_{1122}^{isu} & E_{1111}^{irsu}
\end{bmatrix}
\begin{bmatrix} \varepsilon_{rr}^{o} \\ \varepsilon_{\theta\theta}^{o} \\ \varepsilon_{rr}^{j} \\ \varepsilon_{\theta\theta}^{j} \\ \overline{\varepsilon}_{rr}^{i} \\ \overline{\varepsilon}_{\theta\theta}^{i} \\ \overline{\varepsilon}_{rr}^{ir} \end{bmatrix},
\tag{4.43}
$$

$$
\begin{bmatrix} Q_{rz} \\ Q_{rz}^{k} \\ \overline{Q}_{rz}^{s} \end{bmatrix}
=
\begin{bmatrix} A_{1313} & B_{1313}^{j} & E_{1313}^{i} \\ B_{1313}^{k} & D_{1313}^{jk} & L_{1313}^{kl} \\ E_{1313}^{s} & L_{1313}^{js} & E_{1313}^{is} \end{bmatrix}
\begin{bmatrix} \gamma_{rz}^{o} \\ \gamma_{rz}^{j} \\ \overline{\gamma}_{rz}^{i} \end{bmatrix},
\tag{4.44}
$$

where

$$
\left(F_{\alpha\alpha\beta\beta}^{suj},\, E_{\alpha\alpha\beta\beta}^{isu},\, E_{\alpha\alpha\beta\beta}^{irsu}\right) = \sum_{k=1}^{N} \int_{z_k}^{z_{k+1}} \overline{Q}_{\alpha\alpha\beta\beta}^{(k)} \left(\delta^{s}\delta^{u}\phi^{j},\ \delta^{i}\delta^{s}\delta^{u},\ \delta^{i}\delta^{r}\delta^{s}\delta^{u}\right) dz\,. \tag{4.45}
$$

The explicit forms of above expressions are presented in Appendix A. The other components of stiffness matrices are given in Eqs. (3.42) - (3.45).

4.1.5 Finite Element Model

The generalized displacements $(u_r, u_z, u_r^j, \overline{u}_r^i, \overline{u}_z^i)$ are expressed over each element as a linear combination of the one-dimensional Lagrangian interpolation function ψ_l associated with node l and the nodal values $(u_r)_l, (u_z)_l, (u_r^j)_l, (\overline{u}_r^i)_l, (\overline{u}_z^i)_l$:

$$
\begin{aligned}
u_r &= \sum_{l=1}^{n} (u_r)_l \psi_l \ , \\
u_z &= \sum_{l=1}^{n} (u_z)_l \psi_l \ , \\
u_r^j &= \sum_{l=1}^{n} (u_r^j)_l \psi_l \ , \\
\bar{u}_r^j &= \sum_{l=1}^{n} (\bar{u}_r^j)_l \psi_l \ , \\
\bar{u}_z^j &= \sum_{l=1}^{n} (\bar{u}_z^j)_l \psi_l \ ,
\end{aligned}
\tag{4.46}
$$

where n is the number of nodes in a typical finite element.

Substituting these expressions into the weak statement in Eq. (4.20), the finite element model of a typical element can be obtained as

$$
[K(\Delta)]\{\Delta\} = \{F\}, \tag{4.47}
$$

where $[K(\Delta)]$ is the element stiffness matrix given by

$$
[K] = \begin{bmatrix}
[{}^{11}K] & [{}^{12}K] & [{}^{13}K^k] & [{}^{14}K^s] & [{}^{15}K^s] \\
 & [{}^{22}K] & [{}^{23}K^k] & [{}^{24}K^s] & [{}^{25}K^s] \\
 & & [{}^{33}K^{lk}] & [{}^{34}K^{ls}] & [{}^{35}K^{ls}] \\
 & & & [{}^{44}K^{ns}] & [{}^{45}K^{ns}] \\
sym. & & & & [{}^{55}K^{ns}]
\end{bmatrix}_{\mathrm{L}}
+
\begin{bmatrix}
[\ 0\ ] & [{}^{12}K] & [\ 0\ ] & [\ 0\ ] & [{}^{15}K^s] \\
[{}^{21}K] & [{}^{22}K] & [{}^{23}K^k] & [{}^{24}K^s] & [{}^{25}K^s] \\
[\ 0\ ] & [{}^{32}K^l] & [\ 0\ ] & [\ 0\ ] & [{}^{35}K^{ls}] \\
[\ 0\ ] & [{}^{42}K^n] & [\ 0\ ] & [\ 0\ ] & [{}^{45}K^{ns}] \\
[{}^{51}K^n] & [{}^{52}K^n] & [{}^{53}K^{kn}] & [{}^{54}K^{ns}] & [{}^{55}K^{ns}]
\end{bmatrix}_{\mathrm{NL}} , \tag{4.48}
$$

where $[K]_{\mathrm{L}}$ and $[K]_{\mathrm{NL}}$ denote linear and nonlinear parts, respectively, and $[K]_{\mathrm{NL}}$ is not symmetric. $\{F\}$ is the element force vector containing boundary and transverse force terms

$$
\{F\} = \left\{\{{}^1F\}\ \{{}^2F\}\ \{{}^3F^k\}\ \{{}^4F^s\}\ \{{}^5F^s\}\right\}^{\mathrm{T}} . \tag{4.49}
$$

The element stiffness matrix $[K]$ and the force vector $\{F\}$ are presented in Appendix B. $\{\Delta\}$ is the nodal displacement vector given by

$$\{\Delta\} = \left\{\{u_r\}\ \{u_z\}\ \{u_r^k\}\ \{\bar{u}_r^s\}\ \{\bar{u}_z^s\}\right\}^{\mathrm{T}} . \tag{4.50}$$

The element stiffness matrix $[K\{\Delta\}]$ is a function of nodal displacements, which indicates that the problem is geometrically nonlinear in the nodal displacements. Thus the solution of the nonlinear problem in Eq. (4.47) must be solved by an iterative procedure. In this study, a Newton-Raphson iterative scheme (see Section 4.3) is utilized for the solution of the nonlinear equation.

Reduced integration scheme is used to calculate the stiffness coefficients associated with transverse shear terms.

4.2 Two-Dimensional Model

4.2.1 Kinematics

An N-layer fiber-reinforced rectangular composite plate containing multiple delaminations is considered. (Figure 6). To model the multiple delaminations, the assumed displacement field is supplemented with unit step functions which allow discontinuities in the displacement field. The resulting displacements U_α and U_3 at a generic point x_1, x_2, x_3 in the laminate are assumed to be of the form:

$$U_\alpha(x_\beta,x_3) = u_\alpha(x_\beta) + \phi^j(x_3)\, u_\alpha^j(x_\beta) + \delta^i(x_3)\, \overline{u}_\alpha^i(x_\beta)\,, \tag{4.51}$$

$$U_3(x_\beta,x_3) = u_3(x_\beta) + \delta^i(x_3)\, \overline{u}_3^i(x_\beta)\,, \tag{4.52}$$

where D is the number of delaminations, and M is the number of equivalent single-layers (i.e. number of layers for layer-wise theory and number of sublaminates for sublaminate theory).

The terms u_α and u_3 are the displacements of a point $(x_\beta,0)$ on the reference surface of the laminate, u_α^j are nodal values of the displacements in the x_α direction of each equivalent single-layer, and $\overline{u}_\alpha^i$ and $\overline{u}_3^i$ represent possible jumps in the slipping and opening displacements respectively at $L(i)$-th delaminated interface. $L(i)$-th denotes the location of interface where i-th delamination lies (Figure 7). $\phi^j(z)$ and $\delta^i(z)$ are linear Lagrangian interpolation function through the thickness of the laminate, and unit step function, respectively.

Following the procedure in Chia [108], the nonlinear strain tensor with initial curvature of plate in the sense of von Kármán nonlinearity is derived.

Consider a volume element hdx_1dx_2 from an initially deflected plate and let the vertical distance of an arbitrary point from the reference surface be $x_3(x_1)$ (Figure 9). Defining $\xi(x_\alpha)$ and $\overline{\xi}^i(x_\alpha)$ as a globally deflected shape of a plate and a shape of an initial opening of an each delamination, respectively, the position vector of the point in the undeformed state is

$$\vec{r}_o = x_\alpha \vec{e}_\alpha + \left(\xi + \delta^i \overline{\xi}^i + x_3\right)\vec{e}_3 \ , \tag{4.53}$$

where $\vec{e}_\alpha$ and $\vec{e}_3$ are unit vectors along x_α and x_3 axis.

The position vector in deformed status is

$$\vec{r} = (x_\alpha + U_\alpha)\vec{e}_\alpha + \left(\xi + \delta^i \overline{\xi}^i + x_3 + U_3\right)\vec{e}_3 \ . \tag{4.54}$$

From the Eq. (4.54), the length squared of the line segment on the undeformed surfaces is given by

$$\begin{aligned} ds_o^2 &= d\vec{r}_o \bullet d\vec{r}_o \\ &= \left[\delta_{\alpha\beta} + \left(\xi + \delta^i \overline{\xi}^i + x_3\right)_{,\alpha}\left(\xi + \delta^r \overline{\xi}^r + x_3\right)_{,\beta}\right]dx_\alpha dx_\beta + dx_3^2 + 2\left[\xi + \delta^i \overline{\xi}^i + x_3\right]_{,\alpha} dx_\alpha dx_3 \end{aligned} \tag{4.55}$$

where $\delta_{\alpha\beta}$ denotes Kronecker delta.

Substituting Eqs. (4.50) and (4.51) into Eq. (4.54), the square of the line segment on deformed state is given by

$$\begin{aligned} ds^2 &= d\vec{r} \bullet d\vec{r} \\ &= \left[\left\{\delta_{\alpha\gamma} + \left(u_\gamma + \phi^j u_\gamma^j + \delta^i \overline{u}_\gamma^i\right)_{,\alpha}\right\}\left\{\delta_{\beta\gamma} + \left(u_\gamma + \phi^k u_\gamma^k + \delta^r \overline{u}_\gamma^r\right)_{,\beta}\right\}\right. \\ &\quad \left. + \left(\xi + \delta^i \overline{\xi}^i + x_3 + u_3 + \delta^i \overline{u}_3^i\right)_{,\alpha}\left(\xi + \delta^r \overline{\xi}^r + x_3 + u_3 + \delta^r \overline{u}_3^r\right)_{,\beta}\right]dx_\alpha dx_\beta \\ &\quad + \left[\phi_{,3}^j u_\alpha^j \phi_{,3}^k u_\beta^k + 1\right]dx_3^2 \\ &\quad + 2\left[\left\{1 + \left(u_\gamma + \phi^j u_\gamma^j + \delta^i \overline{u}_\gamma^i\right)_{,\alpha}\right\}\phi_{,3}^k u_\alpha^k + \left(\xi + \delta^i \overline{\xi}^i + x_3 + u_3 + \delta^i \overline{u}_3^i\right)_{,\alpha}\right]dx_\alpha dx_3 \end{aligned} \tag{4.56}$$

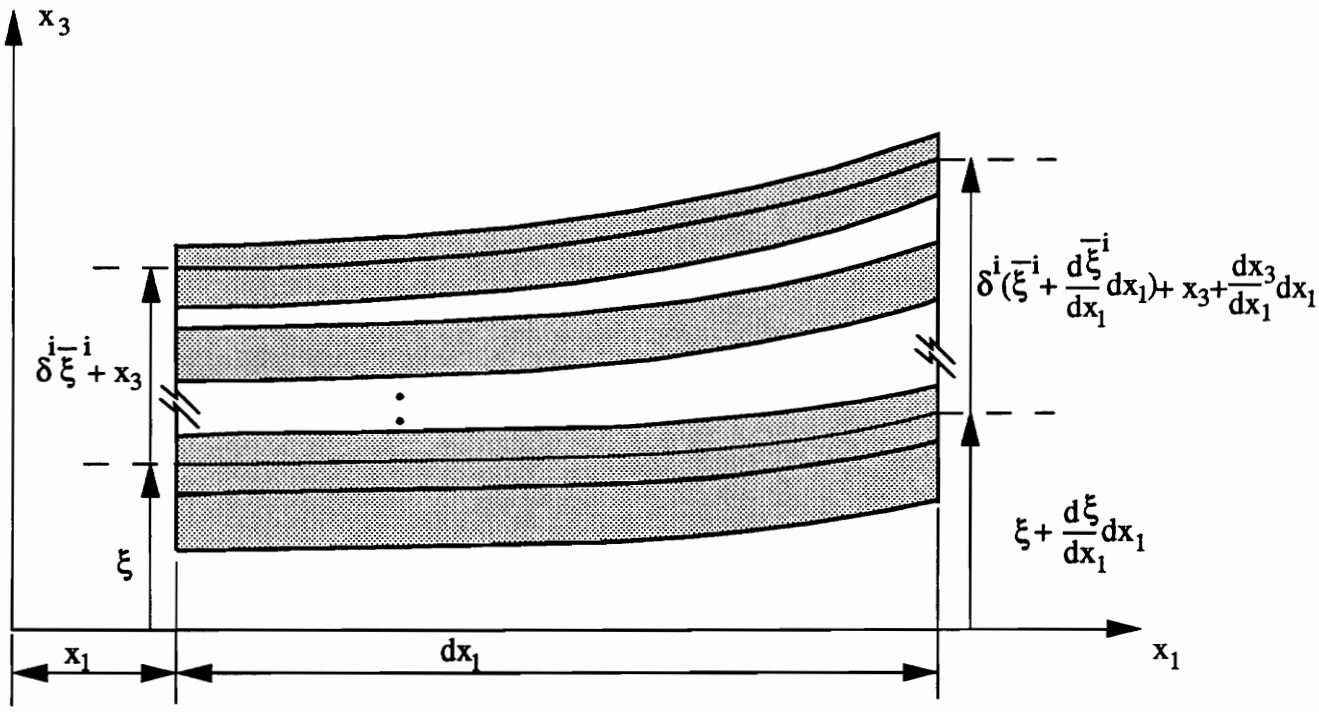

Figure 9. Geometry of the initially deflected rectangular plate element with delaminations

Neglecting the quadratic terms involved in inplane displacements u_α, u^j_α, $\bar{u}^i_\alpha$ according to von Kármán assumption, the difference between ds^2 and ds^2_o, which is the measure of strain, yields

$$ds^2 - ds_o^2 = 2\,(\varepsilon_{\alpha\beta} dx_\alpha dx_\beta + \gamma_{\alpha 3} dx_\alpha dx_3) \ , \tag{4.57}$$

where $\varepsilon_{\alpha\beta}$ and $\gamma_{\alpha 3}$ are the nonlinear strain tensor given by

$$\begin{aligned} \varepsilon_{\alpha\beta} &= \overset{o}{\varepsilon}_{\alpha\beta} + \phi^j \varepsilon^j_{\alpha\beta} + \delta^i \bar{\varepsilon}^i_{\alpha\beta} + \delta^i \delta^s \bar{\varepsilon}^{is}_{\alpha\beta} \ , \\ \gamma_{\alpha 3} &= \overset{o}{\gamma}_{\alpha 3} + \phi^j_3 \gamma^j_{\alpha 3} + \delta^i \bar{\gamma}^i_{\alpha 3} \ , \end{aligned} \tag{4.58}$$

where

$$\overset{o}{\varepsilon}_{\alpha\beta} = \frac{1}{2}\left[u_{\alpha,\beta} + u_{\beta,\alpha} + \frac{1}{2} u_{3,\alpha}(u_3 + 2\xi)_{,\beta} + \frac{1}{2} u_{3,\beta}(u_3 + 2\xi)_{,\alpha} \right] , \tag{4.59}$$

$$\varepsilon^j_{\alpha\beta} = \frac{1}{2}\left(u^j_{\alpha,\beta} + u^j_{\beta,\alpha} \right) , \tag{4.60}$$

$$\begin{aligned} \bar{\varepsilon}^i_{\alpha\beta} = \frac{1}{2}\Big[& \bar{u}^i_{\alpha,\beta} + \bar{u}^i_{\beta,\alpha} + \frac{1}{2} u_{3,\alpha}(\bar{u}^i_3 + 2\bar{\xi}^i)_{,\beta} + \frac{1}{2} u_{3,\beta}(\bar{u}^i_3 + 2\bar{\xi}^i)_{,\alpha} \\ & + \frac{1}{2} \bar{u}^i_{3,\alpha}(u_3 + 2\xi)_{,\beta} + \frac{1}{2} \bar{u}^i_{3,\beta}(u_3 + 2\xi)_{,\alpha} \Big] , \end{aligned} \tag{4.61}$$

$$\bar{\varepsilon}^{is}_{\alpha\beta} = \frac{1}{4}\left[\bar{u}^i_{3,\alpha}(\bar{u}^s_3 + 2\bar{\xi}^s)_{,\beta} + \bar{u}^s_{3,\beta}(\bar{u}^i_3 + 2\bar{\xi}^i)_{,\alpha} \right] , \tag{4.62}$$

$$\overset{o}{\gamma}_{\alpha 3} = u_{3,\alpha}, \qquad \gamma^j_{\alpha 3} = u^j_\alpha, \qquad \bar{\gamma}^i_{\alpha 3} = \bar{u}^i_{3,\alpha} \, . \tag{4.63}$$

4.2.2 Variational Formulation

In order to derive governing equilibrium equation of the present theory, the principle of virtual displacements is used

$$0 = \int_V (\sigma_{\alpha\beta}\delta\varepsilon_{\alpha\beta} + \sigma_{\alpha 3}\delta\gamma_{\alpha 3} - f_i\delta U_i)dV - \oint_S \hat{t}_i\delta U_i dS \ , \tag{4.64}$$

where $\hat{t}_i$ are the specified surface traction forces, and f_i are the body forces. In Eq. (4.64), V is the volume of the plate and S is the boundary of V on which the tractions are specified.

Substituting Eq. (4.58) into Eq. (4.64) and defining specified traction resultants as

$$\left(\hat{N}_\alpha, \hat{N}^j_\alpha, \hat{\overline{N}}^i_\alpha\right) = \int_{z_k}^{z_{k+1}} \hat{t}_\alpha\left(1, \phi^j, \delta^i\right)dx_3 \ , \tag{4.65}$$

$$\left(\hat{Q}_3, \hat{\overline{Q}}^i_3\right) = \int_{z_k}^{z_{k+1}} \hat{t}_3\left(1, \delta^i\right)dx_3 \ , \tag{4.66}$$

the Eq. (4.64) takes the form in the absence of body forces after integrating through the thickness

$$\begin{aligned}
0 = \int_\Omega \Big[& N_{\alpha\beta}\{\delta u_{\alpha,\beta} + \delta u_{3,\alpha}(u_3 + \xi)_{,\beta}\} + N^j_{\alpha\beta}\delta u^j_{\alpha,\beta} \\
& + \overline{N}^i_{\alpha\beta}\{\delta \overline{u}^i_{\alpha,\beta} + \delta u_{3,\alpha}\left(\overline{u}^i_3 + \overline{\xi}^i\right)_{,\beta} + \delta \overline{u}^i_{3,\alpha}(u_3 + \xi)_{,\beta}\} \\
& + \frac{1}{2}\overline{N}^{is}_{\alpha\beta}\{\overline{u}^i_{3,\alpha}\left(\overline{u}^s_3 + \overline{\xi}^s\right)_{,\beta} + \overline{u}^s_{3,\beta}\left(\overline{u}^i_3 + \overline{\xi}^i\right)_{,\alpha}\} \\
& + Q_{\alpha 3}\delta u_{3,\alpha} + Q^j_{\alpha 3}u^j_\alpha + \overline{Q}^i_{\alpha 3}\delta \overline{u}^i_{3,\alpha}\Big]dx_1dx_2 \\
- \int_\Omega & p\delta\left(u_3 + \delta^i\overline{u}^i_3\right)dx_1dx_2 \\
- \int_{\Gamma_1} & \hat{N}_\alpha\delta u_\alpha dS - \int_{\Gamma_2} \hat{Q}_3\delta u_3 dS - \int_{\Gamma_3} \hat{N}^j_\alpha\delta u^j_\alpha dS - \int_{\Gamma_4} \hat{\overline{N}}^i_\alpha\delta \overline{u}^i_\alpha dS - \int_{\Gamma_5} \hat{\overline{Q}}^i_3\delta \overline{u}^i_3 dS \ ,
\end{aligned} \tag{4.67}$$

where p is a specified distributed transverse load and $\Gamma_1, \Gamma_2, \Gamma_3, \Gamma_4, \Gamma_5$ are the portions of the boundary of the reference surface Ω on which $\hat{N}_\alpha, \hat{Q}_3, \hat{N}^j_\alpha, \hat{\overline{N}}^j_\alpha, \hat{\overline{Q}}^j_3$, respectively, are specified. In Eq. (4.67), $\overline{N}^{is}_{\alpha\beta}$ are stress resultants, coming from the nonlinear strain tensor $\overline{\varepsilon}^{is}_{\alpha\beta}$, defined as

$$\overline{N}^{is}_{\alpha\beta} = \int_{-\frac{h}{2}}^{\frac{h}{2}} \sigma_{\alpha\beta}\, \delta^i \delta^s \, dx_3 \, . \tag{4.68}$$

The other stress resultants are defined in Eqs. (3.82) and (3.83).

4.2.3 Equilibrium Equations

The equilibrium equations of the present theory can be derived by integrating the derivatives of the varied quantities by parts and collecting the coefficients of $\delta u_\alpha, \delta u_3, \delta u^j_\alpha, \delta \overline{u}^j_\alpha, \delta \overline{u}^j_3$:

$$N_{\alpha\beta,\alpha} = 0 \ , \tag{4.69}$$

$$Q_{\beta 3,\beta} + [N_{\alpha\beta}(u_{3,\alpha} + \xi_{,\alpha})]_{,\beta} + [\overline{N}^i_{\alpha\beta}(\overline{u}^i_{3,\alpha} + \overline{\xi}^i_{,\alpha})]_{,\beta} = 0 \ , \tag{4.70}$$

$$N^j_{\alpha\beta,\alpha} - Q^j_{\beta 3} = 0 \ , \tag{4.71}$$

$$\overline{N}^i_{\alpha\beta,\alpha} = 0 \ , \tag{4.72}$$

$$\overline{Q}^i_{\beta 3,\beta} + [\overline{N}^i_{\alpha\beta}(u_{3,\alpha} + \xi_{,\alpha})]_{,\beta} + [\overline{N}^{is}_{\alpha\beta}(\overline{u}^s_{3,\alpha} + \overline{\xi}^s_{,\alpha})]_{,\beta} = 0 \ . \tag{4.73}$$

The equilibrium equations consist of $(3+2M+3D)$ differential equations in $(3+2M+3D)$ variables $(u_\alpha, u_3, u^j_\alpha, \overline{u}^i_\alpha, \overline{u}^i_3)$. The geometric nonlinearity is involved only with Eqs. (4.70) and (4.73), which represent the out-of-plane action of the laminate and the sublaminates. The other equations (Eqs. (4.69), (4,71) and (4.72)) are of the same forms as the linear equations given in Eqs. (3.70), (3.72) and (3.73) without inertia terms.

The natural boundary conditions are of the form:

$$\delta u_\alpha: \quad N_\alpha - \hat{N}_\alpha = 0 \qquad \text{on } \Gamma_1 \tag{4.74}$$

$$\delta u_3: \quad Q_3 - \hat{Q}_3 = 0 \qquad \text{on } \Gamma_2 \tag{4.75}$$

$$\delta u^j_\alpha: \quad N^j_\alpha - \hat{N}^j_\alpha = 0 \qquad \text{on } \Gamma_3 \tag{4.76}$$

$$\delta \overline{u}^i_\alpha: \quad \overline{N}^i_\alpha - \hat{\overline{N}}^i_\alpha = 0 \qquad \text{on } \Gamma_4 \tag{4.77}$$

$$\delta \overline{u}^i_3: \quad \overline{Q}^i_3 - \hat{\overline{Q}}^i_3 = 0 \qquad \text{on } \Gamma_5 \tag{4.78}$$

where

$$N_\alpha = N_{\alpha\beta} n_\beta \ , \tag{4.79}$$

$$Q_3 = \left[N_{\alpha\beta}(u_3 + \xi)_{,\alpha} + \overline{N}^i_{\alpha\beta}\left(\overline{u}^i_3 + \overline{\xi}^i\right)_{,\alpha} + Q_{\beta 3} \right] n_\beta \ , \tag{4.80}$$

$$N^j_\alpha = N^j_{\alpha\beta} n_\beta \ , \tag{4.81}$$

$$\overline{N}^i_\alpha = \overline{N}^i_{\alpha\beta} n_\beta \ , \tag{4.82}$$

$$\overline{Q}^i_3 = \left[\overline{N}^i_{\alpha\beta}(u_3 + \xi)_{,\alpha} + \overline{N}^{is}_{\alpha\beta}\left(\overline{u}^s_3 + \overline{\xi}^s\right)_{,\alpha} + \overline{Q}^i_{\beta 3} \right] n_\beta \ . \tag{4.83}$$

Recall that Γ_1 through Γ_5 complement the total boundary Γ such a way that essential boundary conditions are specified:

$$u_\alpha = \hat{u}_\alpha \qquad \text{on } \Gamma - \Gamma_1 \tag{4.84}$$

$$u_3 = \hat{u}_3 \qquad \text{on } \Gamma - \Gamma_2 \tag{4.85}$$

$$u^j_\alpha = \hat{u}^j_\alpha \qquad \text{on } \Gamma - \Gamma_3 \tag{4.86}$$

$$\bar{u}_\alpha^i = \hat{\bar{u}}_\alpha^i \qquad \text{on } \Gamma - \Gamma_4 \tag{4.87}$$

$$\bar{u}_3^i = \hat{\bar{u}}_3^i \qquad \text{on } \Gamma - \Gamma_5 \tag{4.88}$$

4.2.4 Constitutive Equations

Because of the additional stress resultants, $\overline{N}_{\alpha\beta}^{su}$, in the geometric nonlinear formulation, the constitutive equations become different from the linear version.

The constitutive equations of a *k-th* orthotropic lamina in the laminate co-ordinate system are given by

$$\sigma_{\alpha\beta}^{(k)} = \overline{Q}_{\alpha\beta\gamma\omega}^{(k)} \varepsilon_{\gamma\omega}^{(k)} \ , \tag{4.89}$$

$$\sigma_{\alpha 3}^{(k)} = \overline{Q}_{\alpha 3\beta 3}^{(k)} \gamma_{\beta 3}^{(k)} \ , \tag{4.90}$$

where $[\overline{Q}]^{(k)}$ denote the transformed reduced stiffness matrix of the *k-th* layer.

Substitution of Eqs. (4.89) and (4.90) into Eqs. (3.82), (3.83), and (4.68) gives the constitutive equations of the laminate:

$$\begin{bmatrix} N_{\alpha\beta} \\ N_{\alpha\beta}^j \\ \overline{N}_{\alpha\beta}^i \\ \overline{N}_{\alpha\beta}^{ir} \end{bmatrix} = \begin{bmatrix} A_{\alpha\beta\gamma\omega} & B_{\alpha\beta\gamma\omega}^k & E_{\alpha\beta\gamma\omega}^s & E_{\alpha\beta\gamma\omega}^{su} \\ B_{\alpha\beta\gamma\omega}^j & D_{\alpha\beta\gamma\omega}^{jk} & F_{\alpha\beta\gamma\omega}^{sj} & F_{\alpha\beta\gamma\omega}^{suj} \\ E_{\alpha\beta\gamma\omega}^i & F_{\alpha\beta\gamma\omega}^{ik} & E_{\alpha\beta\gamma\omega}^{is} & E_{\alpha\beta\gamma\omega}^{isu} \\ E_{\alpha\beta\gamma\omega}^{ir} & F_{\alpha\beta\gamma\omega}^{irk} & E_{\alpha\beta\gamma\omega}^{irs} & E_{\alpha\beta\gamma\omega}^{irsu} \end{bmatrix} \begin{bmatrix} \varepsilon_{\gamma\omega} \\ \varepsilon_{\gamma\omega}^k \\ \bar{\varepsilon}_{\gamma\omega}^s \\ \bar{\varepsilon}_{\gamma\omega}^{su} \end{bmatrix} , \tag{4.91}$$

$$\begin{bmatrix} Q_{\alpha 3} \\ Q_{\alpha 3}^j \\ \overline{Q}_{\alpha 3}^i \end{bmatrix} = \begin{bmatrix} A_{\alpha 3\beta 3} & B_{\alpha 3\beta 3}^k & E_{\alpha 3\beta 3}^s \\ B_{\alpha 3\beta 3}^j & D_{\alpha 3\beta 3}^{jk} & F_{\alpha 3\beta 3}^{sj} \\ E_{\alpha 3\beta 3}^i & F_{\alpha 3\beta 3}^{ik} & E_{\alpha 3\beta 3}^{is} \end{bmatrix} \begin{bmatrix} \overset{o}{\gamma}_{\beta 3} \\ \gamma_{\beta 3}^k \\ \gamma_{\beta 3}^s \end{bmatrix} , \tag{4.92}$$

where

$$\left(F^{suj}_{\alpha\beta\gamma\omega}, E^{isu}_{\alpha\beta\gamma\omega}, E^{irsu}_{\alpha\beta\gamma\omega}\right) = \sum_{k=1}^{N} \int_{z_k}^{z_{k+1}} \overline{Q}^{(k)}_{\alpha\beta\gamma\omega}\left(\delta^s\delta^u\phi^j,\ \delta^i\delta^s\delta^u,\ \delta^i\delta^r\delta^s\delta^u\right) dx_3 \,. \tag{4.93}$$

The explicit forms of above expressions are presented in Appendix A. The other components of stiffness matrices are given in Eqs. (3.84) - (3.87).

4.2.5 Finite Element Model

The generalized displacements $(u_\alpha, u_3, u^j_\alpha, \overline{u}^i_\alpha, \overline{u}^i_3)$ are expressed over each element as a linear combination of the one-dimensional Lagrangian interpolation function ψ_l associated with node l and the nodal values $(u_\alpha)_l, (u_3)_l, (u^j_\alpha)_l, (\overline{u}^i_\alpha)_l, (\overline{u}^i_3)_l$:

$$\begin{aligned}
u_\alpha &= \sum_{l=1}^{n} (u_\alpha)_l \psi_l \ , \\
u_3 &= \sum_{l=1}^{n} (u_3)_l \psi_l \ , \\
u^j_\alpha &= \sum_{l=1}^{n} (u^j_\alpha)_l \psi_l \ , \\
\overline{u}^i_\alpha &= \sum_{l=1}^{n} (\overline{u}^i_\alpha)_l \psi_l \ , \\
\overline{u}^i_3 &= \sum_{l=1}^{n} (\overline{u}^i_3)_l \psi_l \ ,
\end{aligned} \tag{4.94}$$

where n is the number of nodes in a typical finite element.

Substituting these expressions into the weak statement in Eq. (4.67), the finite element model of a typical element can be obtained as

$$[K(\Delta)]\{\Delta\} = \{F\} \ , \tag{4.95}$$

where $[K(\Delta)]$ is the element stiffness matrix given by

$$
[K] = \begin{bmatrix}
[{}^{\alpha\beta}K] & [{}^{\alpha 3}K] & [{}^{\alpha(\beta+3)}K^{k}] & [{}^{\alpha(\beta+5)}K^{s}] & [{}^{\alpha 8}K^{s}] \\
 & [{}^{33}K] & [{}^{3(\beta+3)}K^{k}] & [{}^{3(\beta+5)}K^{s}] & [{}^{38}K^{s}] \\
 & & [{}^{(\alpha+3)(\beta+3)}K^{lk}] & [{}^{(\alpha+3)(\beta+5)}K^{ls}] & [{}^{(\alpha+3)8}K^{ls}] \\
 & & & [{}^{(\alpha+5)(\beta+5)}K^{ns}] & [{}^{(\alpha+5)8}K^{ns}] \\
sym. & & & & [{}^{88}K^{ns}]
\end{bmatrix}_{\mathrm{L}}
+ \begin{bmatrix}
[\ 0\ ] & [{}^{\alpha 3}K] & [\ 0\ ] & [\ 0\ ] & [{}^{\alpha 8}K^{s}] \\
[{}^{3\beta}K] & [{}^{33}K] & [{}^{3(\beta+3)}K^{k}] & [{}^{3(\beta+5)}K^{s}] & [{}^{38}K^{s}] \\
[\ 0\ ] & [{}^{(\alpha+3)3}K^{l}] & [\ 0\ ] & [\ 0\ ] & [{}^{(\alpha+3)8}K^{ls}] \\
[\ 0\ ] & [{}^{(\alpha+5)3}K^{n}] & [\ 0\ ] & [\ 0\ ] & [{}^{(\alpha+5)8}K^{ns}] \\
[{}^{8\beta}K^{n}] & [{}^{83}K^{n}] & [{}^{8(\beta+3)}K^{nk}] & [{}^{8(\beta+5)}K^{ns}] & [{}^{88}K^{ns}]
\end{bmatrix}_{\mathrm{NL}} , \tag{4.96}
$$

where $[K]_{\mathrm{L}}$ and $[K]_{\mathrm{NL}}$ denote linear and nonlinear parts, respectively. $\{F\}$ is the element force vector containing boundary and transverse force terms

$$
\{F\} = \left\{ \{{}^{\alpha}F\}\ \{{}^{3}F\}\ \{{}^{\alpha(\beta+3)}F^{k}\}\ \{{}^{\alpha(\beta+5)}F^{s}\}\ \{{}^{8}F^{s}\} \right\}^{\mathrm{T}} . \tag{4.97}
$$

The element stiffness matrix $[K]$ and the force vector $\{F\}$ are presented in Appendix B. $\{\Delta\}$ is the nodal displacement vector given by

$$
\{\Delta\} = \{\{u_{\alpha}\}\ \{u_{3}\}\ \{u_{\alpha}^{k}\}\ \{\bar{u}_{\alpha}^{s}\}\ \{\bar{u}_{3}^{s}\}\}^{\mathrm{T}} . \tag{4.98}
$$

The element stiffness matrix $[K(\Delta)]$ is a function of nodal displacements which indicates that the problem is geometrically nonlinear in the nodal displacements. Thus the solution of the nonlinear problem in Eq. (4.95) must be solved by an iterative procedure. In this study, a Newton-Raphson iterative scheme is utilized for the solution of the nonlinear equation.

4.3 Numerical Procedure

4.3.1 Newton-Raphson Method

Finite element formulations of nonlinear differential equations yields nonlinear algebraic equations for each element of the finite element mesh. In Newton-Raphson iteration method, the algebraic equation is transformed in the form:

$$\{R(\Delta)\} = [K(\Delta)]\{\Delta\} - \{F\} \ , \tag{4.99}$$

where $\{R(\Delta)\}$ is a residual vector.

Suppose that the solution of Eq. (4.99) is known at r^{th} iteration for any given load step, the residual vector $\{R(\Delta)\}$ is expanded in a Taylor's series about the known solution $\{\Delta\}^r$

$$\{R(\Delta)\} = \{R(\Delta)^r\} + \left(\frac{\partial\{R\}}{\partial\{\Delta\}}\right)_{\{\Delta\}^r} \left(\{\Delta\}^{r+1} - \{\Delta\}^r\right) + 0(\ ) + \cdots = \{0\} \ . \tag{4.100}$$

Neglecting the higher order terms with respect to $(\{\Delta\}^{r+1} - \{\Delta\}^r)$, Eq. (4.100) can be rewritten as

$$\{R\}^{\mathrm{T}} + [K_{\mathrm{T}}(\Delta)^r]\{\delta\Delta^r\} = \{0\} \ , \tag{4.101}$$

where $\{\delta\Delta^r\}$ is the increment of the solution defined by

$$\{\delta\Delta^r\} = \{\Delta\}^{r+1} - \{\Delta\}^r \ , \tag{4.102}$$

and $[K_{\mathrm{T}}(\Delta)^r]$ is the tangent stiffness matrix defined by

$$[K_T(\Delta)^r] = \left(\frac{\partial\{R\}}{\partial\{\Delta\}} \right)_{\{\Delta\}^r} . \tag{4.103}$$

From Eqs. (4.99) and (4.101),

$$\begin{aligned} \{\delta\Delta^r\} &= -[K_T(\Delta)^r]^{-1}\{R\} \\ &= [K_T(\Delta)^r]^{-1}(\{F\} - [K(\Delta)^r]\{\Delta\}^r) . \end{aligned} \tag{4.104}$$

The residual $\{R(\Delta)^r\}$ is gradually reduced to zero if the procedure converges. The iteration is continued until the convergence criterion is satisfied:

$$\frac{\|\Delta_i^{r+1} - \Delta_i^r\|}{\|\Delta_i^r\|} \leq \varepsilon_{tol.} , \tag{4.105}$$

where $\| \ \|$ denotes an energy norm of the vector and i ranges from 1 to the number of degrees of freedom of the finite element mesh. $\varepsilon_{tol.}$ is a convergence tolerance. The components of the tangent stiffness matrix are presented in Appendix C.

4.3.2 Investigations of Contact Conditions

It is known that the solution may indicate that delaminated sublaminates overlap each other during the postbuckling process even for a single delamination depending on the initial imperfection [41]. Thus, preventing this non-physical sublaminate overlapping phenomenon is necessary for the accurate postbuckling analyses. The present theory allows for an accurate determination of the overlap regions and has a capacity for correction of this problem. Variational formulation of the present theory gives the boundary conditions associated with $\overline{u}_3^i$ (the opening displacement across the delamination) as presented in Eqs. (4.78) and (4.88), which can be interpreted as a contact condition at

the ith delamination surfaces. From the mechanical point of view, $\overline{Q}_3^i$ can be interpreted as contact force at the ith delamination. At contact points, therefore, the delamination opening $\overline{u}_3^i$ must be zero and contact force $\overline{Q}_3^i$ must be nonzero.

Taking the basic assumptions for contact, given in the previous Chapter, into account, the contact algorithm of Method II in Chapter III is used here. Let us consider an overlap region as shown in Figure 10, for instance. Maximum overlap occurs at point 3, and accordingly, specify essential boundary condition $\overline{u}_3^i = 0$ at node 3. Rerun the modified problem until all the overlap region disappear (Figure 10).

In postbuckling analysis, at first, initial imperfections are given and the solution is calculated at the first load step using Newton-Raphson method. The applied load p is increased to $p + \Delta p$, and the above process is repeated until the overlapping appears. Then, the contact process is carried out at each Newton-Raphson iteration step. After the solution is obtained at that load step, the applied load is increased again and the computational algorithm is repeated. The computing flowchart for postbuckling analysis is illustrated in Figure 11.

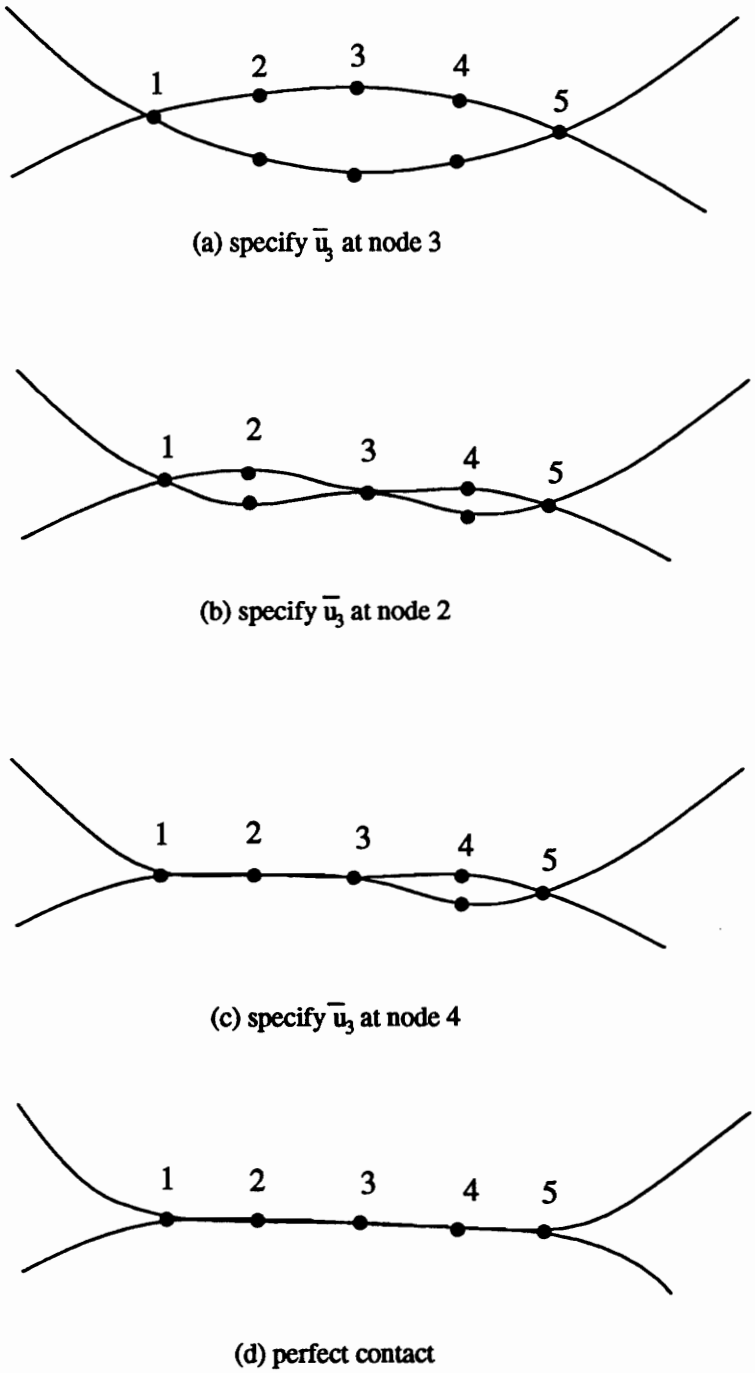

Figure 10. Contact procedure

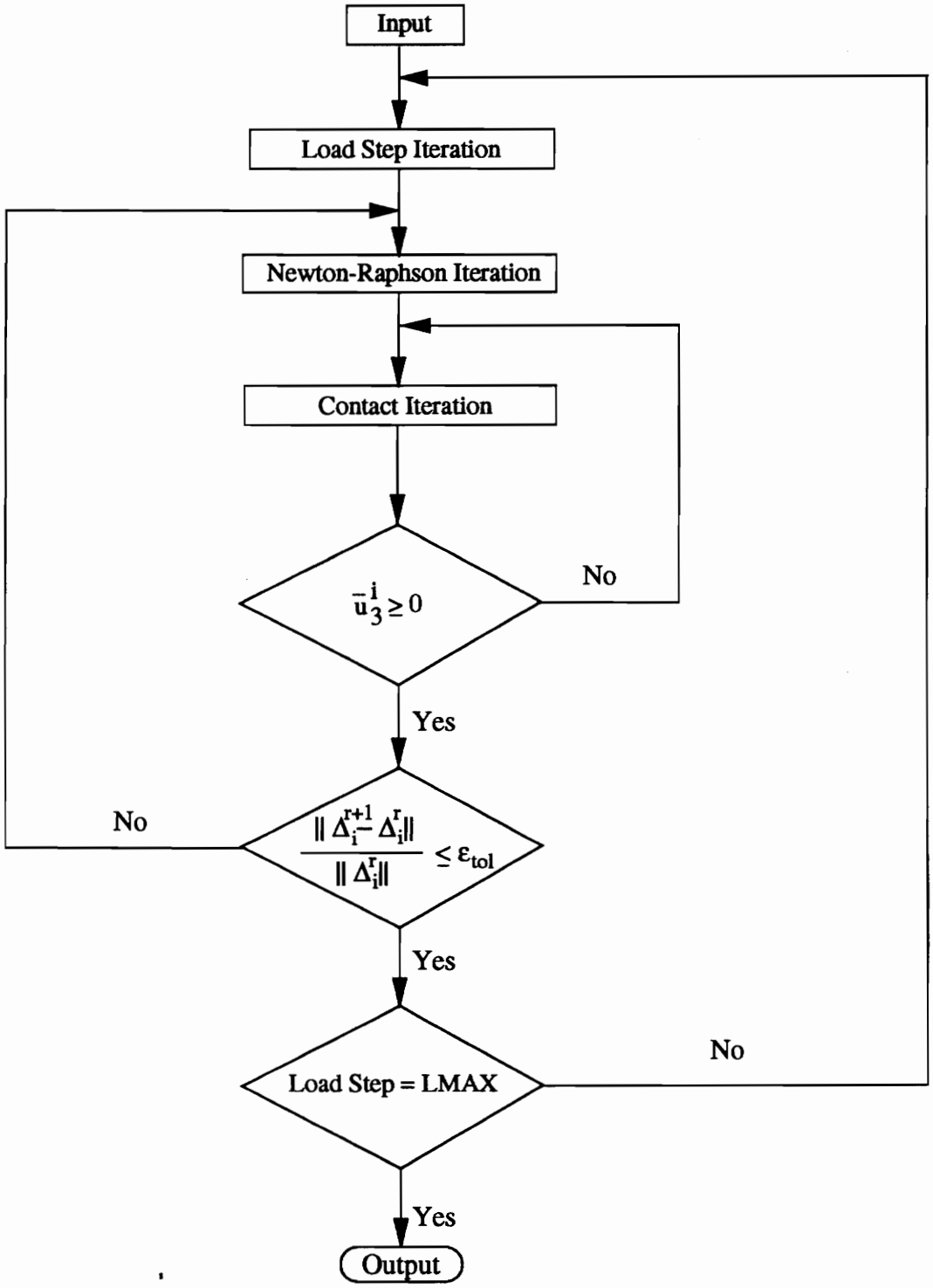

Figure 11. Flowchart for postbuckling analysis

Chapter V

VERIFICATIONS OF THE PRESENT APPROACH

The purpose of this chapter is to verify the capability and versatility of the present approach. For the demonstration, numerical results are presented for the buckling loads, natural frequencies, and postbuckling responses of composites containing through-the-width and embedded delaminations.

Most of the detailed studies concerning buckling and postbuckling of composites with through-the-width delaminations can be found in the next chapter.

5.1 Buckling and Postbuckling Analyses

5.1.1 Through-the-Width Delaminations

As a one-dimensional model, through-the-width delaminations have been studied by many researchers. The displacement fields and stresses in this model are generally assumed to be independent of the x_2 direction (Figure 12). As a result, a one-dimensional finite element model can be used.

Many of the previous investigations applied the symmetry assumption with respect to the half-length of the model for composites with symmetric geometry in the axial direction. As a result, antisymmetric modes have usually been neglected. In this study, however, both symmetric and antisymmetric modes are investigated using a half model of the composite for eigenproblems. A full model is used for antisymmetric modes in postbuckling problems. A typical finite element model is shown in Figure 12.

The following boundary conditions for symmetric and antisymmetric modes are assumed:

at $x_1 = 0$

$$\left.\begin{array}{ll} u_\alpha = 0 & \\ u_3 = 0 & \\ u_\alpha^j = 0 & (j = 1,2...M) \\ \bar{u}_\alpha^i = 0 & (i = 1,2...D) \\ \bar{u}_3^i = 0 & (i = 1,2...D) \end{array}\right\} \text{for clamped} \tag{5.1}$$

$$\left.\begin{array}{ll} u_\alpha = 0 & \\ u_3 = 0 & \\ \bar{u}_\alpha^i = 0 & (i = 1,2...D) \\ \bar{u}_3^i = 0 & (i = 1,2...D) \end{array}\right\} \text{for simply-supported} \tag{5.2}$$

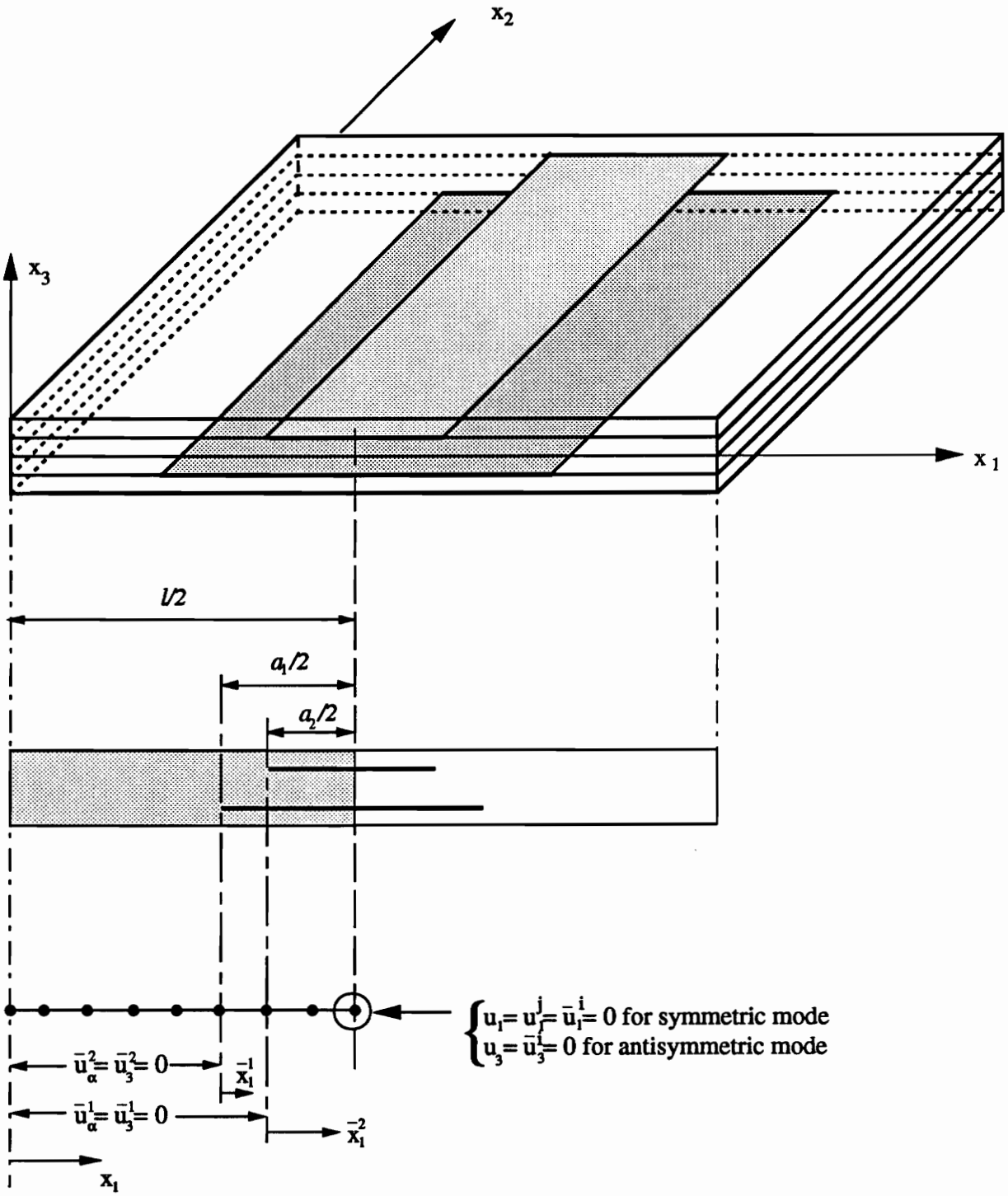

Figure 12. Description of the through-the-width delaminations and the finite element model

at $x = \frac{l}{2}$

$$\begin{aligned} &u_1 = 0 \\ &u_1^j = 0 \quad (j = 1,2...N) \\ &\bar{u}_1^i = 0 \quad (i = 1,2...D) \quad \text{for symmetric mode} \end{aligned} \tag{5.3}$$

$$\begin{aligned} &u_3 = 0 \\ &\bar{u}_3^i = 0 \quad (i = 1,2...D) \quad \text{for antisymmetric mode} \end{aligned} \tag{5.4}$$

For the portion where the ith delamination does not exist, the relative displacements of two delaminated surfaces are specified as follows:

along $x_1 = 0$ to $\frac{1}{2}(l - a_i)$

$$\begin{aligned} &\bar{u}_\alpha^i = 0 \\ &\bar{u}_3^i = 0 \end{aligned} \tag{5.5}$$

As an illustrative example, a specially orthotropic clamped composite laminate containing a centrally-located delamination at the midplane is considered in terms of the change in buckling modes (Figure 13).

For convenience, the following nondimensional quantities are used:

$$P = \frac{p}{p_{cr}}, \quad \bar{a} = \frac{a}{l}, \tag{5.6}$$

where p is the load applied to a composite and p_{cr} is the critical buckling load of the undelaminated composite.

The material being considered in this study is T300/5208 graphite/epoxy and the properties are as follows:

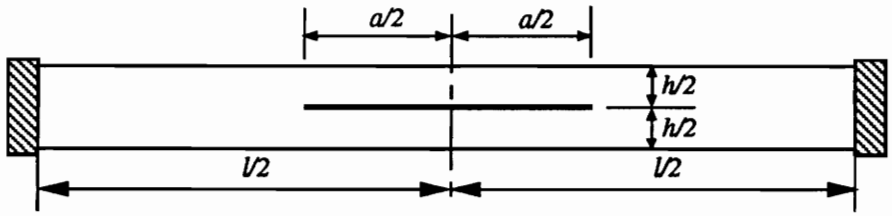

Figure 13. Geometry of a clamped beam-plate containing a through-the-width delamination at midplane

$$
\begin{aligned}
&E_{11} = 181GPa \\
&E_{22} = E_{33} = 10.3GPa \\
&G_{12} = G_{13} = G_{23} = 7.17GPa \\
&\nu_{12} = \nu_{13} = \nu_{23} = 0.28
\end{aligned}
\tag{5.7}
$$

The thickness-to-span ratio (h/l) is assumed to be very small (1/400) , so that the results can be compared with the previous available results based on classical lamination theory. The nondimensional buckling loads for three possible buckling modes (Figure 14) of different delamination length ratios are compared with those from [35] and [47] in Table 1.

The results obtained by Simitses et al. [35] did not apply symmetry assumptions in the axial direction. On the other hand, symmetry was assumed in [47] and thus, the antisymmetric modes were not considered. The present analysis clearly shows that the

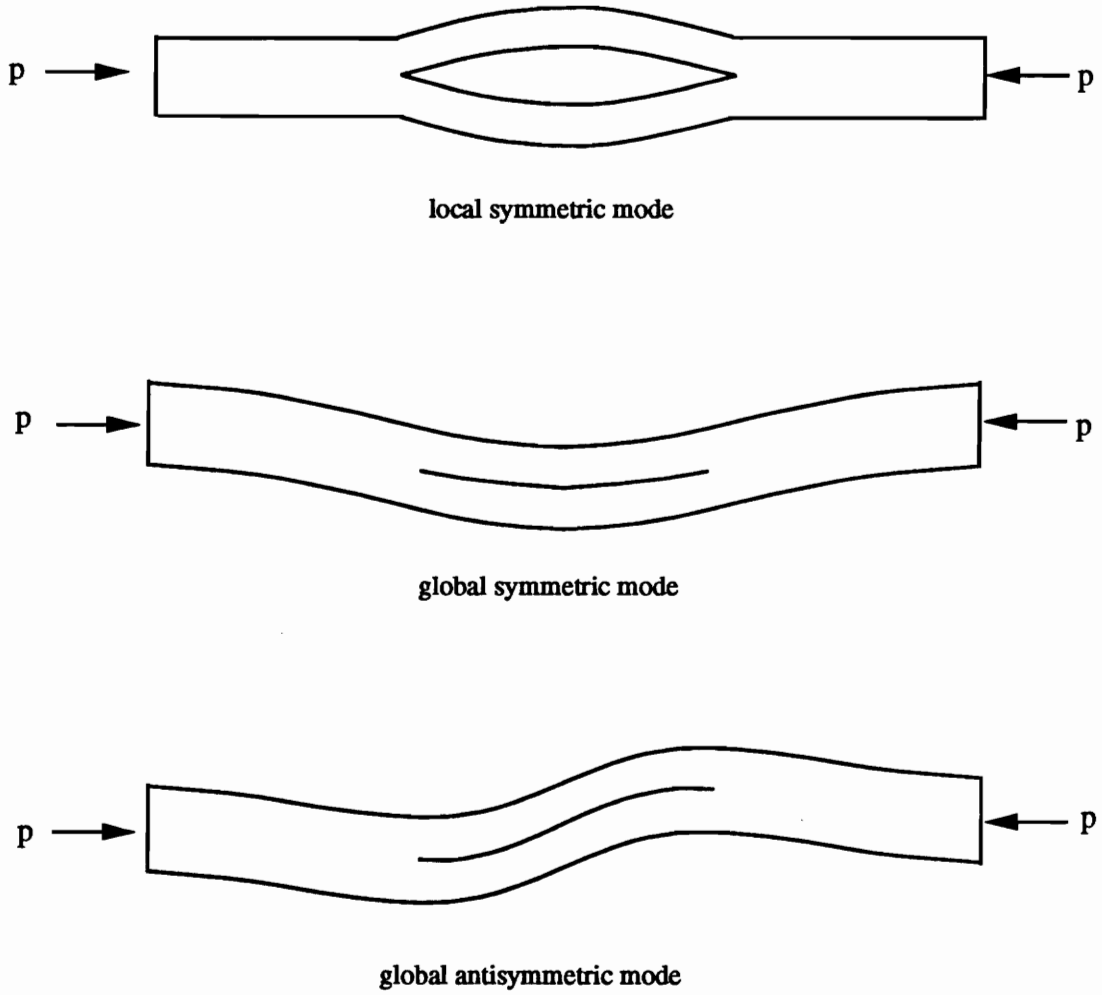

Figure 14. Three possible buckling mode shapes for a composite containing a delamination at midplane

Table 1. Comparison of nondimensional buckling loads for various length of a midplane delamination

a/l	Simitses [35]	Chen [47]	Present		
			Global symmetric	Local symmetric	Anti-symmetric
0.1	0.9999	0.9999	0.9999	15.320	1.9480
0.2	0.9956	0.9956	0.9956	6.0963	1.4360
0.3	0.9638	0.9638	0.9639	2.7176	1.0240
0.4	**0.8481**	**0.8561**	**0.8562**	**1.5358**	**0.8482**
0.5	0.6896	0.6896	0.6898	0.9864	0.7967
0.6	0.5411	0.5411	0.5413	0.6868	0.7929
0.7	0.4310	0.4310	0.4311	0.5058	0.7629
0.8	0.3514	0.3514	0.3515	0.3883	0.6857
0.9	0.2923	0.2933	0.2934	0.3077	0.5947

nondimensional buckling load for global symmetric and antisymmetric modes corresponds to those of Chen [47] and Simitses [35], respectively for $\bar{a} = 0.4$, implying that the antisymmetric mode is obviously the first buckling mode for this specific value of $\bar{a}$. For the other values of $\bar{a}$, the present results for the global symmetric mode are in excellent agreement with the two other solutions.

Nondimensional buckling loads for the three distinguishable buckling modes of a laminate with a single midplane delamination are shown in Figures 15 and 16 for $h/l = 1/400$ and $1/10$, respectively. It is observed that the global symmetric mode representing the solid line is insensitive to the slenderness ratio of the composite. On the other hand, the local symmetric mode shows the most drastic change in load carrying capacity. For a short delamination ($\bar{a} < 0.25$) , the global symmetric mode is apparently the first buckling mode for both slenderness ratios. Between $\bar{a} = 0.25$ and $\bar{a} = 0.45$, however, the global antisymmetric mode becomes the first buckling mode shape for the thick composite, whereas the antisymmetric mode governs the buckling behavior for a very small range of $\bar{a}$ (near 0.4) for the thinner composite. This is because the shear effect becomes significant for a thicker plate, and thus, enhances the antisymmetric mode. Near $\bar{a} = 0.5$, buckling loads of all the three modes are very close to one another, suggesting that the composite may take any of these buckling mode shapes depending on its shape of initial imperfection. For a longer delamination ($\bar{a} > 0.5$) , the buckling load of the local symmetric mode is slightly lower than for the global symmetric mode for the thick composite, but still greater than the local symmetric mode of the thinner composite. The antisymmetric mode is beyond these two modes for both cases, so that failure loads follow either the global or local symmetric buckling mode depending on the thickness-to-span ratio.

The postbuckling analysis is carried out for $\bar{a} = 0.4$, where both symmetric and antisymmetric modes are close each other. Since the deflection at the center is always

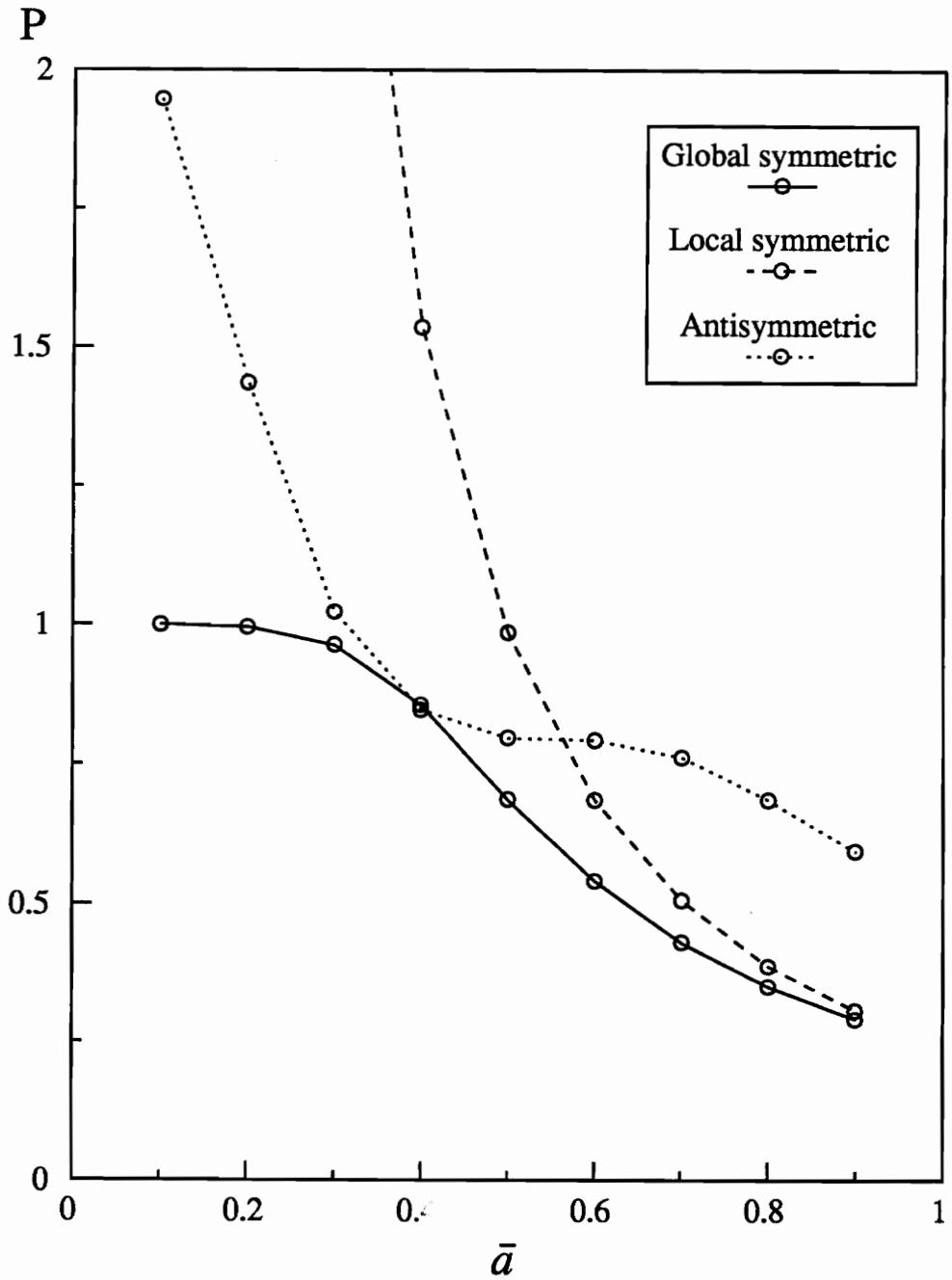

Figure 15. Buckling load vs. delamination length for a composite containing a delamination at midplane with h/l = 1/400

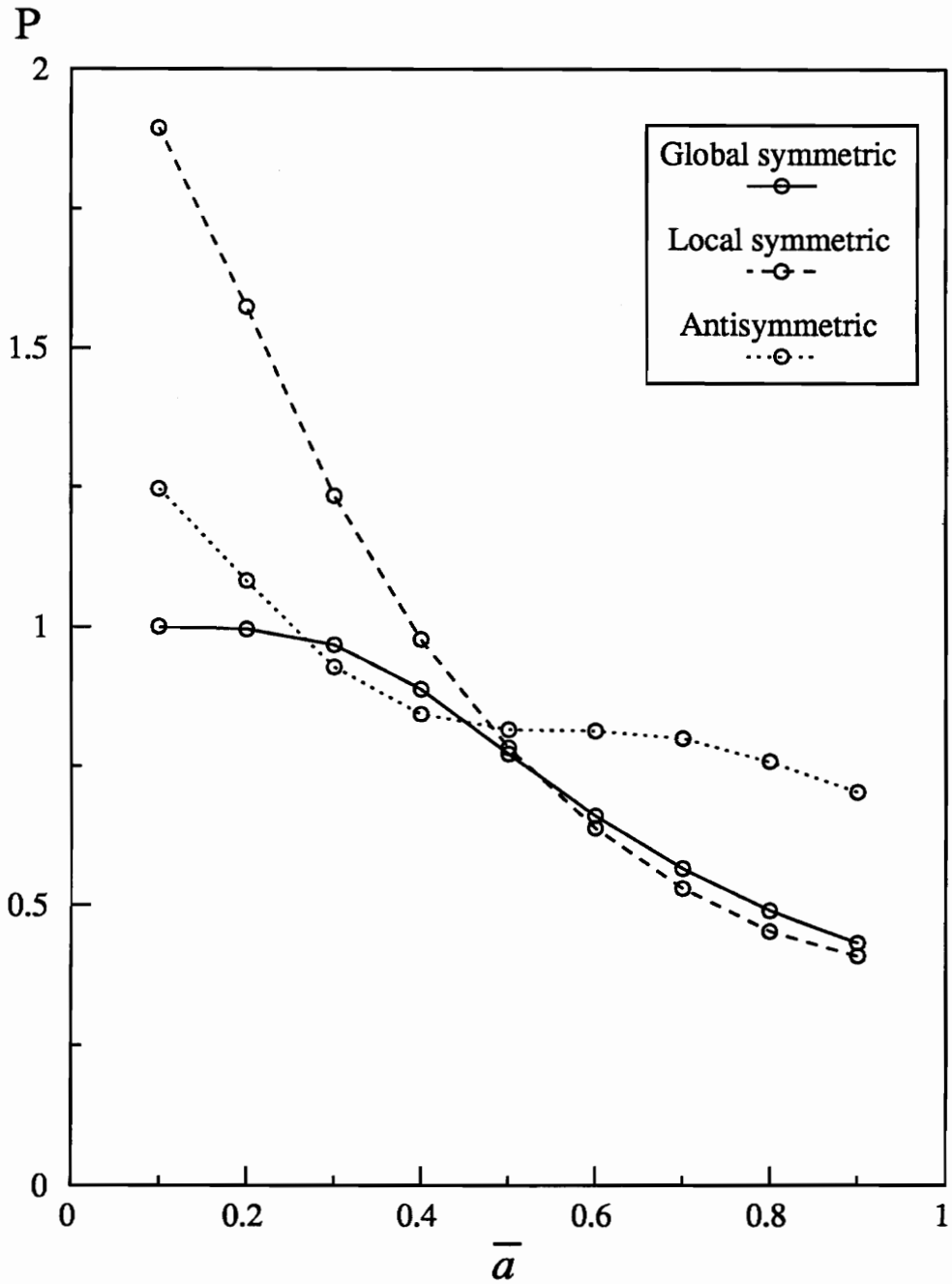

Figure 16. Buckling load vs. delamination length for a composite containing a delamination at midplane with h/l = 1/10

zero for antisymmetric mode, the load-end shortening curve is considered (Figure 17). It should be noted that an initial imperfection of the composite is necessary in order to initiate a nontrivial postbuckling response.

In this case, initial imperfections are taken as one and two half-waves for symmetric and antisymmetric modes, respectively:

$$\begin{aligned} \xi &= \frac{1}{2} w_o h\left(1 - \cos\frac{2\pi x_1}{l}\right) \quad \text{for the symmetric mode} \\ \xi &= w_o h \sin\frac{2\pi x_1}{l} \quad \text{for the antisymmetric mode} \end{aligned} \tag{5.8}$$

where h is the thickness, and l is the length of the plate, respectively, as shown in Figure 13. In Eq. (5.8), w_o is the fraction of initial deflection with respect to the plate thickness at the center.

Initial delamination opening ($\bar{\xi}'$) is assumed to be zero for both cases because the buckling mode shapes are obviously global for both symmetric and antisymmetric modes as given in Table 1. While the initial imperfection exactly satisfy the clamped boundary conditions for the symmetric mode, it does not satisfy the boundary conditions exactly, but the difference is negligible for this antisymmetric case. In Figure 17, the end shortening is normalized with respect to length of the composite as $U = u_1/l$.

As soon as the composite reaches its delamination buckling load, it suddenly loses load-carrying capacity for both cases. So, the delamination buckling load itself can be considered as the global buckling load in this case (Figure 17).

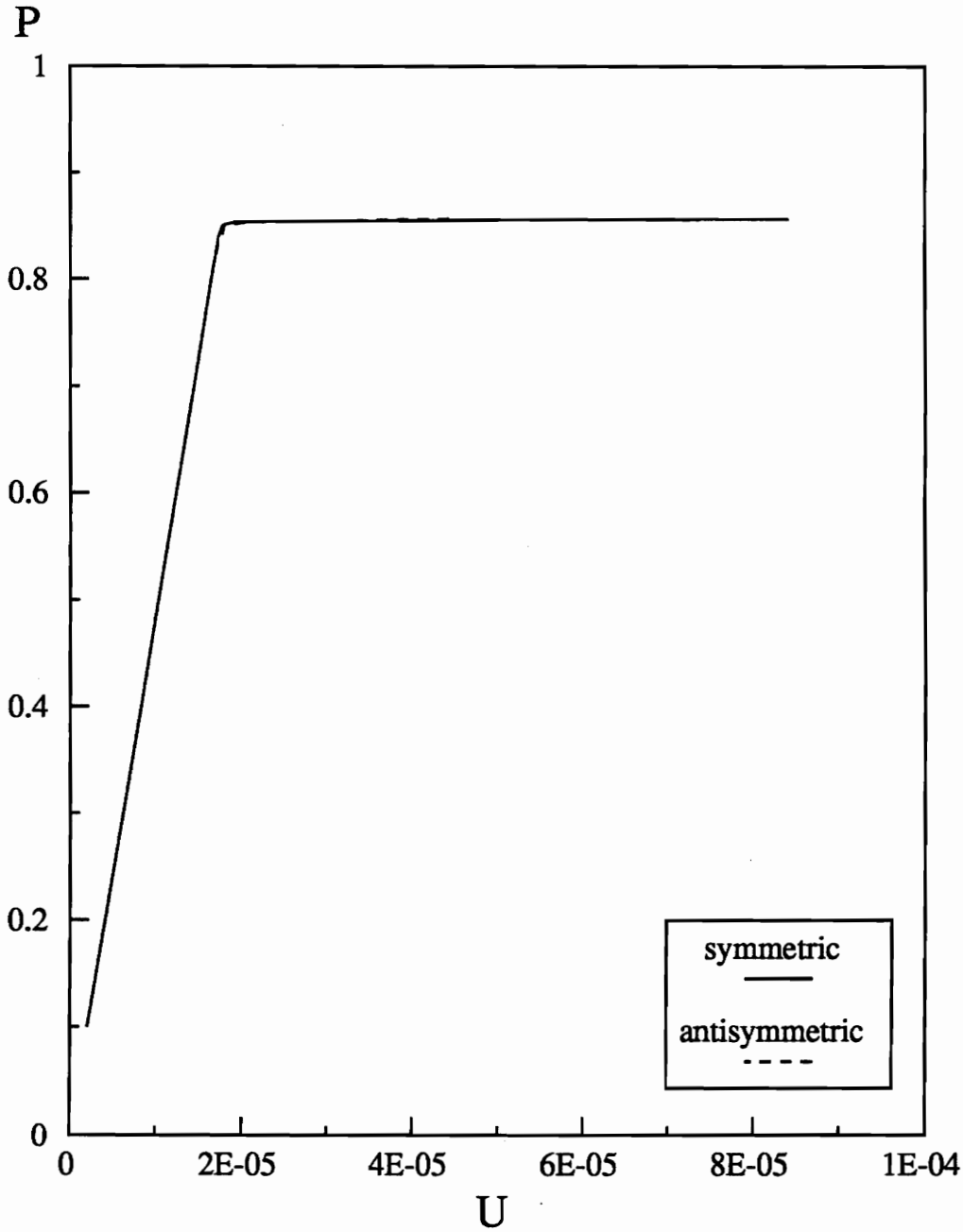

Figure 17. Load-end shortening curve for a composite containing a delamination ($\bar{a}$ = 0.4) at midplane

5.1.2 Embedded Delaminations

5.1.2.1 Axisymmetric Circular Delaminations

Because of its circumferential axisymmetry, the problem can be simplified to a one-dimensional problem when axisymmetric finite element is used to formulate it. Although the present formulation can be applicable to polar anisotropic materials, all the examples considered are isotropic materials for an illustrative purpose.

Single delamination

A clamped isotropic circular plate containing a concentric penny-shaped delamination at its midplane is considered (Figure 18). The plate is under uniform circumferential compressive load. The critical buckling loads with respect to the delamination radius are presented for two different thickness-to-span ratios. In the first case, the thickness-to-span ratio is assumed to be very small ($h/R = 1/500$), so that the results can be compared with the previous results of classical lamination theory [81]. Secondly, a moderately thick plate ($h/R = 1/10$) is considered in order to investigate the effect of thickness-to-span ratio on the buckling loads and buckling modes.

The buckling coefficients for the three distinguishable buckling modes are shown in Figures 19 and 20. In these Figures, the buckling loads are normalized as:

$$P = \frac{pR^2}{D_r} \tag{5.9}$$

where

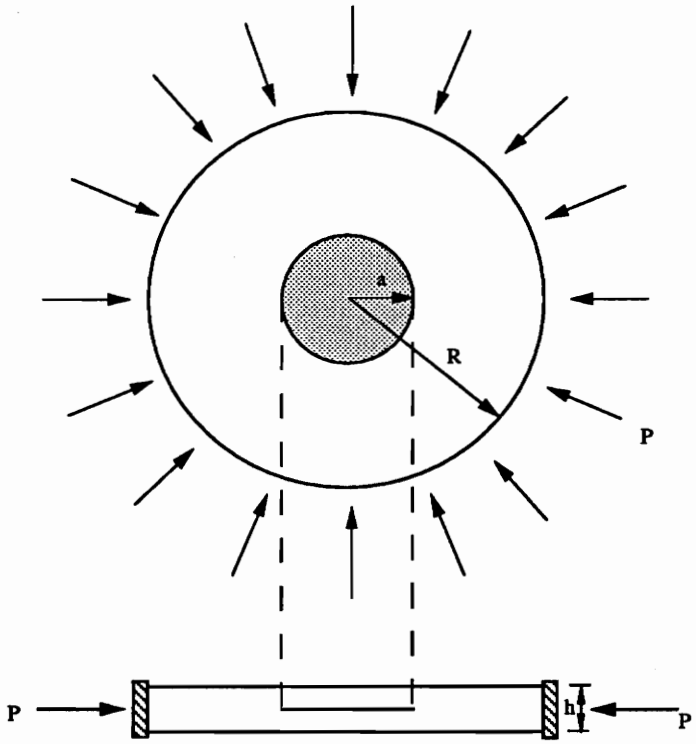

Figure 18. Geometry of a circular plate containing a concentric penny-shaped delamination at midplane

$$D_r = \frac{E_r h^3}{12(1-\nu^2)} \quad . \tag{5.10}$$

Delamination radius is normalized with respect to the radius of the plate as $\bar{a} = a/R$.

The present results show good agreement with the results reported in [81] as shown in Figure 19. Unlike the case of through-the-width delaminations, the slenderness of the plate seldom affects buckling loads and modes. For the range of delamination radius, the global symmetric mode is dominant, and the buckling load of the antisymmetric mode is far beyond that of the global symmetric mode.

As another example, the present postbuckling solutions are compared with the previous results [77] in Table 2 for the case of near-the-surface delamination ($t/h = 0.1$). In

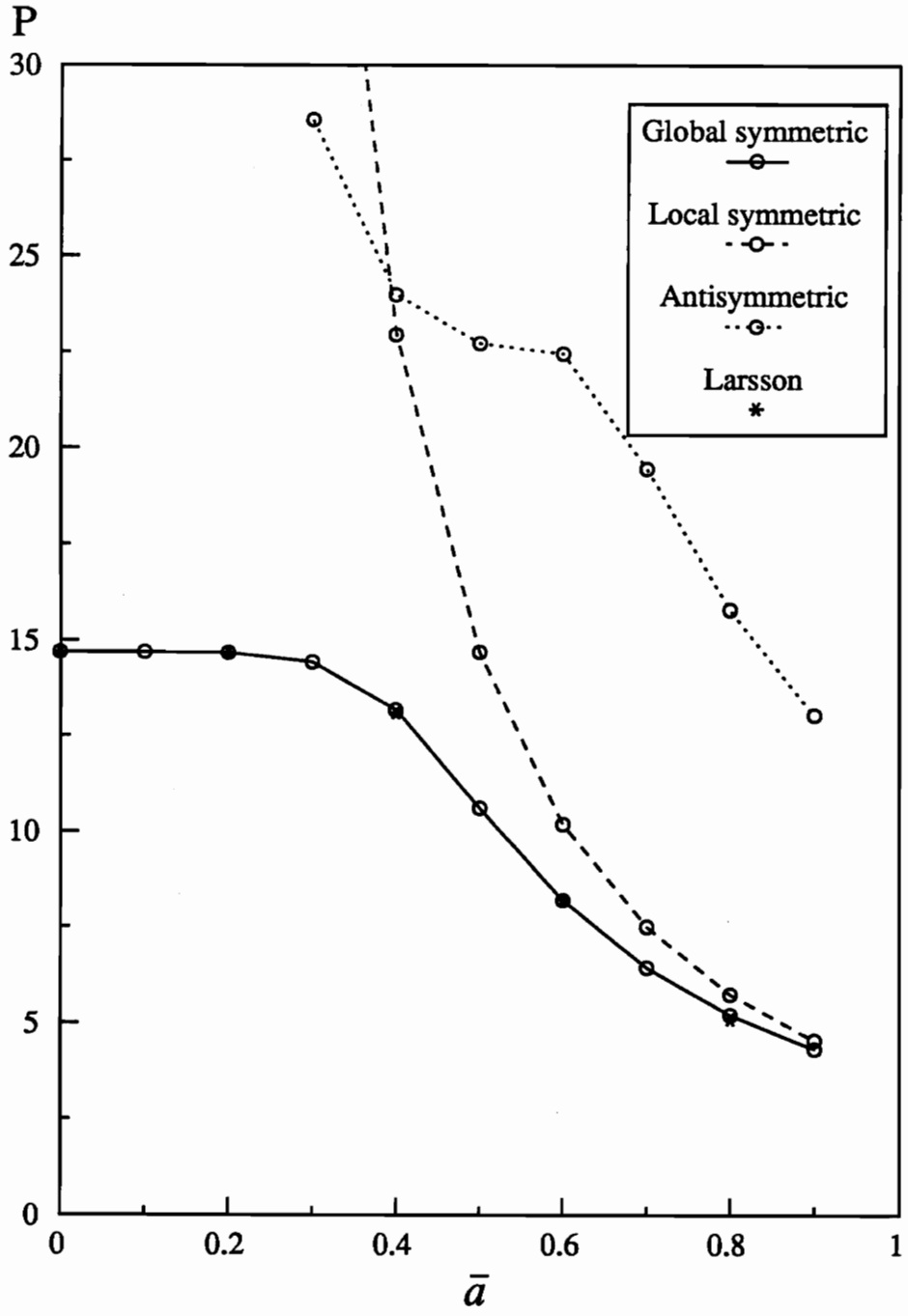

Figure 19. Buckling loads vs. delamination radius for a circular plate containing a single midplane penny-shaped delamination with h/R = 1/500

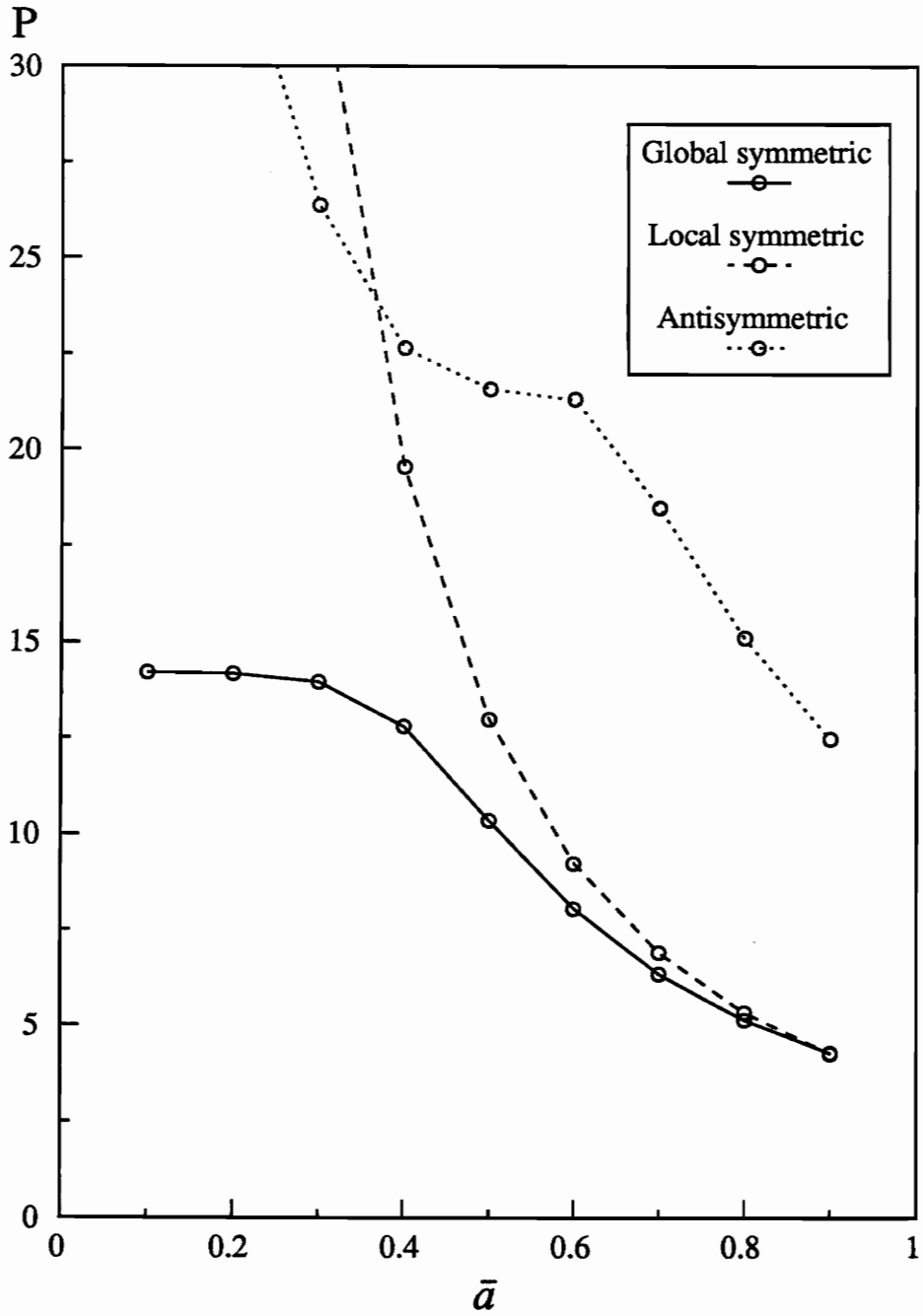

Figure 20. Buckling loads vs. delamination radius for a circular plate containing a single midplane penny-shaped delamination with h/R = 1/10

Table 2, P and U are nondimensional applied compressive load and end shortening, respectively, defined as:

$$P = \frac{p}{p_{cr}} \quad , \qquad U = \left\{12(1-\nu^2)u_r(R)/R\right\}^{1/2} \frac{a}{h} \quad . \tag{5.11}$$

where p_{cr} is the buckling load of the undelaminated plate, and $u_r(R)$ is a radial displacement at the supports.

For two different delamination sizes, $\bar{a} = 0.125$ and 0.25, the present results show excellent agreement with Yin's results [77].

Multiple delaminations

In order to investigate the effect of multiple penny-shaped delaminations in a circular plate, an isotropic clamped circular plate with three equidistant delaminations having same radii ($a_1 = a_2 = a_3 = a$) is considered. The buckling loads for the first symmetric and antisymmetric buckling modes are represented in terms of delamination sizes. Unlike the through-the-width delamination case, the symmetric mode is dominant for the whole range of $\bar{a}$ (Figure 21).

The next example is three equidistant delaminations with different radii as shown in Figure 22. The postbuckling deformation is shown in Figure 23, compared to the undelaminated case. The delamination radii and the deflection at the center of the plate are normalized as $\bar{a}_i = a_i/R$ and $W = u_z/h$.

At the load level of first buckling load (near $P = 0.4$), the bottom sublaminate buckles down and the other parts deflect up together. As load increased to $P = 0.65$, the second bifurcation point is reached, and thus the second sublaminate buckles down with increasing the opening of the first delamination, and the deformation of the whole part

Table 2. Comparison of postbuckling solution for a penny-shaped delamination at midplane of a circular plate

a/R=0.125			a/R=0.25		
P	U		P	U	
	Yin [77]	Present		Yin [77]	Present
0.6416	3.2098	3.2100	0.1604	3.2103	3.2103
0.6464	3.2219	3.2219	0.1616	3.2222	3.2219
0.6551	3.2436	3.2436	0.1638	3.2436	3.2441
0.6758	3.2943	3.2945	0.1689	3.2946	3.2942
0.6960	3.3432	3.3433	0.1740	3.3441	3.3436
0.7361	3.4384	3.4384	0.1946	3.5367	3.5370
0.7763	3.5311	3.5312	0.2158	3.7255	3.7249
0.8562	3.7085	3.7084	0.2611	4.0987	4.0983
0.9668	3.9412	3.9408	0.3106	4.4715	4.4711
0.9838	3.9761	3.9755	0.3649	4.8477	4.8475
0.9877	3.9845	3.9835	0.4245	5.2293	5.2289
0.9896	3.9888	3.9873	0.4897	5.6171	5.6171
0.9908	3.9919	3.9901	0.5604	6.0097	6.0098
0.9917	3.9945	3.9925	0.6742	6.5933	6.5936
0.9926	3.9971	3.9955	0.7852	7.1171	7.1192
0.9933	3.9991	3.9980	0.8857	7.5629	7.5748

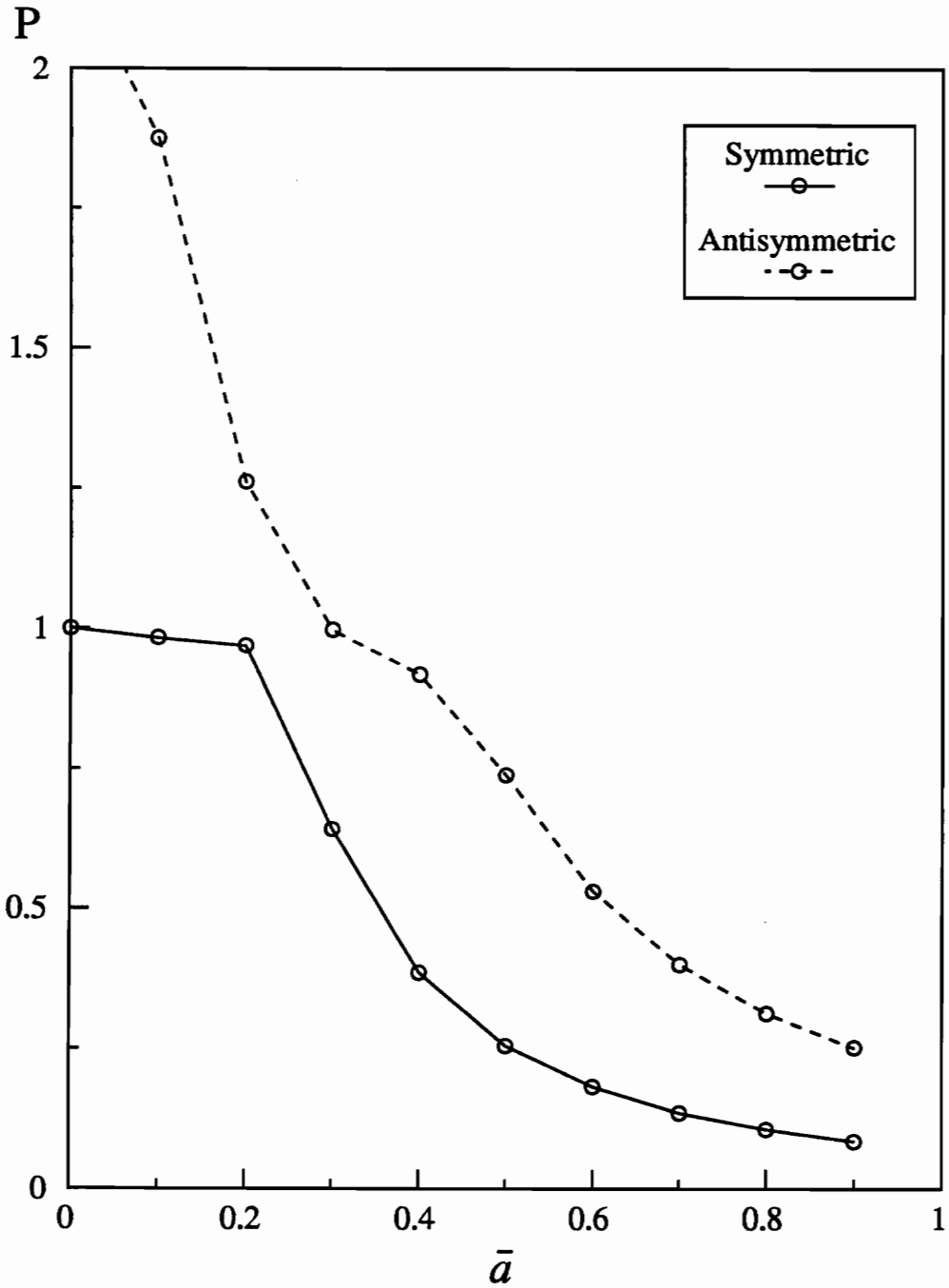

Figure 21. Buckling loads vs. delamination radius for a circular plate containing three equidistant uniform, penny-shaped delaminations

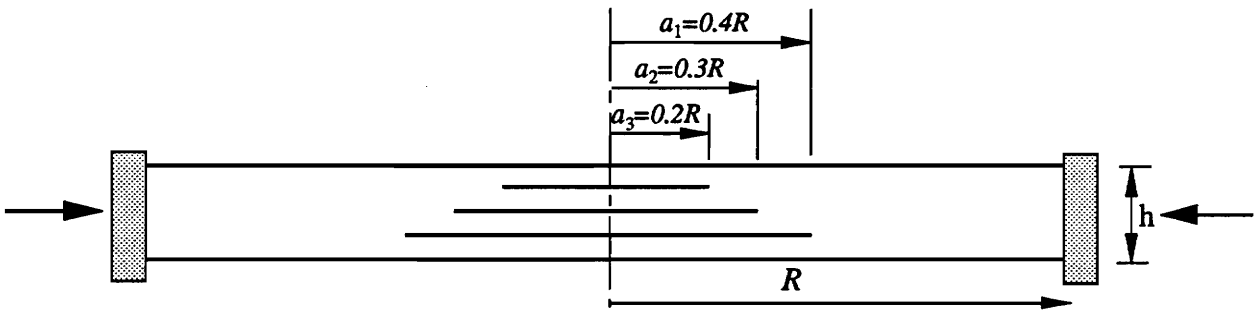

Figure 22. Geometry of a clamped circular plate containing three equidistant penny-shaped delaminations with $\bar{a}_1 = 0.4$, $\bar{a}_2 = 0.3$, $\bar{a}_3 = 0.2$

is accelerated upward. At increased load, these two delaminations open continuously, and the whole part substantially buckles upward. It is shown that the shortest delamination ($\bar{a}_3 = 0.2$) stays closed during the postbuckling process.

5.1.2.2 Two-Dimensional Delaminations

A two-dimensional square-shaped concentric delamination in a square plate is considered. The problem geometry and finite element mesh are shown in Figure 24. The material used is T300/5208 graphite/epoxy. The plate is specially orthotropic and simply-supported along all edges with low thickness-to-span ratio ($h/l = 1/10$). A delamination is assumed to lie near the surface ($t/h = 0.2$). The buckling loads for the cases

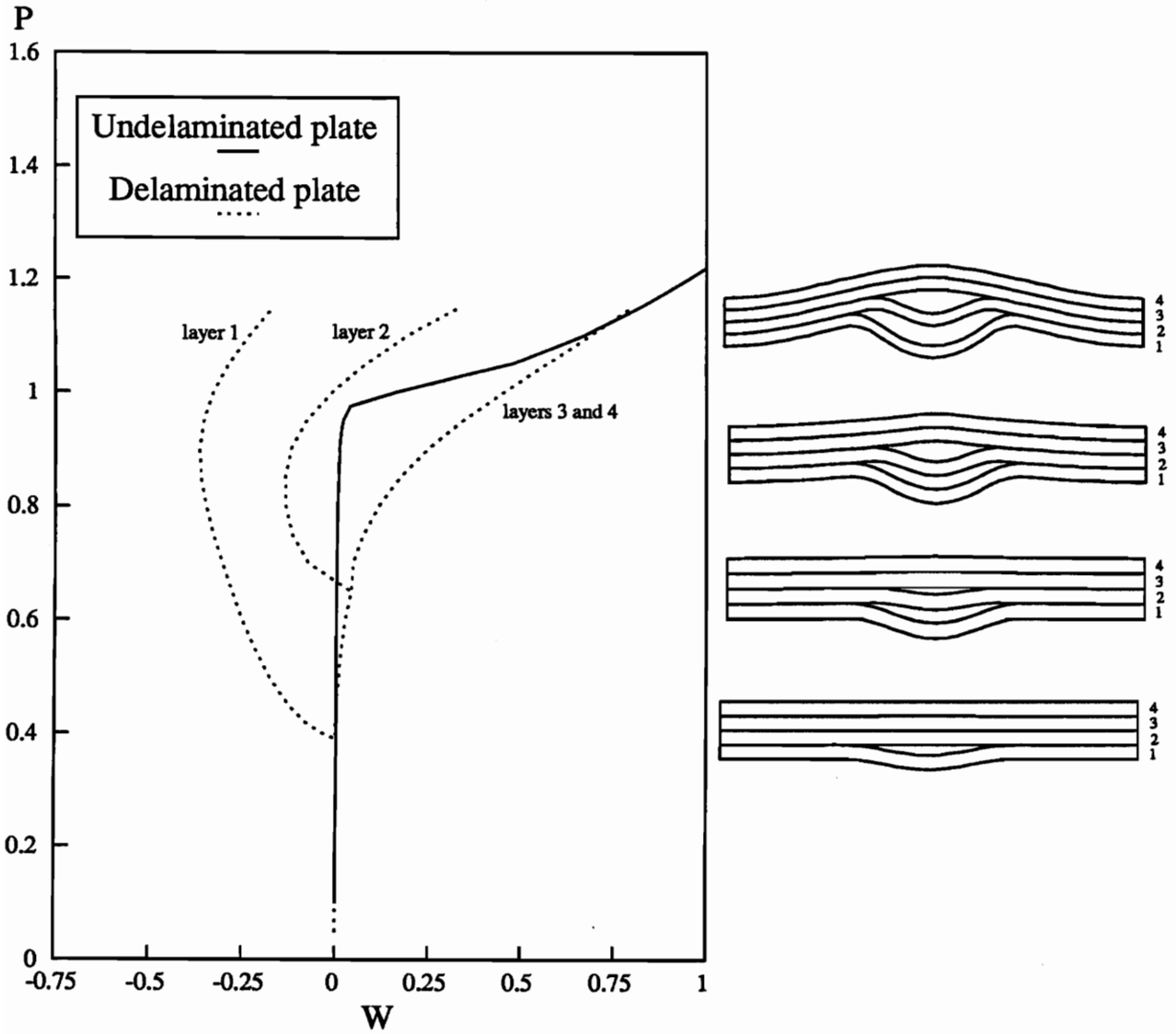

Figure 23. Load-deflection curve for a circular plate containing three equidistant penny-shaped delaminations with $\bar{a}_1 = 0.4$, $\bar{a}_2 = 0.3$, $\bar{a}_3 = 0.2$

of uniaxial and biaxial compressive loads are normalized with respect to those of the undelaminated plate in Figure 25. It is seen that the buckling coefficient for a biaxial compressive load is more sensitive to delamination than the one for a uniaxial load.

As another example, a simply-supported $[\pm\theta]_4$ antisymmetric angle-ply laminate with a square delamination of $\bar{a} = 0.4$ at its midplane is considered. The material properties are as follows:

$$\begin{aligned} &\frac{E_{11}}{E_{22}} = 40 \\ &\frac{G_{23}}{E_{22}} = 0.5\,, \quad \frac{G_{13}}{E_{22}} = \frac{G_{12}}{E_{22}} = 0.6 \\ &\nu_{23} = \nu_{13} = \nu_{12} = 0.25 \end{aligned} \tag{5.12}$$

In order to save computing time, the sublaminate approach is used. Simply-supported boundary conditions of the quadrant of the plate for one and two half-waves are presented in Figure 26. The buckling loads are normalized as $P = pl^2/E_{22}h^3$. The nondimensional buckling loads for one half-wave and two half-wave modes in the loading direction are shown in Figure 27 for both undelaminated and delaminated composites under uniaxial compressive loading. It can be seen that the reduction in buckling loads due to the delamination for the mode of one half-wave is almost constant for all the range of lamination angle θ. On the other hand, the difference in buckling loads between delaminated and undelaminated cases for the two half-wave mode is substantially reduced as the lamination angle approaches 90°. As a result, the buckling loads for the delaminated composite are not much different from the undelaminated case for $\theta > 60$ where the two half-wave mode is dominant, while they are quite lower values than the undelaminated case for $\theta < 60$.

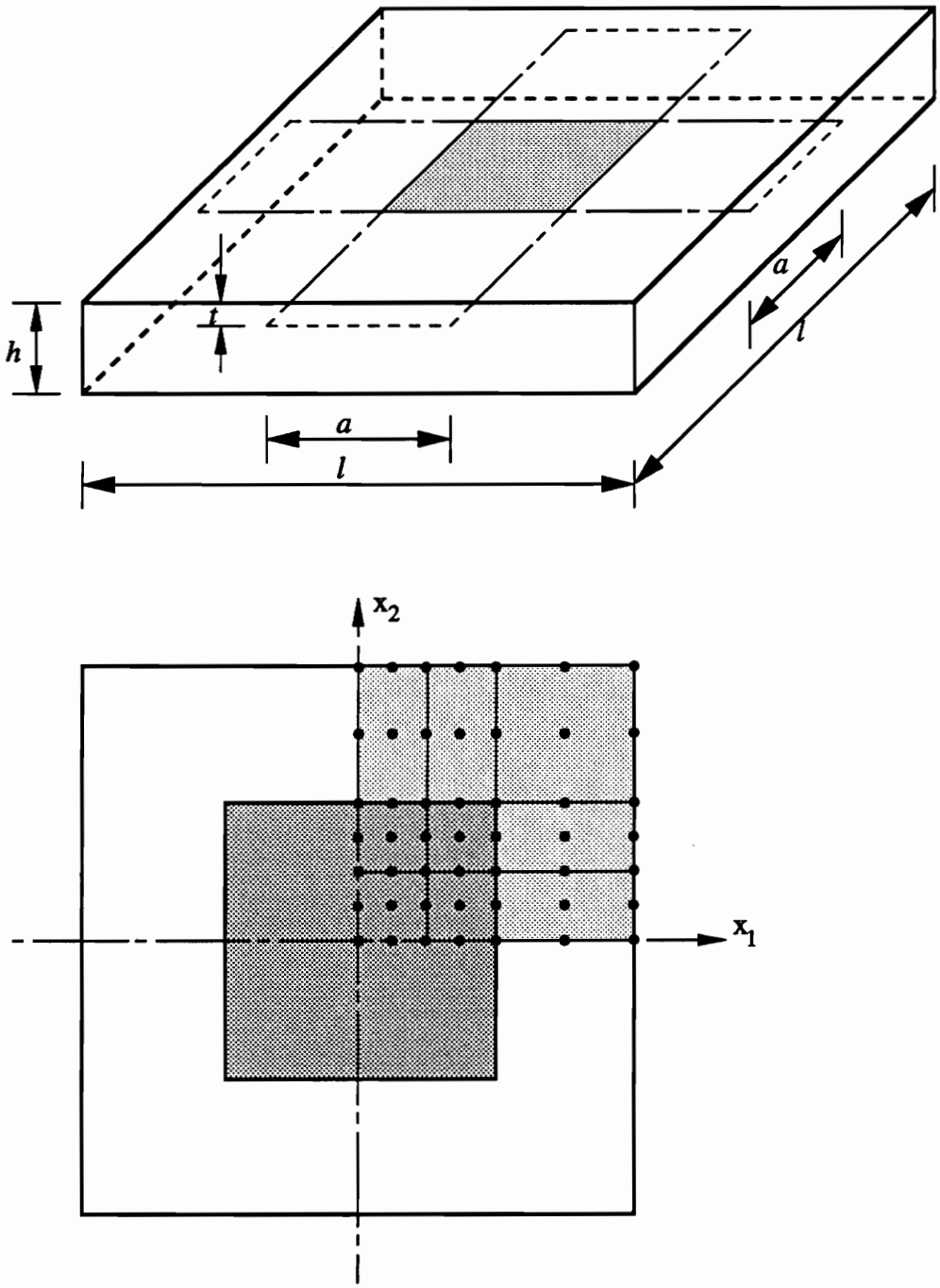

Figure 24. Geometry of a square plate containing a single square delamination and the finite element mesh

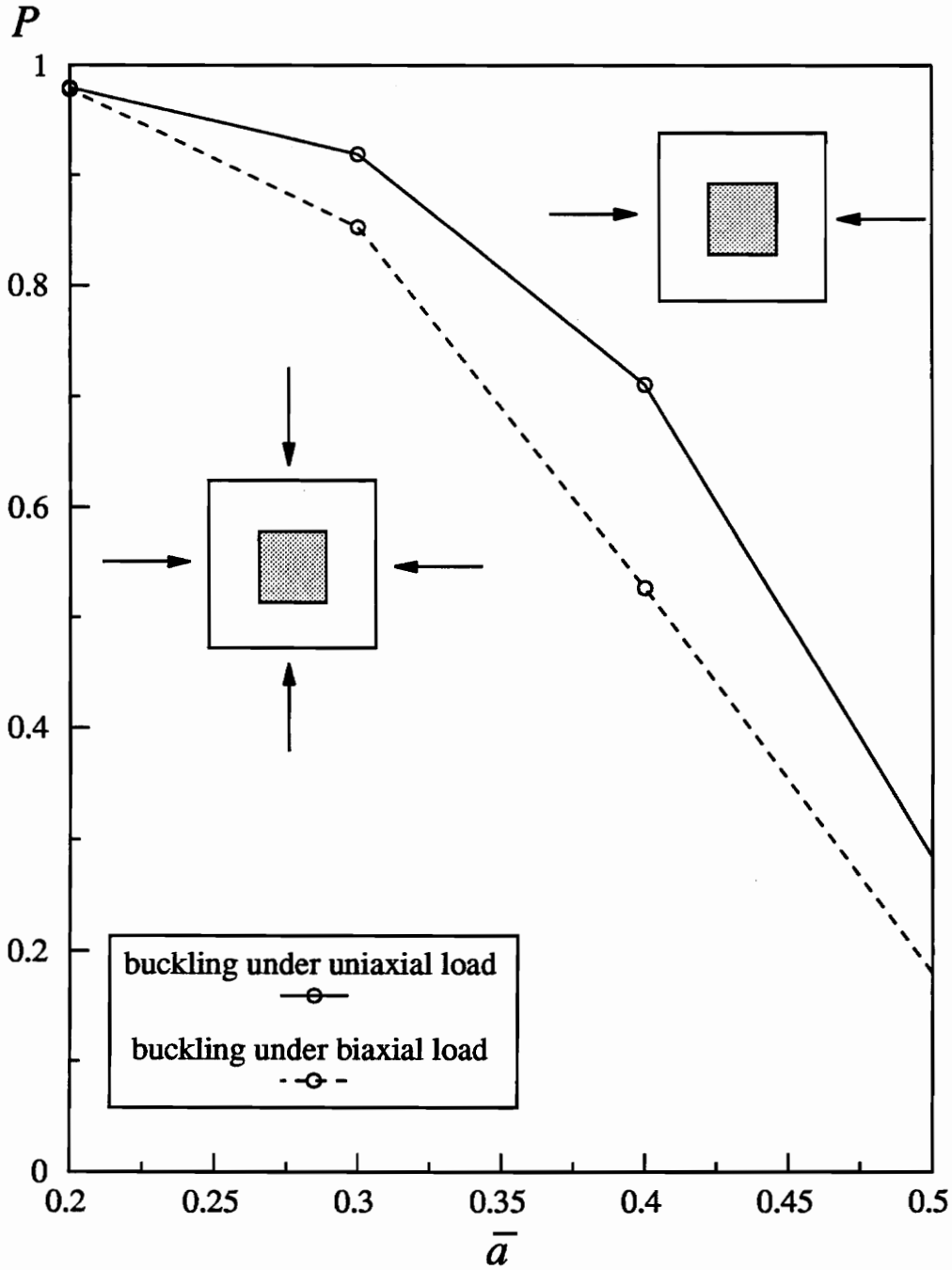

Figure 25. Buckling loads vs. delamination size for a square orthotropic plate under uniaxial and biaxial compressive loads

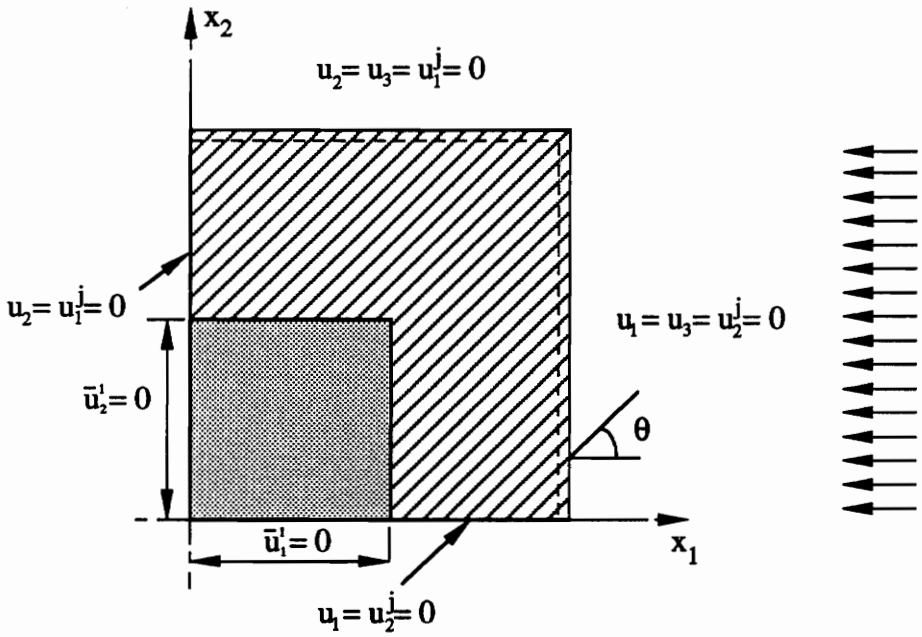

(a) one half-wave in loading direction

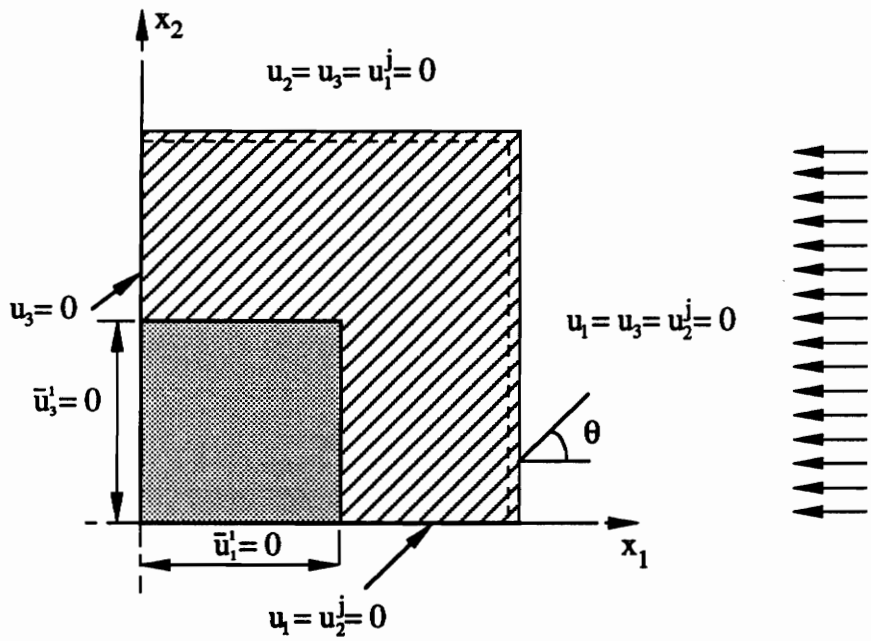

(b) two half-waves in loading direction

Figure 26. Boundary conditions of the simply-supported quarter-plate model for one half-wave and two half-waves in the loading direction

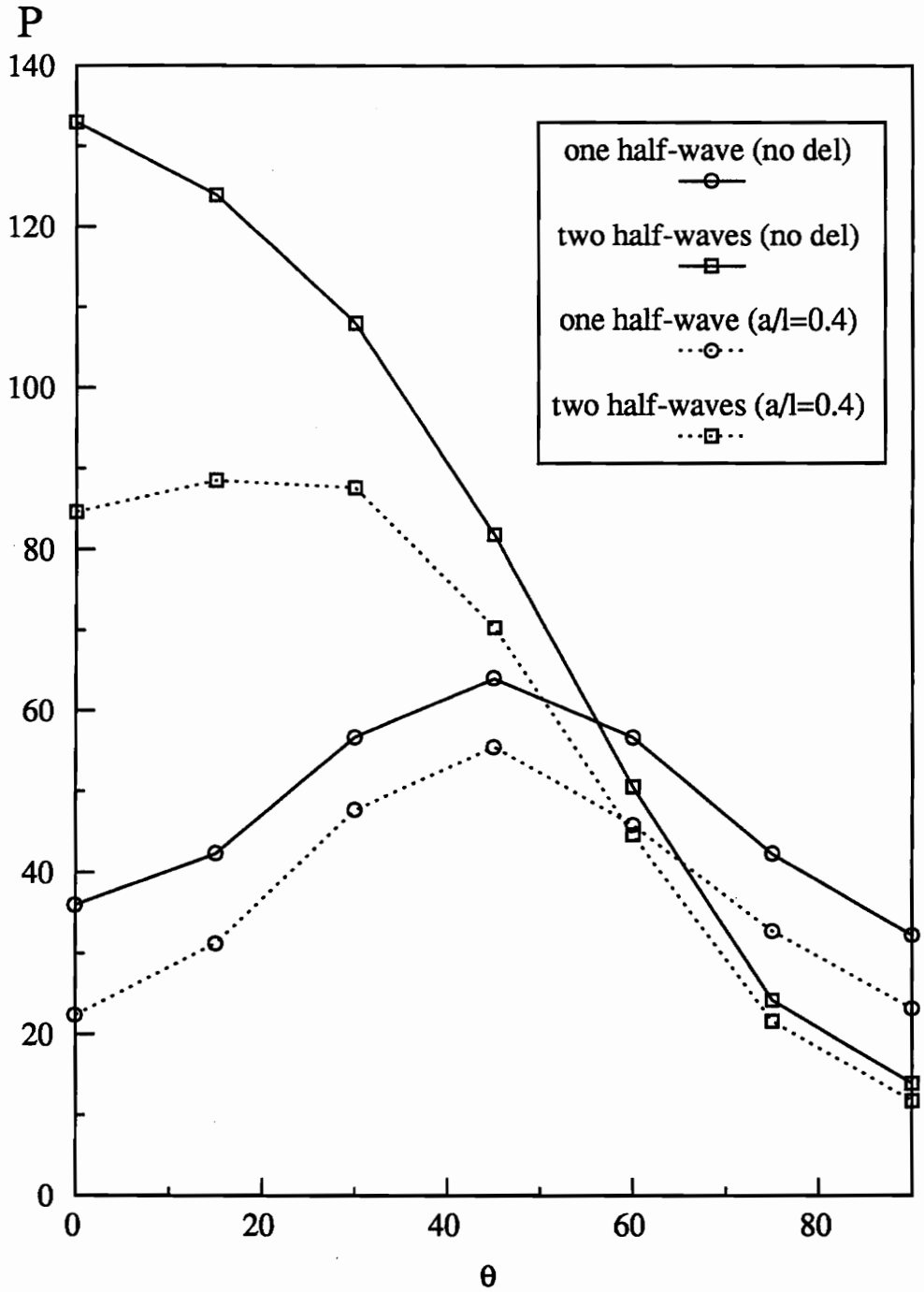

Figure 27. Buckling loads vs. lamination angle for undelaminated and delaminated angle-ply composite plates

5.2 Free Vibration Analysis

5.2.1 Through-the-Width Delaminations

5.2.1.1 Isotropic Clamped Beam

For the verification of the capability for vibration analysis of the present theory, a comparison with a previously available result is made. The first three nondimensional natural frequencies of a clamped beam with a various lengths of a delamination located symmetrically both in the axial direction and through the width are compared with Wang's results [67] in Table 3. The thickness-to-span ratio is assumed to be very small and the material is isotropic with Poisson's ratio $\nu = 0.3$ for the comparison.

It should be mentioned that the delamination always remains completely closed during the motion. The normalized natural frequencies in Table 3 are defined as

$$\Omega = \sqrt{\frac{\rho h}{EI}}\, l^2 \omega \ . \tag{5.13}$$

There is an excellent agreement between the two theories for all ranges of $\bar{a}$.

As another example, a delamination is located close to the surface ($\bar{t} = 0.2$). For $\bar{a} = 0.3$, the calculated first vibration mode shape is demonstrated in Figure 28(a). As shown in the Figure, the delamination opens when the beam vibrates upward. When the beam vibrates downward, however, this mode shape is inadequate for representing the motion because there may be an overlapping between two sublaminates. In fact, the delamination should close when the beam goes down (Figure 28(c)).

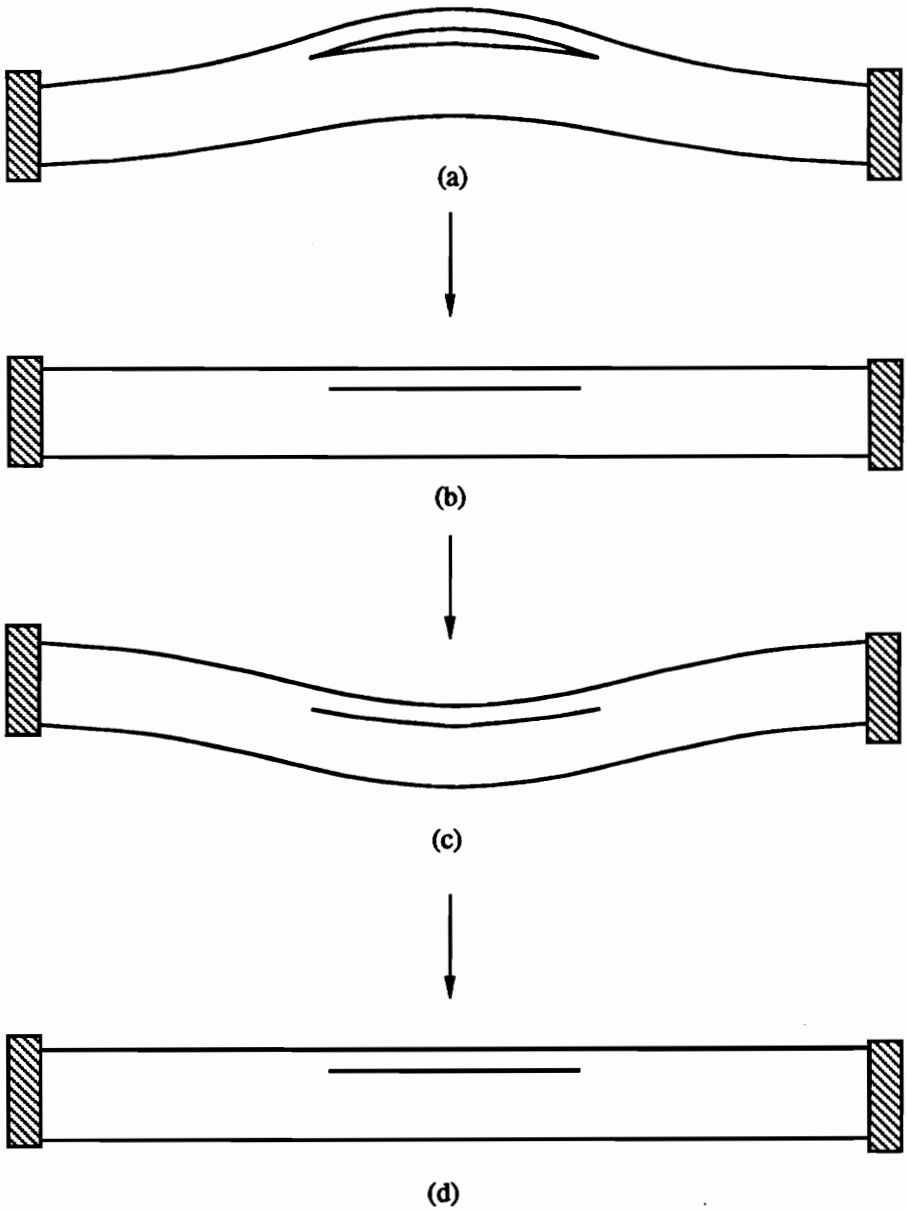

Figure 28. Vibration mode change during the period of the motion for a clamped beam with $\bar{t} = 0.2$, $\bar{a} = 0.3$

Figure 29. Natural vibration mode shape for a clamped beam with $\bar{t} = 0.2$, $\bar{a} = 0.6$

Consequently, the beam does not exhibit classical vibration modes, and strictly speaking, the natural vibration frequencies cannot be defined in this case, as noted by Andruet and Plaut [109].

However, assuming that the two delaminated parts have the same velocities as well as same deflections at status (b) in Figure 28, a total period can be approximated by adding half of the period of two states, and further, the combined natural frequencies can be estimated as follows:

$$\omega = \frac{2\omega_{\text{open}} \times \omega_{\text{closed}}}{\omega_{\text{open}} + \omega_{\text{closed}}} \quad . \tag{5.14}$$

The first nondimensional natural frequencies for the cases of delamination opening, delamination closing, and combined modes are presented for $\bar{a} = 0.3$ and 0.6 in Table

Table 3. Natural frequencies of a clamped beam with a midplane delamination.

	Wang [67]			Present analysis		
a/l	1st	2nd	3rd	1st	2nd	3rd
0	22.39	61.67	120.91	22.36	61.61	120.68
0.1	22.37	60.76	120.81	22.36	60.74	120.62
0.2	22.35	55.97	118.76	22.35	55.95	118.69
0.3	22.23	49.00	109.04	22.23	48.97	109.03
0.4	21.83	43.87	93.57	21.82	43.86	93.51
0.5	20.88	41.45	82.29	20.88	41.50	82.23
0.6	19.29	40.93	77.64	19.28	41.01	77.64
0.7	17.23	40.72	77.05	17.22	40.80	77.12
0.8	15.05	39.01	75.33	15.05	39.04	75.39
0.9	13.00	35.38	69.17	12.99	35.38	69.16

Table 4. Natural frequencies of a clamped beam with t/h=0.2.

	a/l=0.3	a/l=0.6
opening delamination mode	22.08	12.05
closing delamination mode	22.32	21.29
combined mode	22.20	15.39

4. It should be noted that the velocity-matching assumption appears to be somewhat inappropriate for a longer delamination ($\bar{a} = 0.6$). This is because the first vibration mode for delamination opening shows almost pure local vibration of the thin upper layer (Figure 29) while delamination opening-suppressed mode is global. This results in substantial difference in vibration frequencies between the two cases. Therefore, more accurate analysis appears to be necessary for local-mode type vibration of delaminated composites.

5.2.1.2 Composite Cantilever Beam

A cantilever beam with $[0/\theta]_S$ stacking sequence is considered in order to investigate the delamination effect on natural frequencies (Figure 30). Two delaminations with $\bar{a}_1 = \bar{a}_2 = 0.5$ are assumed to exist at the midplane and $[0/\theta]$ interface at the center of the composite. The material used is T300/5208 graphite epoxy.

The natural frequency is normalized with respect to the natural frequency of the undelaminated beam (ω_{perf}):

$$\Omega = \frac{\omega}{\omega_{perf}} \quad . \tag{5.15}$$

The first natural frequencies for undelaminated and delaminated composites are compared with respect to change in lamination angle θ in Figure 31. For all the cases considered, both delaminations are shown to remain closed during the whole period of motion. It can be seen that a delamination at the midplane has more effect on natural frequency than the one at the $[0/\theta]$ interface. It also appears that the composite with two delaminations has lower frequencies than the single delamination cases for all the

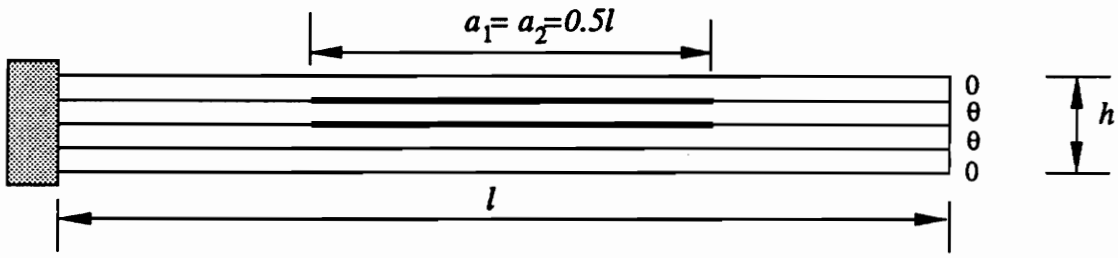

Figure 30. Geometry of a composite cantilever beam containing two delaminations

range of θ, as expected. As θ increases, the delamination effect on frequencies also increases.

5.2.2 Embedded Delamination

Vibration of a circular plate with a concentric penny-shaped delamination at midplane is studied. Thickness-to-radius ratio (h/R) is assumed to be 1/10, and the material is isotropic with $\nu = 0.3$. In Figure 32, the first natural frequency is demonstrated with respect to delamination size for clamped and simply-supported boundary conditions. The natural frequencies being considered in Figure 32 are normalized as

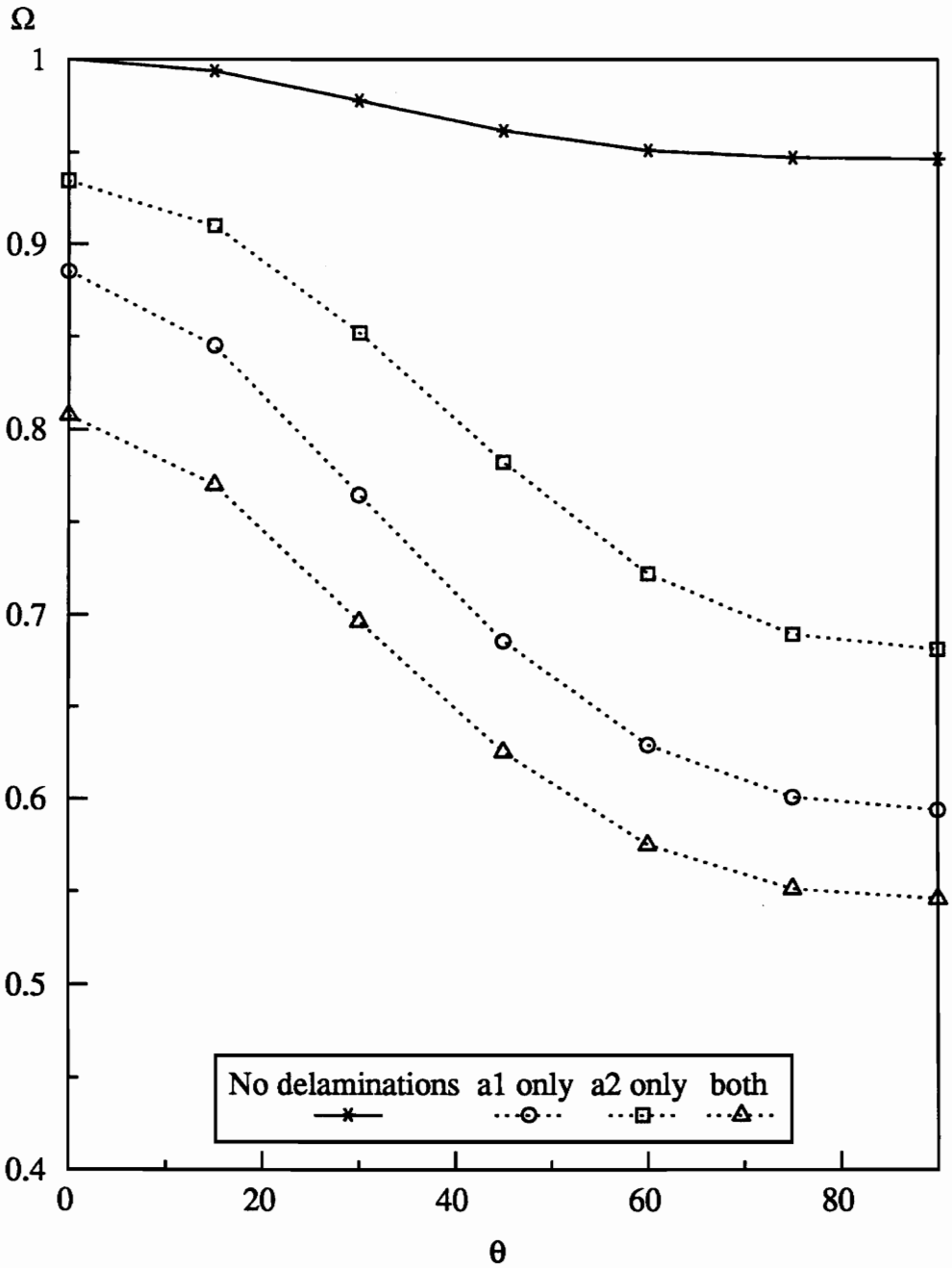

Figure 31. Natural frequencies vs. fiber angle for $[0/\theta]_S$ composites containing one and two delaminations with $\bar{a}_1 = \bar{a}_2 = 0.5$

$$\Omega = \frac{\omega}{R^2}\sqrt{\frac{D_r}{\rho}} \quad . \tag{5.16}$$

It should be noted that the vibration mode shape for the first frequency is always the global mode with a delamination completely closed for both boundary conditions. Therefore, the vibration mode shape obtained is physically admissible during the motion of the plate. As is shown in Figure 32, the effect of delamination on the vibration frequencies of a simply-supported circular plate is almost negligible even for quite a large delamination. Referring to Figures 20 and 32, it can also be seen that the natural frequency is less sensitive to delamination than is buckling load.

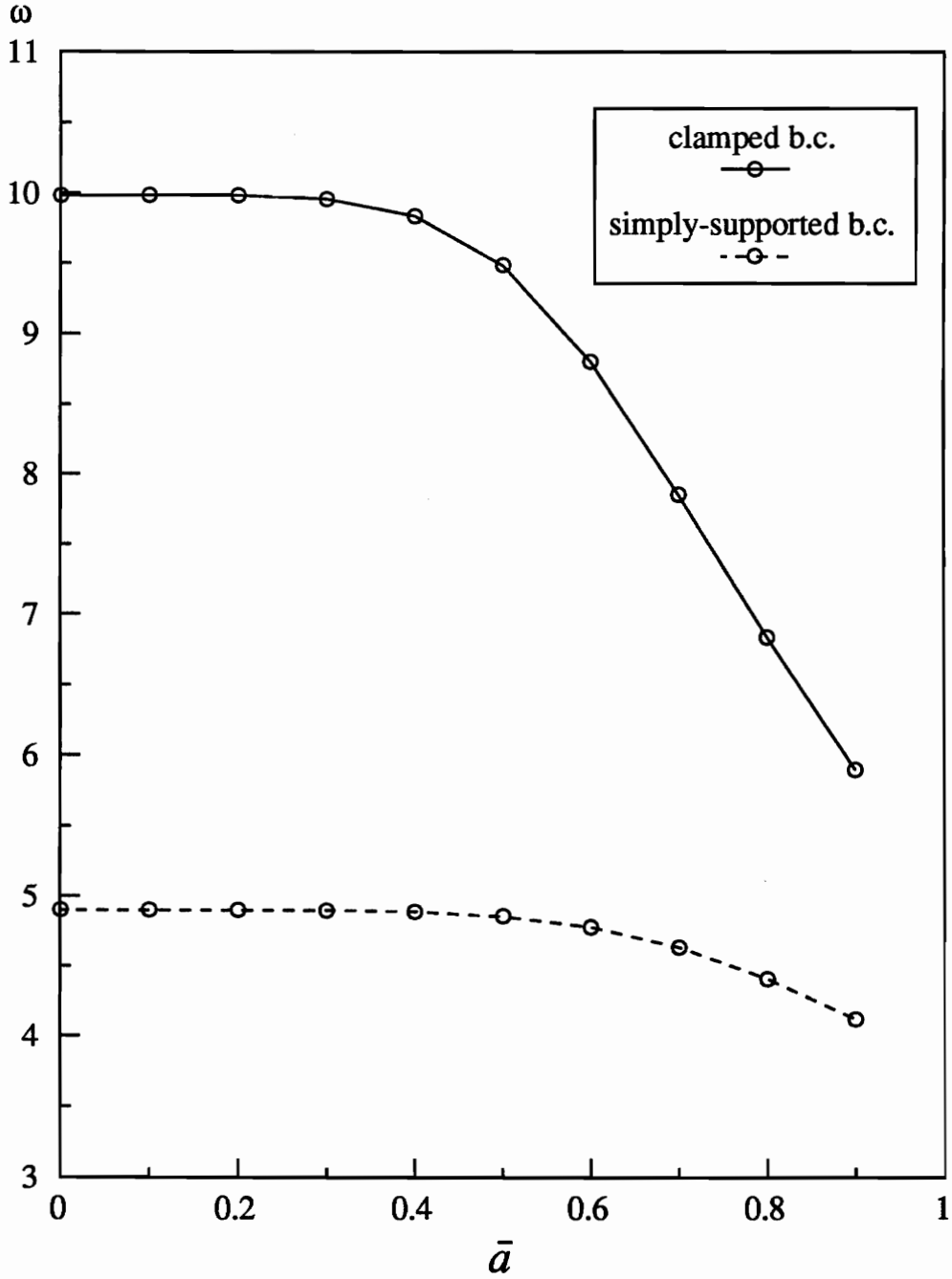

Figure 32. Natural frequencies vs. delamination radius for a circular plate containing a single midplane penny-shaped delamination

Chapter VI

BUCKLING AND POSTBUCKLING FOR THROUGH-THE-WIDTH DELAMINATIONS

In this chapter, numerical results are presented for buckling and postbuckling problems of composites with through-the-width delaminations.

Both single and multiple delamination problems are studied in the framework of eigenvalue analysis and geometric nonlinear postbuckling analysis. The effects of initial imperfections, contact condition between delaminated surfaces, and material anisotropy are investigated. The effects of configurations of delamination such as location, size, and number on the buckling and postbuckling responses of delaminated composites are also investigated qualitatively and quantitatively. Finally, a comparison between layer-wise and sublaminate theories is made with respect to accuracy and efficiency.

6.1 Single Delamination

The problem geometry is illustrated in Figure 33. For convenience, the following non-dimensional quantities are used:

$$\bar{t} = \frac{t}{h}, \quad P = \frac{p}{p_{cr}}, \quad \bar{a} = \frac{a}{l}, \tag{6.1}$$

where p is the load applied to a composite and p_{cr} is the critical buckling load of the undelaminated composite.

The material being used in this study is T300/5208 graphite/epoxy.

6.1.1 The Effects of Initial Imperfections and Contact Condition

A specially orthotropic clamped composite laminate containing a single through-the-width delamination at its center ($e/l = 0.5$) with $\bar{t} = 0.2$ and $\bar{a} = 0.3$ is considered (Figure 33). The thickness-to-span ratio is assumed to be $h/l = 1/400$. In order to satisfy the clamped boundary conditions, the initial imperfection is taken as:

$$\begin{aligned} \xi &= \frac{1}{2} w_o h \left(1 - \cos \frac{2\pi x_1}{l} \right), \\ \bar{\xi}^i &= \frac{1}{2} \bar{w}_o^i h \left(1 - \cos \frac{2\pi \bar{x}_1^i}{a_i} \right), \end{aligned} \tag{6.2}$$

where h is the thickness, and l is the length of the plate, respectively, as shown in Figure 33. In Eq.(6.2), w_o is the fraction of initial deflection with respect to the plate thickness

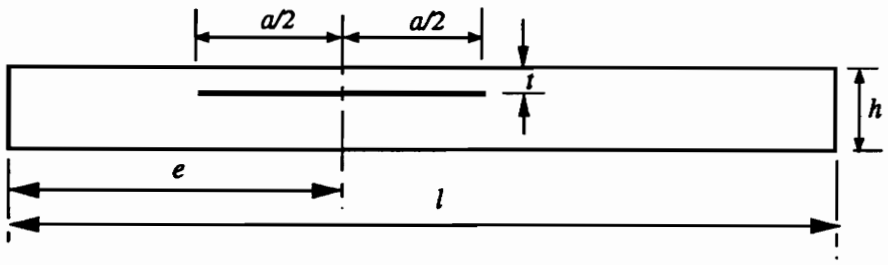

Figure 33. Geometry of a composite containing single through-the-width delamination

at the center and $\overline{w}_o^i$ is the fraction of initial opening of the ith delamination with respect to the plate thickness at the center. The global co-ordinate x_1 and the local co-ordinate $\overline{x}_1^i$ are shown in Figure 12.

Recall that ξ and $\overline{\xi}^i$ denote a globally deflected shape of the composite and a shape of delamination opening, respectively. Note that the initial imperfections exactly satisfy the clamped boundary condition. Bifurcation analysis reveals that the nondimensional buckling load is $P = 0.436$. The first buckling mode shape for this problem is shown in Figure 34.

The postbuckling solutions for various initial imperfections are discussed in the following paragraphs. The out-of plane deflection in these discussions is normalized as $W = u_3/h$ at the center of the beam-plate.

First, the initial imperfection is assumed to be the same shape as the buckling mode. In this case, the ratio of global imperfection (w_o) with respect to the local imperfection

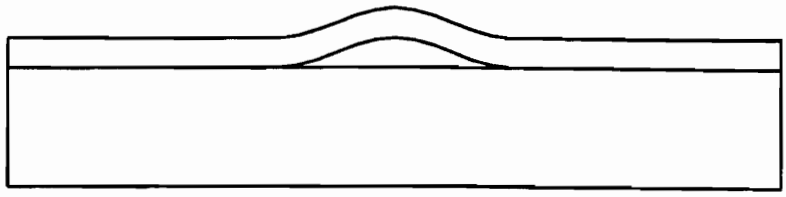

Figure 34. Buckling mode shape for $\bar{a}$ = 0.3 and $\bar{t}$ = 0.2

($\overline{w}_o^i$) is 0.008/1. In the computation, therefore, $w_o = 0.008 \times 10^{-3}$ and $\overline{w}_o^i = 1.0 \times 10^{-3}$ are used to simulate the imperfection of buckling mode shape. For all the other cases, The initial delamination opening ($\overline{w}_o^i$) is set to zero, thus only the global initial imperfection (w_o) is used.

It is seen that the curve with imperfection of buckling mode (Figure 35) is identical to that with a small positive imperfection (Figure 36). As soon as the composite reaches the buckling load ($P = 0.436$), the top thin delaminated layer starts to buckle in the positive x_3 direction because the imperfection is positive, and the bottom thick layer gradually deflects downward.

At the load level of $P = 0.7$, the deformation of the lower layer is accelerated, rendering the upper layer substantially deflected downward. Finally, the whole part of the plate loses its load-carrying capacity at $P = 0.8$. As the magnitude of the initial imperfection increases to $w_o = 0.025$ (Figure 37), the bottom layer deflects upward in a

small magnitude until $P = 0.5$, and then it starts to deflect downward. The final failure load is still the same as the one for smaller imperfection.

For $w_o = 0.035$ (Figure 38), the top layer deflects up monotonically and the bottom layer also deflects up in a small magnitude until $P = 0.6$ and suddenly deflects down around $P = 0.75$. The failure seems to occur at almost the same load level as the previous cases.

As the imperfection is increased to $w_o = 0.04$ (Figure 39), the delamination buckling load can hardly be distinguished. The top layer starts to deflect as soon as the load is applied. But, the bottom thick layer remains almost flat until the load reaches near $P = 0.8$. That is, this magnitude of initial imperfection is equivalent to the eccentricity from the local buckling of the top layer. Thus, the whole part can either deflect up or down. At increased load, the bottom part buckles downward violently at the lower level of the load than that of the smaller imperfection.

For larger magnitude of positive imperfections (Figures 40 and 41), however, the response is significantly different. The delamination buckling load is not distinguishable at all, and the composite starts to deflect upward with a delamination opening as soon as the load is applied. For $w_o = 0.1$, above the load level of $P = 0.8$, two layers overlap each other (Figure 40) suggesting that the necessity of contact condition. For this reason, the load-deflection curve is redrawn with contact condition for this problem (Figure 41). Figure 41 shows that contact occurs between two layers above the load level of $P = 0.8$, as expected.

In order to investigate this contact effect more rigorously, relatively small and large negative initial imperfections ($w_o = -0.001, -0.1$) are considered. The load-deflection curves for $w_o = -0.001$ are shown in Figure 42 for the analyses with and without contact condition. For the case without contact condition, since the top layer has larger negative displacement compared to the bottom layer, it penetrates the lower part above the

buckling load level. Sheinman et al. [41] obtained this physically inadmissible postbuckling deformation for a delaminated beam, and explained that local buckling cannot occur for this deformation process. However, when the contact condition is imposed on the problem, the postbuckling response is surprisingly different from the one without contact. Until the buckling load, both parts contact, with negligibly small contact force. At the buckling load, the contact force is suddenly increased due to the top layer which tries to buckle down. Since the bending stiffness of the bottom layer is much higher than that of the top part, the bottom layer does not deflect, but the contact force generated from these two layers pushes the top layer back upward substantially. First they seem to stay together, and then, the upper part buckles up due to the very small magnitude of imperfection and the global equilibrium path is the same as the case for $w_o = 0.001$.

From these observation, it can be seen that the almost flat composite ($w_o = \pm 0.001$) and the composite with imperfection of buckling mode yield identical results.

For a larger negative initial imperfection ($w_o = -0.1$) (Figure 43), the load deflection curve shows again a physically unacceptable deformed mode when the contact condition is not applied. On the other hand, the curve with contact condition shows a significantly different deformation pattern. That is, the delamination effect is negligible. The plate behaves as if there is no delamination in it. In fact, the delamination opens at the buckling load, but the opening is so small that it does not affect the global behavior of the structure. Accordingly, the failure may occur at the load level of the undelaminated plate case ($P = 1$).

The load-end shortening curve is given in Figure 44 for various initial imperfections. The end-shortening is normalized as $U = u_1/l$. It can be seen that the load-carrying capacity of the composite varies significantly depending on the magnitudes and directions

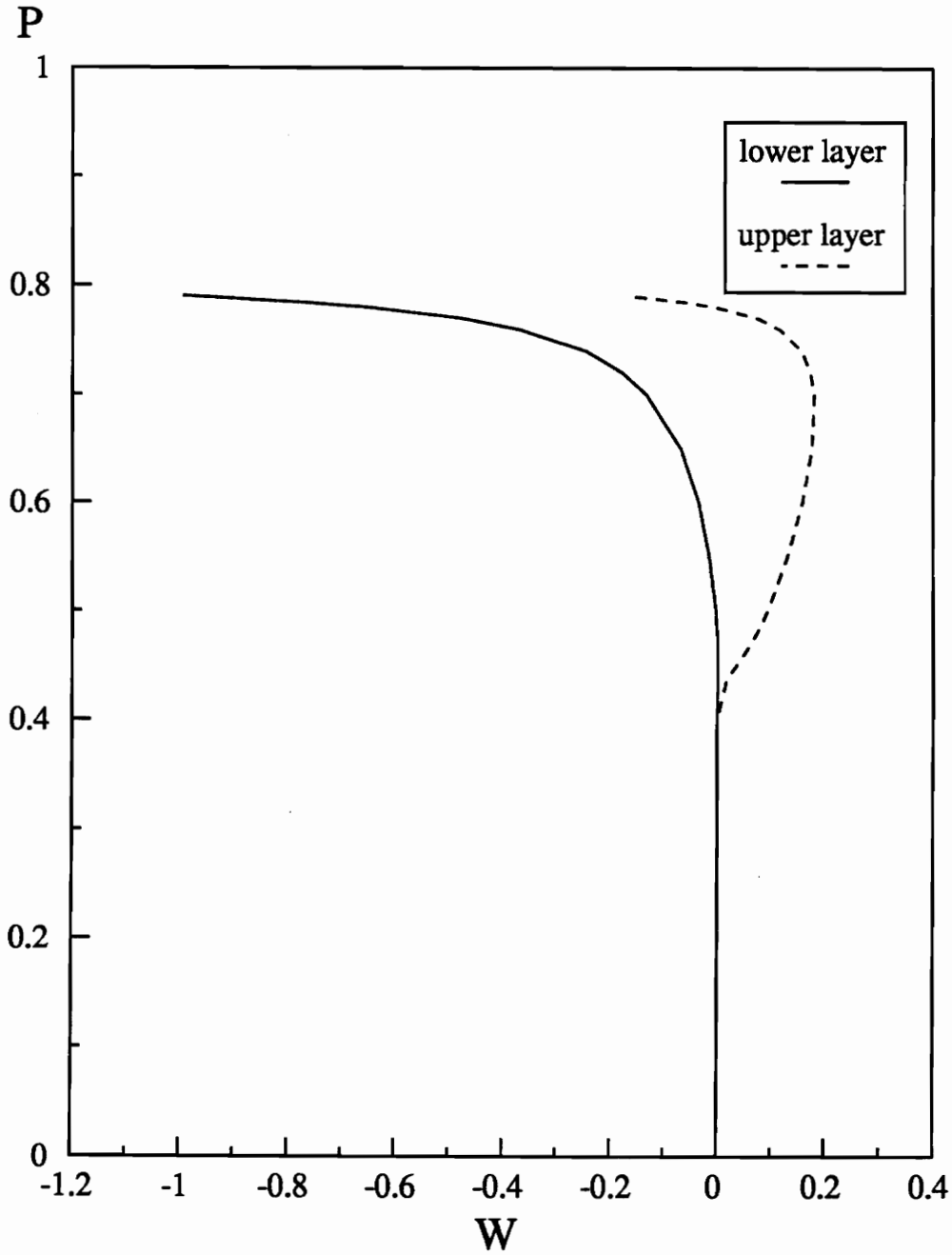

Figure 35. Load-deflection curve of a delaminated composite ($\bar{a}$ = 0.3 and $\bar{t}$ = 0.2) with imperfection of buckling mode shape

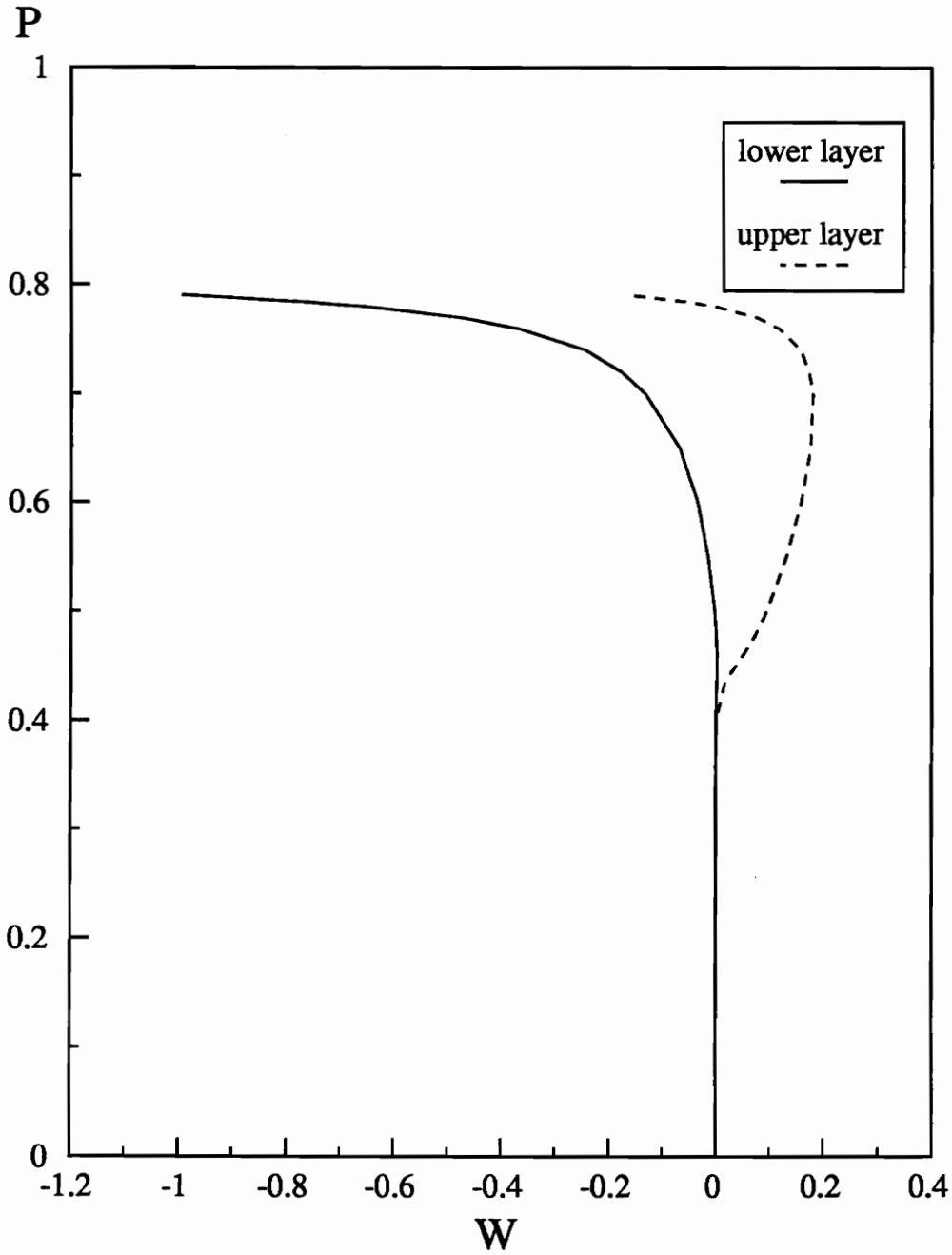

Figure 36. Load-deflection curve of a delaminated composite ($\bar{a}$ = 0.3 and $\bar{t}$ = 0.2) with imperfection of w_o = 0.001.

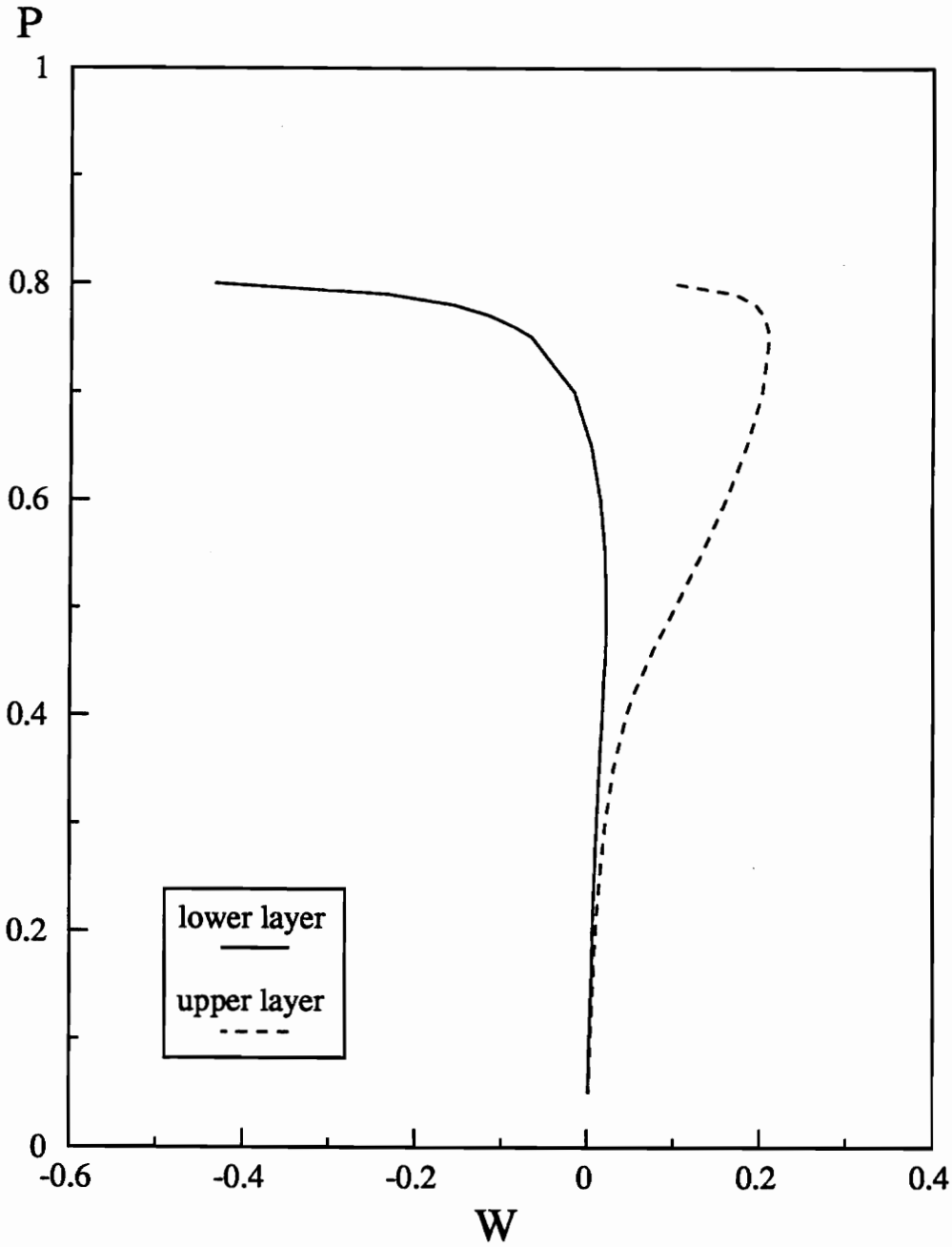

Figure 37. Load-deflection curve of a delaminated composite ($\bar{a}$ = 0.3 and $\bar{t}$ = 0.2) with imperfection of w_o = 0.025.

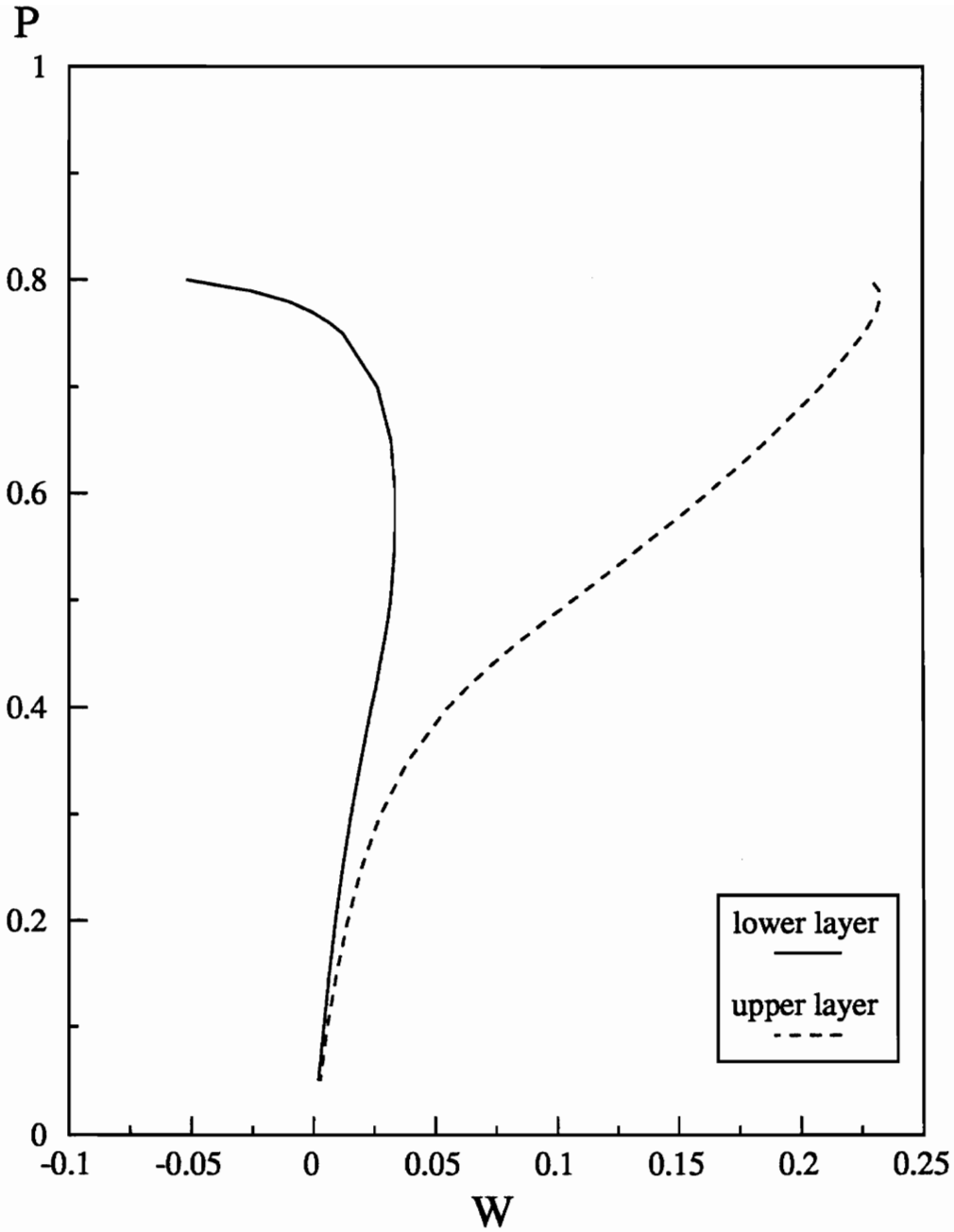

Figure 38. Load-deflection curve of a delaminated composite ($\bar{a}$ = 0.3 and $\bar{t}$ = 0.2) with imperfection of w_o = 0.035.

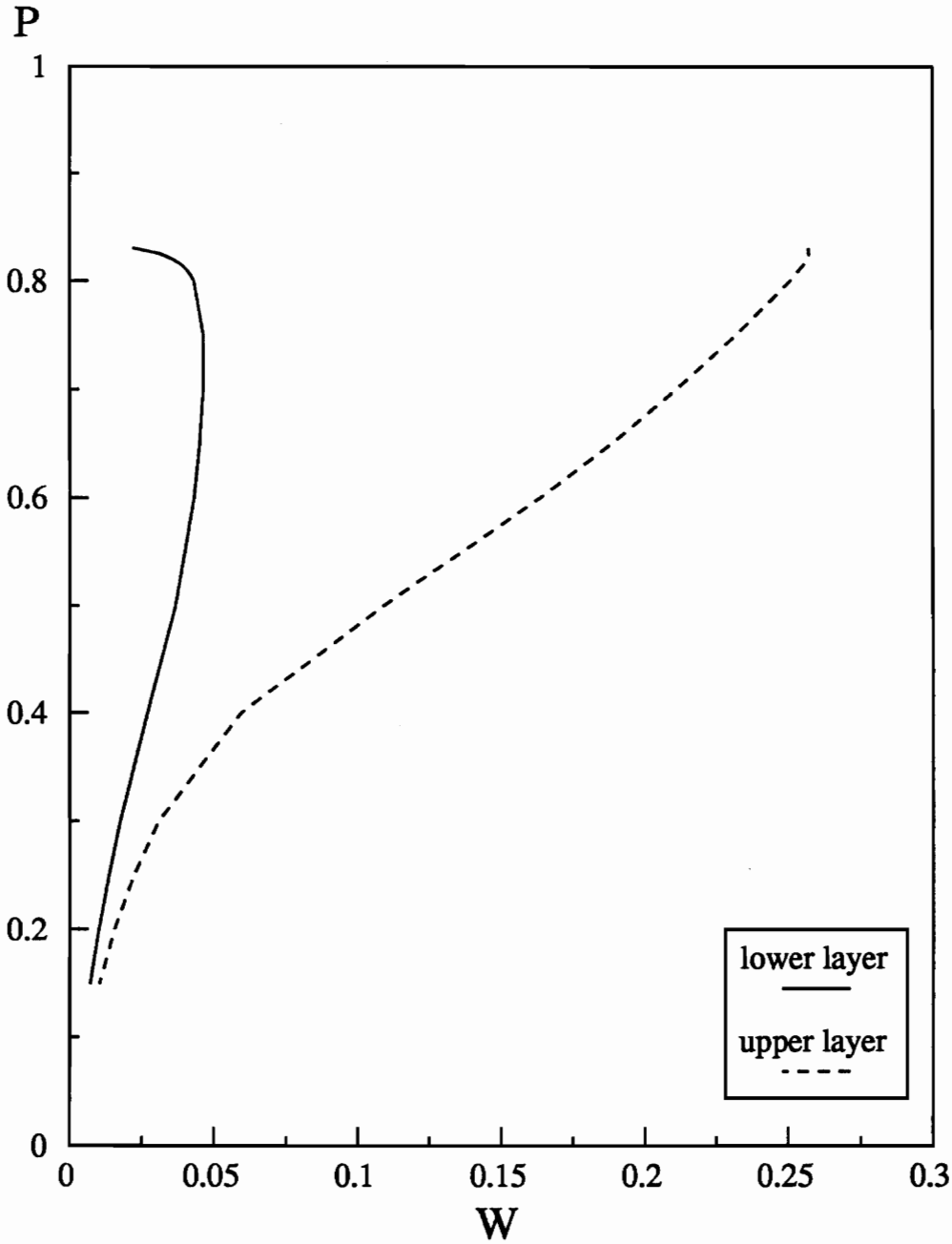

Figure 39. Load-deflection curve of a delaminated composite ($\bar{a}$ = 0.3 and $\bar{t}$ = 0.2) with imperfection of w_o = 0.04.

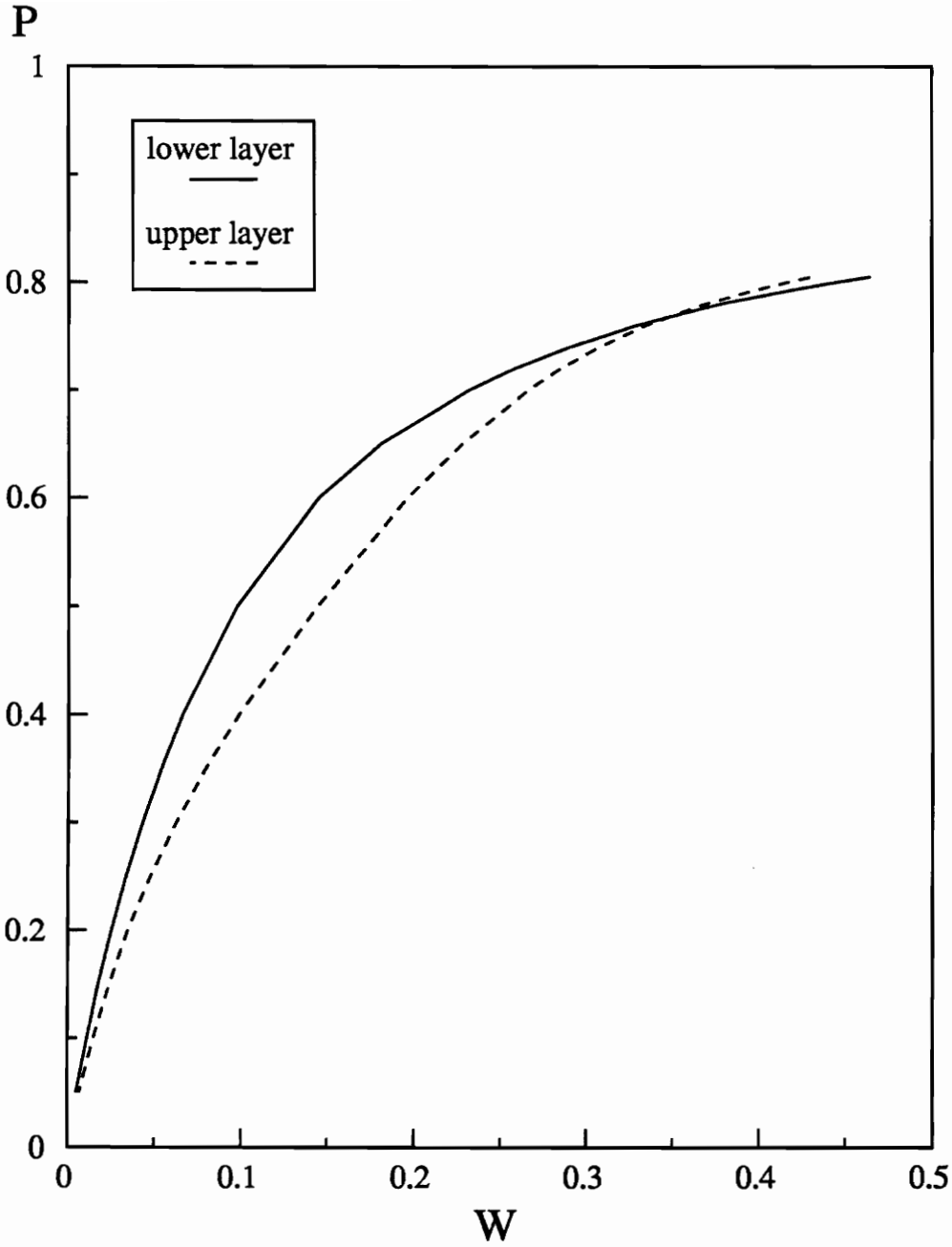

Figure 40. Load-deflection curve of a delaminated composite ($\bar{a}$ = 0.3 and $\bar{t}$ = 0.2) with imperfection of w_o = 0.1 (without contact condition)

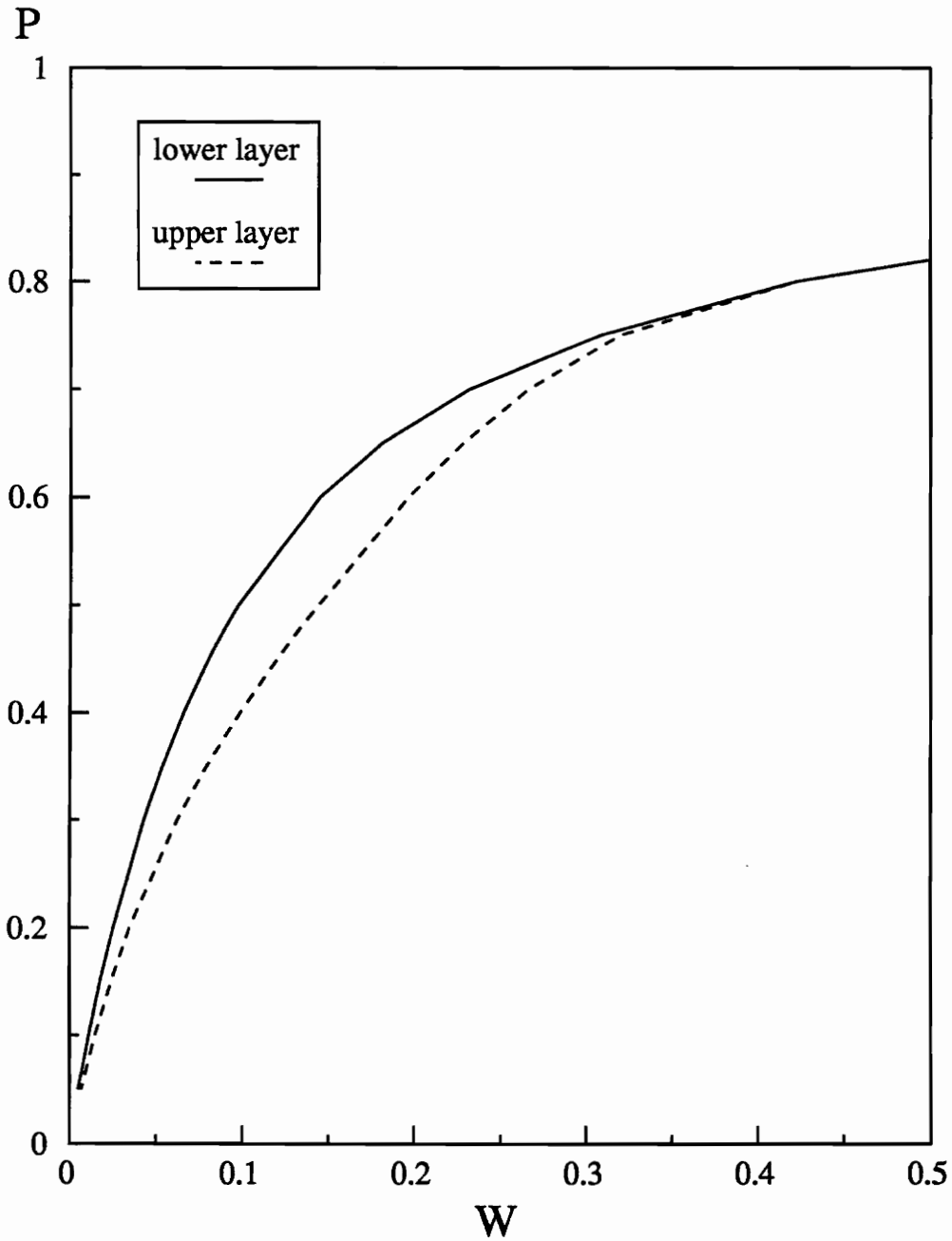

Figure 41. Load-deflection curve of a delaminated composite ($\bar{a}$ = 0.3 and $\bar{t}$ = 0.2) with imperfection of w_o = 0.1 (with contact condition)

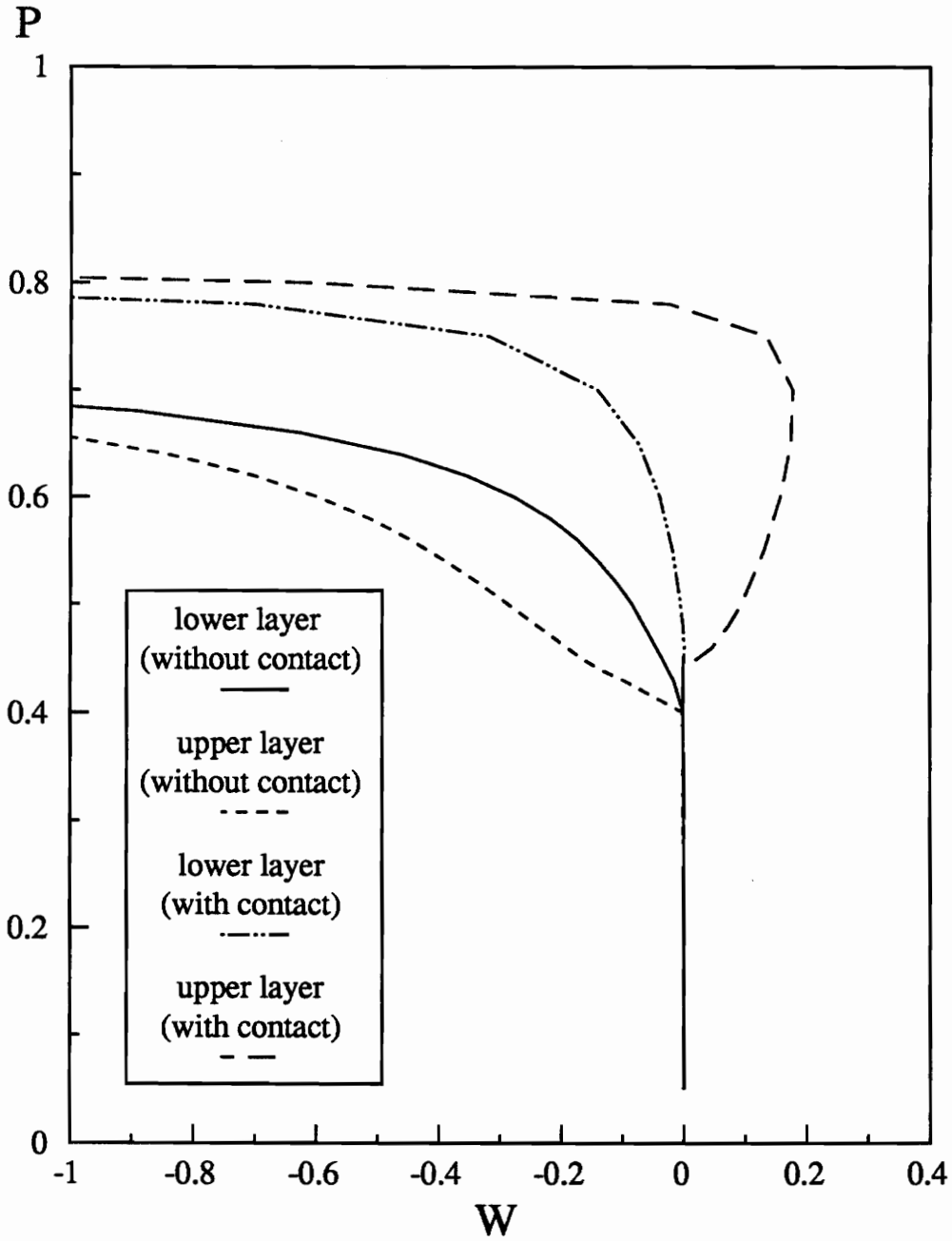

Figure 42. Load-deflection curve of a delaminated composite ($\bar{a}$ = 0.3 and $\bar{t}$ = 0.2) with imperfection of w_o = -0.001

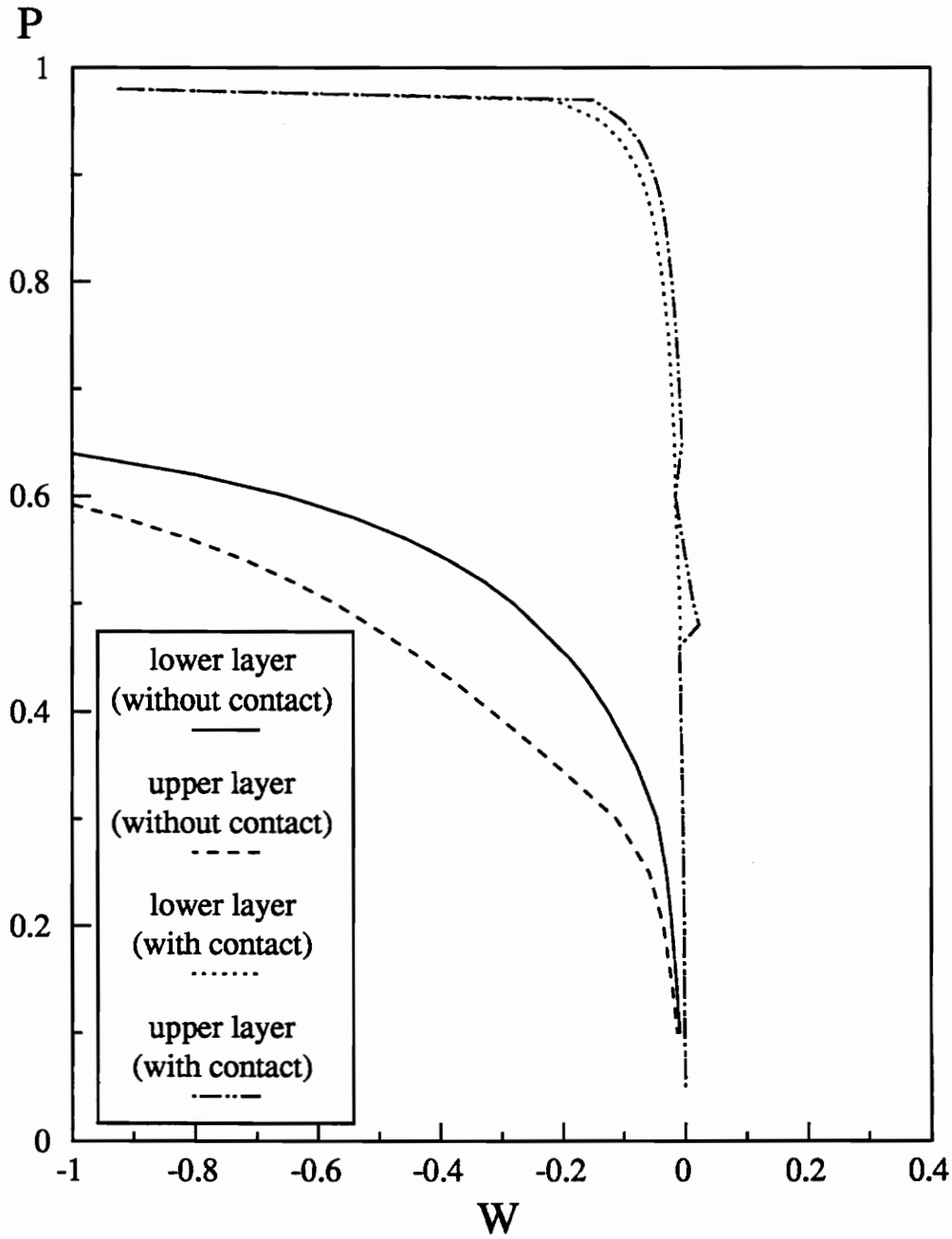

Figure 43. Load-deflection curve of a delaminated composite ($\bar{a}$ = 0.3 and $\bar{t}$ = 0.2) with imperfection of w_o = -0.1

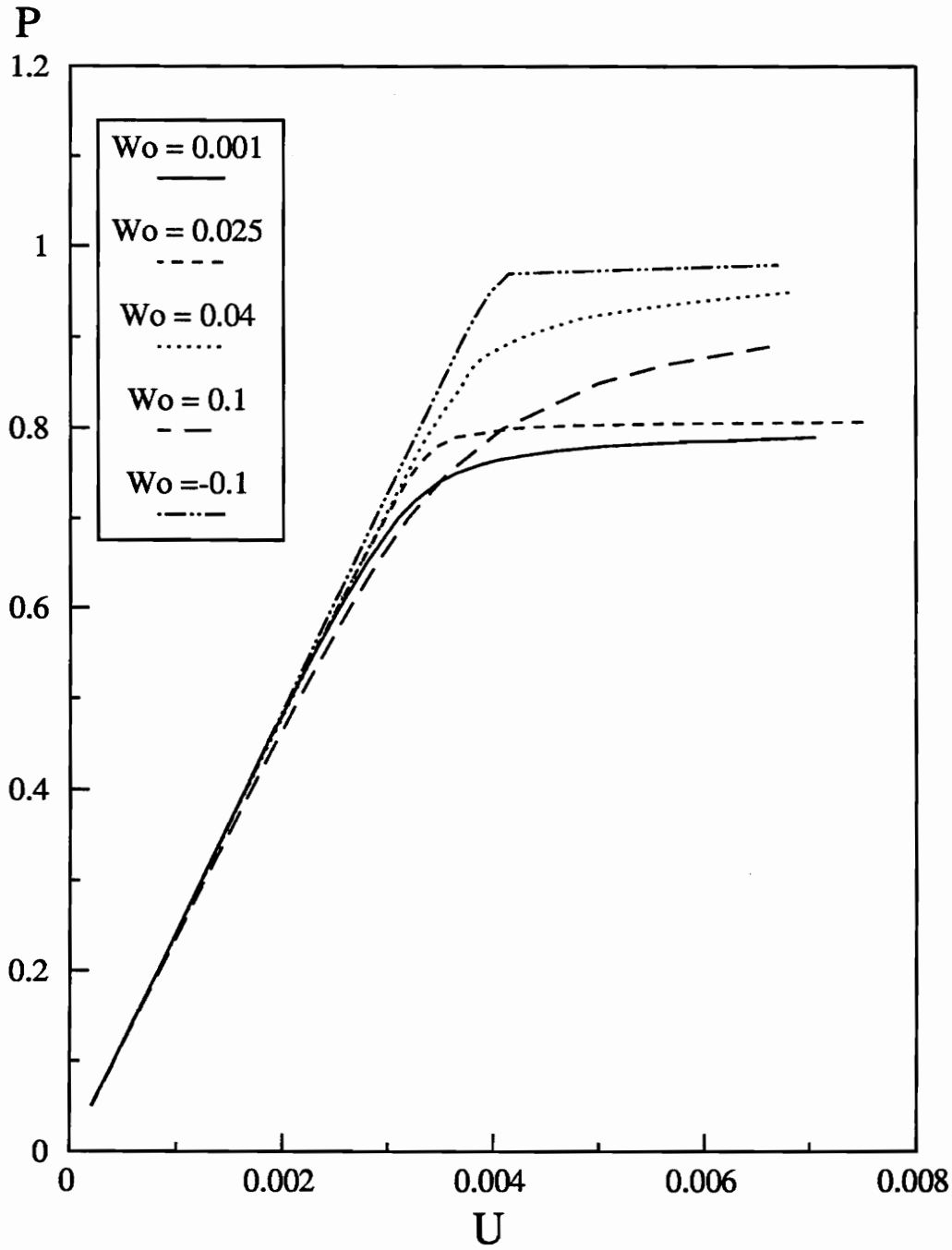

Figure 44. Load-end shortening curve of a delaminated composite ($\bar{a}$ = 0.3 and $\bar{t}$ = 0.2) for various initial imperfections.

of initial imperfections. Except the curve with $w_o = 0.1$, which did not show local buckling, the slopes of all the other curves are identical until the load reaches the local buckling load ($P = 0.436$). Above the buckling load, the composite with large negative imperfection shows sudden loss in load-carrying capacity near $P = 1$ while the composite with large positive imperfection exhibits gradual reduction in load-carrying capacity.

6.1.2 The Effects of Location and Length of Delamination

The effect of delamination location along the axial direction of the composite on the buckling load is shown in Figures 45, 46, and 47 for $\bar{a} = 0.2,\ 0.4$ and 0.6 , respectively. A midplane delamination ($\bar{t} = 0.5$) is centered at several axial locations (e) along the span (l) of the composite (Figure 33).

It is found that the local one half-wave mode is increasingly sensitive to axial delamination position as delamination length increases and the buckling load is generally lowest when the delamination lies in the center of the composite. The buckling load for the global one half-wave mode reaches its highest value when the delamination is centered. The two half-wave mode also varies with axial delamination location, but it does not exhibit a general tendency for various delamination lengths. For $\bar{a} = 0.2$, the global one half-wave mode is dominant for the entire range of e/l . However, for $\bar{a} = 0.4$ and $\bar{a} = 0.6$, the two half-wave and local one half-wave modes govern the buckling, respectively, (Figures 46 and 47) as a delamination approaches the center of the composite.

Next, the effect of through-the-thickness location of delamination on the buckling and postbuckling response is investigated for various delamination lengths ($\bar{a} = 0.3,\ 0.5,\ 0.9$). As a delamination approaches to the midplane of the composite, the buckling load increases for all the cases.

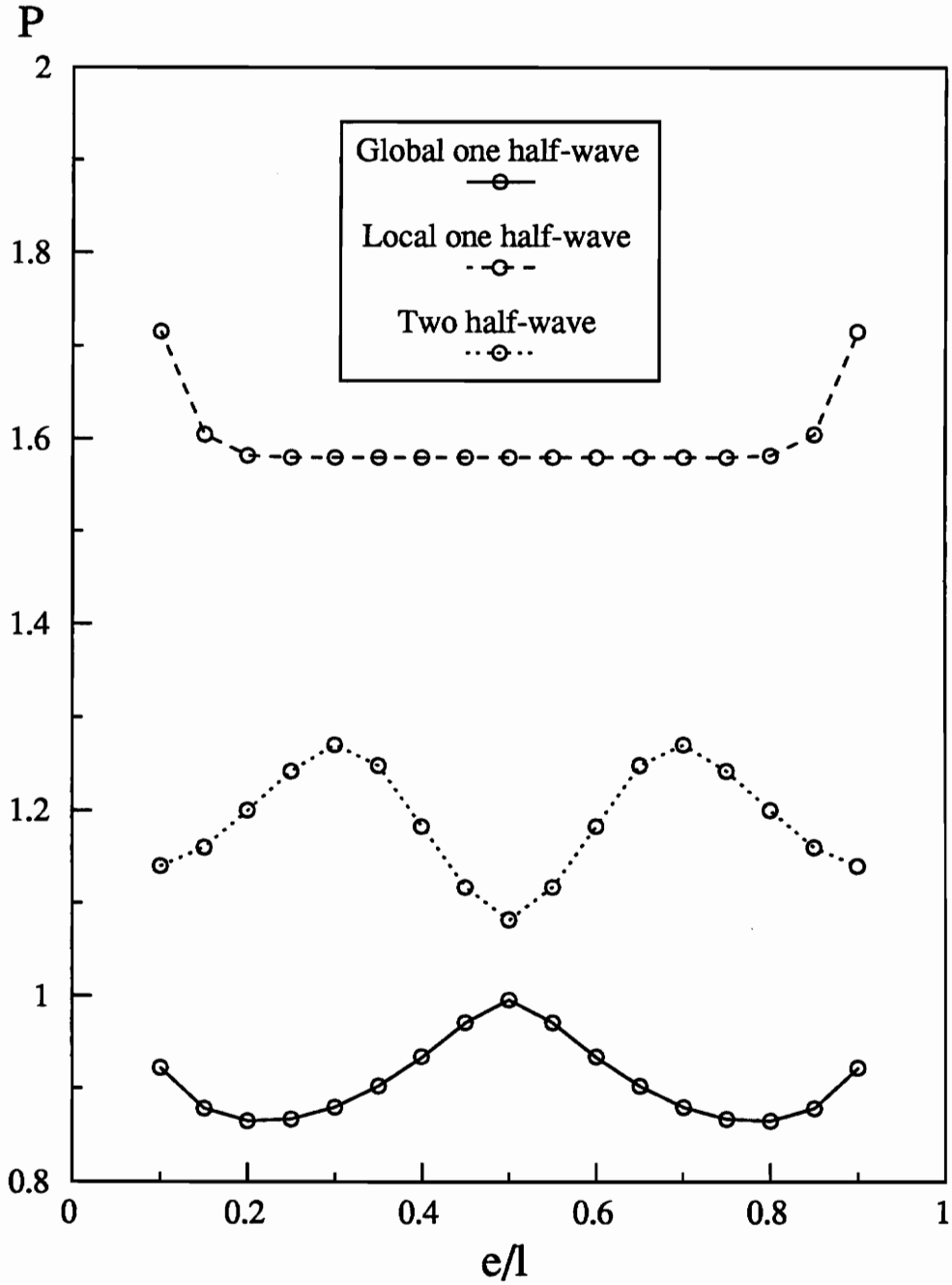

Figure 45. Effect of axial location of a delamination at midplane for $\bar{a}$ = 0.2

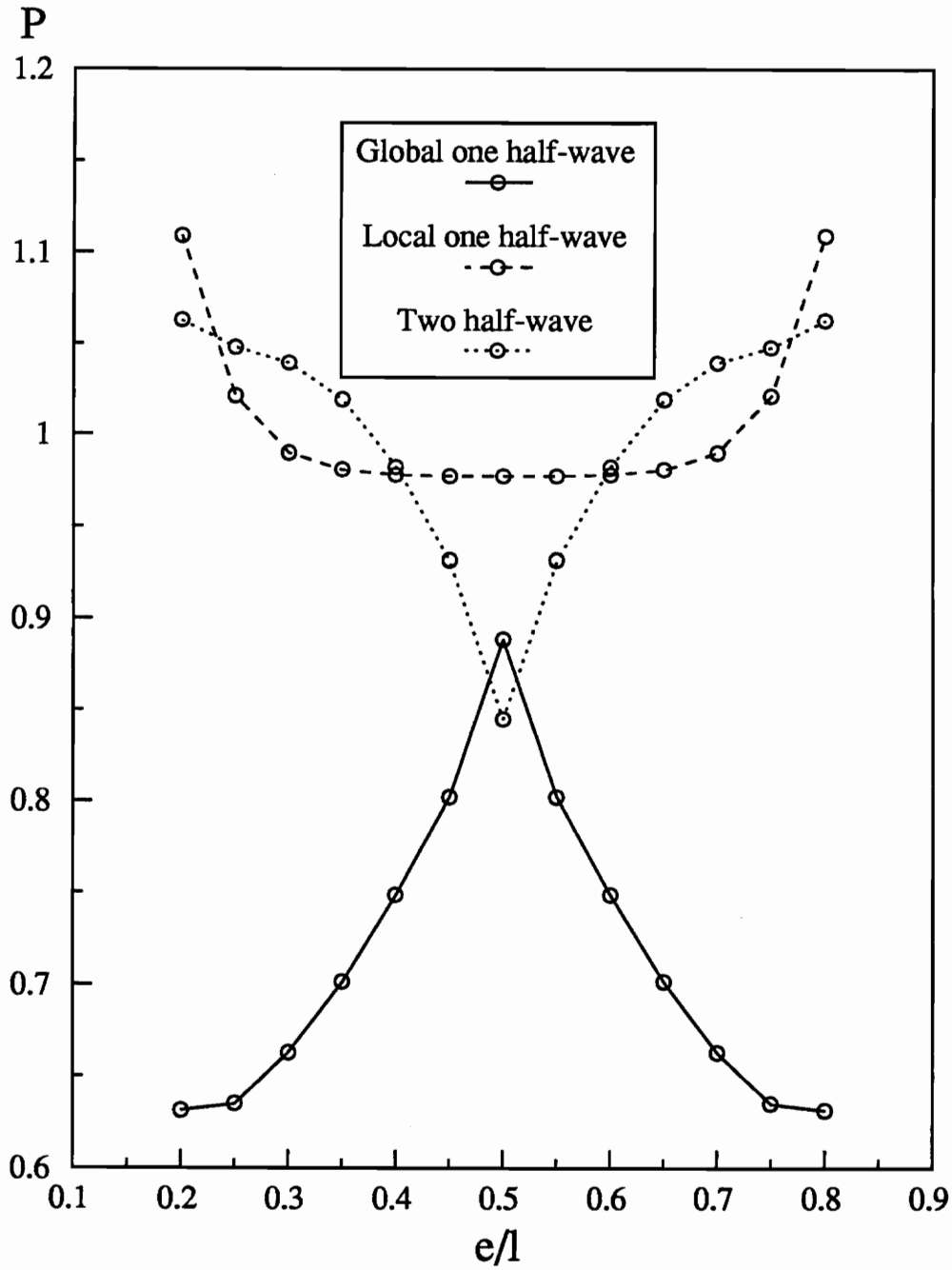

Figure 46. Effect of axial location of a delamination at midplane for $\bar{a}$ = 0.4

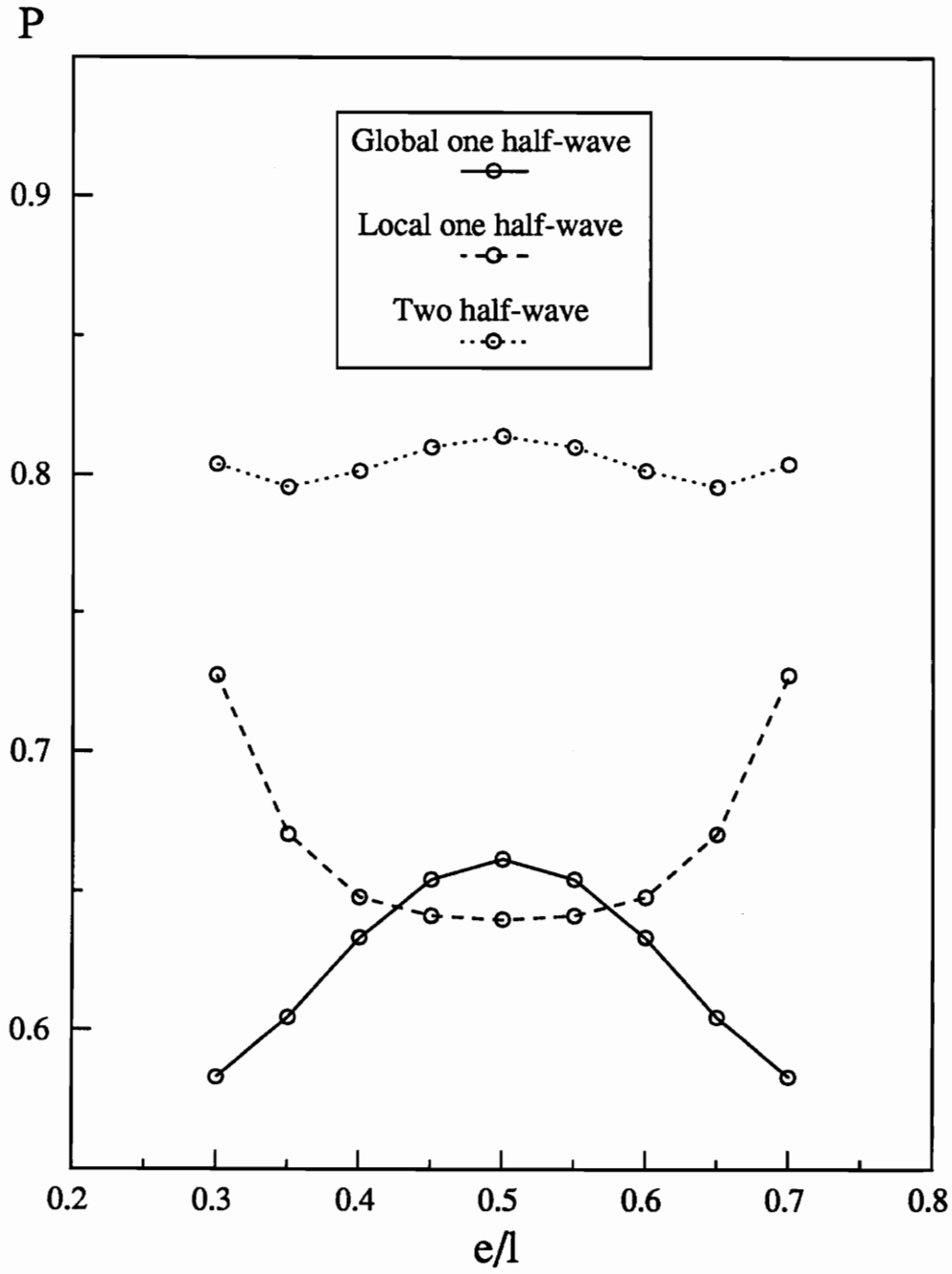

Figure 47. Effect of axial location of a delamination at midplane for $\bar{a}$ = 0.6

For $\bar{a} = 0.3$ (Figure 48), the characteristics of post-critical deformation changes from local to global buckling between $\bar{t} = 0.1$ and $\bar{t} = 0.3$, hence the ultimate load-carrying capacity for $\bar{t} = 0.3$ is larger than that of $\bar{t} = 0.1$. As the delamination comes closer to the midplane ($\bar{t} = 0.4$) the ultimate load-carrying capacity seems to be almost the same as the undelaminated case. The delamination is shown to remain closed during the postbuckling process. For $\bar{a} = 0.5$ (Figure 49), the ultimate load-carrying capacity seems to be insensitive to $\bar{t}$. The postbuckling deformation is changed from the local mode ($\bar{t} = 0.1,\ 0.3$) to the global-local mixed mode ($\bar{t} = 0.4$). For a relatively long delamination ($\bar{a} = 0.9$), as a delamination approaches the midplane, the ultimate load-carrying capacity decreases substantially (Figure 50), implying that the delamination located near the midplane is potentially more dangerous than the near-the-surface one.

It is seen that the global structure can still carry the load although local buckling occurs, especially for a near-the-surface delamination. As a delamination approaches the midplane of the composite, the range between the local and global bifurcation points reduces gradually, suggesting that the postbuckling response changes from local to global deformation.

6.1.3 The Effect of Anisotropy

Even an initially symmetric laminate can be locally unsymmetric when it contains a delamination, and may thus exhibit bending-extension coupling. In this example, this bending-extension coupling effect is studied for [0/90/90//0], [90/0/0//90] and [90/0/0//0] simply-supported cross-ply laminates as shown in Figure 51. Here, // denotes an interface where a delamination lies. The thickness-to-span ratio is assumed to be 1/10, and three delamination lengths $\bar{a} = 0.3, 0.5, 0.8$ are considered.

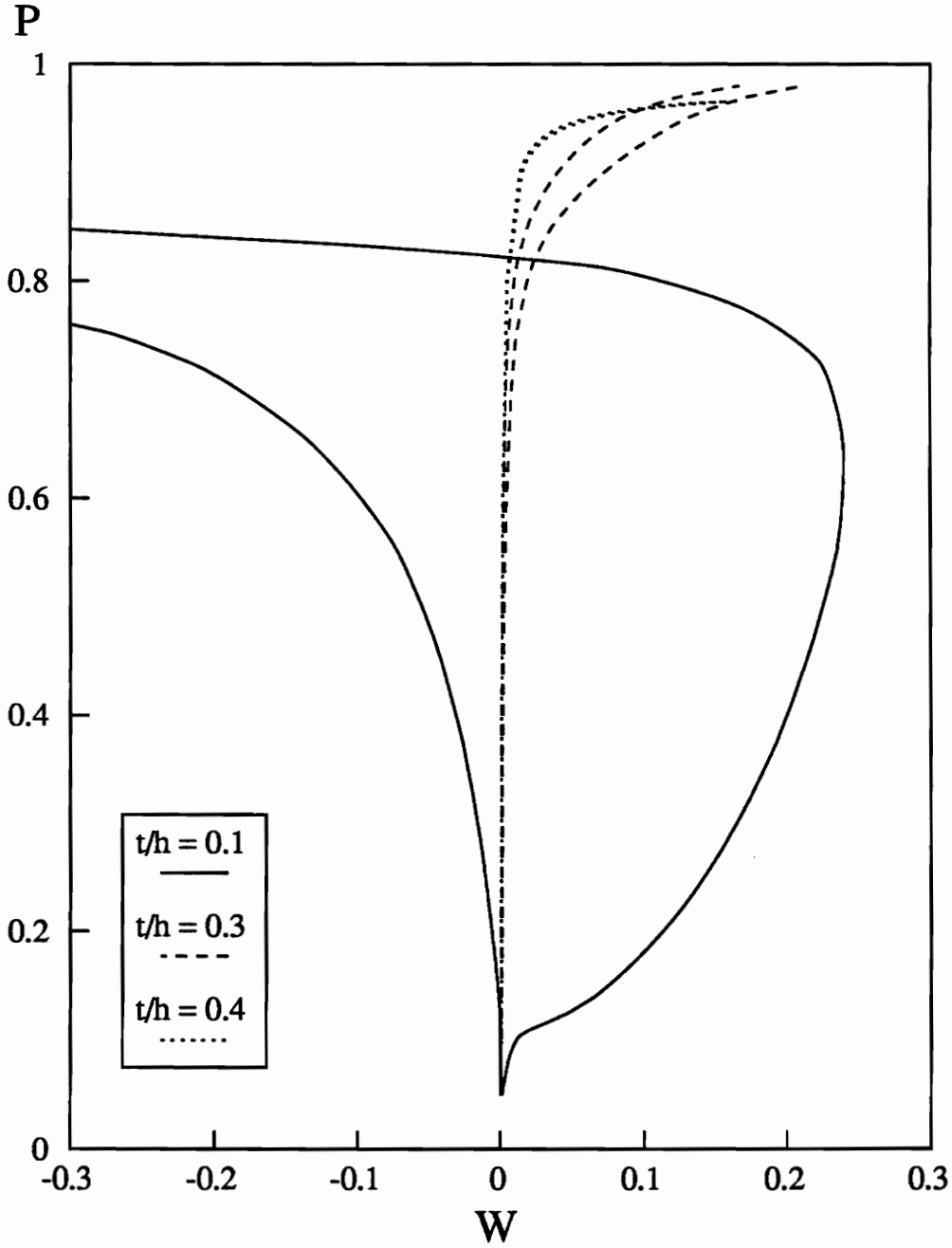

Figure 48. Load-deflection curve of a delaminated composite with $\bar{a}$ = 0.3 for various through-the-thickness location of delaminations ($\bar{t}$)

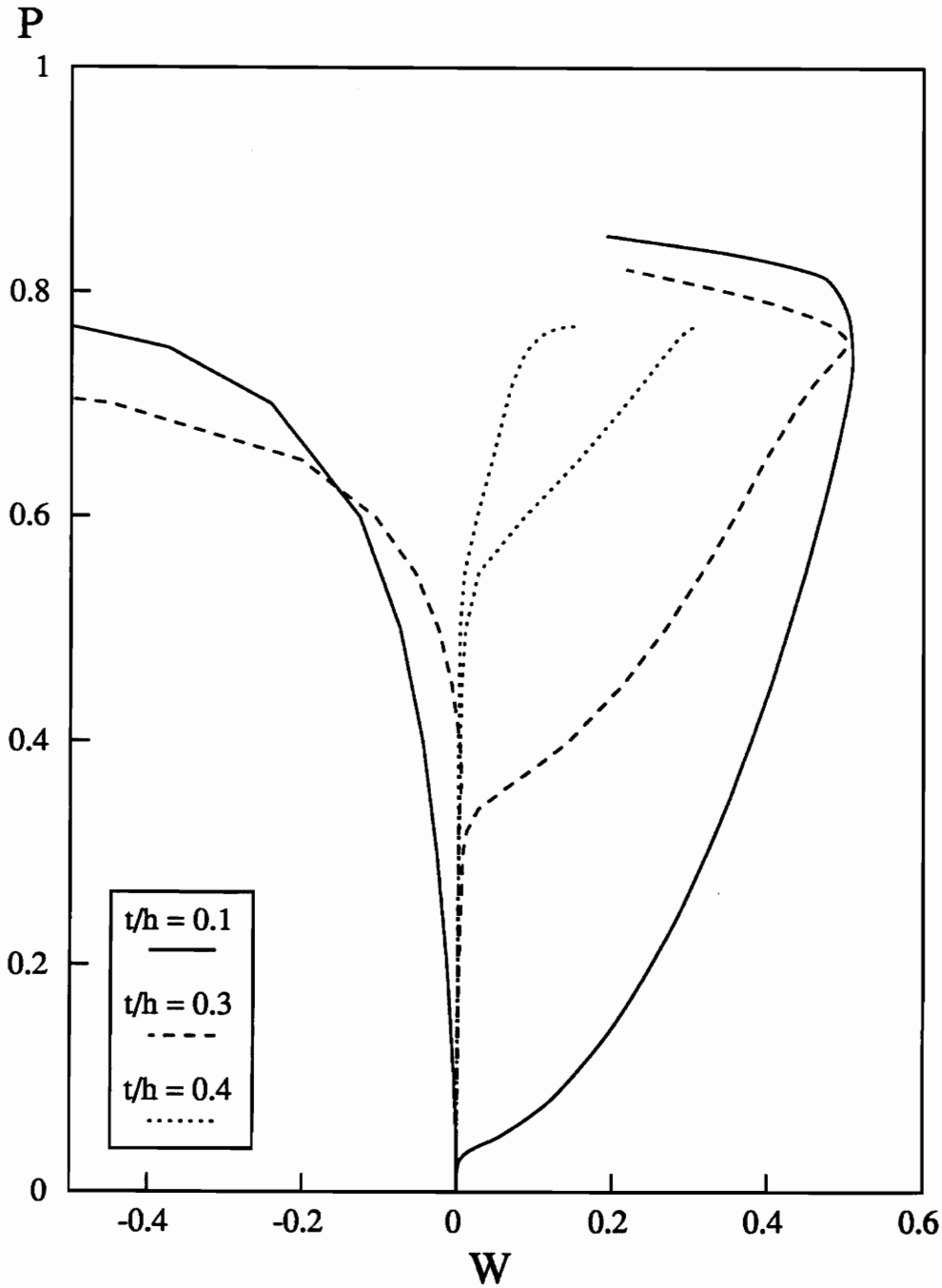

Figure 49. Load-deflection curve of a delaminated composite with $\bar{a}$ = 0.5 for various through-the-thickness location of delaminations ($\bar{t}$)

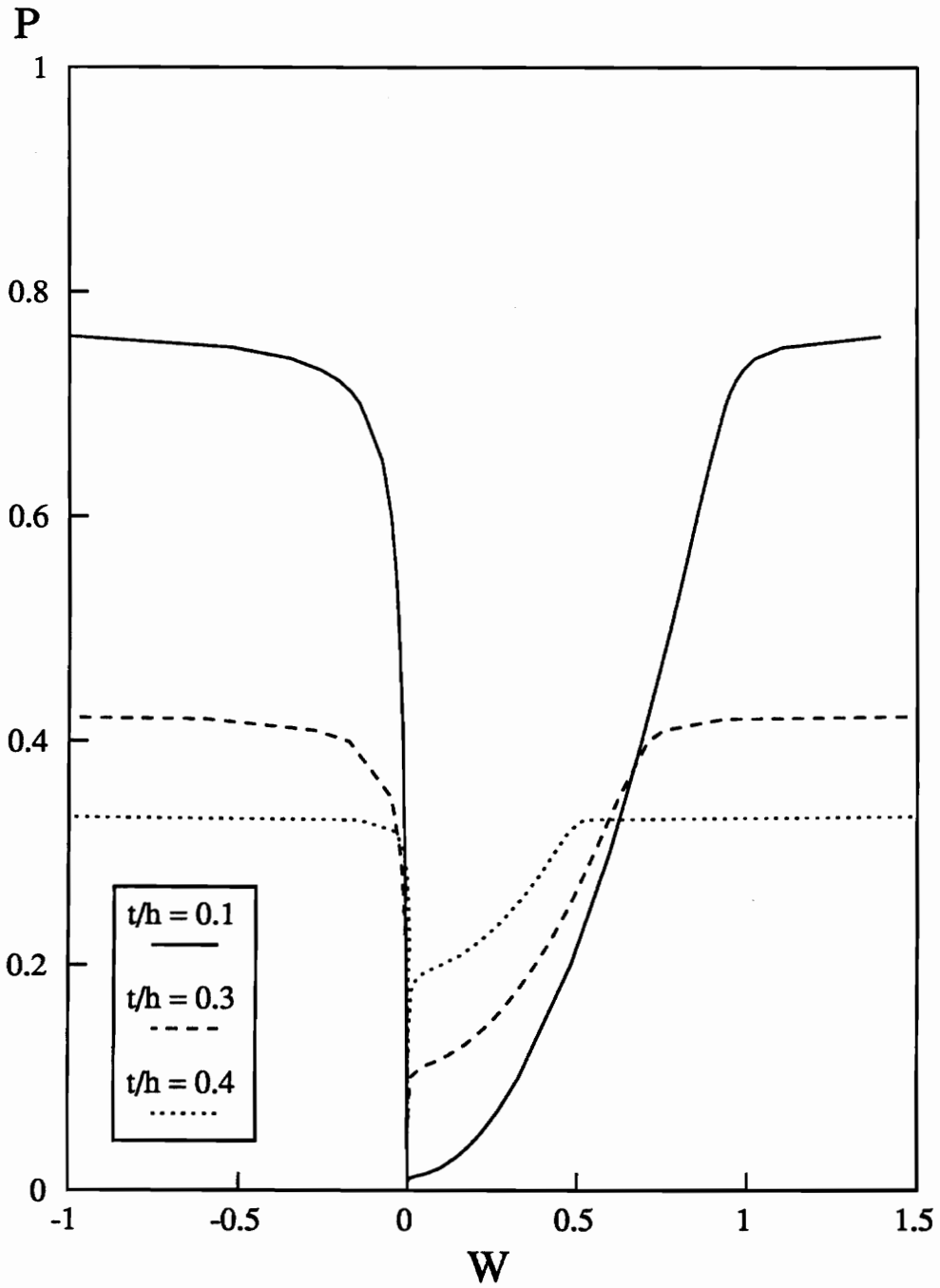

Figure 50. Load-deflection curve of a delaminated composite with $\bar{a}$ = 0.9 for various through-the-thickness location of delaminations ($\bar{t}$)

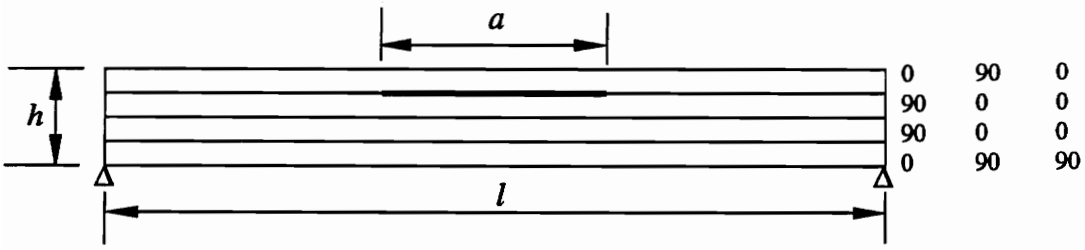

Figure 51. Geometry of simply-supported cross-ply laminates containing a delamination between 3rd and 4th layers.

It is noted that initial imperfection is not required to initiate the postbuckling deformation for simply-supported boundary condition, because a delamination itself can be considered as an imperfection. As a result, no initial imperfection is used in this analysis. The out-of plane deflection considered in Figures 52 - 54 is normalized by $W = u_3/h$ at the center of the composite.

The horizontal lines in Figures 52 and 53 indicate calculated buckling loads from bifurcation analysis for each delamination length. Load-deflection curves are demonstrated for the [0/90/90//0] laminate in Figure 52. For all delamination lengths, the bottom sublaminate tends to deflect downward immediately due to bending-extension coupling. But for $\bar{a} = 0.3$, the debonded region is relatively small compared with the whole length of the composite, thus the coupling effect is negligible. However, for $\bar{a} = 0.5$ and 0.8, the laminate loses its load-carrying capacity well below the predicted

buckling load due to the coupling, and the delamination opens rapidly at load levels well below the buckling load.

On the other hand, for the [90/0/0//90] laminate, the bottom sublaminate tends to deflect upward, due to the bending-extension coupling with load applied (Figure 53). At the same time, the compliant top layer can hardly carry the load, resulting in the eccentricity which causes the bottom part to buckle downward.

These two effects balance each other, and the structure remains straight with a very small delamination opening until the buckling load level of the undelaminated plate regardless the delamination length. It is shown that the predicted buckling load significantly underestimates the global buckling of the structure. That is, in this case, the bending-extension coupling is shown to have a stabilization effect on the buckling of a delaminated composite, contrary to conclusions of other investigators [40,41,48].

The significant disagreements of buckling loads between the eigenvalue and postbuckling analyses come from the fact that the prebuckling effects are neglected in the eigenvalue analysis.

As another case, the delaminated upper part is replaced with a stiff layer (0 °). The load-deflection curves are plotted for delaminated and undelaminated composites in Figure 54. The delamination always remains closed during the whole process of postbuckling deformation for all the delamination lengths considered. This is because the lower part deflects upward just as in (90/0/0//90), but the hard upper layer does not buckle first. Accordingly, there is a perfect contact between the top and the bottom parts, and the existence of delamination hardly affect the global structural behavior. The whole structure starts to deflect due to global bending-extension coupling with load applied as shown in Figure 54.

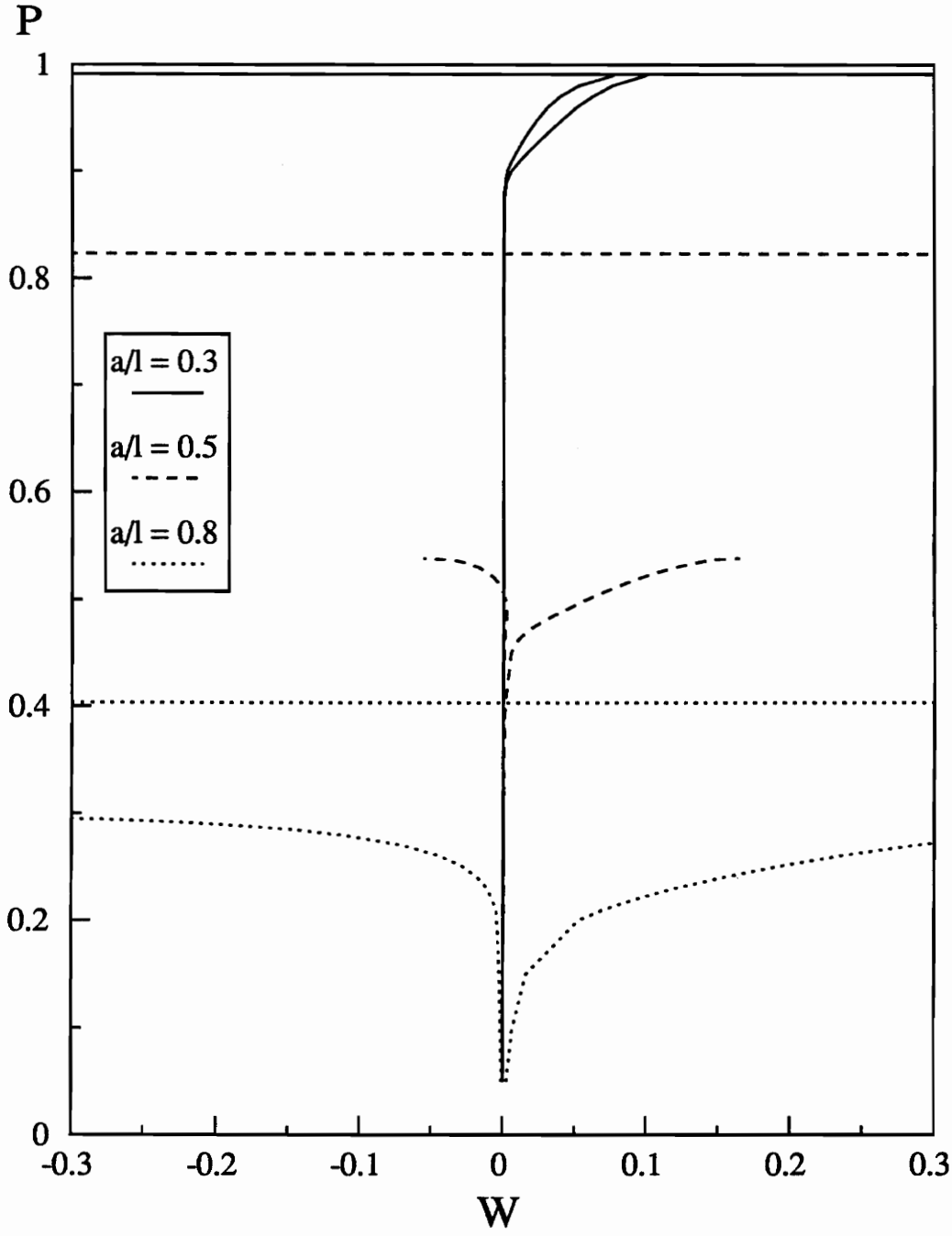

Figure 52. Load-deflection curve of a simply-supported [0/90/90//0] laminate with a delamination

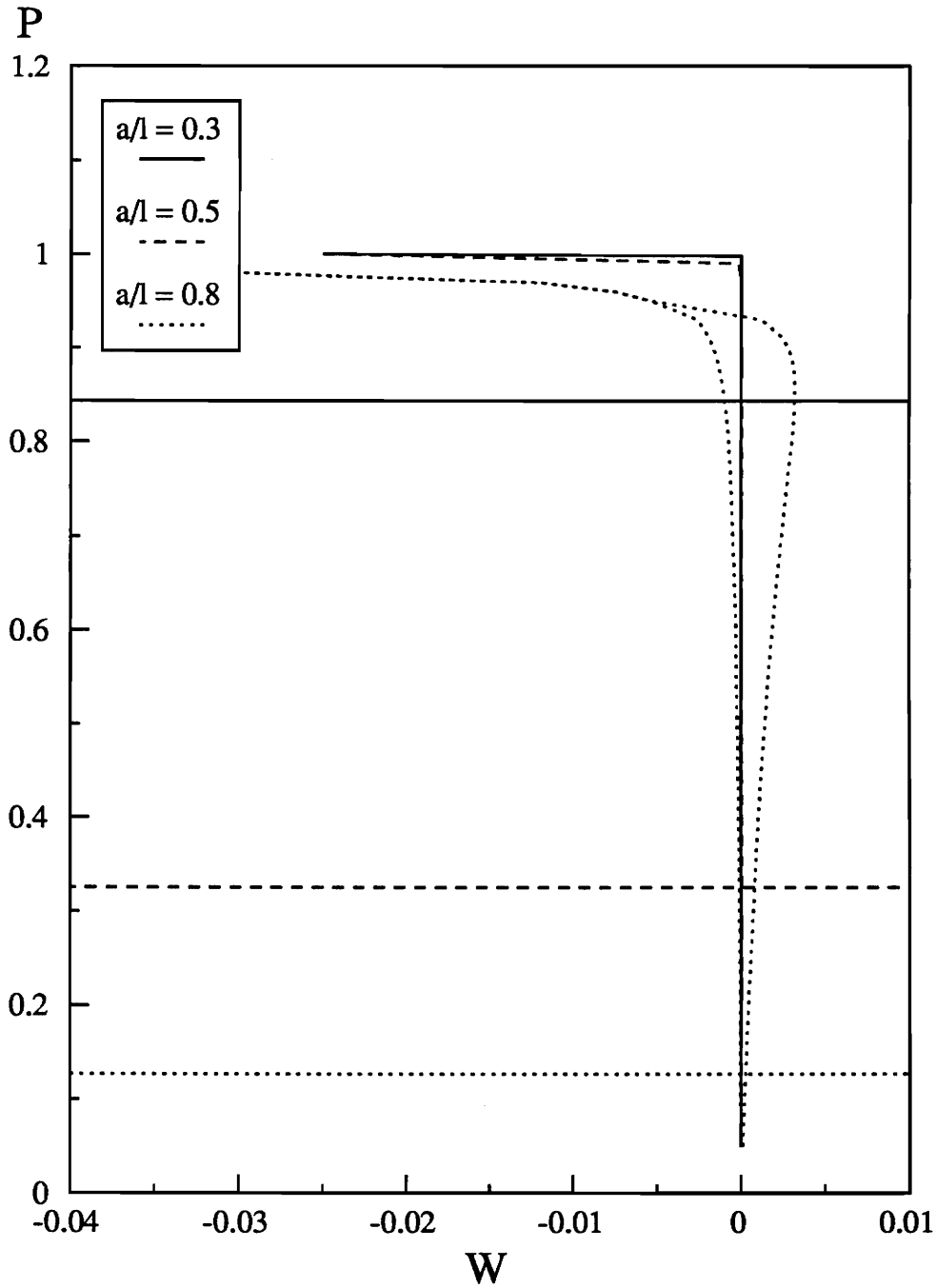

Figure 53. Load-deflection curve of a simply-supported [90/0/0//90] laminate with a delamination

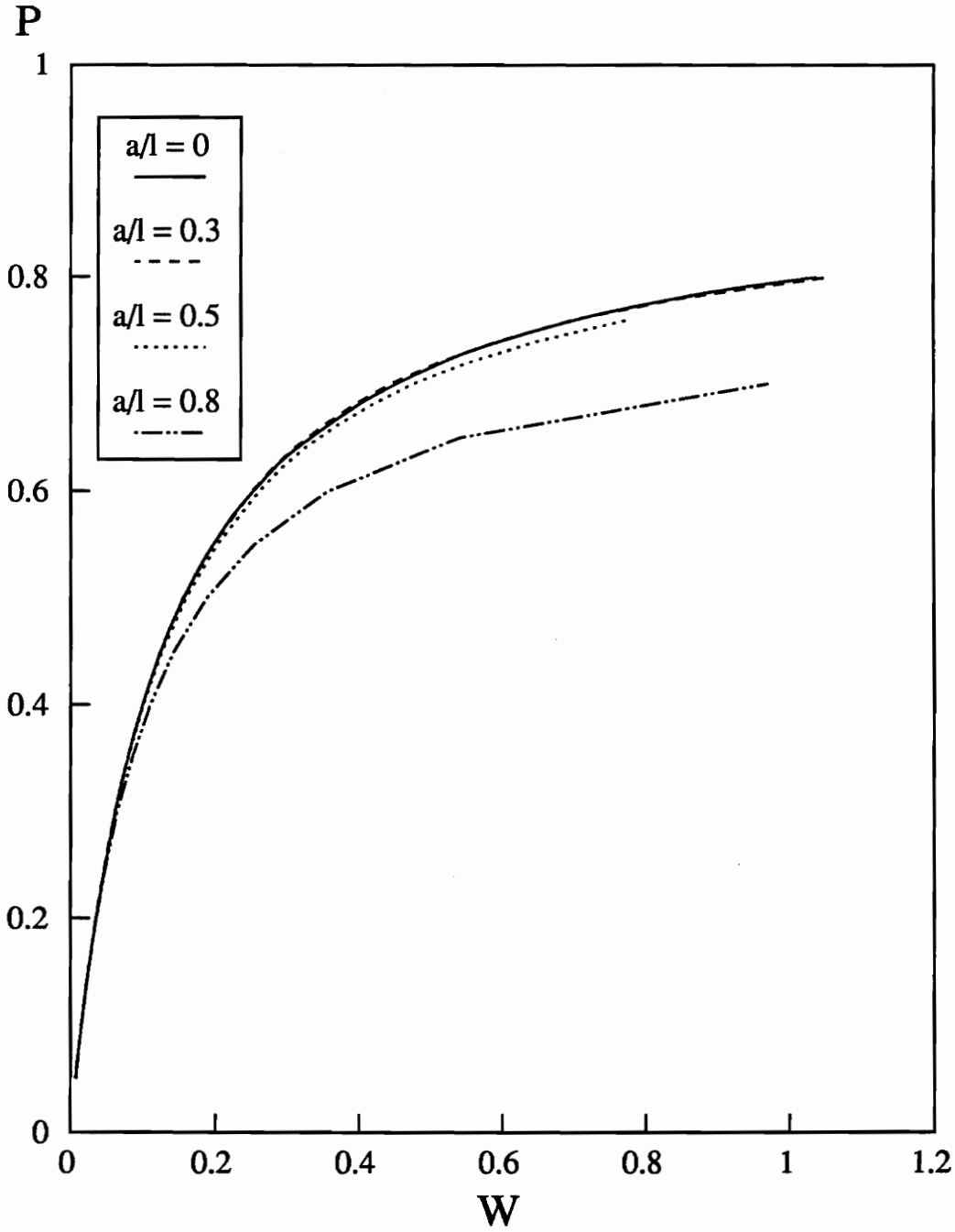

Figure 54. Load-deflection curve of a simply-supported [90/0/0//0] laminate with a delamination

6.2 Multiple Delaminations

6.2.1 Two and Three Delaminations

For comparison purpose, an example by Wang et al. [56] is reconsidered here as shown in Figure 55. This example demonstrates the effects of nondimensional delamination lengths, locations through the thickness, and number of delaminations on the buckling load. Two delaminations symmetrically located with respect to midplane, and three delaminations with an additional one at the midplane are investigated. All delaminations are assumed to have the same length.

Nondimensional parameters are defined as:

$$\bar{t} = \frac{t}{h}\ , \quad P = \frac{p}{p_{cr}}\ , \quad \bar{a} = \frac{a}{l}\ . \tag{6.3}$$

The material properties of random short-fiber SMC-R50 composite considered in this study are as follows [56]:

$$\begin{aligned} &E_{11} = 1.58\times10^{6}\text{psi} \\ &E_{22} = E_{33} = 1.1\times10^{6}\text{psi} \\ &G_{13} = 0.36\times10^{6}\text{psi} \\ &\nu_{12} = 0.31 \\ &\nu_{13} = 0.22 \end{aligned} \tag{6.4}$$

Nondimensional buckling loads versus delamination lengths are presented in Figures 56 - 61. It is assumed that the all the delamination opening displacements ($\bar{u}_3^i$) are forced to set to zero for contact constrained antisymmetric mode. In the figures, SWC, SWOC,

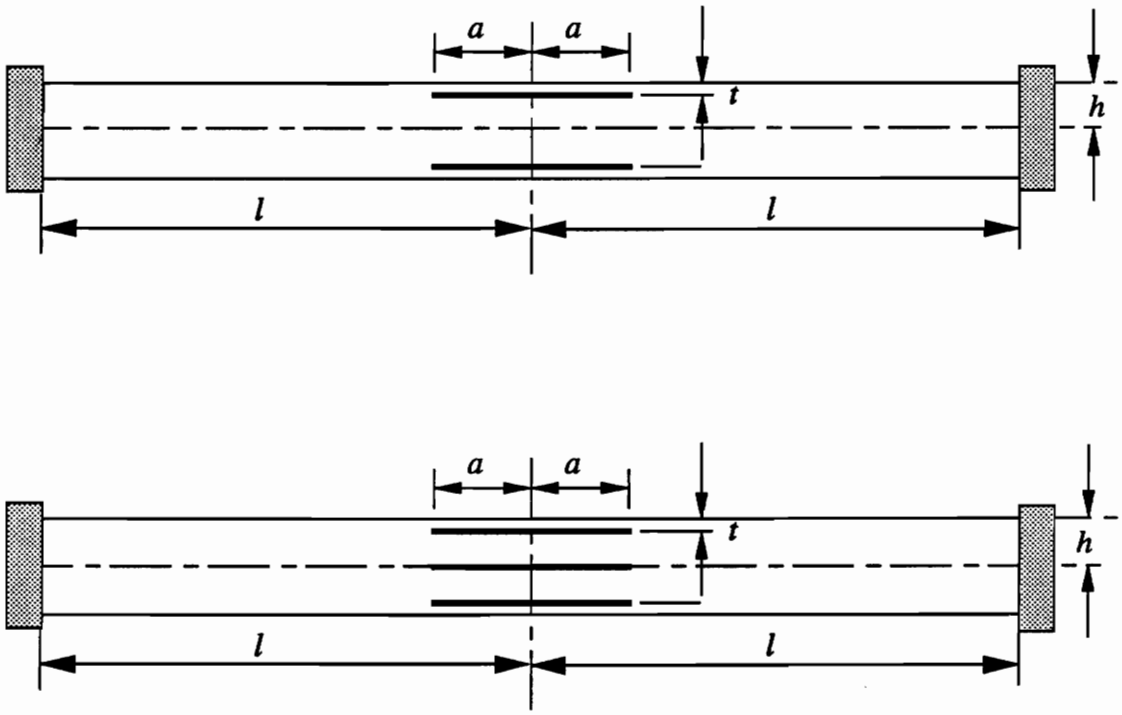

Figure 55. Geometry of two and three symmetrically located delaminations with respect to midplane

AWC, AWOC denote symmetric modes with and without contact condition and antisymmetric modes with and without contact condition, respectively.

The first symmetric and antisymmetric buckling modes are presented for the case of $\bar{t} = 0.25$ with two and three delaminations in Figures 56 and 57, respectively. In this case, the outer delaminated regions are much thinner in comparison to the inner regions for both cases. Therefore, the symmetric thin-film buckling mode is dominant for both cases and the buckling load for all the range of $\bar{a}$ does not show any differences between the two and three delamination cases. While the contact effect for the symmetric mode is negligible, the effect for the antisymmetric mode is significant. When an additional delamination is introduced at the midplane, the buckling load for the antisymmetric mode is dramatically reduced, whereas the symmetric mode hardly changes.

In the case of a composite with three delaminations of $\bar{t} = 0.5$ (Figures 58 and 59), the antisymmetric buckling mode obviously dominates bifurcation point for the range of $\bar{a} = 0.1$ to 0.4. In this case, the additional delamination has great contribution to the antisymmetric mode for relatively short delamination cracks. Consequently, the composite with an additional delamination at the midplane exhibits a much lower critical buckling load than the composite with two shorter delaminations due to the antisymmetric mode. Wang et al. [56] did not predict this antisymmetric mode because they used a symmetry assumption. It is shown that the contact effects are negligible for both modes in a composite with equidistant delaminations.

Composites with delaminations near the midplane ($\bar{t} = 0.75$) are considered in Figures 60 and 61. Both contact methods (M1, M2) described in Chapter III are used to predict buckling load for a symmetric mode. Unlike the other cases considered, the contact effects are shown to be significant for the symmetric as well as the antisymmetric mode. The buckling load without contact condition for three delaminations is the same as the one for $\bar{t} = 0.25$, because the thickness of the thinner layer is the same. However,

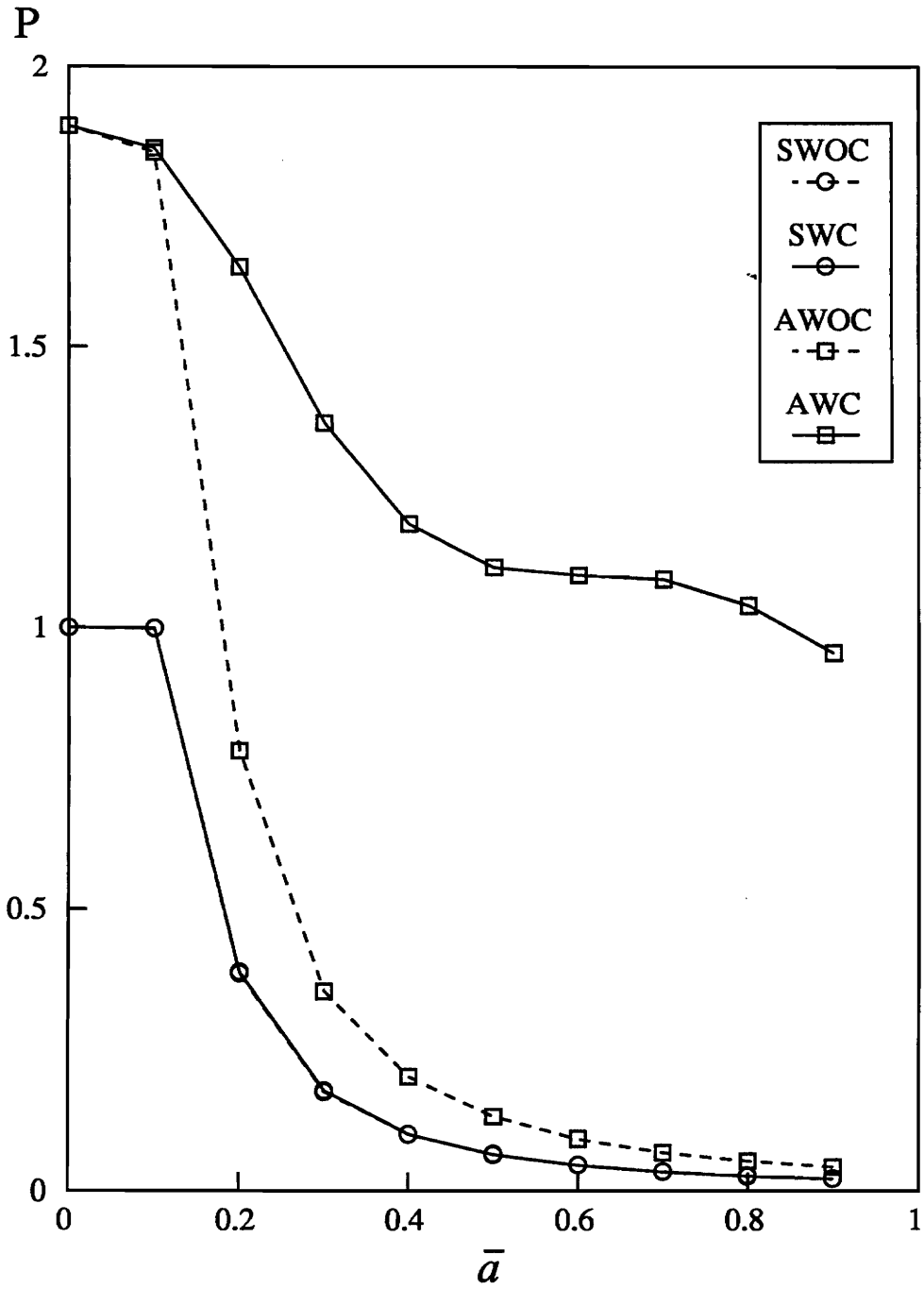

Figure 56. Buckling load vs. delamination lengths for a composite containing two delaminations for $\bar{t}$ = 0.25 with and without contact condition

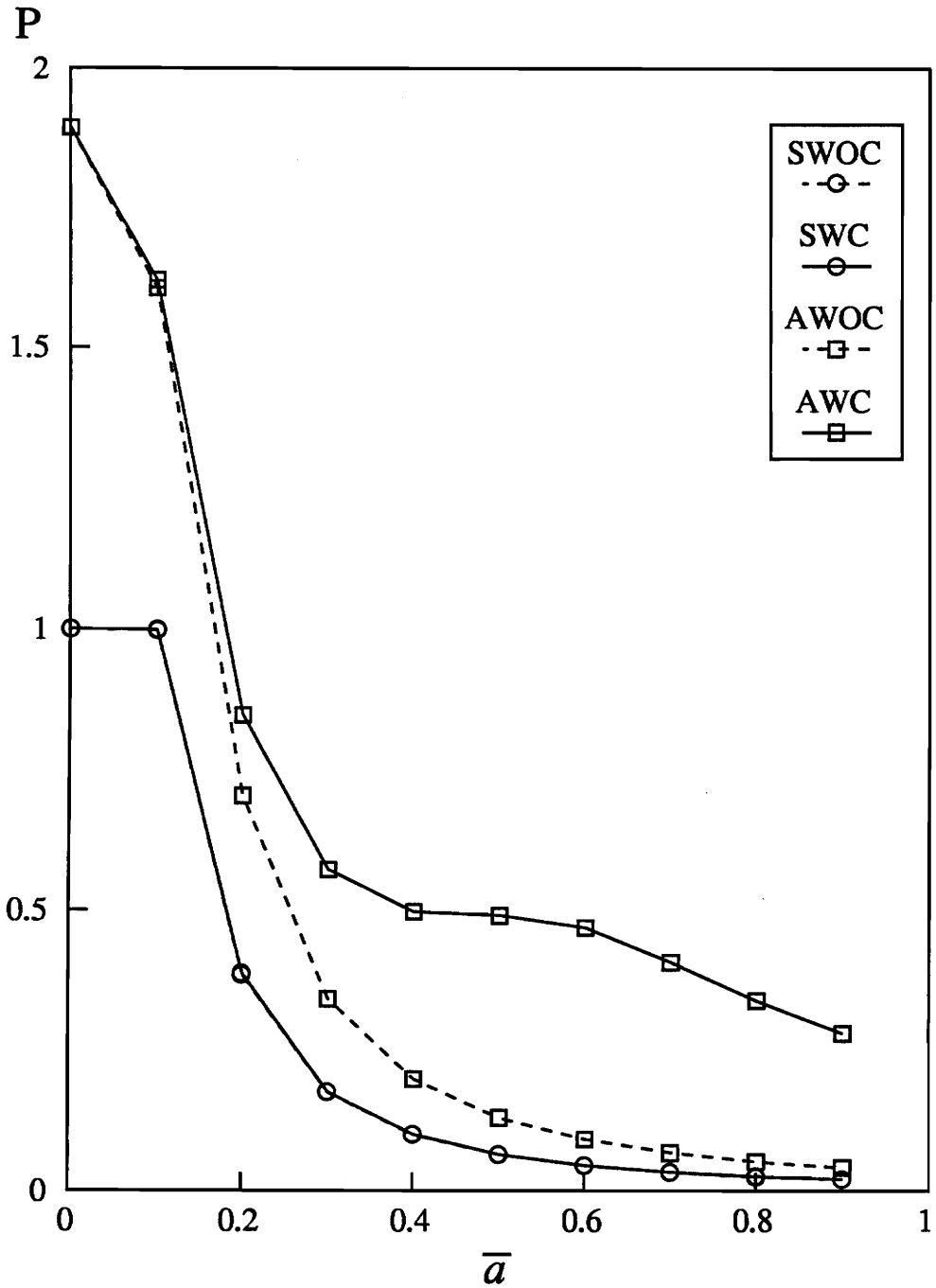

Figure 57. Buckling load vs. delamination lengths for a composite containing three delaminations for $\bar{t}$ = 0.25 with and without contact condition

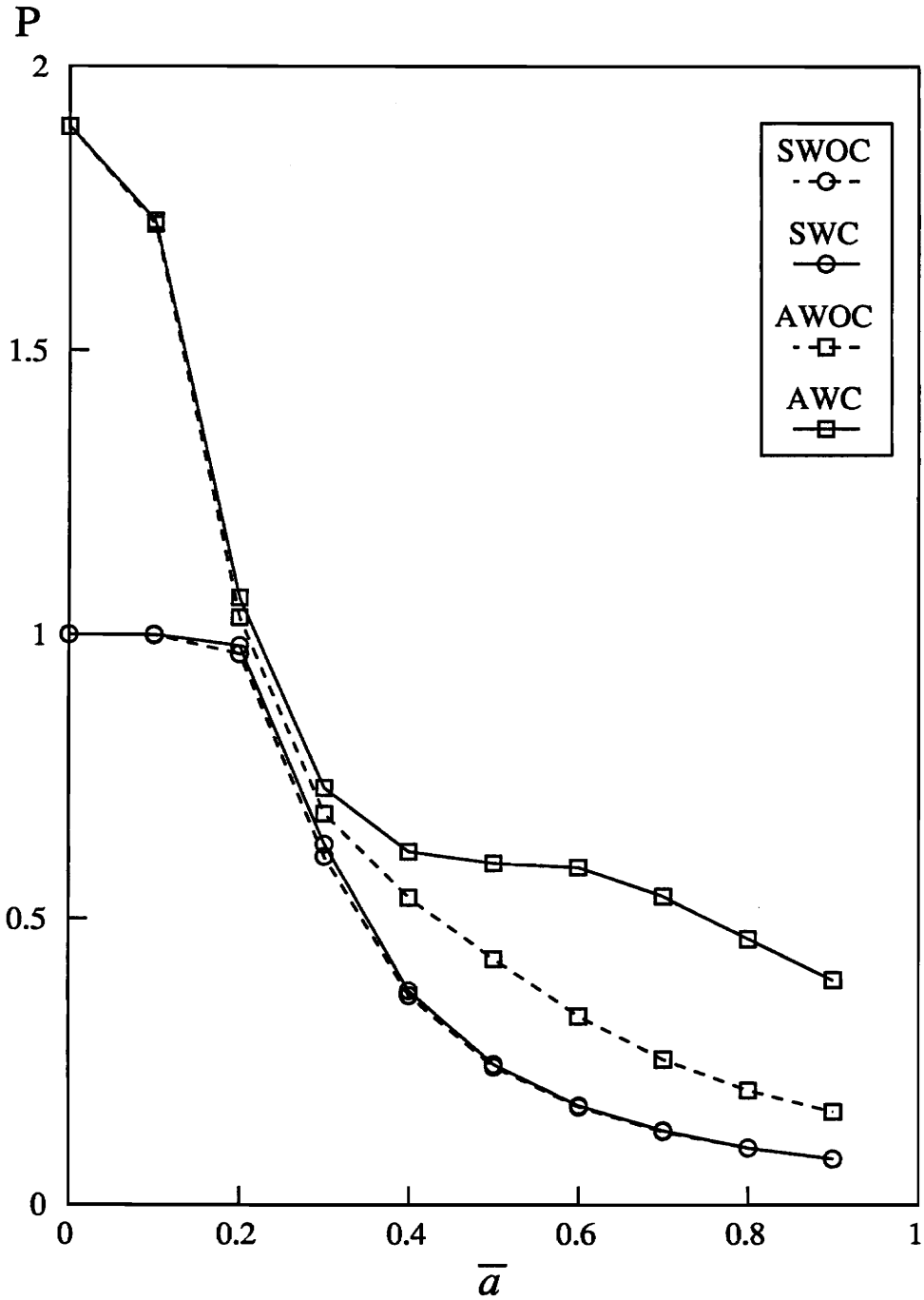

Figure 58. Buckling load vs. delamination lengths for a composite containing two delaminations for $\bar{t}$ = 0.5 with and without contact condition

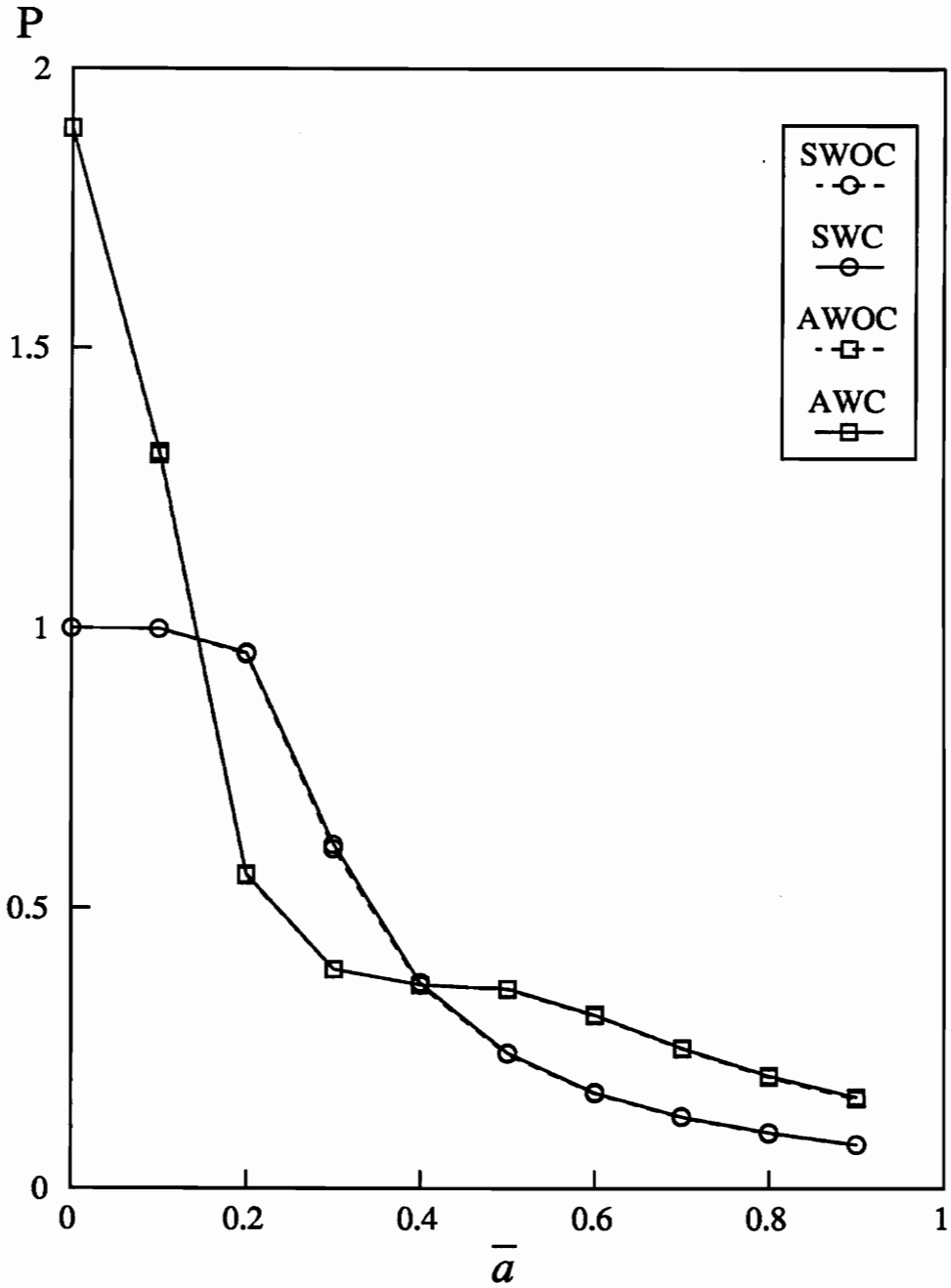

Figure 59. Buckling load vs. delamination lengths for a composite containing three delaminations for $\bar{t}$ = 0.5 with and without contact condition

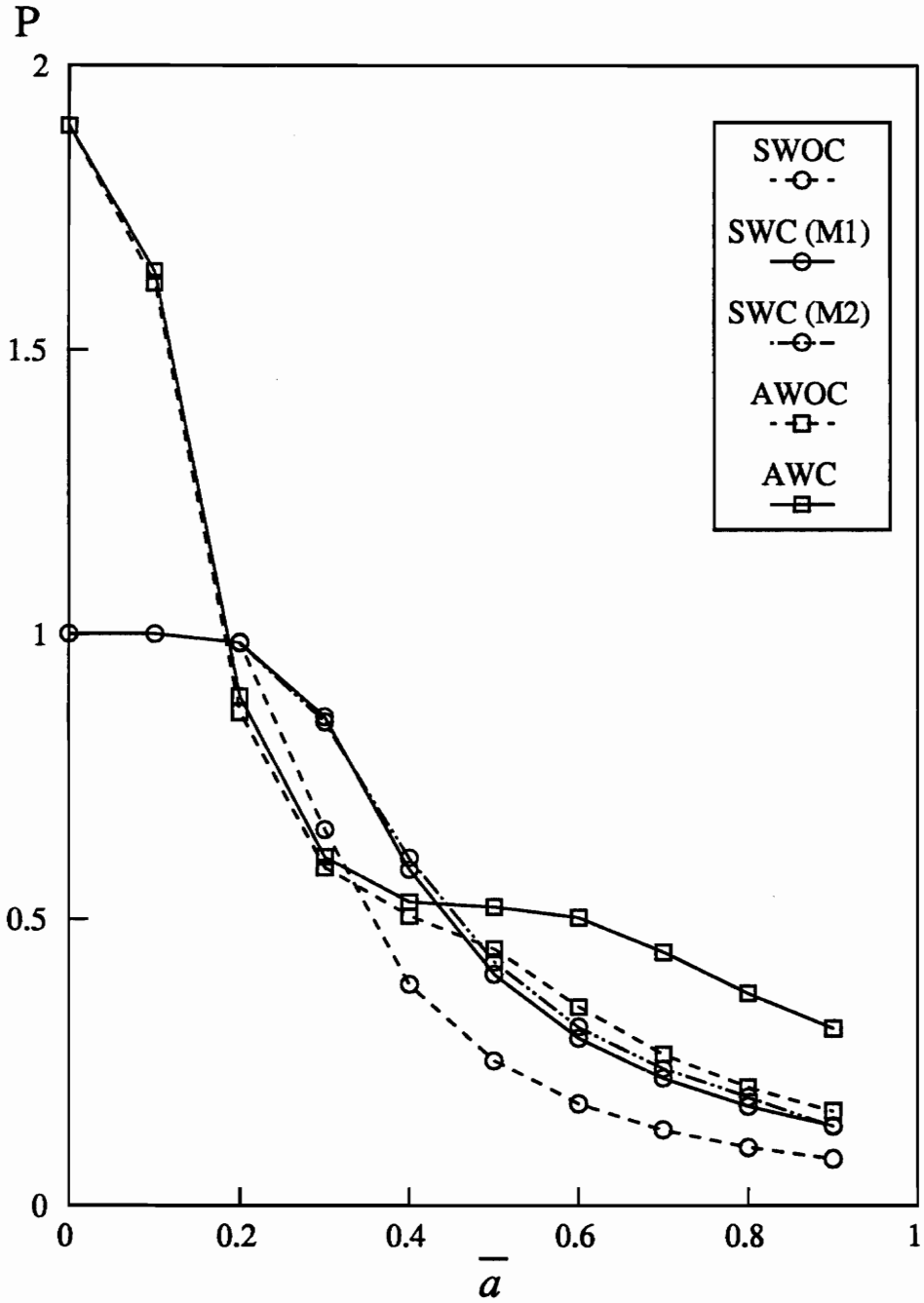

Figure 60. Buckling load vs. delamination lengths for a composite containing two delaminations for $\bar{t}$ = 0.75 with and without contact condition

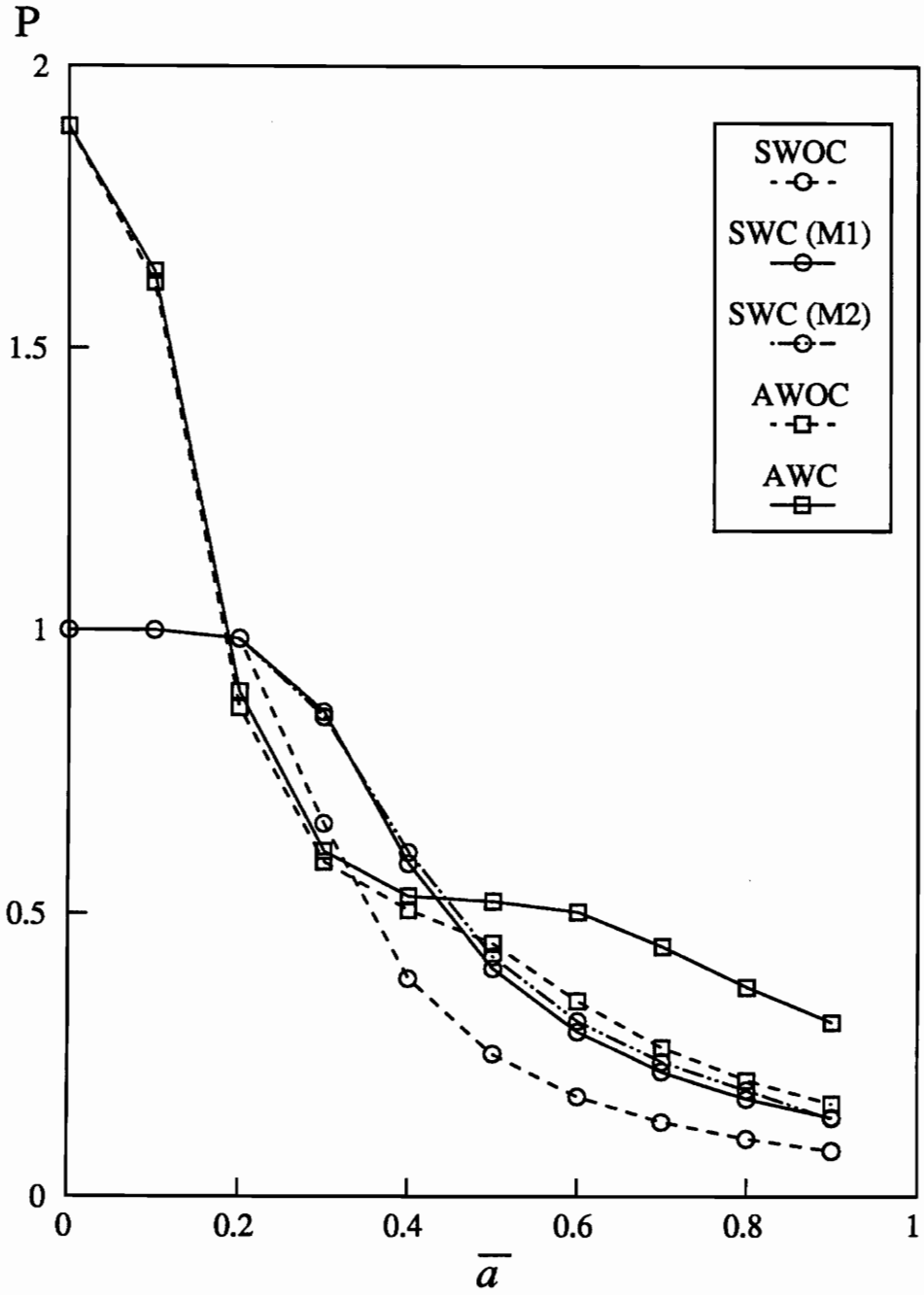

Figure 61. Buckling load vs. delamination lengths for a composite containing three delaminations for $\bar{t}$ = 0.75 with and without contact condition

the contact constrained buckling load is much higher than that of the unconstrained one, implying that neglecting the contact condition for the thinner core layer may cause totally erroneous results. In general, Method 1 predicts more conservative buckling loads than Method 2, but the difference seems to be quite small. As a result, the contact constrained curves for both two and three delaminations yield almost the same trends for both modes, showing that the antisymmetric mode is the first buckling mode for $\bar{a} = 0.2$ to 0.4.

In order to investigate the failure process of the compressed composite with multiple delaminations, postbuckling analyses are presented for $\bar{a} = 0.3$. The first two or three lowest symmetric buckling mode shapes and an antisymmetric mode are shown in Figures 62 - 64 for $\bar{t} = 0.25$, 0.5 and 0.75, respectively. It can be seen that the several lowest buckling loads are very close to one another. For this reason, the postbuckling solution is obtained for imperfections of these mode shapes.

For all the results given, the magnitudes of the initial imperfections (w_o and $\overline{w}_o^i$) are determined in the following way: First, calculate the buckling mode and identify the ratio of the deflections of the each sublaminate at the center of the composite. Secondly, set the maximum deflection from the buckling mode to 1×10^{-3} as an imperfection (either w_o or $\overline{w}_o^i$ depending on the mode shape), and set the others according to the ratio in the buckling mode.

Load-deflection curves are shown in Figures 65 and 66 for two delaminations with initial imperfections of the first and the second buckling mode shapes. For the first mode imperfection, The lower delamination always remains closed, and the composite acts as if it contains only an upper delamination. For the second mode imperfection, however, both delaminations start to open at the buckling load. As the load level approaches $P = 0.75$, the whole part buckles abruptly. The load-end shortening relation is illustrated in Figure 67 for two delaminations with $\bar{t} = 0.25$. The postbuckling defor-

mation for the second buckling mode shape shows sudden loss in load-carrying capacity while that of first mode shape shows gradual reduction in load-carrying capacity.

For three delaminations with $\bar{t} = 0.25$ (Figures 68 and 69), the load-deflection curves show the same trends as that of the two delamination cases. However, the ultimate load-carrying capacity for the three delamination cases are shown to be slightly below the two delamination cases, whereas the bifurcation points are the same for both the first and second buckling mode shapes, respectively. The load-end shortening curves for these cases are shown in Figure 70. The load-end shortening curve for the antisymmetric case coincides with the symmetric cases until the load reaches the first buckling load ($P = 0.1764$). Above this load level, the curves for symmetric modes slightly change their slope, while the antisymmetric case continues as an extension of the prebuckling path. At a buckling load of the antisymmetric mode ($P = 0.5722$), the composite with the antisymmetric mode can no longer sustain the load. Usually, it is known that a sudden buckling mode change may occur when two end-shortening curves cross each other [110]. It should be noted here that the curves with symmetric and antisymmetric modes do not necessarily represent the postbuckling deformed mode change phenomenon. As a consequence, although the buckling load for the antisymmetric mode shape is far beyond that of the symmetric mode shape, the final load-carrying capacity of the antisymmetrically buckled composite is substantially lower than that of the symmetric modes. This implies that as soon as a delaminated composite buckles in an antisymmetric mode, it cannot carry the load, and thus does not exhibit postbuckling deformation.

For $\bar{t} = 0.5$ with two delaminations, the load-deflection curves for the first buckling mode imperfection are shown in Figure 71. The upper delamination opens and lower delamination remains closed as for the case of $\bar{t} = 0.25$. For the second mode imperfection, the postbuckling deformation is shown in Figure 72. The noticeable point

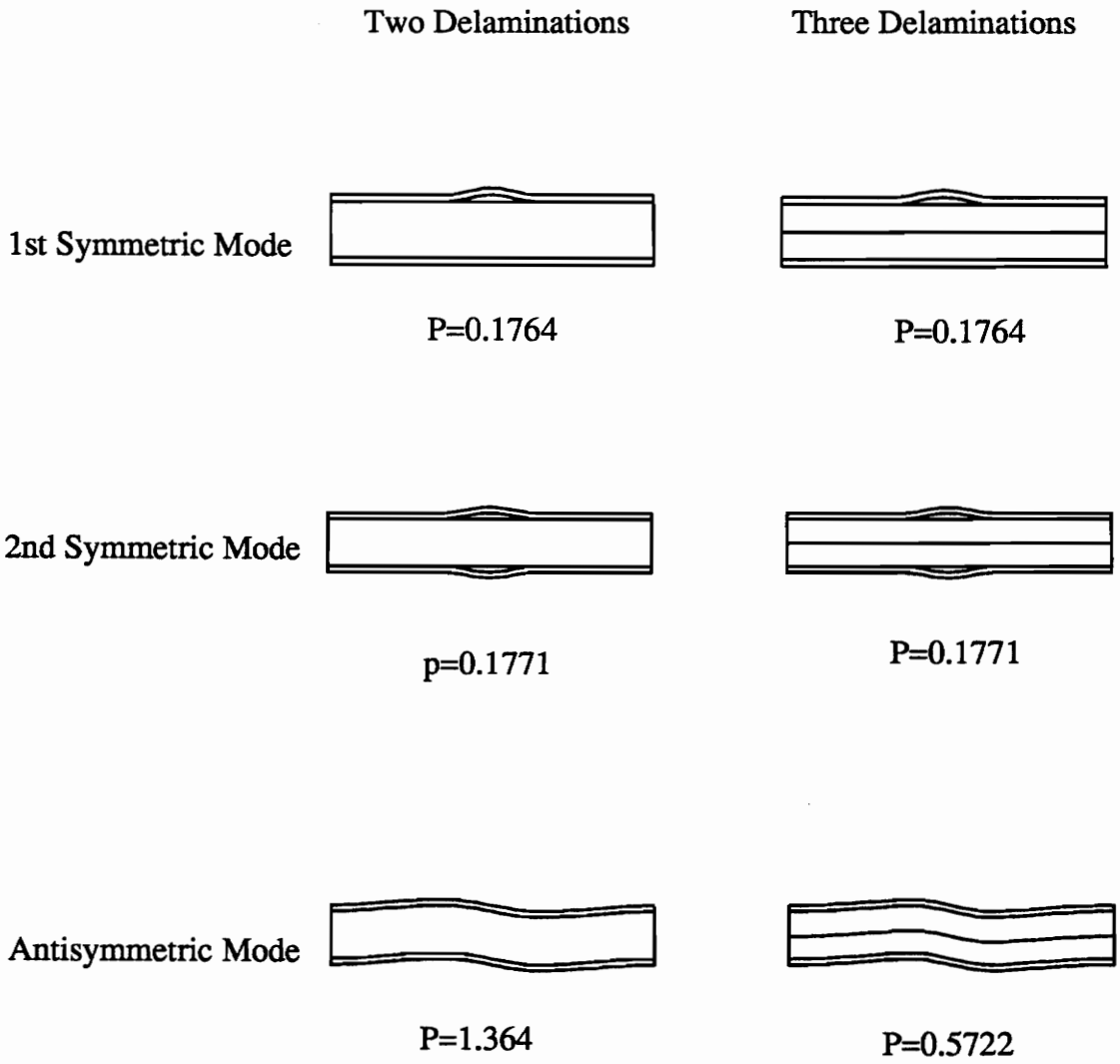

Figure 62. Buckling loads and mode shapes for two and three delaminations with $\bar{t} = 0.25$

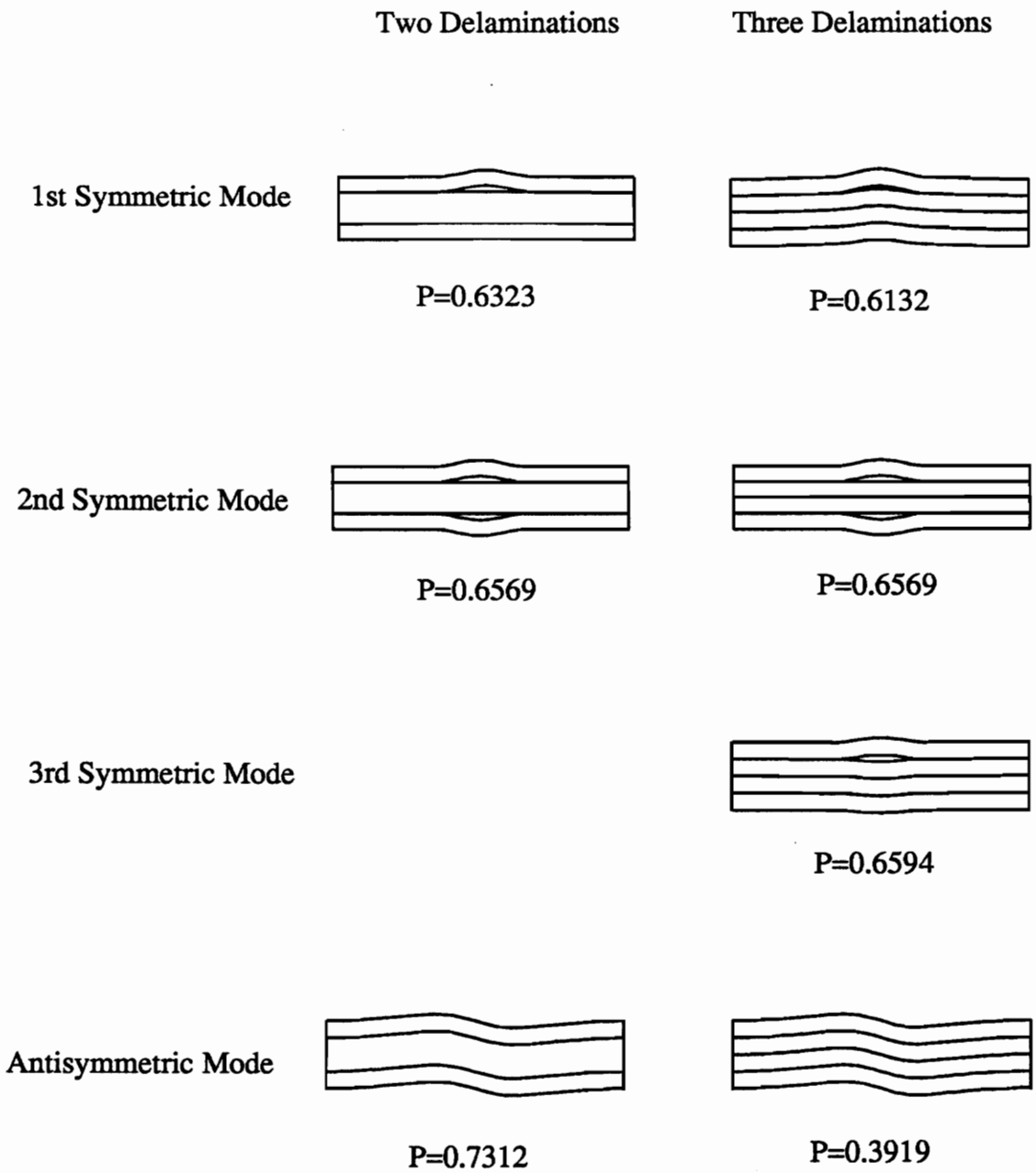

Figure 63. Buckling loads and mode shapes for two and three delaminations with $\bar{t} = 0.5$

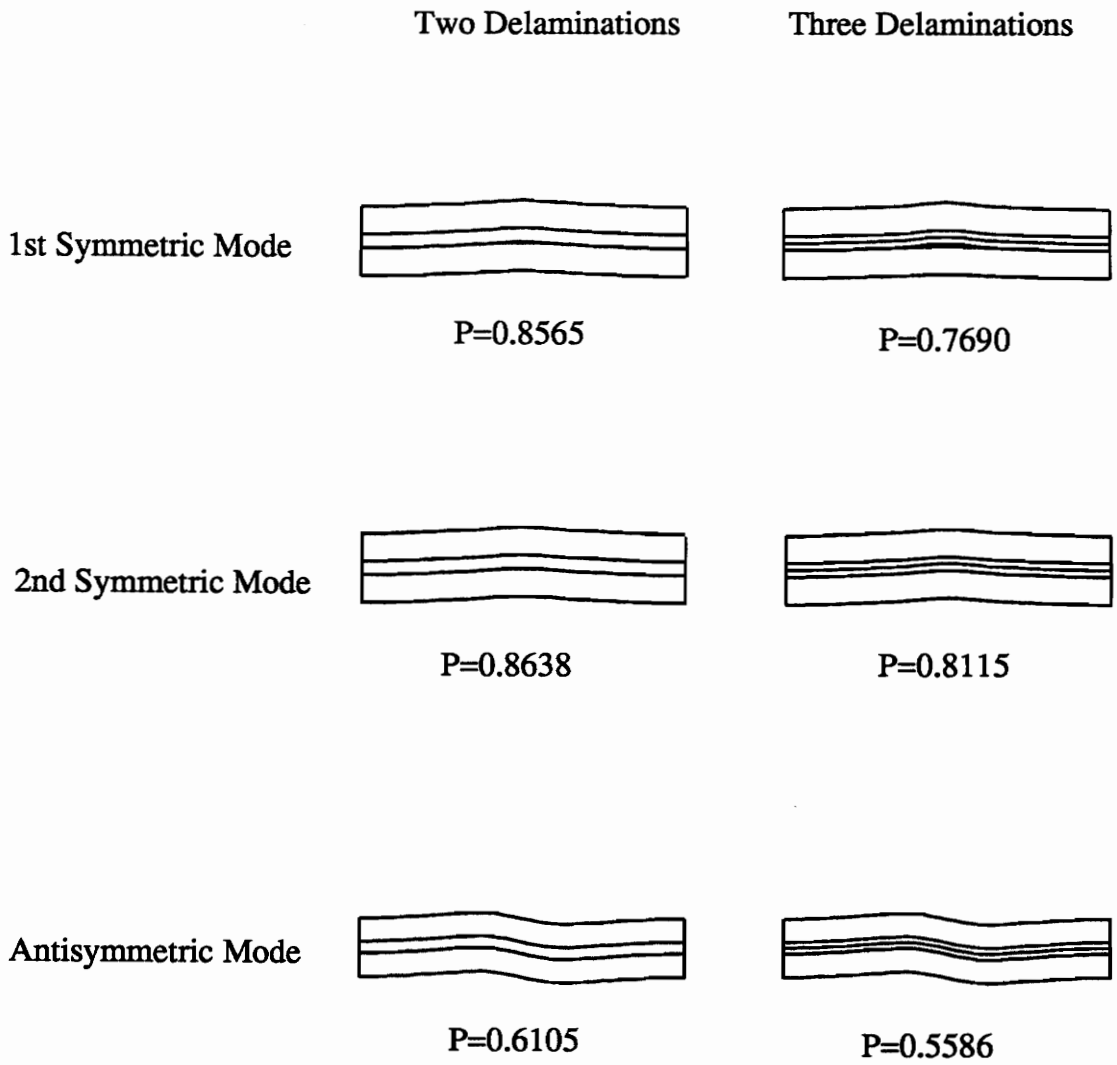

Figure 64. Buckling loads and mode shapes for two and three delaminations with $\bar{t} = 0.75$

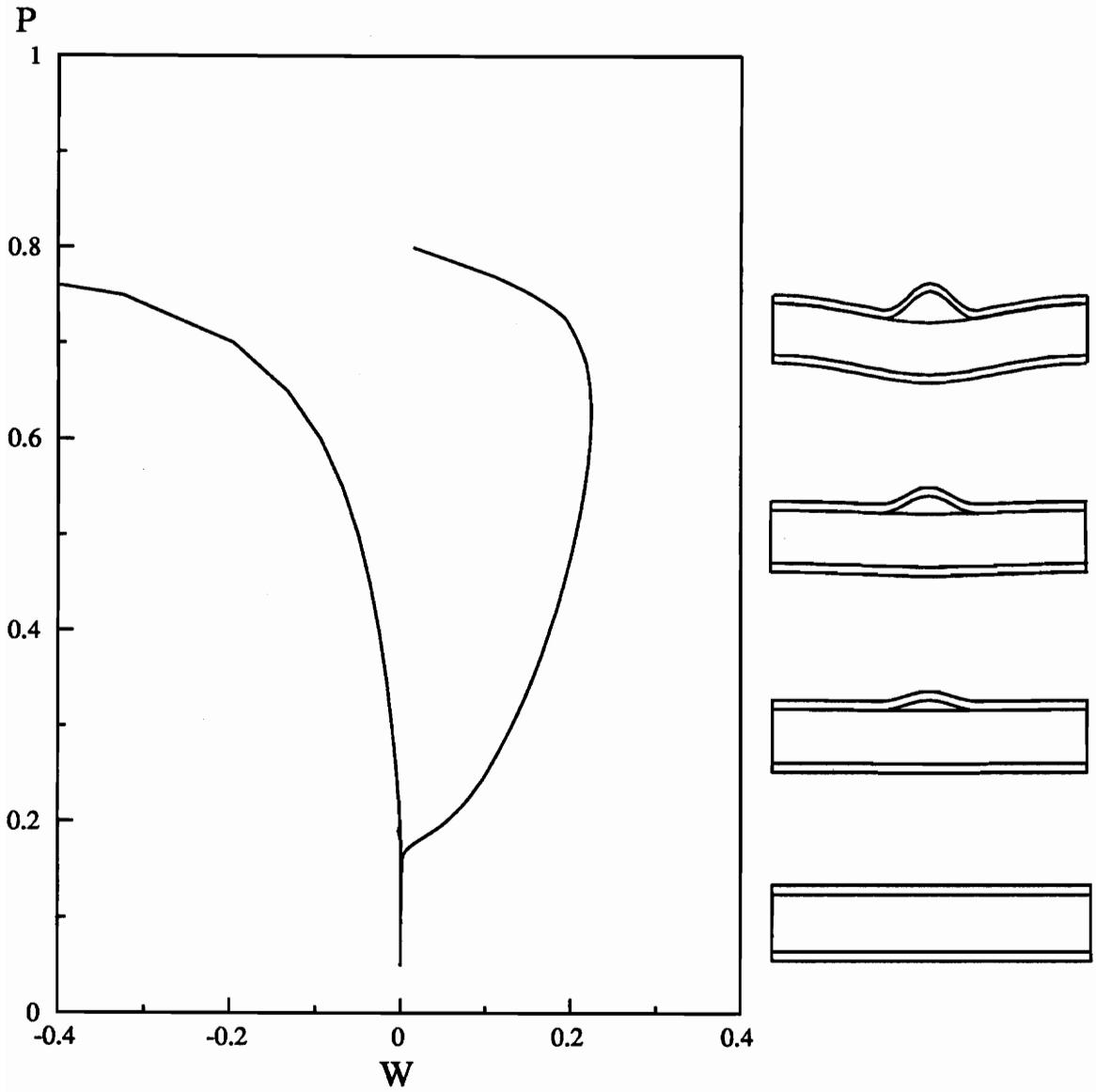

Figure 65. Load-deflection curve for a composite containing two delaminations for $\bar{t} = 0.25$ with imperfection of first symmetric buckling mode

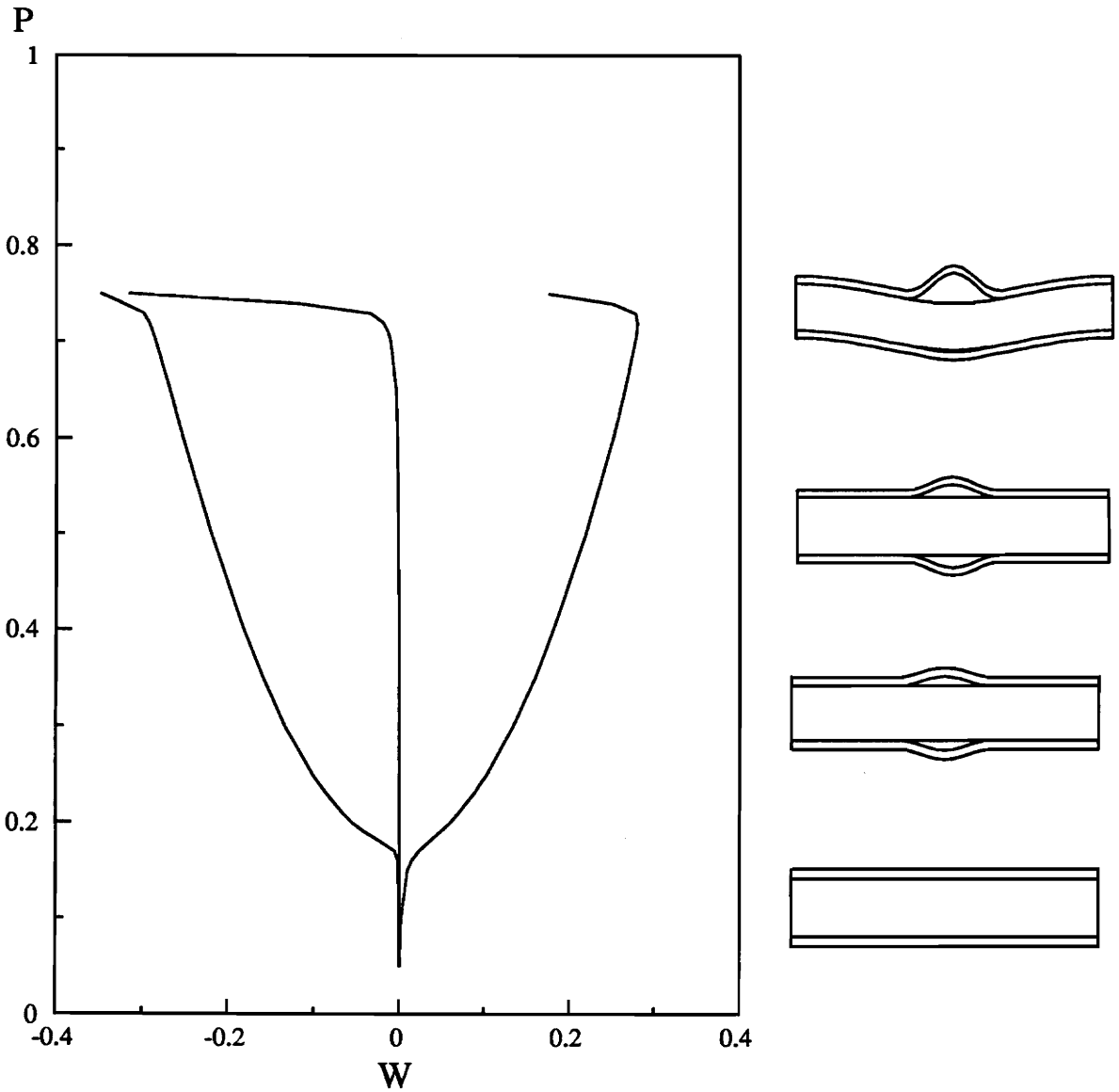

Figure 66. Load-deflection curve for a composite containing two delaminations for $\bar{t} = 0.25$ with imperfection of second symmetric buckling mode

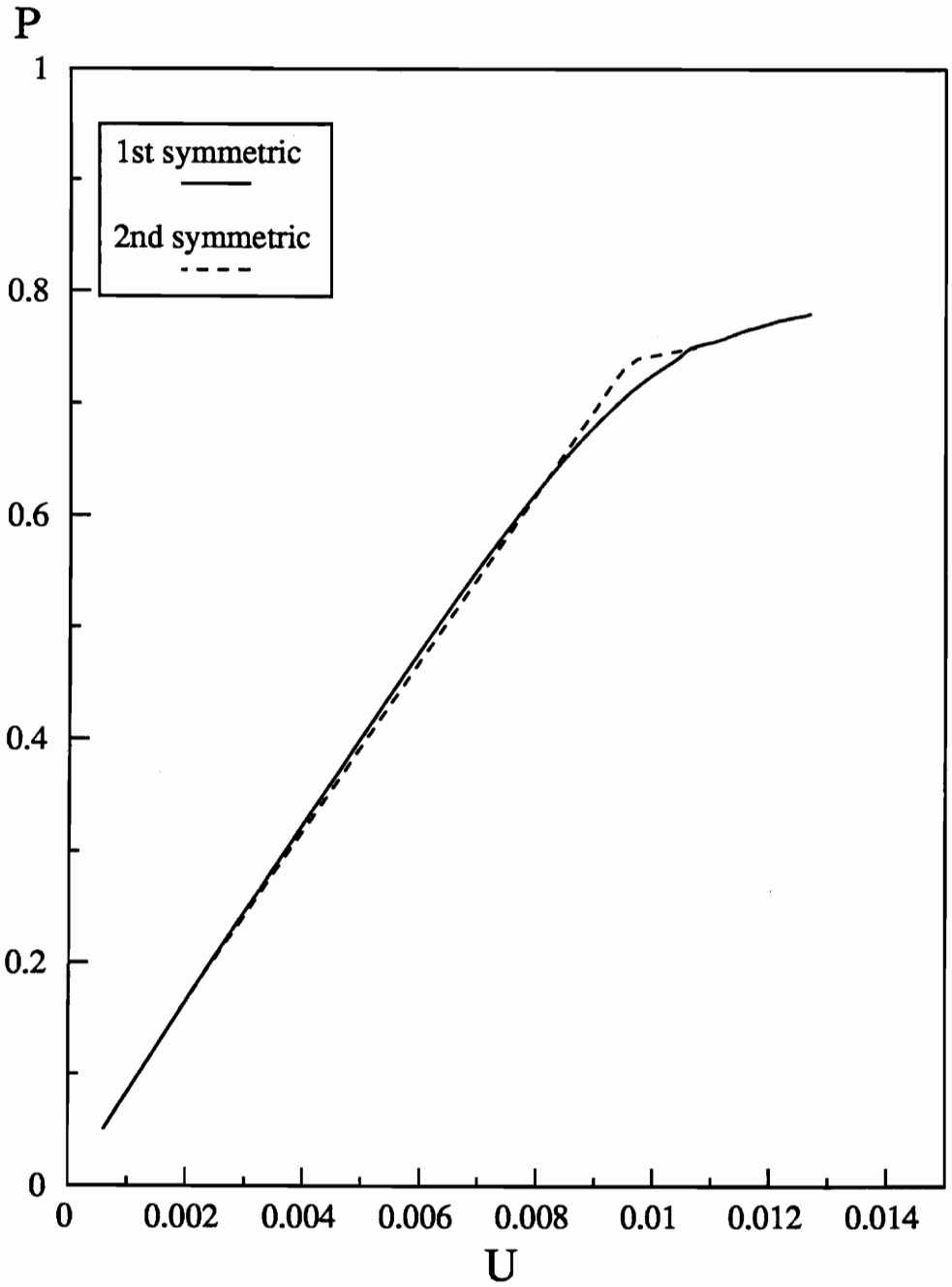

Figure 67. Load-end shortening curve for a composite containing two delaminations for $\bar{t} = 0.25$ with various initial imperfections

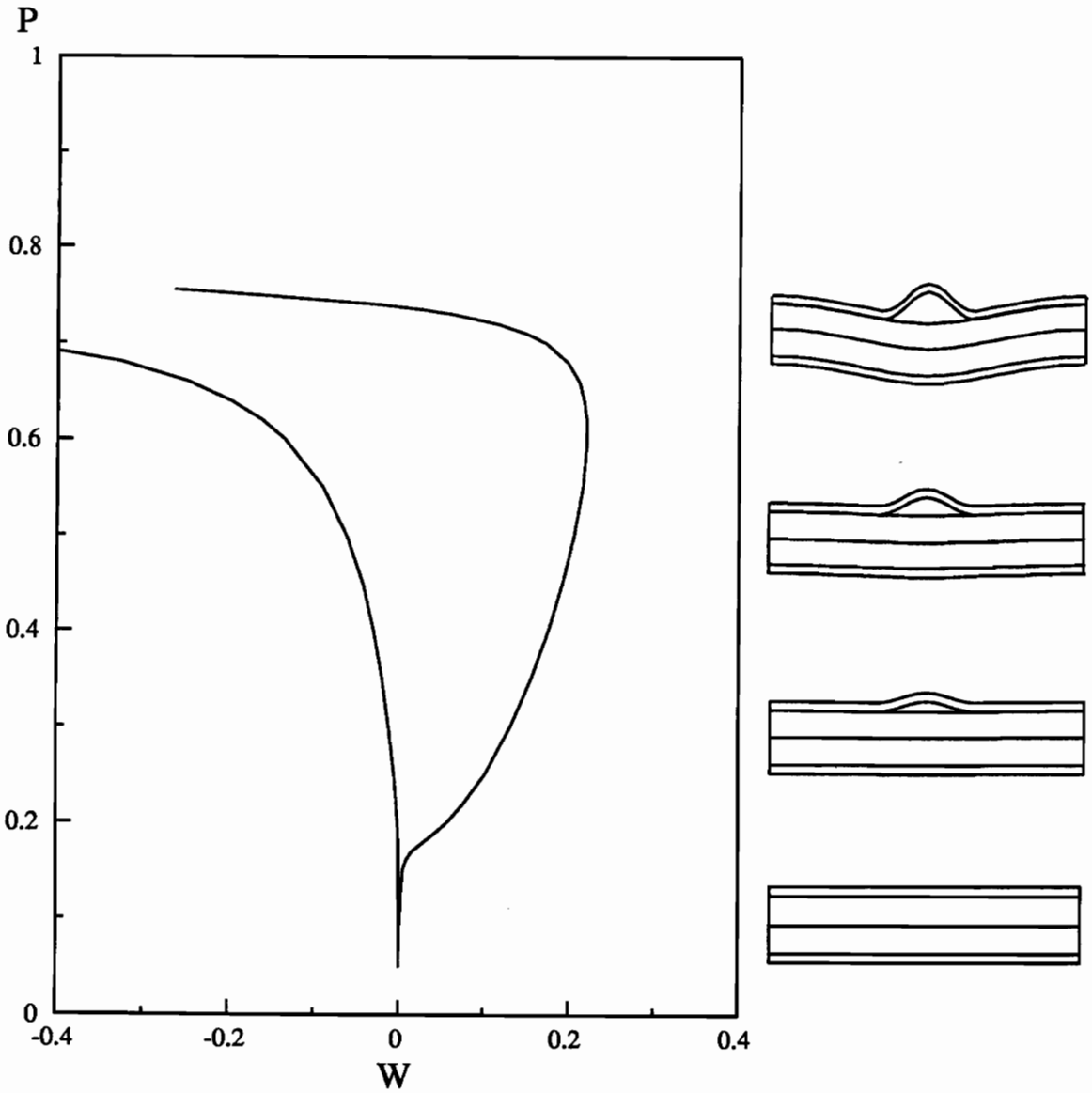

Figure 68. Load-deflection curve for a composite containing three delaminations for $\bar{t} = 0.25$ with imperfection of first symmetric buckling mode

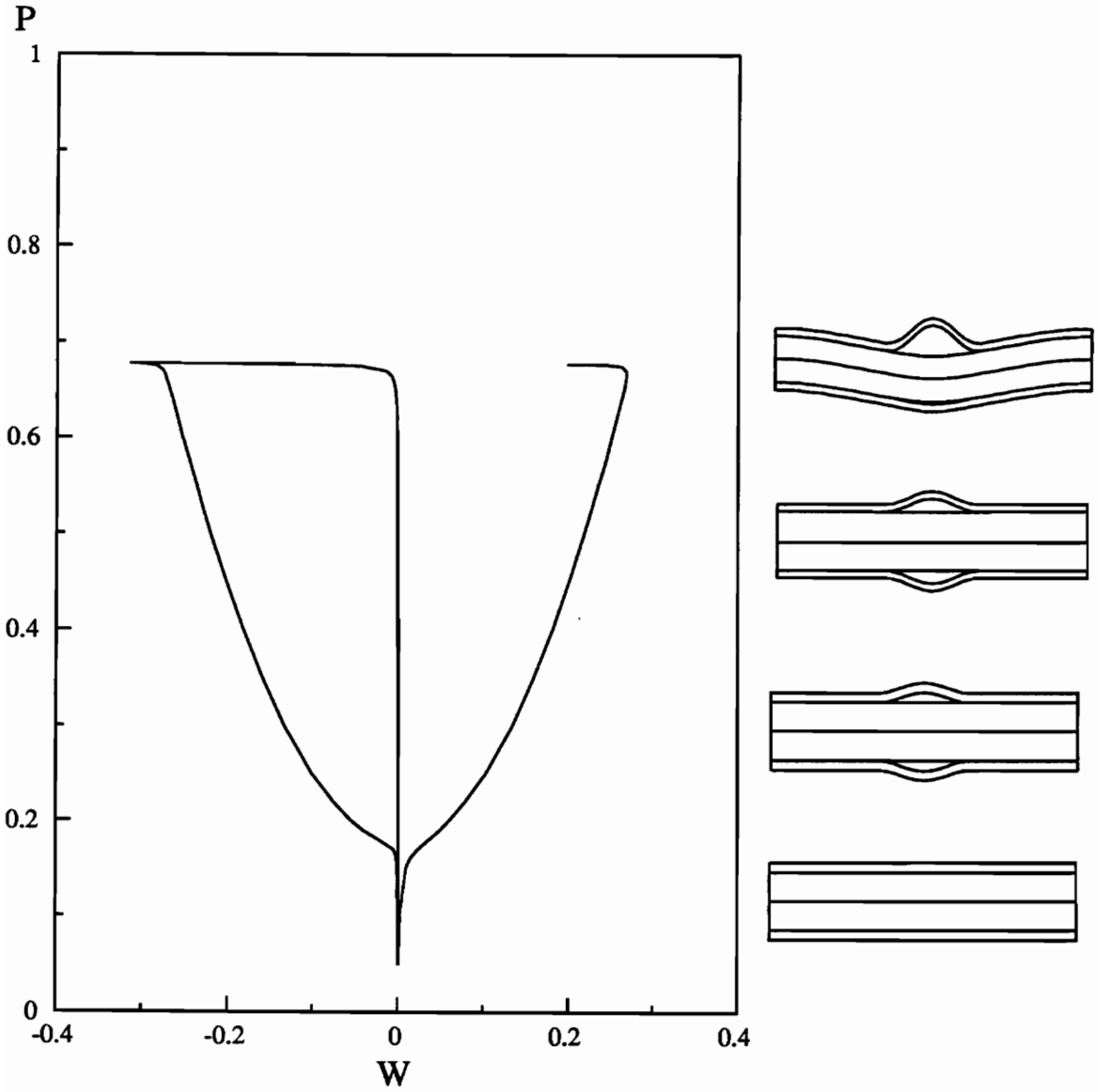

Figure 69. Load-deflection curve for a composite containing three delaminations for $\bar{t} = 0.25$ with imperfection of second symmetric buckling mode

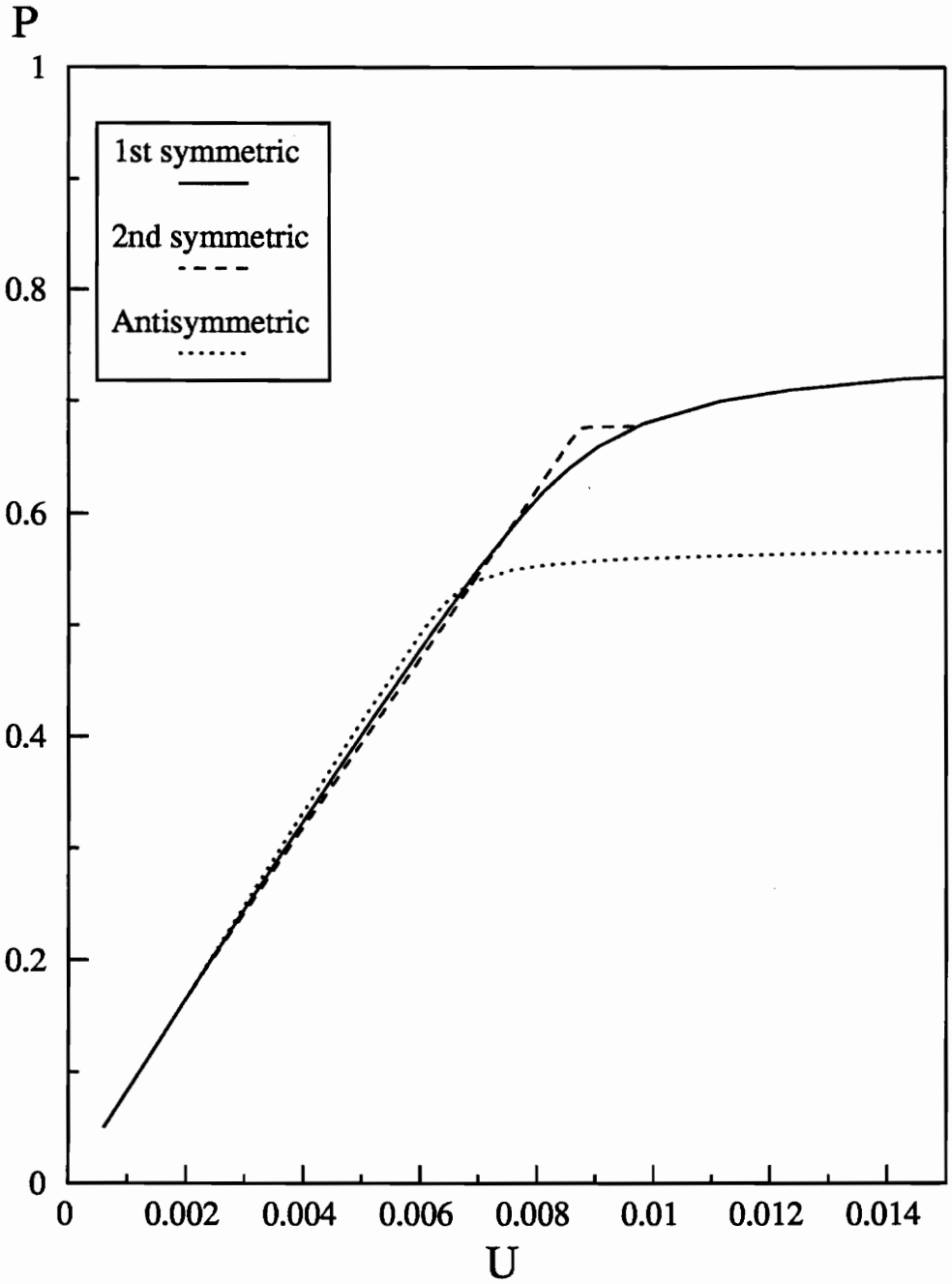

Figure 70. Load-end shortening curve for a composite containing three delaminations for $\bar{t} = 0.25$ with various initial imperfections

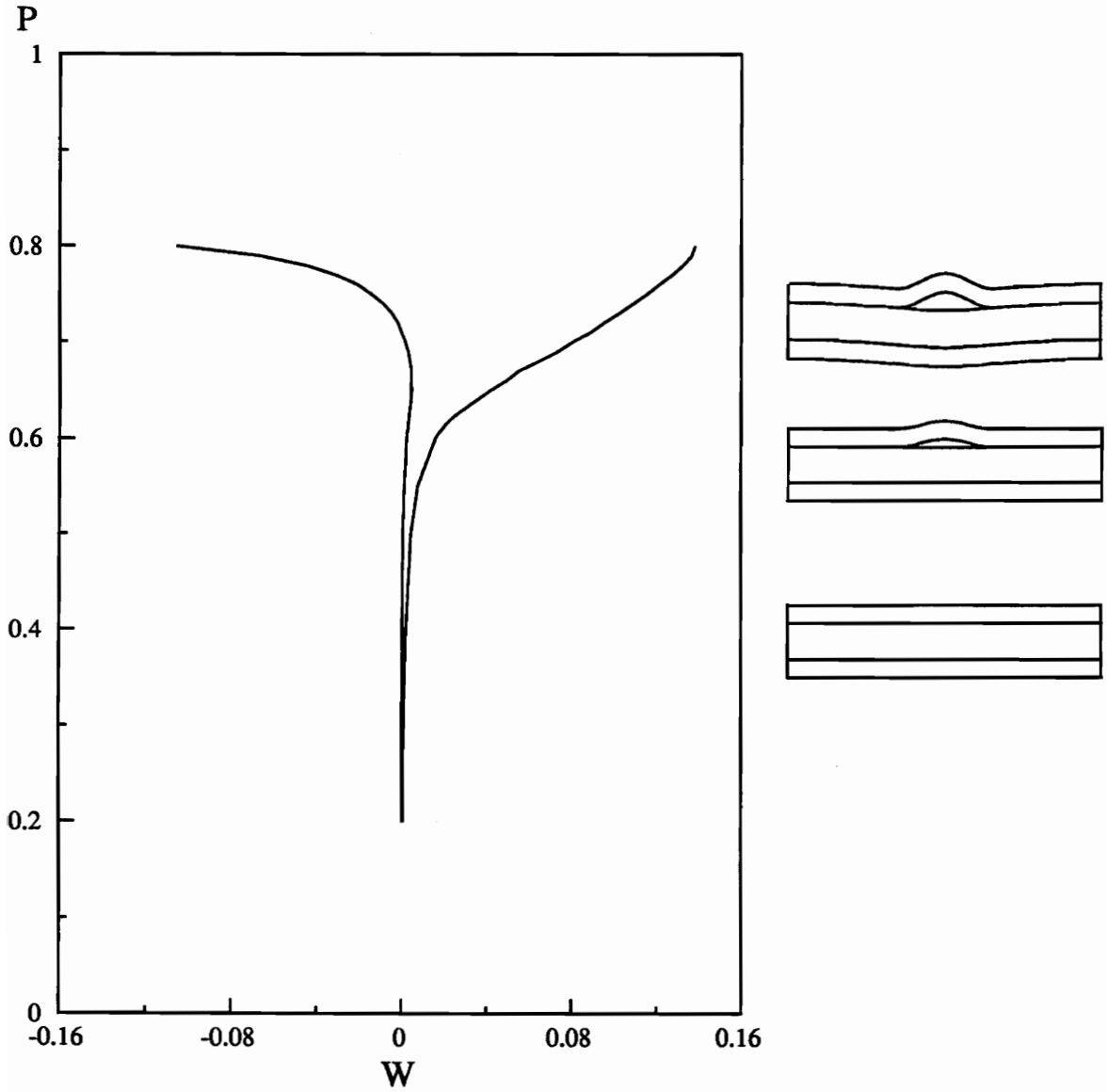

Figure 71. Load-deflection curve for a composite containing two delaminations for $\bar{t} = 0.5$ with imperfection of first symmetric buckling mode

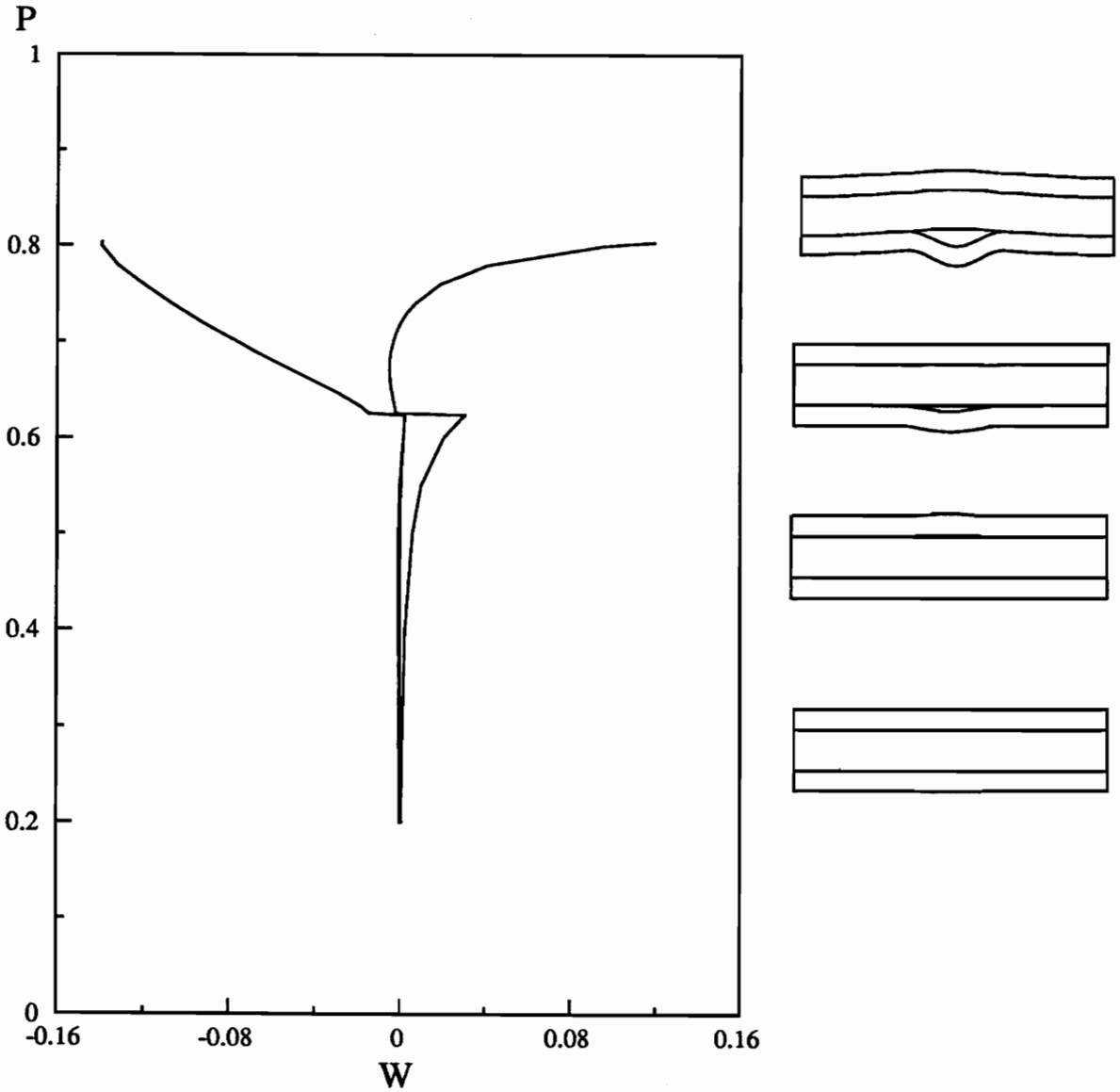

Figure 72. Load-deflection curve for a composite containing two delaminations for $\bar{t} = 0.5$ with imperfection of second symmetric buckling mode

here is that the composite first exhibits prebuckling delamination opening until the load reaches the buckling load and then, at a buckling load, the composite exhibits a transition into another buckling mode which is same as the previous case (first buckling mode imperfection). This example illustrates well the capability of the present method for problems in which multiple equilibrium paths exist. Load-end shortening curves (Figure 73) indicate that the composite buckled in antisymmetric mode exhibits much lower load-carrying capacity than that of symmetric modes. In this case, both symmetric modes show identical load-end shortening curves.

For $\bar{t} = 0.5$ with three delaminations, the first buckling mode shape is antisymmetric. For the symmetric buckling mode shape imperfections, the postbuckling behavior is global mode having all delaminations closed regardless of the shape of the initial imperfection. As a result, the delamination buckling load itself is a buckling load of the overall structure, and the load-carrying capacity is remarkably lower than the two delamination cases (Figure 74).

For $\bar{t} = 0.75$, for both symmetric and antisymmetric modes, the buckling load itself is the overall load-carrying capacity. The composite with three delaminations has slightly lower buckling loads than that of two delaminations as shown in Figures 75 and 76.

6.2.2 Seven Delaminations

It is assumed that there are seven interfaces in the laminate where delamination may exist, and each sublaminate has the same thickness (Figure 77). The thickness-to-span ratio (h/l) is assumed to be 1/10.

The nondimensional buckling load of the fully delaminated composite is compared (Figure 78) with a composite containing a single delamination at the outermost interface

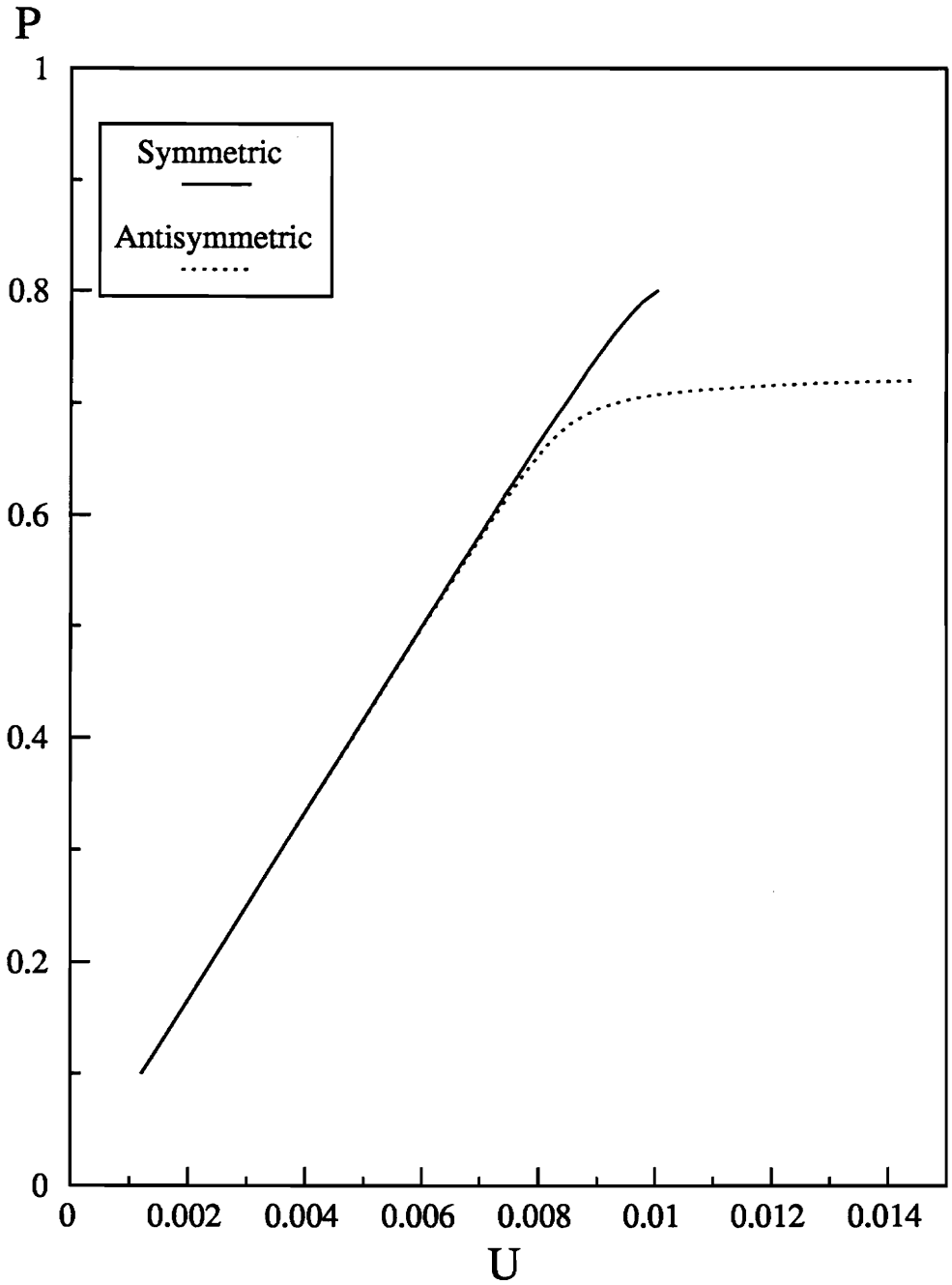

Figure 73. Load-end shortening curve for a composite containing two delaminations for $\bar{t} = 0.5$ with various initial imperfections

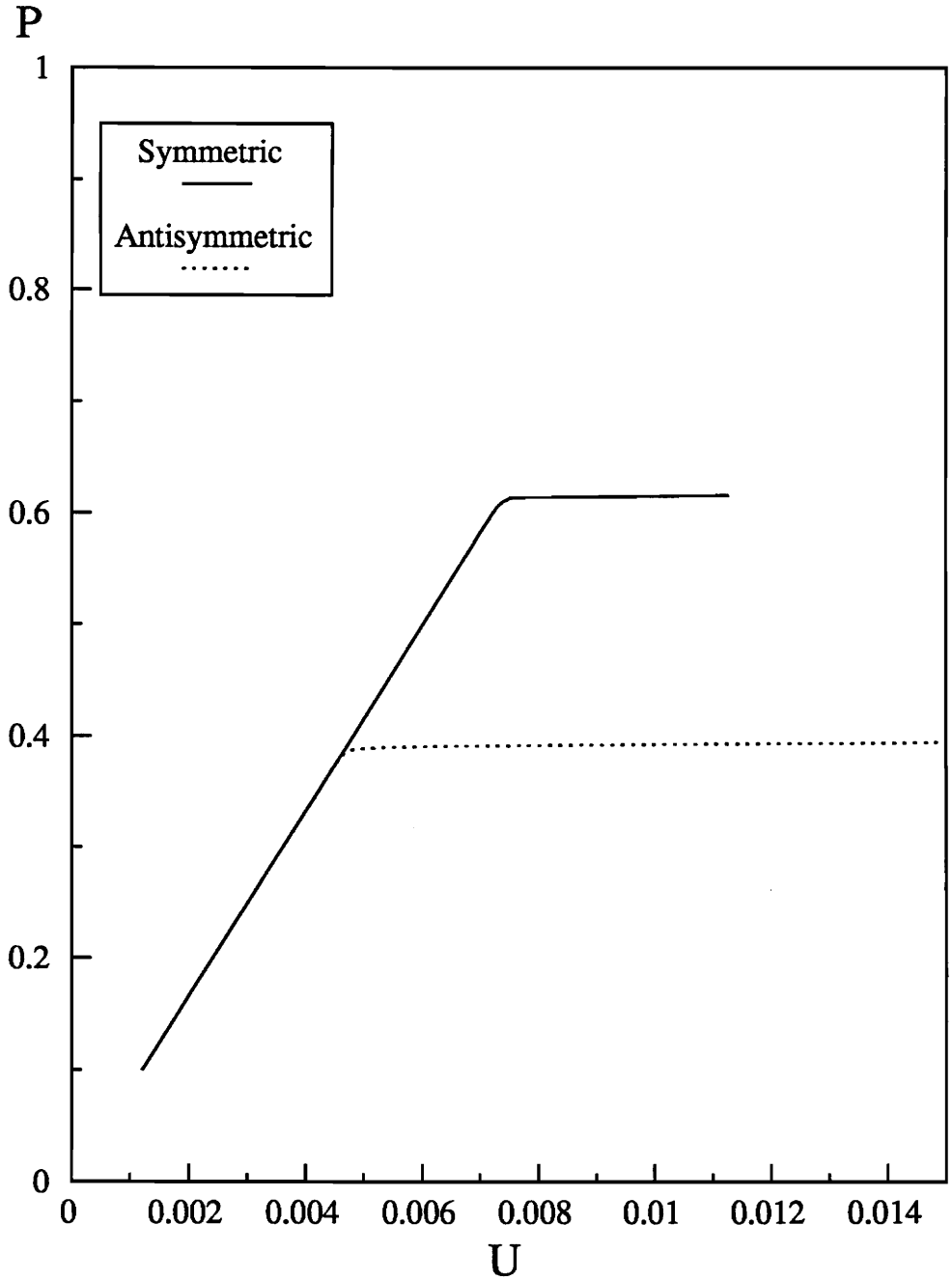

Figure 74. Load-end shortening curve for a composite containing three delaminations for $\bar{t} = 0.5$ with various initial imperfections

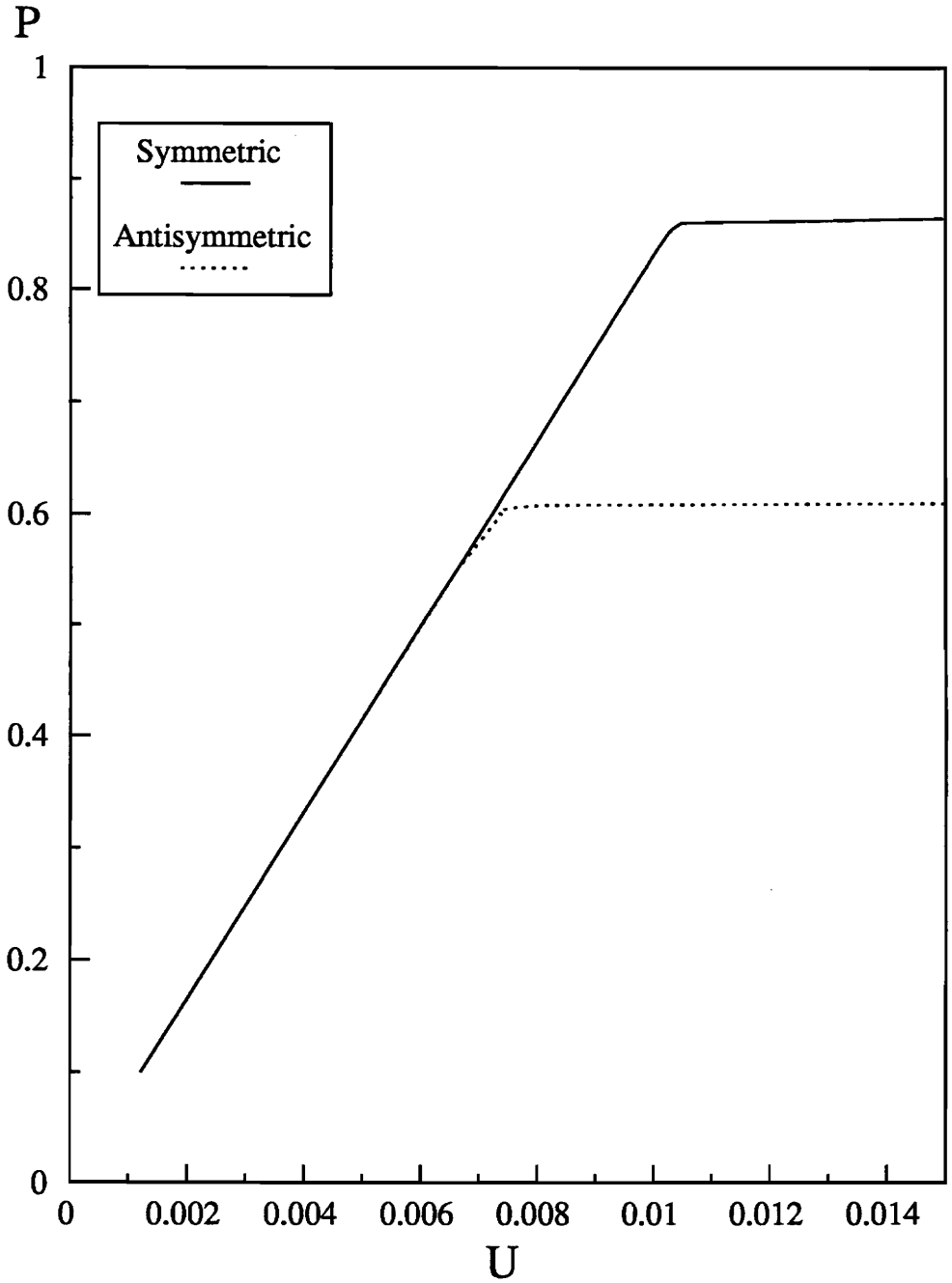

Figure 75. Load-end shortening curve for a composite containing two delaminations for $\bar{t} = 0.75$ with various initial imperfections

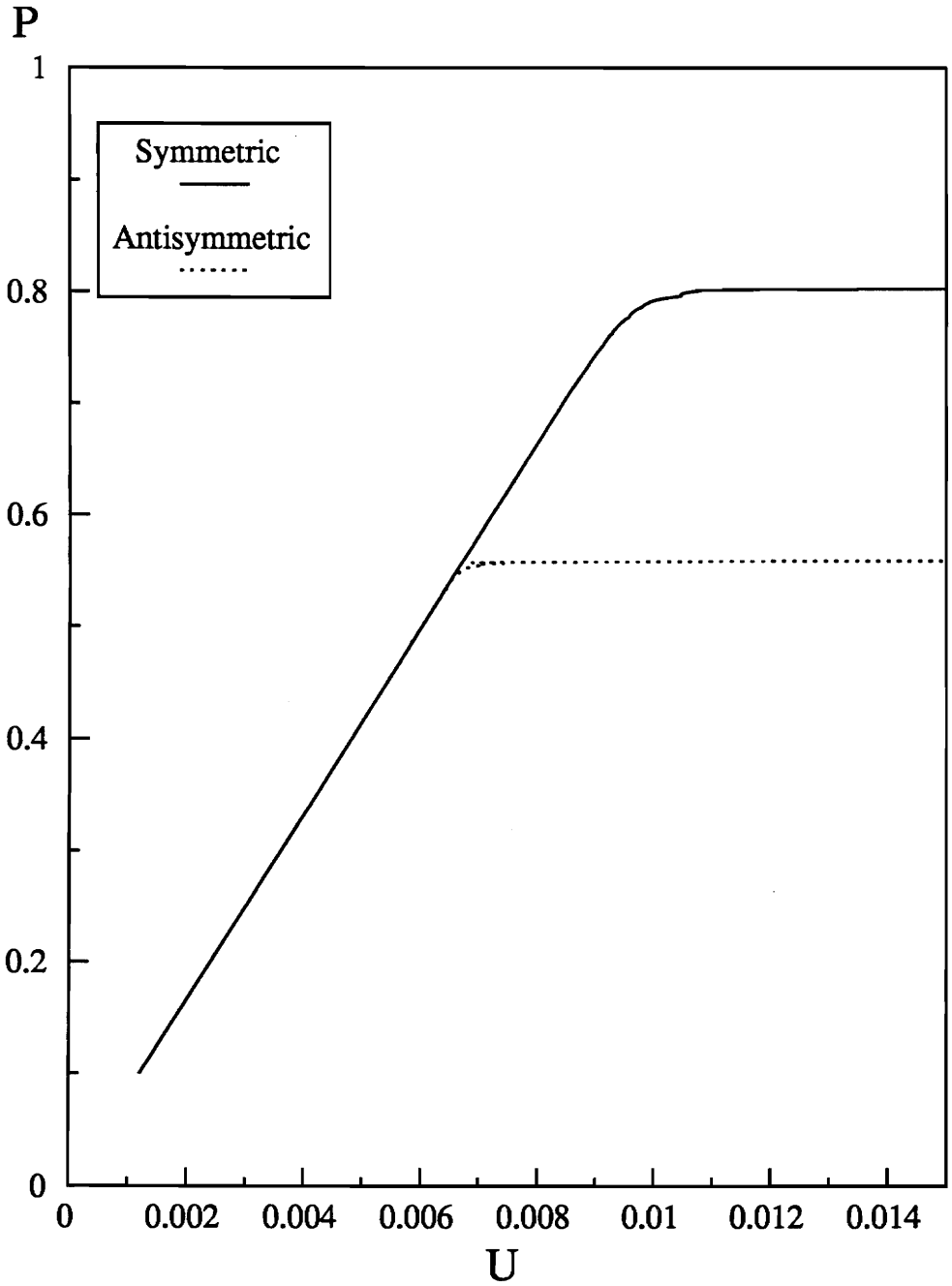

Figure 76. Load-end shortening curve for a composite containing three delaminations for $\bar{t} = 0.75$ with various initial imperfections

and a composite with a triangular delamination distribution. It is noted that the single and triangularly distributed delamination cases yield almost identical results over the entire region of $\bar{a}$. That is, the thin-film type local symmetric mode dominates buckling for these two cases. This result suggests that the longest delamination existing in the outermost layer governs the buckling load and mode shape and the shorter ones seldom contribute to the buckling load for triangular case. However, the buckling load of the fully delaminated composite is far below the other two cases, by 40% for short delamination lengths. This is because the antisymmetric mode, which is insignificant for the other two cases, becomes responsible for buckling for multiple short uniform delaminations. The global symmetric buckling mode occurs only for very short delaminations, e.g. $\bar{a} < 0.1$ for one and triangular delaminations, $\bar{a} < 0.05$ for full uniform delaminations. Local buckling is predicted for longer delaminations, so that all the three cases coincide for relatively long delamination cracks ($\bar{a} > 0.3$) .

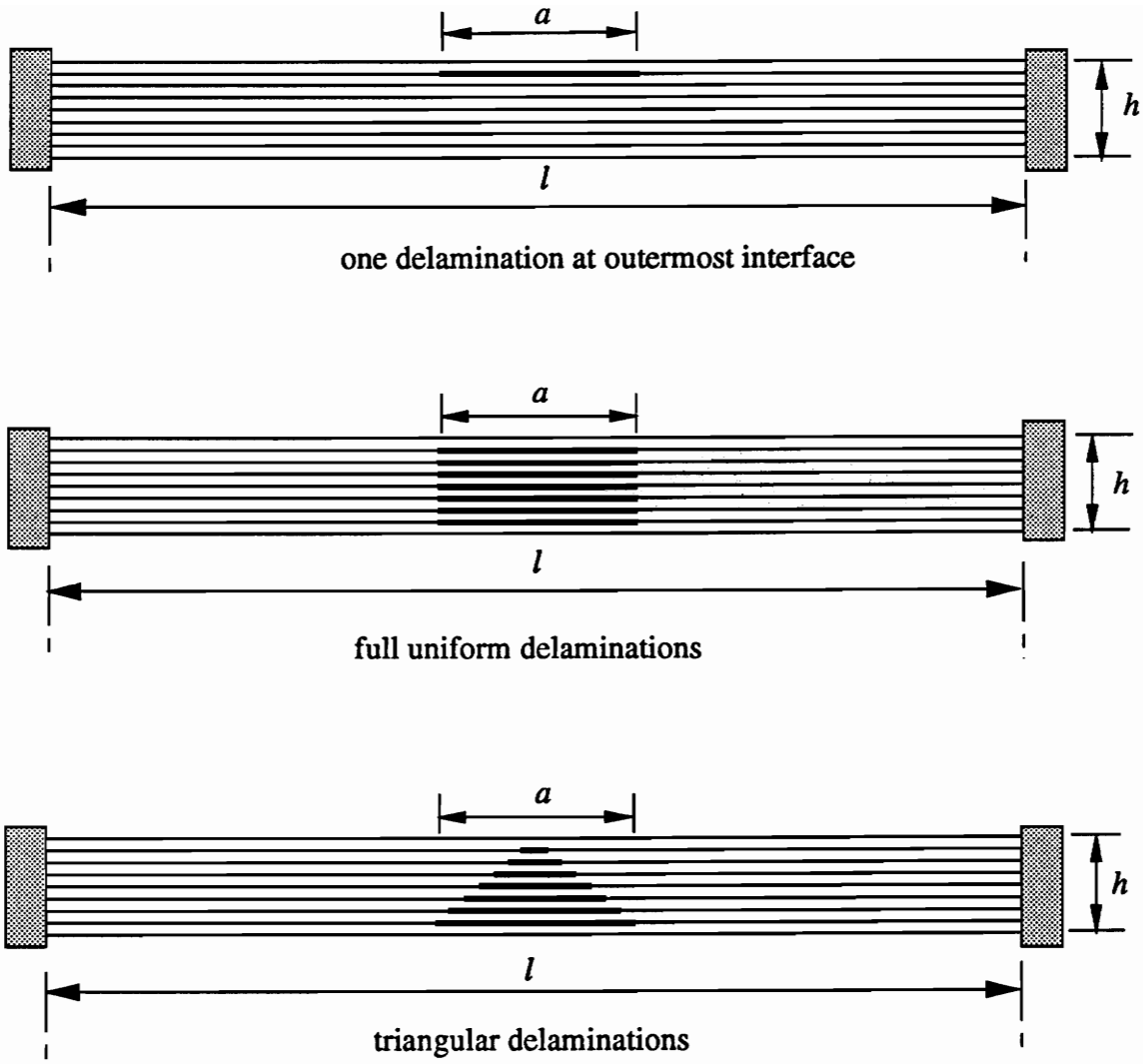

Figure 77. Geometry for composites containing one, triangular and full uniform delaminations

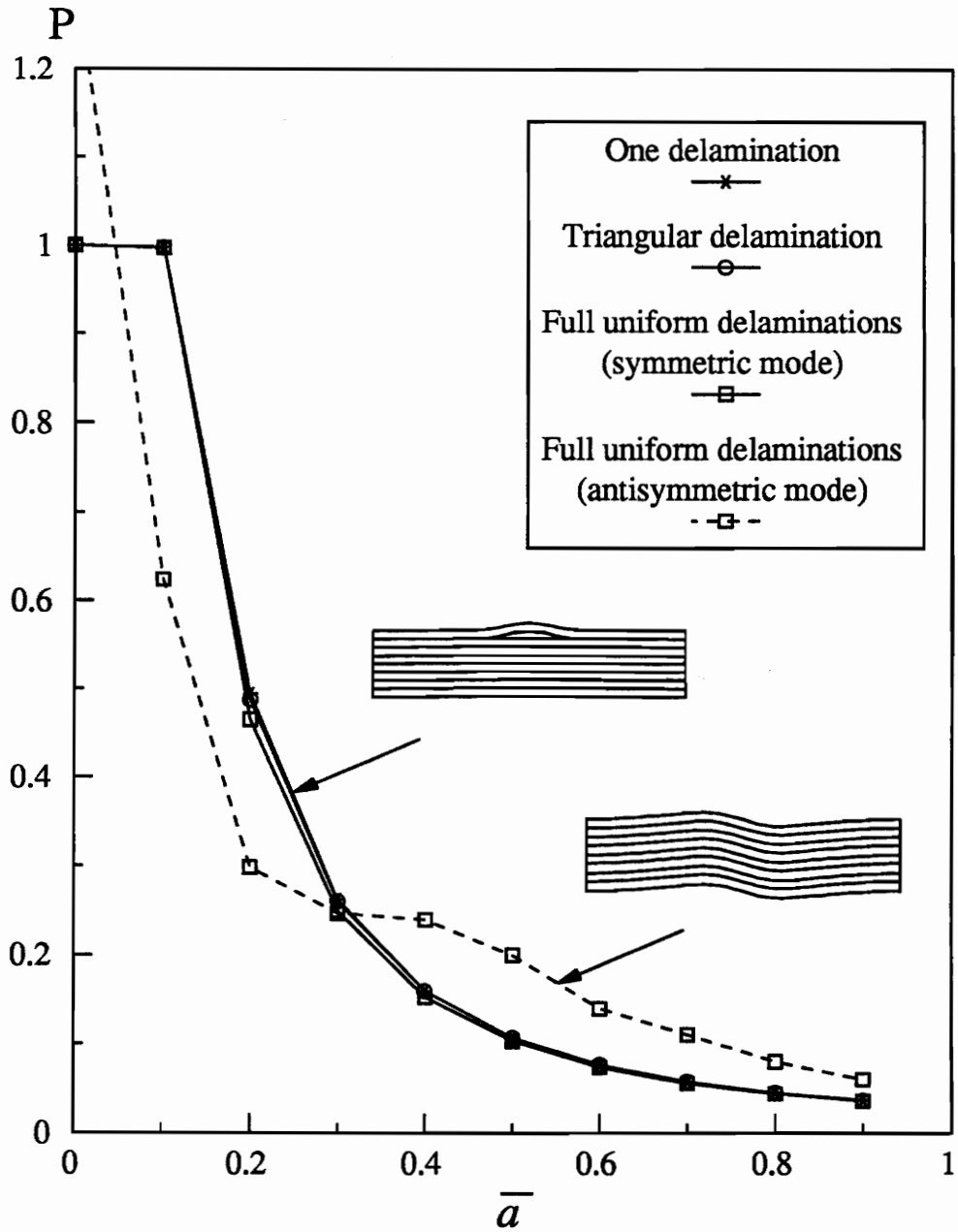

Figure 78. Buckling load vs. delamination lengths for composites containing one, triangular , and full uniform delaminations.

6.3 Layer-Wise Model vs. Sublaminate Model

6.3.1 Buckling Response of Delaminated Composites

The accuracy and efficiency of the layer-wise model and sublaminate model are investigated for a clamped quasi-isotropic composite containing a through-the-width delamination at its midplane. The thickness-to-span ratio is assumed to be 1/50 and the stacking sequence is $[0/90/\pm 45]_s$.

The first three nondimensional buckling loads are presented and CPU time for each analysis is given in Table 5. For all analyses given, ten quadratic one-dimensional elements are used for the full model of the composite and the IBM 3090 Mainframe is used for computation. For both layer-wise and sublaminate theories, results are obtained considering two cases: first, the coupling stiffness terms (A_{1112}, B^i_{1112}, and D^{ij}_{1112}) are neglected, that is, the degrees of freedom per node is $2+M+2D$ (u_1, u_3, u^i_1, $\bar{u}^i_1$, $\bar{u}^i_3$). The coupling terms are included in the second case, so the degrees of freedom per node is $3+2M+3D$ (u_1, u_2, u_3, u^i_1, u^i_2, $\bar{u}^i_1$, $\bar{u}^i_2$, $\bar{u}^i_3$). The buckling loads are nondimensionalized with respect to the critical buckling load of an undelaminated composite calculated by the uncoupled sublaminate approach.

For the undelaminated case ($a/l=0$), the coupling effect seems to be negligible for both theories. However, as delamination size increases, the difference between two results for both theories slightly increases up to 3.5 % for $a/l=0.8$. This is due to the fact that the delaminated sublaminates are no longer symmetric, so that the coupling stiffnesses B^i_{1112} become significant.

Table 5. Comparison between the layer-wise and sublaminate theories for buckling loads of a $[0/90/45/-45]_s$ laminate with a midplane delamination

a/l		0	0.2	0.4	0.6	0.8
Layer-wise without coupling	1st	.99846	.89096	.63478	.37248	.23727
	2nd	1.9901	.96597	.68786	.38301	.24579
(10 sec.) 252 D.O.F	3rd	3.7647	1.9420	.72920	.65964	.48646
Layer-wise with coupling terms	1st	.99541	.86685	.61919	.36090	.22938
	2nd	1.9840	.96067	.67221	.37060	.23768
(55 sec.) 462 D.O.F	3rd	3.7536	1.8809	.70590	.64137	.47002
Sublaminate without coupling	1st	1	.90459	.64141	.37543	.23789
	2nd	1.9968	.96932	.68951	.38415	.24677
(2 sec.) 126 D.O.F	3rd	3.7866	1.9604	.73249	.66274	.48806
Sublaminate with coupling	1st	0.9999	.87983	.62634	.36382	.22966
	2nd	1.9967	.96698	.67437	.37019	.23840
(6 sec.) 210 D.O.F.	3rd	3.7862	1.8947	.70741	.64526	.47120

The proposed sublaminate theory is seen to be in excellent agreement with the layer-wise theory in predicting buckling loads for both coupled and uncoupled cases with significant computational time savings.

6.3.2 Postbuckling Analysis of Multiply Delaminated Composites

In this section, 8-layered simply-supported quasi-isotropic and unidirectional composite laminates with two delaminations are considered for postbuckling responses. The delaminations are assumed to exist in the first and sixth interfaces of the composites (Figure 79).

No initial imperfection is used in the analyses because delaminations can initiate the postbuckling deformations for simply-supported boundary conditions. Three different delamination lengths with four different lay-ups are considered. First, the postbuckling deformations for $[0/\pm 45/90]_s$ laminate are shown in Figures 80 - 82. In Figure 80, the load-deflection curves for two uniform delaminations are shown.

As soon as the laminate is subjected to applied load, the top sublaminate tends to deflect upward due to bending-extension coupling, and opens the upper delamination slightly, and the curves for both approaches almost coincide until $P = 0.3$. Near $P = 0.3$, the thin bottom layer buckles down accelerating the eccentricity in force distribution. As load increases, the upper delamination closes and two upper sublaminates deflect upward globally, and the difference between the two approaches becomes significant. For long lower delamination and shorter upper delamination (Figure 81), the postbuckling mechanism is same and the global behavior of the composite is similar to uniform delamination case. But, the lower delamination opens at a lower load level, and

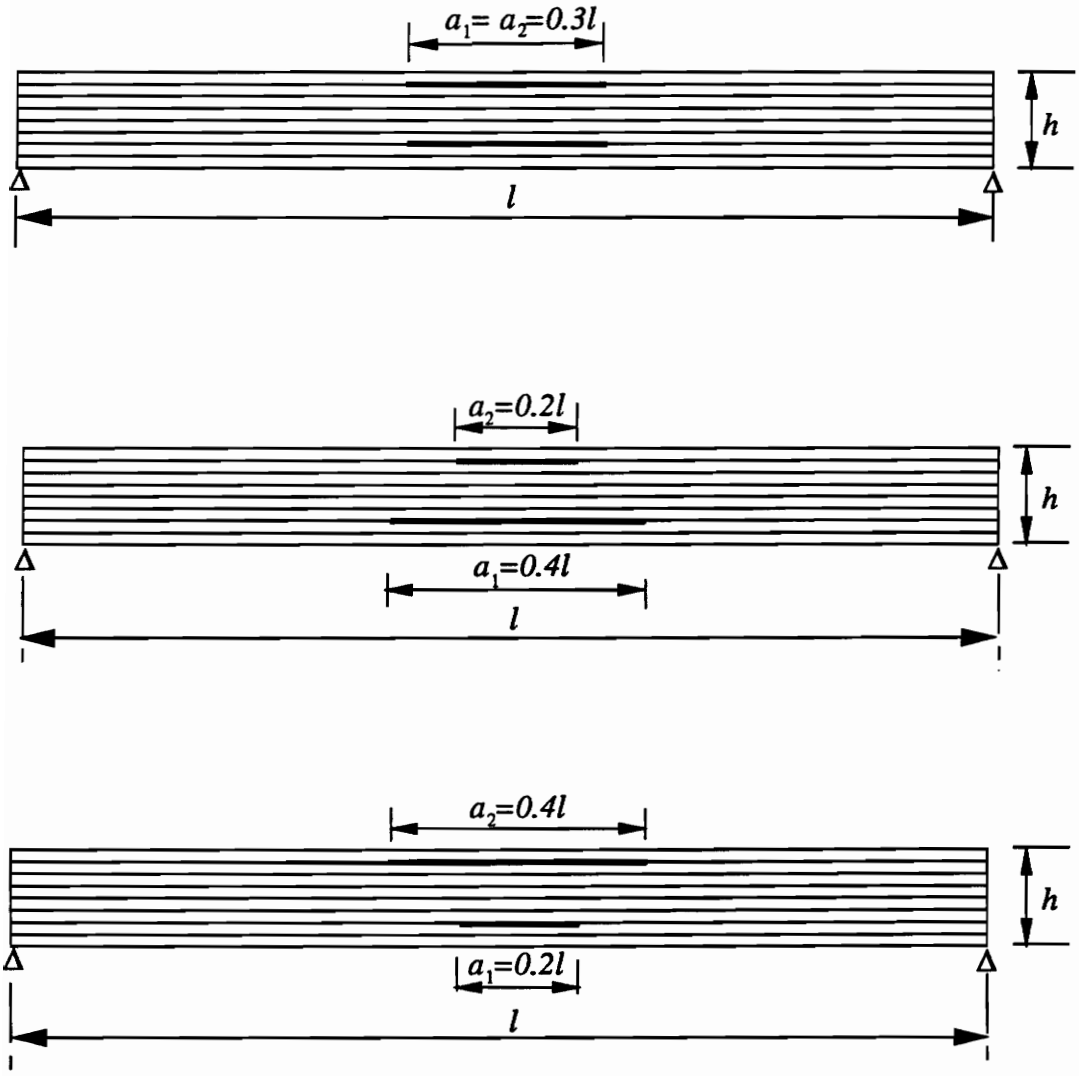

Figure 79. Geometry of an 8-layered quasi-isotropic composite containing two delaminations

global failure may occur sooner than for the uniform delamination case. The difference between the two approaches is small.

For short lower and longer upper delaminations (Figure 82), the situation is quite different. The bottom and middle sublaminates deflect together downward because the lower delamination size is so small that these two sublaminates act as one sublaminate having large bending-extension coupling. But, the upper sublaminate tends to deflect up due to another bending-extension coupling. Near $P = 0.3$, the top sublaminate suddenly pops down, closing the upper delamination, and the whole part still deflects down. This is because the effect of force eccentricity due to global downward bending is greater than the coupling effect of upper sublaminate at this load level. At increased load, both lower and upper delaminations open.

The postbuckling deformations for $[0/90/\pm 45]_s$ laminates are depicted in Figures 83 - 85. In this case, the top sublaminate exhibits high bending-extension coupling effects. Thus, the upper delamination tends to open as soon as load is applied, and the lower delamination remains closed for the whole postbuckling process in the case of uniform and long upper delaminations (Figures 83 and 85). In these cases, the result of layer-wise theory is significantly different from that of sublaminate theory due to the high coupling effect. For a long lower delamination, however, the thin bottom layer buckles first and the resulting force eccentricity makes the whole part deflect upward closing the upper delamination as for the $[0/\pm 45/90]_s$ case (Figure 84).

For a quasi-isotropic laminate having stiff layer in the core and relatively compliant layer in the outer region ($[45/90/-45/0]_s$) , the postbuckling deformations are shown in Figures 86 - 88. It is seen that no delamination opening occurs and no local buckling load is distinguishable for all three cases. For uniform and long lower delamination cases, the composite deflects upward gradually while the composite deflects downward

for the long upper delamination case. The difference of the two approaches is shown to be negligible.

The postbuckling analyses of a unidirectional fiber composite ($[0]_8$) are presented in Figures 89 - 91. In this case, the composite does not exhibit bending-extension coupling, and the only postcritical deformation driving force is the eccentricity in force distribution due to the delaminations. For both uniform and long lower delamination cases, the upper delamination always remains closed while the lower delamination opens monotonically. Around $P = 0.8$, the whole part deflects upward. For a composite having a long upper delamination, the global structure remains almost straight with delaminations closed until the buckling load for undelaminated composite. Global buckling occurs near $P = 1$. The effect of delamination is shown to be negligible in this case. It also appears that there are no differences between the layer-wise and sublaminate approaches for unidirectional composites, as expected.

From the results obtained here, it can be seen that the sublaminate approaches always overestimate the load-carrying capacity compared with the layer-wise solution. While the difference between these two approaches is shown to be negligible for global type buckling ($[45/90/-45/0]_s$), it is significant for high bending-stretching coupled sublaminate buckling ($[0/90/\pm 45]_s$).

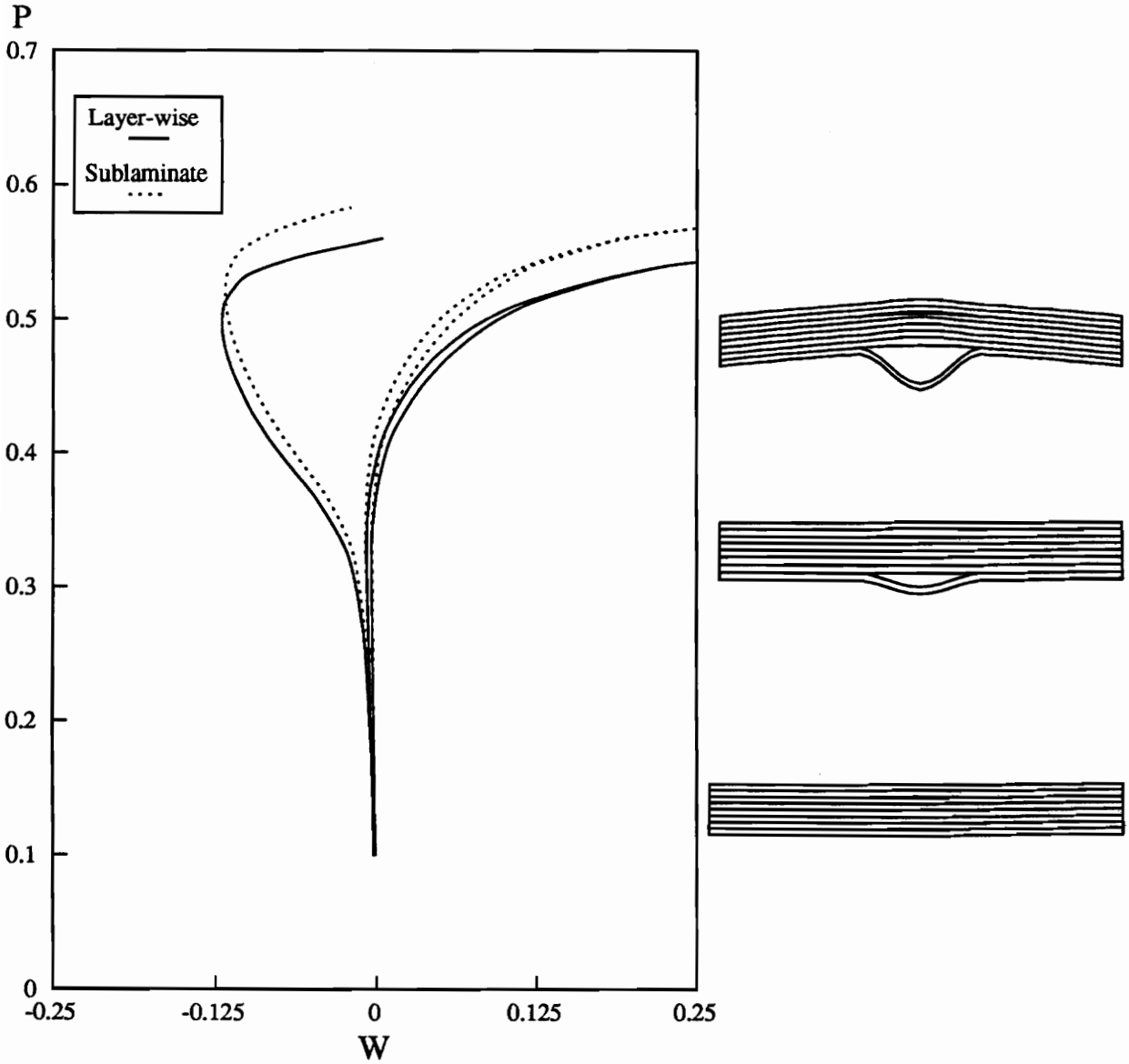

Figure 80. Load-deflection curve for a $[0/\pm 45/90]_S$ composite with $\bar{a}_1 = 0.3$, $\bar{a}_2 = 0.3$

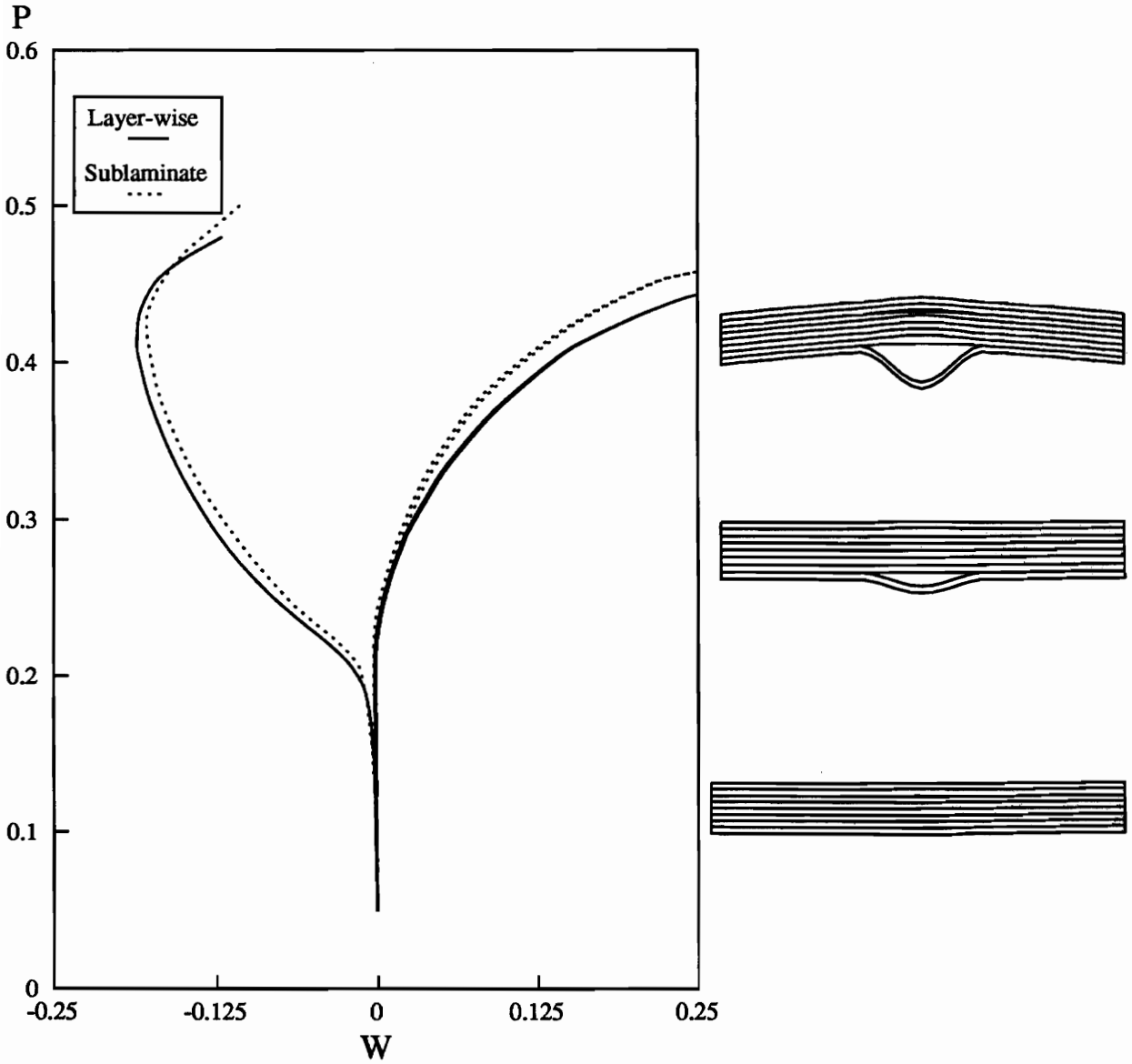

Figure 81. Load-deflection curve for a $[0/\pm 45/90]_S$ composite with $\bar{a}_1 = 0.4$, $\bar{a}_2 = 0.2$

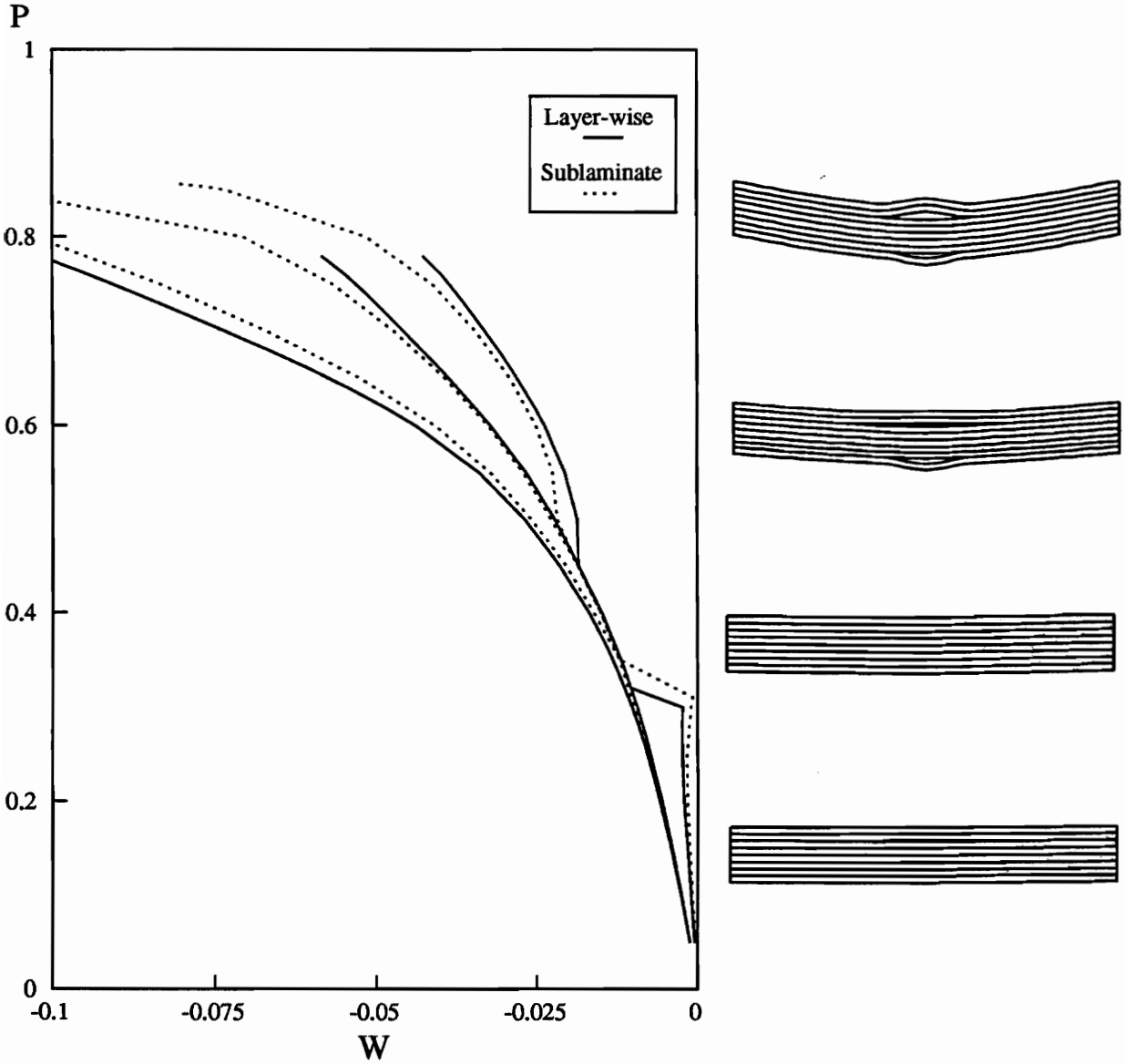

Figure 82. Load-deflection curve for a $[0/\pm 45/90]_S$ composite with $\bar{a}_1 = 0.2$, $\bar{a}_2 = 0.4$

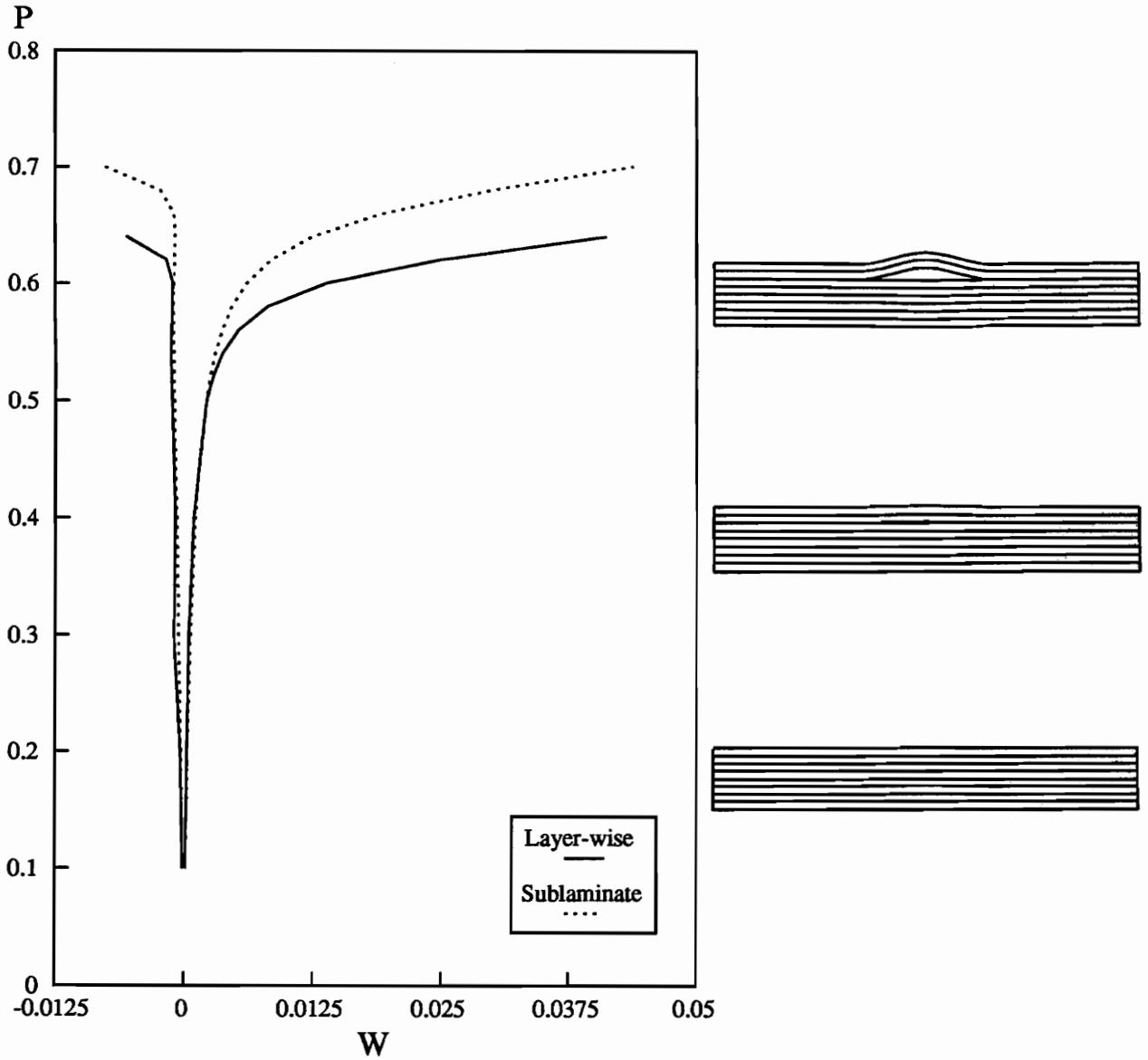

Figure 83. Load-deflection curve for a $[0/90/\pm 45]_S$ composite with $\bar{a}_1 = 0.3$, $\bar{a}_2 = 0.3$

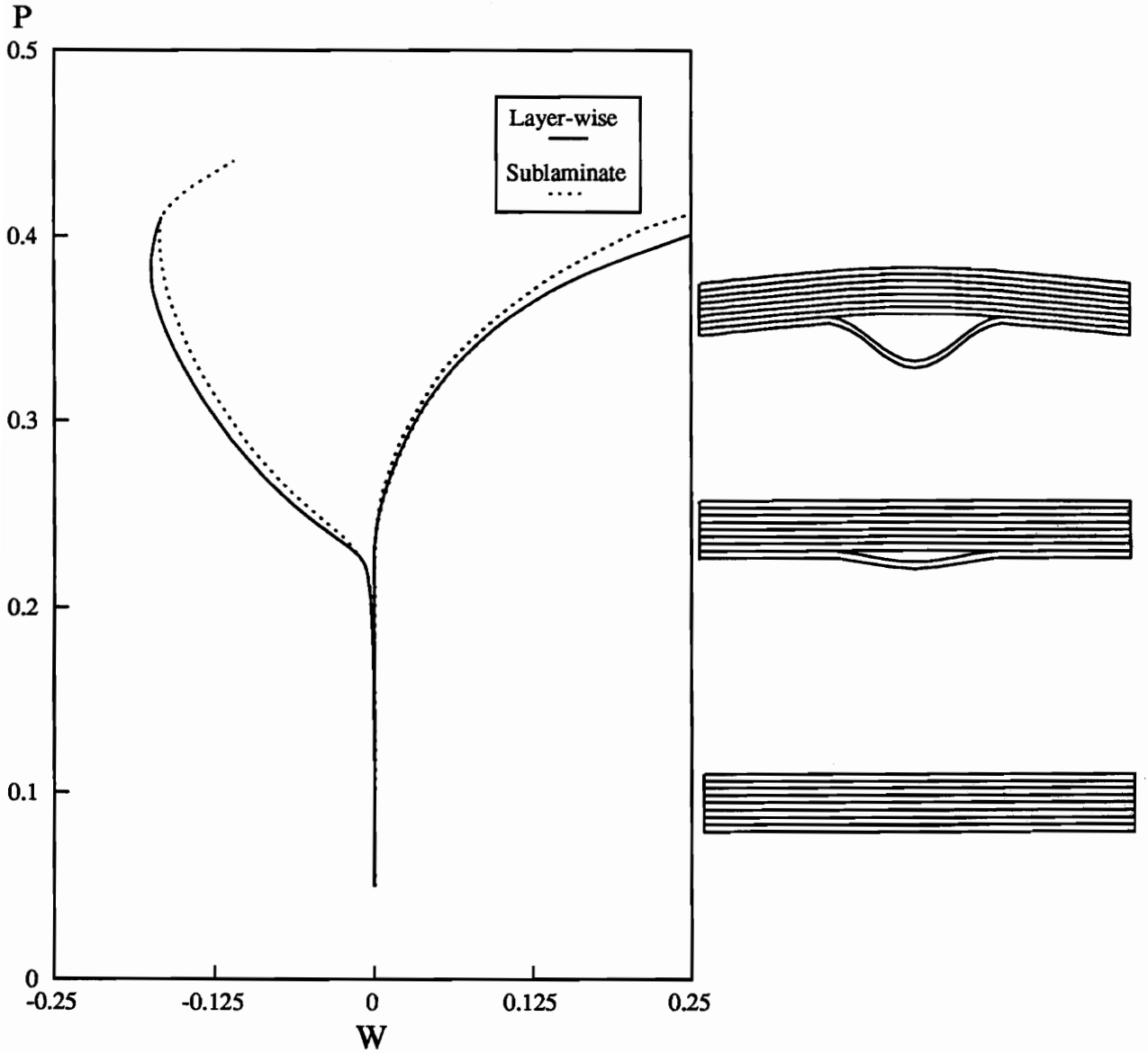

Figure 84. Load-deflection curve for a $[0/90/\pm 45]_S$ composite with $\bar{a}_1 = 0.4$, $\bar{a}_2 = 0.2$

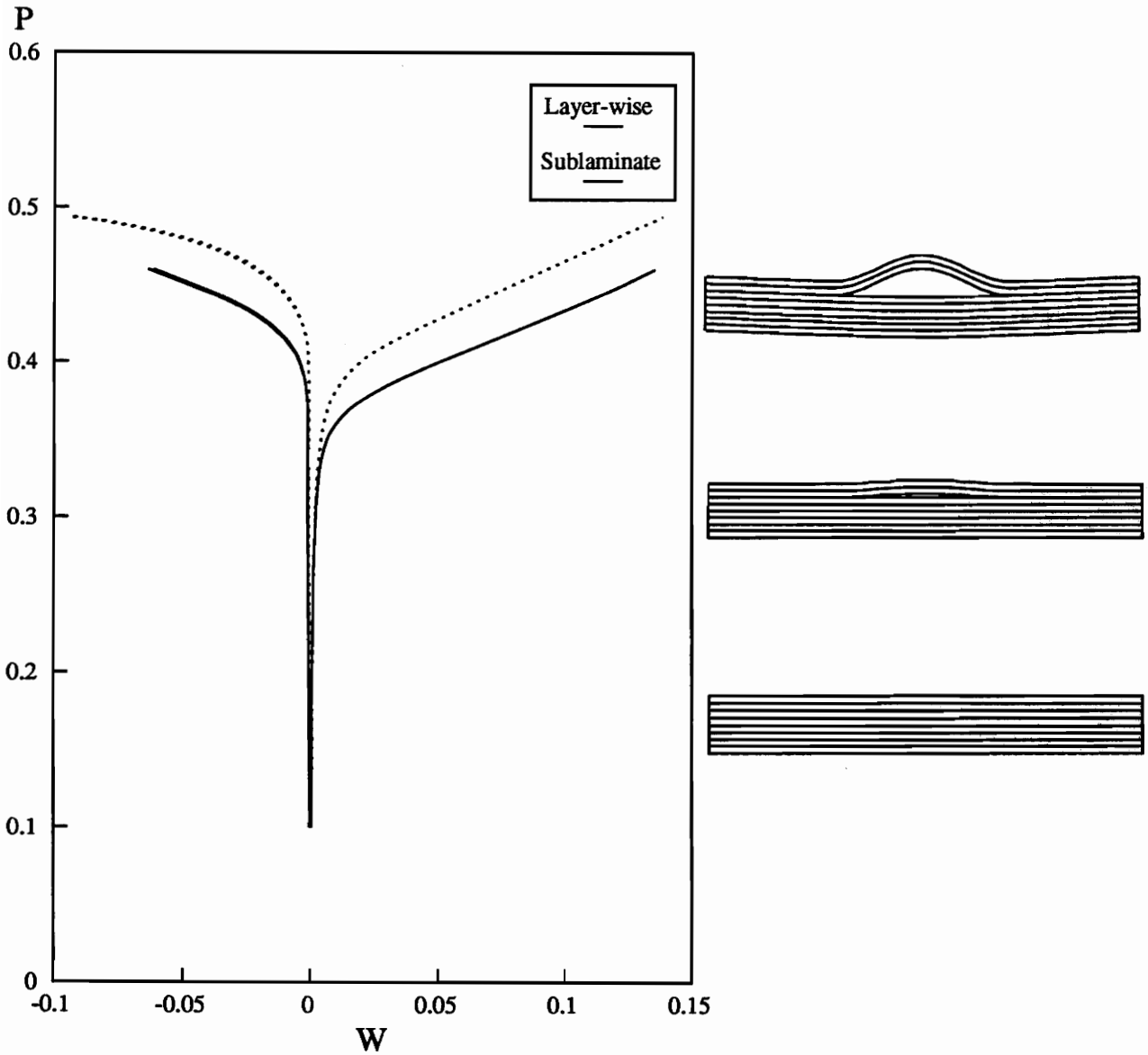

Figure 85. Load-deflection curve for a $[0/90/\pm 45]_S$ composite with $\bar{a}_1 = 0.2$, $\bar{a}_2 = 0.4$

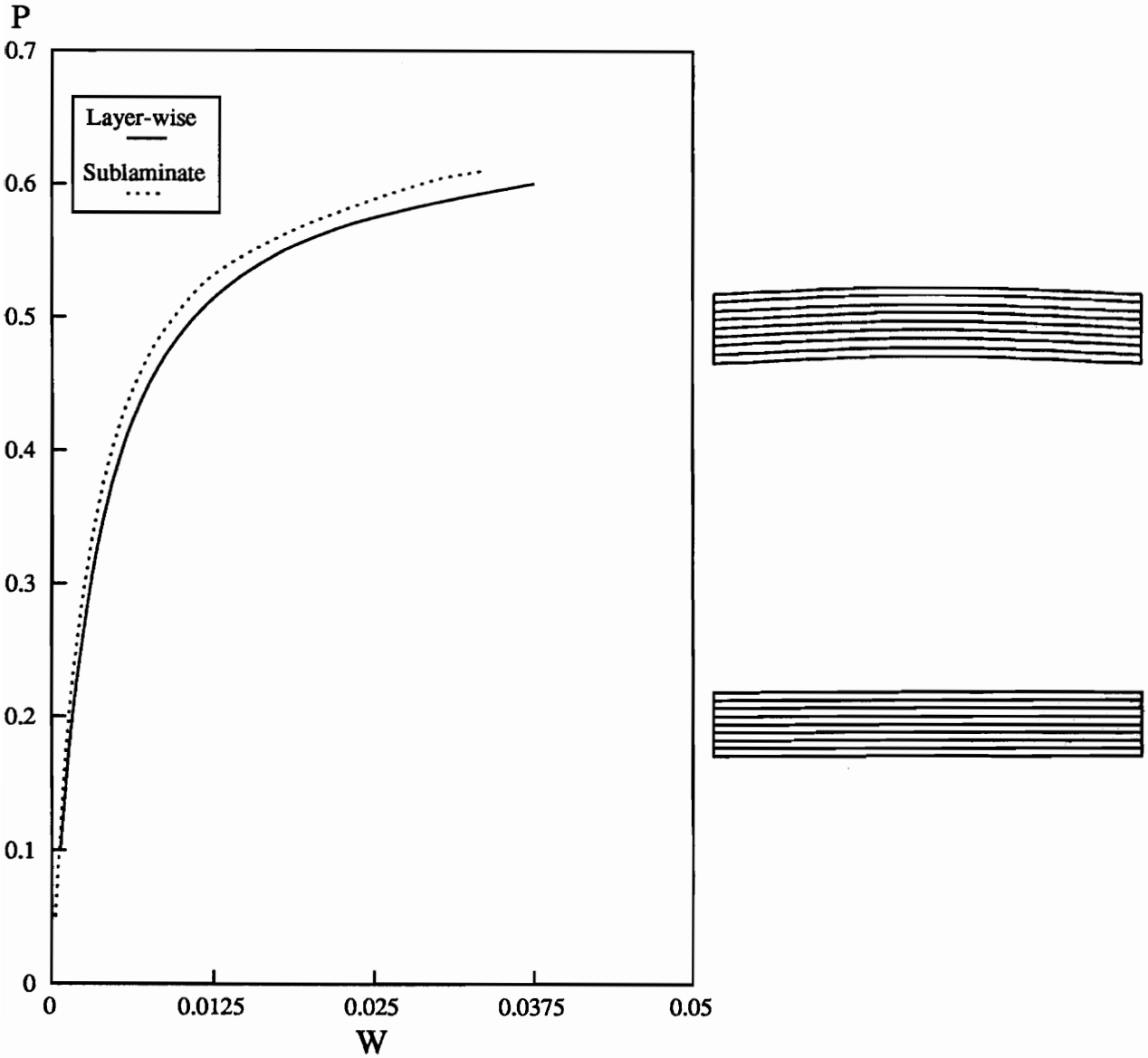

Figure 86. Load-deflection curve for a $[45/90/-45/0]_S$ composite with $\bar{a}_1 = 0.3$, $\bar{a}_2 = 0.3$

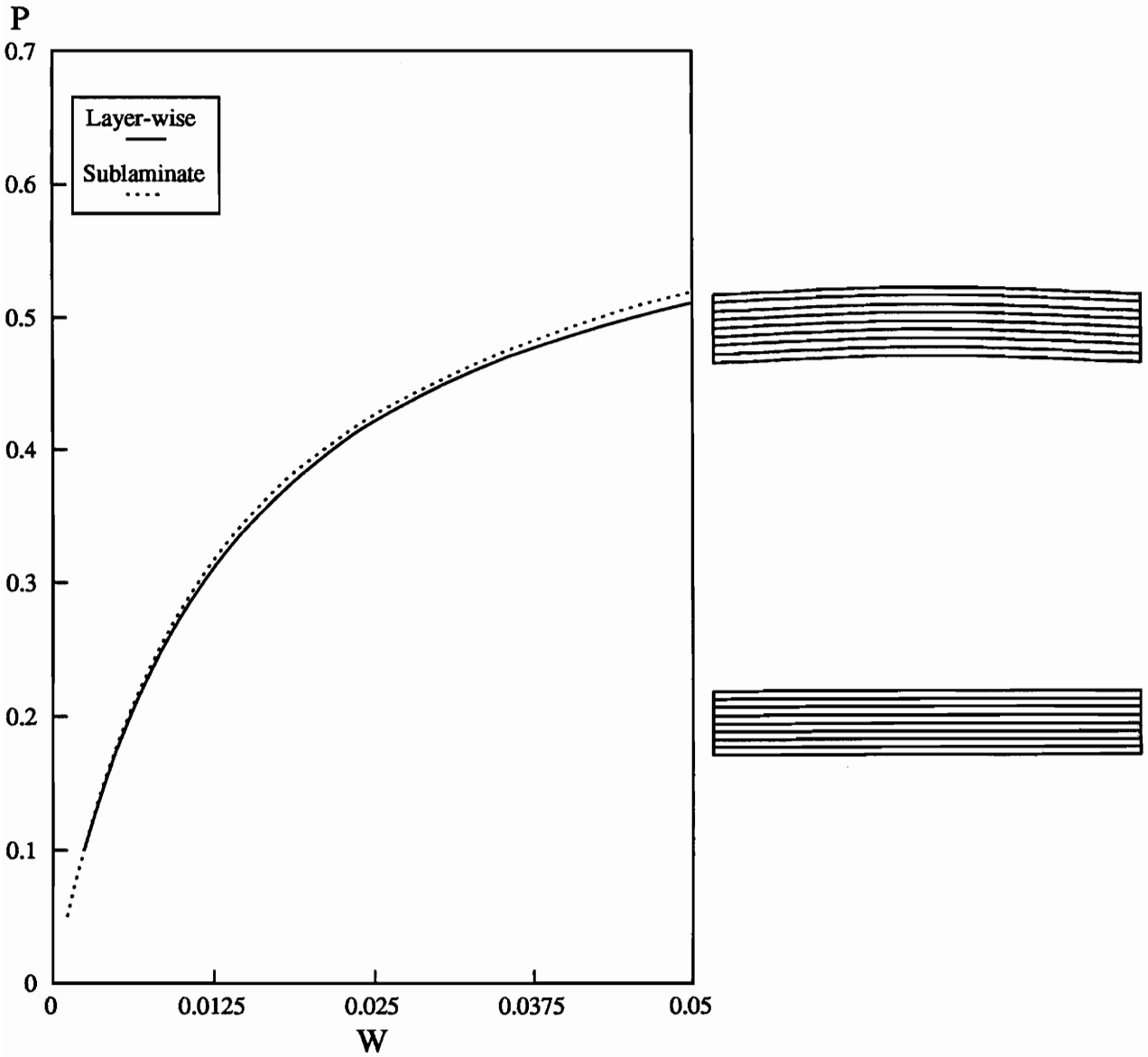

Figure 87. Load-deflection curve for a $[45/90/-45/0]_S$ composite with $\bar{a}_1 = 0.4$, $\bar{a}_2 = 0.2$

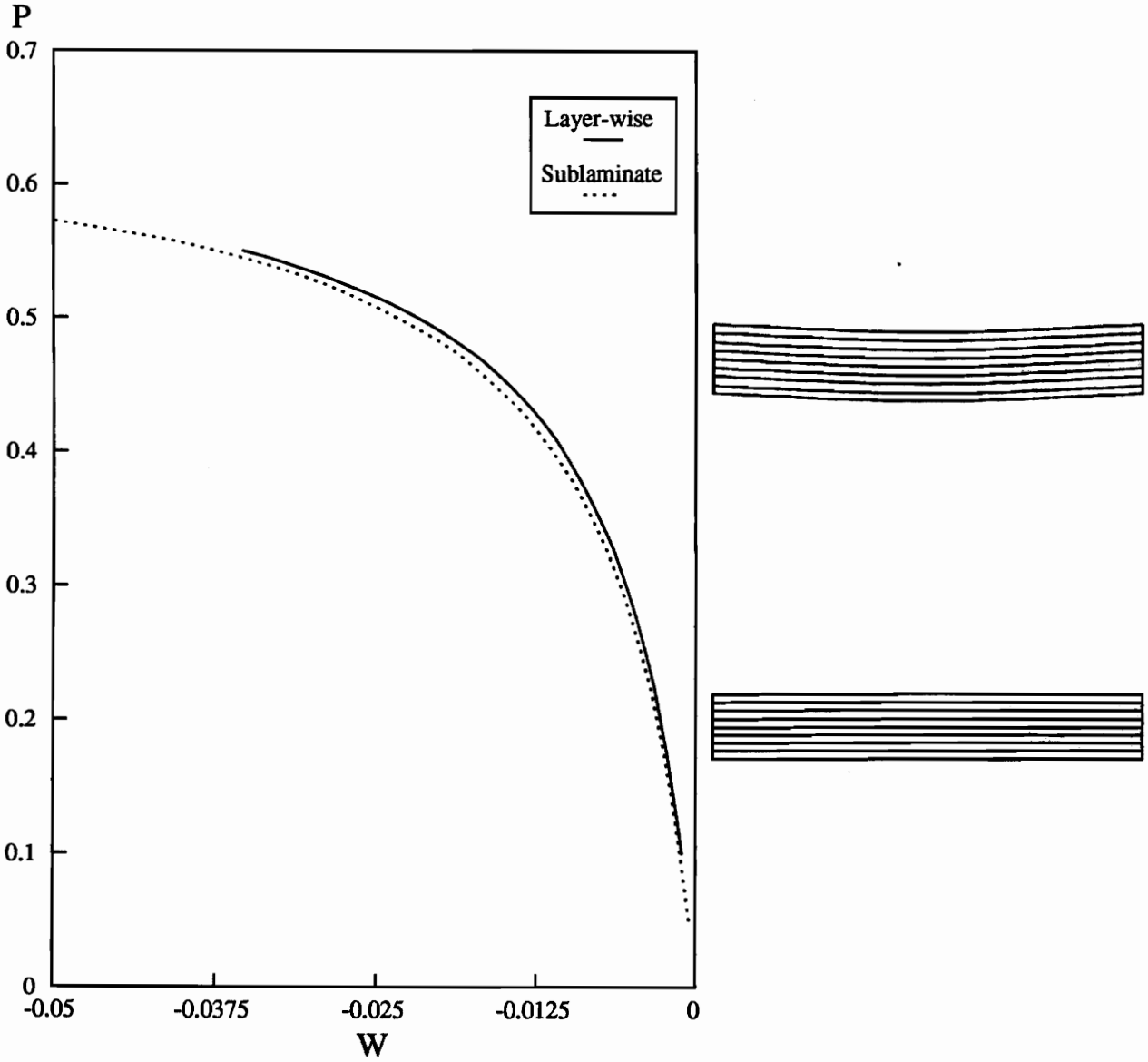

Figure 88. Load-deflection curve for a $[45/90/-45/0]_S$ composite with $\bar{a}_1 = 0.2$, $\bar{a}_2 = 0.4$

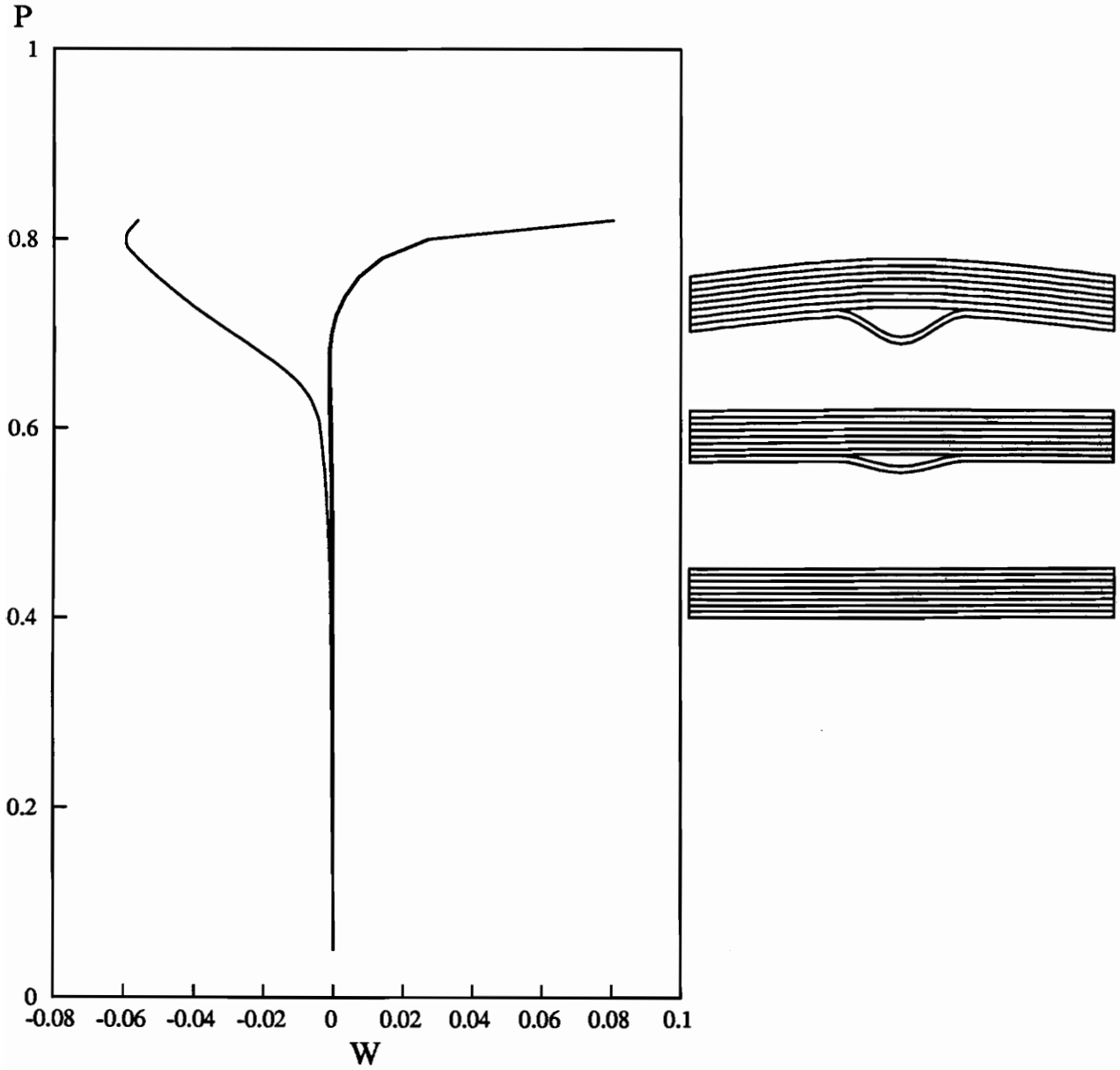

Figure 89. Load-deflection curve for a $[0]_8$ composite with $\bar{a}_1 = 0.3$, $\bar{a}_2 = 0.3$

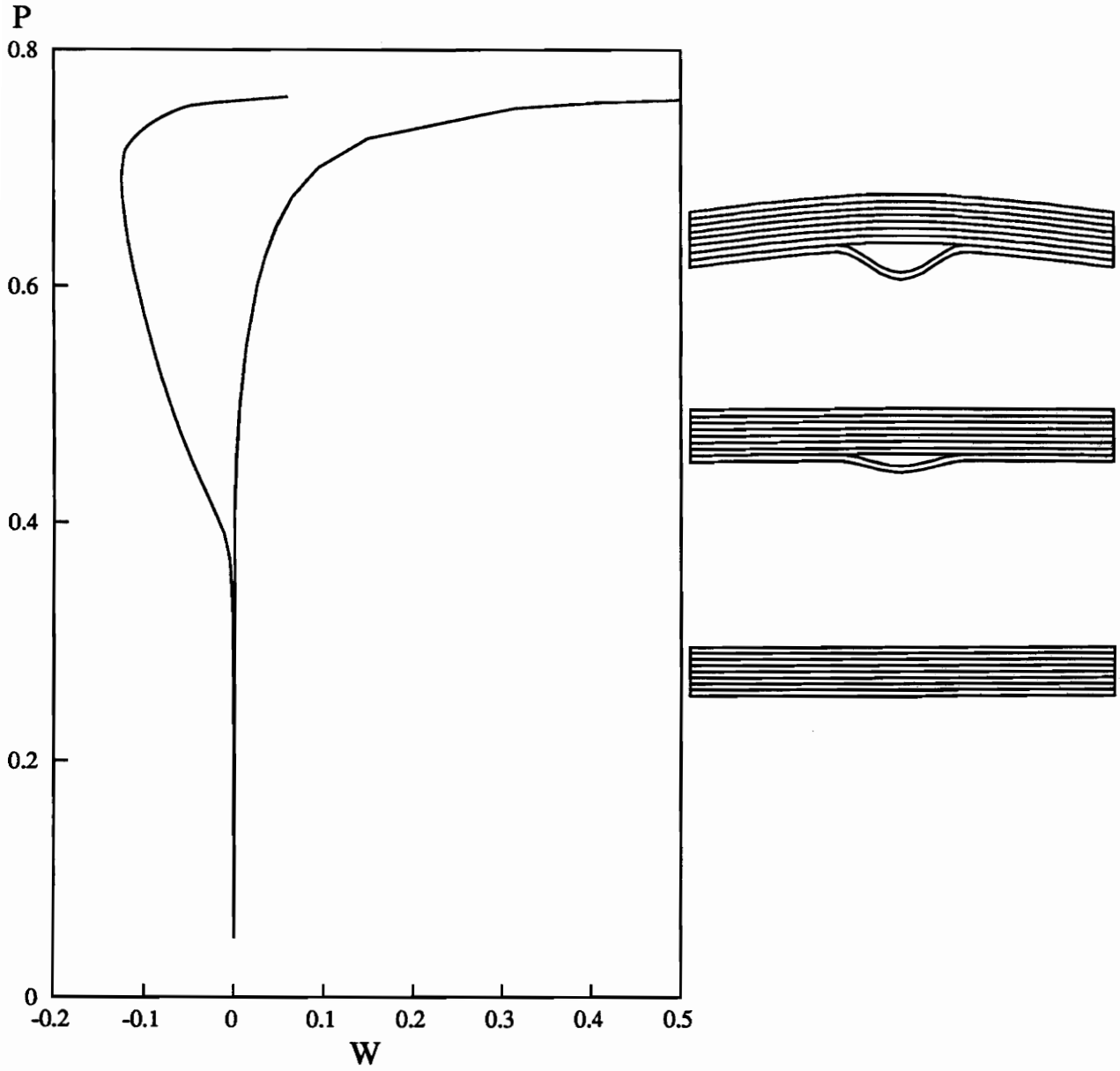

Figure 90. Load-deflection curve for a $[0]_8$ composite with $\bar{a}_1 = 0.4$, $\bar{a}_2 = 0.2$

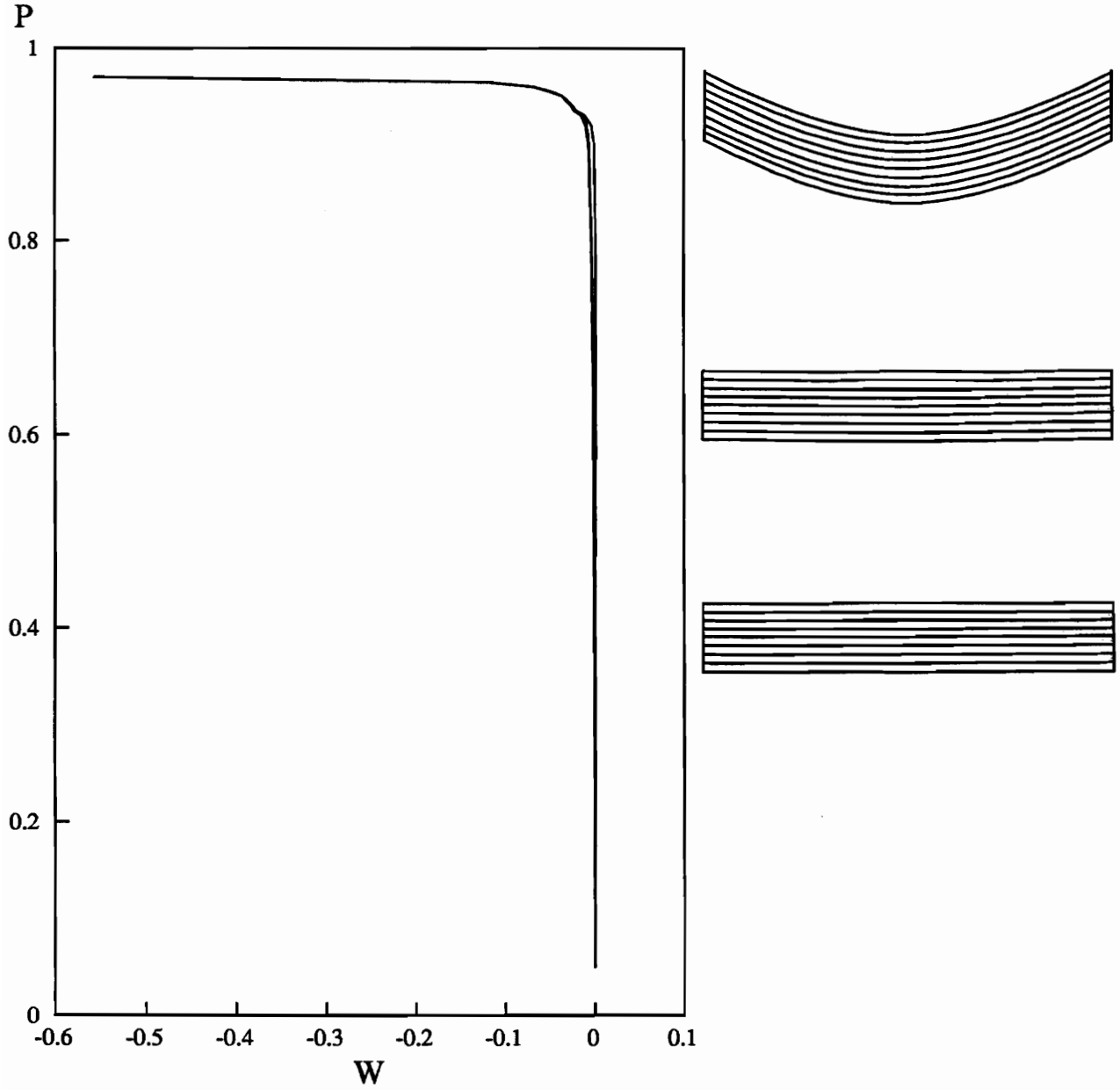

Figure 91. Load-deflection curve for a $[0]_8$ composite with $\bar{a}_1 = 0.2$, $\bar{a}_2 = 0.4$

Chapter VII

SUMMARY AND CONCLUSIONS

A one- and two-dimensional, layer-wise and sublaminate finite element model is developed to study the compressive stability and free vibration of composite plates with multiple delaminations. The model is capable of predicting accurate buckling loads, natural frequencies, and postbuckling response for various configurations such as through-the-width, concentric penny-shaped, and rectangular delaminations. All the possible buckling modes, including global, local, and global-local coupled symmetric modes and the antisymmetric mode are considered. The effects of composite geometry and locations, sizes, number and shapes of delamination on compressive behavior and vibration characteristics of composites are parametrically studied. The effects of material anisotropy, contact behavior of delaminated surfaces and initial imperfections of composites are also considered.

Based on the above theoretical developments and numerical results, the following concluding remarks are made:

1. The thickness-to-span ratio of a delaminated composite affects the buckling load and mode shapes for the through-the-width delamination case. For thick composites, depending on the delamination length, composites with midplane delamination can buckle in local or global symmetric modes, or even in an *antisymmetric* mode. However, the thickness-to-span ratio does not cause substantial change in buckling loads and mode shapes for penny-shaped midplane delaminations in circular plates under circumferential load. The buckling modes are always global symmetric.
2. For an embedded square midplane delamination in angle-ply laminates, the delamination effect is almost constant for one half-wave buckling mode as lamination angle θ changes while it strongly depends upon θ for two half-wave buckling mode.
3. In order to obtain physically admissible vibration frequencies and mode shapes of composites with a through-the-width delamination, two states of mode shapes in which a delamination opens and closes are considered separately. By combining the frequencies of the two vibration mode states, the natural frequency of a delaminated composite is approximated. While this weighted frequency method is quite reasonable for global-type vibration modes (small delamination opening), the method is somewhat inappropriate for highly local-type vibration modes, and more accurate analysis seems to be necessary.
4. The postbuckling response of a delaminated composite is very sensitive to the amplitude and the direction of the initial imperfection. This is especially true for near-the-surface delaminations. This is because there are many equilibrium paths, and the composite can take any path depending on the initial imperfections. For a relatively large magnitude of imperfection in the direction of the thicker sublaminate, delamination buckling does not occur, showing that the presence of this imperfection has a beneficial contribution on the postbuckling response of a delaminated composite.

5. Buckling loads and mode shapes are influenced by axial and through-the-thickness locations of through-the-width delaminations. For a given length of delamination, the buckling load decreases as the delamination approaches the surface of the plate. The ultimate load-carrying capacity also decreases as a delamination is closer to the surface when the delamination is relatively short. However, for a longer delamination, the load-carrying capacity is shown to increase as the delamination approaches the surface. In general, the difference between local buckling load and ultimate global buckling load increases as the delamination approaches the surface.
6. The effect of anisotropy on the buckling and postbuckling response of delaminated composites is significant. The bifurcation analysis for highly anisotropic sublaminates may lead to erroneous results, and accordingly postbuckling analysis is necessary. For compliant inner and stiff outer layers ($[0/90/90//0]_s$), the bending - extension coupling significantly reduced the buckling load and increased the postbuckling deformation. However, for stiff inner and compliant outer layers ($[90/0/0//90]_s$), the coupling shown to be a *stabilization effect* for delamination buckling and postbuckling deformation contradicting other previous conclusions [40,41,48]. This is because the contact effects of delaminated surfaces were neglected in those previous works.
7. For composites with two and three through-the-width delaminations, the buckling and postbuckling responses are shown to be very sensitive to location of delaminations. As the two outer delaminations approach to the midplane of the composite, the buckling loads for symmetric modes are monotonically increased, while the buckling load for antisymmetric mode reaches the lowest value when the delaminations are located equidistantly. When composites buckle in an antisymmetric mode, there is no postbuckling deformation, and thus this antisymmetric mode can be considered to be catastrophic.

8. For some configurations of multiple delaminations, although the first buckling load for the antisymmetric mode is much greater than for the symmetric mode, the ultimate load-carrying capacity is significantly lower than the symmetric case due to the unstable nature of the antisymmetric mode. In this case, sudden *mode change* in postbuckling deformation is expected.
9. Composites with seven uniform, equidistant through-the-width delaminations have a much lower buckling load for short delaminations than that for a single delamination at the outermost layer and that of a triangular delamination shape due to the antisymmetric mode. It is noted that the larger the number of delaminations, the more dominant is the antisymmetric mode for short uniform delaminations. The buckling mode is still symmetric even for equidistant multiple penny-shaped delaminations in a circular plate.
10. For composites containing multiple delaminations, the *contact* effects between delaminated surfaces become significant, and the proposed simple contact algorithm is shown to be very efficient for solving the problem.
11. For a composite with a stiff core (0°), the composite buckles globally with all delaminations closed, implying that the stiff core is potentially helpful for damage tolerance of composites for delaminations. For composites with a compliant core, the composite is more prone to delamination opening, and the postbuckling deformation depends on the configuration of the delaminations.
12. The proposed *sublaminate* theory predicts buckling loads and mode shapes accurately for delaminated composites with significantly reduced computational cost and time compared to the layer-wise theory. For the postbuckling response, however, it is not as accurate as for the bifurcation case. This is because the coupling effects that comes from material anisotropy may be overlooked in sublaminate approach which is based on averaged properties of each sublaminate. The layer-wise ap-

proach, which models laminates layer-by-layer, is, therefore, preferred for more accurate postbuckling analysis of delaminated composites.

As a natural extension of the present study, the following can be recommended:

1. Buckling and postbuckling behavior of composites with delaminations under combined shear and compressive loads
2. Thermal and moisture effects on the stability of composites containing delaminations
3. More rigorous approach for the vibration of delaminated composites, which can predict interaction between open and closed delamination states accurately.
4. Delamination propagation with appropriate fracture criterion and final failure prediction of delaminated composites

REFERENCES

1. Starnes, J. H., Rhodes, M. D. and Williams, J. G. "Effect of Impact Damage and Holes on the Compressive Strength of a Graphite/Epoxy Laminate," *Nondestructive Evaluation and Flaw Criticality for Composite Materials, ASTM STP 696, R. B. Pipes, Ed.,* 1979, pp. 145-171.
2. Jones, R. "Damage Tolerance of Advanced Composite Materials: Compression," *Role of Fracture Mechanics in Modern Technology , G. C. Sih, H. Nisitani and T. Ishihara (editors),* Elsevier Science Publishers B. V. (North-Holland), 1987, pp. 653-663.
3. Reddy, J. N. "A Generalization of Two Dimensional Theories of Laminated Composite Plates," *Communications in Applied Numerical Methods,* Vol. 3, 1987, pp. 173-180.
4. Yang, P. C., Norris, C. H., Stavsky, Y., "Elastic Wave Propagation in Heterogeneous Plates," *International Journal of Solids and Structures,* Vol. 2, 1966, pp. 665-684.
5. Whitney, J. M., "The Effect of Transverse Shear Deformation on the Bending of Laminated Plates," *Journal of Composite Materials,* Vol. 3, 1973, pp. 534-547.
6. Whitney, J. M. and Sun, C. T., "A Higher Order Theory for Motion of Laminated Composites," *Journal of Sound and Vibration,* Vol. 30, 1973, pp. 85-97.
7. Lo, K. H., Christensen, R. M. and Wu, E. M., "A Higher-Order Theory of Plate Deformation Part 2;Laminated Plates," *ASME Journal of Applied Mechanics,* Vol. 44, 1977, pp. 669-676.
8. Reddy, J. N., "A Simple Higher-Order Theory for Laminated Composite Plates," *ASME Journal of Applied Mechanics,* Vol. 51, 1984, pp. 745-752.

9. Reddy, J. N., "On Refined Computational Models of Composite Laminates," *International Journal for Numerical Methods in Engineering,* Vol. 27, 1989, pp. 233-265.

10. Reddy, J. N., "A Review of Refined Theories of Laminated Composite," *Shock and Vibration Digest,* Vol. 22, 1990, pp. 3-17.

11. Noor, A. K. and Burton, W. S., "Assessment of Computational Models for Multilayered Anisotropic Plates ," *Composite Structures,* Vol. 14, 1990, pp. 233-265.

12. Rohwer, K., "Application of Higher Order Theories to the Bending Analysis of Layered Composite Plates," *International Journal of Solids and Structures,* Vol. 29, 1992, pp. 105-119.

13. Pryor, C. W. and Barker, R. M., "A Finite Element Analysis Including Transverse Shear Effects for Application to Laminated Plates," *AIAA Journal,* Vol. 9, 1971, pp. 912-917.

14. Srinivas, S., "Refined Analysis of Composite Laminates," *Journal of Sound and Vibration,* Vol. 30, 1973, pp. 495-507.

15. Mau, S. T., "A Refined Laminated Plate Theory," *ASME Journal of Applied Mechanics,* Vol. 40, 1973, pp. 606-607.

16. Seide, P., "An Improved Approximate Theory for the Bending of Laminated Plates," *Mechanics Today,* Vol. 5, 1980, pp. 451-466.

17. Spilker, R. L., Chou, S. C. and Opringer, O., "Alternate Hybrid-Stress Elements for Analysis of Multilayer Composite Plates," *Journal of Composite Materials,* Vol. 11, 1977, pp. 51-70.

18. Chaudhuri, R. A., "Triangular Finite Element for Analysis of Thick Laminated Plates," *International Journal for Numerical Methods in Engineering,* Vol. 24, 1987, pp. 1203-1224.

19. Reissner, E., "On a Mixed Variational Theorem and On Shear Deformable Plate Theory," *International Journal for Numerical Methods in Engineering,* Vol. 23, 1986, pp. 193-198.

20. Toledano, A. and Murakami, H., "A Composite Plate Theory for Arbitrary Laminate Configurations," *ASME Journal of Applied Mechanics,* Vol. 54, 1987, pp. 181-189.

21. DiSciuva, M., "Development of an Anisotropic Multilayered Shear-Deformable Rectangular Plate Element," *Computers and Structures,* Vol. 21, 1985, pp. 789-796.

22. DiSciuva, M., "An Improved Shear-Deformation Theory for Moderately Thick Multilayered Anisotropic Shells and Plates," *ASME Journal of Applied Mechanics,* Vol. 54, 1987, pp. 589-596.

23. Cho, K. N., Striz, A. G. and Bert, C. W., "Bending Analysis of Thick Bimodular Laminates by Higher Order Individual-Layer Theory," *Composite Structures,* Vol. 15, 1990, pp. 1-24.

24. Reddy, J. N., Barbero, E. J., "A Plate Bending Element Based On a Generalized Laminated Plate Theory ," *International Journal for Numerical Methods in Engineering,* Vol. 28, 1989, pp. 2275-2292.

25. Barbero, E. J. and Reddy, J. N., "Nonlinear Analysis of Composite Laminates Using a Generalized Laminated Plate Theory," *AIAA Journal,* Vol. 28, 1990, pp. 1987-1994.

26. Epstein, M. and Huttelmaier, H. P., "A Finite Element Formulation for Multilayered and Thick Plates," *Computers and Structures,* Vol. 16, 1983, pp. 645-650.

27. Barboni, R. and Gaudenzi, P., "A Three Dimensional Finite Element Analysis of Edge Effects in Composite Materials," *Composite Materials - Design and Analysis; Proceeding of the 2nd International Conference on Computer Aided Design in Composite Material Technology,* Free University of Brussels and Wessex Institute of Technology, 1990, eds. W. P. Wilde, W. R. Blain, pp. 239-247.

28. Robbins, D. H. and Reddy, J. N., "Modelling of Thick Composites Using a Layer-Wise Laminate Theory," *CCMS Report 91-10,* Virginia Polytechnic Institute and State University, 1991.

29. Lee, C. Y. and Liu, D., "An Interlaminar Stress Continuity Theory for Laminated Composite Analysis," *Computers and Structures,* Vol. 42, 1992, pp. 69-78.

30. Owen, D. R. J. and Li, Z. H., "A Refined Analysis of Laminated Plates by Finite Element Displacement Methods I-Fundamentals and Static Analysis," *Computers and Structures,* Vol. 26, 1987, pp. 907-914.

31. Owen, D. R. J. and Li, Z. H., "A Refined Analysis of Laminated Plates by Finite Element Displacement Methods II-Vibration and Stability," *Computers and Structures,* Vol. 26, 1987, pp. 915-923.

32. Wanthal, S. P. and Yang, H. T. Y., "Three-Dimensional Finite Element Formulations for Laminated Plates," *Journal of Reinforced Plastics and Composites,* Vol. 10, 1991, pp. 330-355.

33. Griffin, O. H., "The Use of Computers in the Evaluation of Three Dimensional Stress Effects in Composite Material Products," *Composite Materials - Design and Analysis; Proceeding of the 2nd International Conference on Computer Aided Design in Composite Material Technology,* Free University of Brussels and Wessex Institute of Technology, 1990, eds. W. P. Wilde, W. R. Blain, pp. 171-187.

34. Chai, H., Babcock, C. D. and Knauss, W. B. "One-Dimensional Modelling of Failure in Laminated Plates by Delamination Buckling," *International Journal of Solids and Structures,* Vol. 17, 1981, pp. 1069-1083.

35. Simitses, G. J., Sallam, S. and Yin, W. L. "Effect of Delamination of Axially Loaded Homogeneous Laminated Plates," *AIAA Journal,* Vol. 23, 1985, pp. 1437-1444.

36. Sallam, S. and Simitses, G. J., "Delamination Buckling and Growth of Flat Cross-Ply Laminates," *Composite Structures,* Vol. 4, 1985, pp. 361-381.

37. Yin, W. L., Sallam, S. and Simitses, G. J., "Ultimate Axial Load Capacity of a Delaminated Beam-Plate," *AIAA Journal,* Vol. 24, 1986, pp. 123-128.

38. Bolotin, V. V., Zebelyan, Z. K. and Kurzin, A. A. "Stability of Compressed Components with Delamination-Type Flaws," *Probl. Proch.,* Vol. 7, 1981, pp. 813-819.

39. Sheinman, I., Bass, M. and Ishai, O., "Effect of Delamination on Stability of Laminated Composite Strip," *Composite Structures,* Vol. 11, 1989, pp. 227-242.

40. Yin, W. L., "The Effects of Laminated Structures on Delamination Buckling and Growth," *Journal of Composite Materials,* Vol. 22, 1988, pp. 502-517

41. Sheinman, I. and Souffer, M., "Postbuckling Analysis of Composite Delaminated Beams," *International Journal of Solids and Structures,* Vol. 27, 1991, pp. 639-646.

42. Moshaiov, A. and Marshall, J., "Analytical Determination of Critical Load of Delaminated Plates" *Journal of Ship Research,* Vol. 35, 1991, pp. 87-90.

43. Somers, M., Weller, T. and Abramovich, H., "Influence of Predetermined Delaminations on Buckling and Postbuckling Behavior of Composite Sandwich Beams," *Composite Structures,* Vol. 17, 1991, pp. 295-329.

44. Tracy, J. T. and Pardoen, G. C., "The Effect of Delamination on the Fundamental and Higher order Buckling Loads of Laminated Beams," *Journal of Composite Testing and Research,* Vol. 11, 1989, pp. 87-93.

45. Kardomateas, G. A. and Schmueser, D. W., "Buckling and Postbuckling of Delaminated Composites under Compressive Loads Including Shear Effects," *AIAA Journal,* Vol. 26, 1988, pp. 337-343.

46. Kardomateas, G. A., "Large Deformation Effects in the Postbuckling Behavior of Composite with Thin Delaminations," *AIAA Journal,* Vol. 27, 1988, pp. 624-631.

47. Chen, H. P., "Shear Deformation Theory for Compressive Delamination Buckling and Growth," *AIAA Journal,* Vol. 29, 1991, pp. 813-819.

48. Chen, H. P., "A Delamination Buckling and Growth for Unsymmetric Laminates by Shear Deformation Theory," *Proceeding of AIAA/ASME/ASCE/AHS/ASC 32th SDM Conference* Baltimore, Maryland, 1991, pp. 896-905.

49. Vizzini, A. J. and Lagace, P. A., "The Buckling of a Delaminated Sublaminate on Elastic Foundation," *Journal of Composite Materials,* Vol. 21, 1985, pp. 1106-1117.

50. Anastasiad, J. S. and Simitses, G. J., "Spring Simulated Delamination of Axially-Loaded Flat Laminates," *Composite Structures,* Vol. 17, 1991, pp. 67-85.

51. Kardomateas, G. A., "Effect of an Elastic Foundation on the Buckling and Postbuckling of Delaminated Composites under Compressive Loads," *ASME Journal of Applied Mechanics,* Vol. 55, 1988, pp. 238-241.

52. Suemasu, H., "Analytical Study of Shear Buckling and Postbuckling of Composite Plates with a Delamination," *JSME International Journal, Series I,* Vol. 34, 1991, pp. 135-142.

53. Madenzi, E., "Delamination Growth and Buckling in an Orthotropic Strip," *International Journal of Solids and Structures,* Vol. 27, 1991, pp. 1773-1888

54. Whitcomb, J. D., "Finite Element Analysis of Instability Related Delamination Growth," *Journal of Composite Materials,* Vol. 15, 1981, pp. 403-426.

55. Wang, S. S., Zahlan, N. M. and Suemasu, H., "Compressive Stability of Delaminated Random Short-Fiber Composites, Part I-Modelling and Methods of Analysis," *Journal of Composite Materials,* Vol. 19, 1985, pp. 296-316.

56. Wang, S. S., Zahlan, N. M. and Suemasu, H., "Compressive Stability of Delaminated Random Short-Fiber Composites, Part II- Experimental and Analytical Results" *Journal of Composite Materials,* Vol. 19, 1985, pp. 317-333.

57. Williams, J. F., Stouffer, O. C., Illic, S. and Jones, R., "An Analysis of Delamination Behavior," *Composite Structures,* Vol. 5, 1986, pp. 203-216.

58. Shaw, D. and Tsai, M. Y., "Analysis of Delamination in Compressively Loaded Laminates," *Composite Science and Technology,* Vol. 34, 1989, pp. 1-17.

59. Chaouk, H. and Steven, G. P., "Closure Effects in Delaminated Graphite Epoxy Laminate under Compression," *Theoretical Applied Fracture Mechanics,* Vol. 8, 1987, pp. 79-85.

60. Jones, R. and Callinan, R. J., "Analysis of Compression Failure in Fiber Composite Laminates," *Progress in Science and Engineering of Composites,* ICCM-IV, Tokyo, 1982, pp.

61. Kapania, R. K. and Wolfe, D. R., "Delamination Buckling and Growth in Axially-Loaded Beam-Plate," *Proceeding of AIAA/ASME/ASCE/AHS/ASC 28th SDM Conference* Monterey, California, 1987, pp. 766-775.

62. Kapania, R. K. and Wolfe, D. R., "Buckling of Axially-Loaded Beam-Plate with Multiple Delamination," *Advances in Macro-Mechanics of Composite Material Vessels and components,* D. Hui, T. J. Kojik, PVP Vol. 146 PD Vol. 18., ASME New York, 1988, pp. 1-10.

63. Kutlu, Z. and Chang, F. K., "Modelling Compression Failure of Laminated Composites Containing Multiple Through-the-Width Delaminations," *Journal of Composite Materials,* Vol. 26, 1992, pp. 350-387.

64. Breivik, N. L., "Compression of Thick Laminated Composite Beams with Initial Impact-Like Damage," *Master Thesis,* Virginia Polytechnic Institute and State University, 1992

65. Lee, J., Gürdal, Z. and Griffin, O. H., "A Layer-Wise Approach for the Bifurcation Problems in Composites with Delaminations," *Proceeding of AIAA/ASME/ASCE/AHS/ASC 33th SDM Conference* Dallas, Texas, 1992, pp. 10-20.

66. Ramkumar, R. L., Kulkarni, S. V. and Pipes, R. B., "Free Vibration Frequencies of a Delaminated Beam," *34th Annual Technical Conference, Reinforced/Composites Institute, Society of Plastics Industry,* 1979, Section 22-E, pp. 1-5

67. Wang, J. T. S., Lyn, Y. Y. and Gibby, J. A., "Vibration of Split Beams," *Journal of Sound and Vibration,* Vol. 84, 1982, pp. 491-502.

68. Yin, W. L. and Jane, K. C., "Vibration of a Delaminated Beam-Plate Relative to Buckled States," *Proceeding of AIAA/ASME/ASCE/AHS/ASC 29th SDM Conference* Williamsburg, Virginia, 1988, pp. 860-870

69. Chen, H. P. and Goggin, P., "Free Vibration of a Compressed Delaminated Plate," *Proceeding of AIAA/ASME/ASCE/AHS/ASC 33th SDM Conference* Dallas, Texas, 1992, pp. 1830-1840.

70. Tracy, J. T. and Pardoen, G. C., "Effect of Delamination on the Natural Frequencies of Composite Laminates," *Journal of Composite Materials,* Vol. 23, 1989, pp. 1200-1215.

71. Shen, M. H. H. and Grady, J. E., "Free Vibrations of Delaminated Beams," *Proceeding of AIAA/ASME/ASCE/AHS/ASC 32th SDM Conference* Baltimore, Maryland, 1991, pp. 3017-3025.

72. Kachanov, L. M., "Separation Failure of Composite Materials," *Polymer Mechanics,* Vol. 12, 1976, pp. 812-815.

73. Bottega, W. J., Maewal, A., "Delamination Buckling and Growth in Laminates," *ASME Journal of Applied Mechanics,* Vol. 50, 1983, pp. 184-189.

74. Bottega, W. J., Maewal, A., "Dynamics of Delamination Buckling," *International Journal of Nonlinear Mechanics,* Vol. 18, 1983, pp. 449-463.

75. Yin, W. L., "Axisymmetric Buckling and Growth of a Circular Delamination in a Compressive Laminate," *International Journal of Solids and Structures,* Vol. 21, 1985, pp. 503-514.

76. Yin, W. L. and Fei, Z. "Buckling Load of a Circular Plate with a Concentric Delamination," *Mechanics Research Communication,* Vol. 11, 1984, pp. 337-344.

77. Yin, W. L. and Fei, Z. "Delamination Buckling and Growth in a Clamped Circular Plate," *AIAA Journal,* Vol. 26, 1988, pp. 438-445.

78. Partridge, C., Waechter, R. T., Williams, J. F. and Jones, R., "Understanding Delamination Behavior in a Circular Laminate," *Theoretical and Applied Fracture Mechanics,* Vol. 13, 1990, pp. 99-104.

79. Bruno, D. and Grimaldi, A., "Delamination Failure of Layered Composite Plates Loaded in Compression," *International Journal of Solids and Structures,* Vol. 26, 1990, pp. 313-330.

80. Grimaldi, A. and Reddy, J. N., "On Delamination in Plates;Unilateral Contact Approach," *Report VPI-E 82-83,* Virginia Polytechnic Institute and State University, 1982

81. Larsson, P. L., "On Delamination Buckling and Growth in Circular and Annular Orthotropic Plates," *International Journal of Solids and Structures,* Vol. 27, 1991, pp. 15-28.

82. Larsson, P. L., "On Multiple Delamination Buckling and Growth in Composite Plates," *International Journal of Solids and Structures,* Vol. 27, 1991, pp. 1623-1637.

83. Konish, D. Y. and Johnson, W. R., "Fatigue Effects on Delaminations and Strength Degradations in Graphite/Epoxy Laminates," *Composite Materials, ASTM STP 674* 1979, pp. 597-619.

84. Ashizawa, M., "Fast Interlaminar Fracture of a Compressively Loaded Composite Containing a Defect," *fifth DOD/NASA Conference on Fibrous Composites in Structural Design* , New Orleans, Louisiana, 1981

85. Chai, H. and Babcock, C. D., "Two-Dimensional Modelling of Compressive Failure in Delaminated Laminates," *Journal of Composite Materials,* Vol. 19, 1985, pp. 67-98.

86. Kassapoglou, C., "Buckling, Postbuckling and Failure of Elliptical Delaminations in Laminates under Compression," *Composite Structures,* Vol. 9, 1988, pp. 139-159.

87. Kassapoglou, C. and Hammer, J. "Design and Analysis of Composite Structures with Manufacturing Flaws," *Journal of American Helicopter Society,* Vol. 35, 1990, pp. 46-52.

88. Shivakumar, K. N. and Whitcomb, J. D., "Buckling of Sublaminates in a Quasi-Isotropic Composite Laminates," *Journal of Composite Materials,* Vol. 19, 1985, pp. 2-19.

89. Flanagan, G., "Two-Dimensional Delamination Growth in Composite Laminates under Compression Loading," *Composite Materials, ASTM STP 972* 1988, pp. 180-190.

90. Peck, S. O. and Springer, G. S., "The Behavior of Delaminations in Composite Plates-Analytical and Experimental Results," *Journal of Composite Materials,* Vol. 25, 1991, pp. 907-927.

91. Cairns, D. S., Minguet, P. J. and Abdallah, M. G. "Theoretical and Experimental Response of Composite Laminates with Delaminations Loaded in Compression," *Proceeding of AIAA/ASME/ASCE/AHS/ASC 33th SDM Conference* Dallas, Texas, 1992, pp. 1-9.

92. Yin, W. L. and Jane, K. C., "Refined Buckling and Postbuckling Analysis of Two Dimensional Delaminations - I. Analysis and Validation," *International Journal of Solids and Structures,* Vol. 29, 1992, pp. 591-610.

93. Yin, W. L. and Jane, K. C., "Refined Buckling and Postbuckling Analysis of Two Dimensional Delaminations - II. Results for Anisotropic Laminates and Conclusion," *International Journal of Solids and Structures,* Vol. 29, 1992, pp. 611-639.

94. Chai, H., "Buckling and Postbuckling Behavior of Elliptical Plates; Part I-Analysis," *ASME Journal of Applied Mechanics,* Vol. 57, 1990, pp. 981-988.

95. Chai, H., "Buckling and Postbuckling Behavior of Elliptical Plates; Part II-Results," *ASME Journal of Applied Mechanics,* Vol. 57, 1990, pp. 989-994.

96. Davidson, B. D., "Delamination Buckling: Theory and Experiment," *Journal of Composite Materials,* Vol. 25, 1991, pp. 1351-1378.

97. Davidson, B. D., "A Determination of the Strength and Mode of Failure of Compression Loaded Laminates Containing Multiple Delaminations," *Jet Propulsion Laboratory,* Internal Document D-6447, 1989.

98. Steinmetz, G., Arendts, F. J. and Nething, R. "Delamination Buckling of Laminated Plates," *Developments in the Science and Technology of Composite Materials,* Fourth European Conference on Composite Materials, Stuttgart, F. R. G., 1990, pp. 495-502.

99. Cochelin, B. and Potier-Ferry, M., "A Numerical Model for Buckling and Growth of Delaminations in Composite Laminates," *Computer Methods in Applied Mechanics and Engineering,* Vol. 89, 1991, pp. 361-380.

100. Mukherjee, Y. X., Xie, Z. and Ingraffea, A. R., "Delamination Buckling of Laminated Plates," *International Journal for Numerical Methods in Engineering,* Vol. 32, 1991, pp. 1321-1337.

101. Barbero, E. J. and Reddy, J.N. "Modelling of Delamination in Composite Laminates using a Layer-Wise Plate Theory," *International Journal of Solids and Structures,* Vol. 28, 1991, pp. 373-388.

102. Whitcomb, J. D., "Three Dimensional Analysis of a Postbuckled Embedded Delaminations," *Journal of Composite Materials,* Vol. 23, 1989, pp. 862-889.

103. Irwin, G. R., "Fracture," *Handbuch der Physik,* Vol. 6, 1958, p. 551.

104. Whitcomb, J. D., "Comparison of Full 3-D, Thin-Film 3-D, and Thin-Film Plate Analysis of a Postbuckled Embedded Delamination," *Journal of Composite Technology and Research,* Vol. 11, 1989, pp. 154-157.

105. Reddy, J. N., *Energy and Variational Methods in Applied Mechanics,* John Wiley, New York, 1984.

106. Jones, R. M., *Mechanics of Composite Materials,* Hemisphere Publishing Corporation, New York, 1975.

107. Reddy, J. N., *An Introduction to the Finite Element Method,* McGraw-Hill, New York, 1984.

108. Chia, C. Y., *Nonlinear Analysis of Plates,* McGraw-Hill, New York, 1980.

109. Andruet, R. H. and Plaut, R. H., "Behavior of a Cracked Rotating Shaft during Passage through a Critical Speed," Unpublished Paper of Department of Civil Engineering, Virginia Polytechnic Institute and State University, 1992

110. Stein, M., "Loads and Deformation of Buckled Rectangular Plates," *NASA TR R-40, 1959.*

Appendix A

LAMINATE STIFFNESSES

The laminate stiffnesses for both layer-wise and sublaminate theories are calculated to be

$$(A_{\alpha\beta\gamma\omega}, A_{\alpha 3\beta 3}) = \sum_{k=1}^{N} (\overline{Q}^k_{\alpha\beta\gamma\omega}, \overline{Q}^k_{\alpha 3\beta 3}) h^k$$

$$(E^i_{\alpha\beta\gamma\omega}, E^i_{\alpha 3\beta 3}) = \sum_{k=L(i)}^{N} (\overline{Q}^k_{\alpha\beta\gamma\omega}, \overline{Q}^k_{\alpha 3\beta 3}) h^k$$

$$(E^{is}_{\alpha\beta\gamma\omega}, E^{is}_{\alpha 3\beta 3}) = \sum_{k=L(\max(i,s))}^{N} (\overline{Q}^k_{\alpha\beta\gamma\omega}, \overline{Q}^k_{\alpha 3\beta 3}) h^k$$

$$E^{isu}_{\alpha\beta\gamma\omega} = \sum_{k=L(\max(i,s,u))}^{N} \overline{Q}^k_{\alpha\beta\gamma\omega} h^k$$

$$E^{isuv}_{\alpha\beta\gamma\omega} = \sum_{k=L(\max(i,s,u,v))}^{N} \overline{Q}^k_{\alpha\beta\gamma\omega} h^k$$

For layer-wise model

$$B^{j}_{\alpha\beta\gamma\omega} = \frac{1}{2}\left(\overline{Q}^{j-1}_{\alpha\beta\gamma\omega}h^{j-1} + \overline{Q}^{j}_{\alpha\beta\gamma\omega}h^{j}\right)$$

$$B^{j}_{\alpha3\beta3} = \overline{Q}^{j-1}_{\alpha3\beta3} - \overline{Q}^{j}_{\alpha3\beta3}$$

$$D^{jj}_{\alpha\beta\gamma\omega} = \frac{1}{3}\left(\overline{Q}^{j-1}_{\alpha\beta\gamma\omega}h^{j-1} + \overline{Q}^{j}_{\alpha\beta\gamma\omega}h^{j}\right)$$

$$D^{j(j+1)}_{\alpha\beta\gamma\omega} = \frac{1}{6}\,\overline{Q}^{j}_{\alpha\beta\gamma\omega}h^{j}$$

$$D^{jj}_{\alpha3\beta3} = \frac{\overline{Q}^{j-1}_{\alpha3\beta3}}{h^{j-1}} + \frac{\overline{Q}^{j}_{\alpha3\beta3}}{h^{j}}$$

$$D^{j(j+1)}_{\alpha3\beta3} = -\frac{\overline{Q}^{j}_{\alpha3\beta3}}{h^{j}}$$

$$F^{ij}_{\alpha\beta\gamma\omega} = \frac{1}{2}\left(\overline{Q}^{j-1}_{\alpha\beta\gamma\omega}h^{j-1} + \overline{Q}^{j}_{\alpha\beta\gamma\omega}h^{j}\right) \quad j > L(i)$$

$$F^{ij}_{\alpha\beta\gamma\omega} = \frac{1}{2}\,\overline{Q}^{j}_{\alpha\beta\gamma\omega}h^{j} \quad j = L(i)$$

$$F^{ij}_{\alpha3\beta3} = \overline{Q}^{j-1}_{\alpha3\beta3} - \overline{Q}^{j}_{\alpha3\beta3} \quad j > L(i)$$

$$F^{ij}_{\alpha3\beta3} = -\,\overline{Q}^{j}_{\alpha3\beta3} \quad j = L(i)$$

$$F^{isj}_{\alpha\beta\gamma\omega} = \frac{1}{2}\left(\overline{Q}^{j-1}_{\alpha\beta\gamma\omega}h^{j-1} + \overline{Q}^{j}_{\alpha\beta\gamma\omega}h^{j}\right) \quad j > L(\max(i,s))$$

$$F^{isj}_{\alpha\beta\gamma\omega} = \frac{1}{2}\,\overline{Q}^{j}_{\alpha\beta\gamma\omega}h^{j} \quad j = L(\max(i,s))$$

$$F^{irsj}_{\alpha\beta\gamma\omega} = \frac{1}{2}\left(\overline{Q}^{j-1}_{\alpha\beta\gamma\omega}h^{j-1} + \overline{Q}^{j}_{\alpha\beta\gamma\omega}h^{j}\right) \quad j > L(\max(i,r,s))$$

$$F^{irsj}_{\alpha\beta\gamma\omega} = \frac{1}{2}\,\overline{Q}^{j}_{\alpha\beta\gamma\omega}h^{j} \quad j = L(\max(i,r,s))$$

For sublaminate model

$$B^{j}_{\alpha\beta\gamma\omega} = \frac{1}{H^{j-1}}\left[\hat{B}^{j-1}_{\alpha\beta\gamma\omega} - z_{L(j\text{-}2)}\hat{A}^{j-1}_{\alpha\beta\gamma\omega}\right] - \frac{1}{H^{j}}\left[\hat{B}^{j}_{\alpha\beta\gamma\omega} - z_{L(j)}\hat{A}^{j}_{\alpha\beta\gamma\omega}\right]$$

$$B^{j}_{\alpha3\beta3} = \frac{\hat{A}^{j-1}_{\alpha3\beta3}}{H^{j-1}} - \frac{\hat{A}^{j}_{\alpha3\beta3}}{H^{j}}$$

$$D^{jj}_{\alpha\beta\gamma\omega} = \frac{1}{(H^{j-1})^2}\left[\hat{D}^{j-1}_{\alpha\beta\gamma\omega} - 2z_{L(j\text{-}2)}\hat{B}^{j-1}_{\alpha\beta\gamma\omega} + z^2_{L(j\text{-}2)}\hat{A}^{j-1}_{\alpha\beta\gamma\omega}\right] + \frac{1}{(H^{j})^2}\left[\hat{D}^{j}_{\alpha\beta\gamma\omega} - 2z_{L(j)}\hat{B}^{j}_{\alpha\beta\gamma\omega} + z^2_{L(j)}\hat{A}^{j}_{\alpha\beta\gamma\omega}\right.$$

$$D^{j(j+1)}_{\alpha\beta\gamma\omega} = -\frac{1}{(H^{j})^2}\left[\hat{D}^{j}_{\alpha\beta\gamma\omega} - (z_{L(j\text{-}1)} + z_{L(j)})\hat{B}^{j}_{\alpha\beta\gamma\omega} + z_{L(j\text{-}1)}z_{L(j)}\hat{A}^{j}_{\alpha\beta\gamma\omega}\right]$$

$$D^{jj}_{\alpha3\beta3} = \frac{\hat{A}^{j-1}_{\alpha3\beta3}}{(H^{j-1})^2} + \frac{\hat{A}^{j}_{\alpha3\beta3}}{(H^{j})^2}$$

$$D^{j(j+1)}_{\alpha3\beta3} = -\frac{\hat{A}^{j}_{\alpha3\beta3}}{(H^{j})^2}$$

$$F^{ij}_{\alpha\beta\gamma\omega} = \frac{1}{H^{j-1}}\left[\hat{B}^{j-1}_{\alpha\beta\gamma\omega} - z_{L(j\text{-}2)}\hat{A}^{j-1}_{\alpha\beta\gamma\omega}\right] - \frac{1}{H^{j}}\left[\hat{B}^{j}_{\alpha\beta\gamma\omega} - z_{L(j)}\hat{A}^{j}_{\alpha\beta\gamma\omega}\right] \quad j > i+1$$

$$F^{ij}_{\alpha\beta\gamma\omega} = -\frac{1}{H^{j}}\left[\hat{B}^{j}_{\alpha\beta\gamma\omega} - z_{L(j)}\hat{A}^{j}_{\alpha\beta\gamma\omega}\right] \quad j = i+1$$

$$F^{ij}_{\alpha3\beta3} = \frac{\hat{A}^{j-1}_{\alpha3\beta3}}{H^{j-1}} - \frac{\hat{A}^{j}_{\alpha3\beta3}}{H^{j}} \quad j > i+1$$

$$F^{ij}_{\alpha3\beta3} = -\frac{\hat{A}^{j}_{\alpha3\beta3}}{H^{j}} \quad j = i+1$$

$$F^{isj}_{\alpha\beta\gamma\omega} = \frac{1}{H^{j-1}}\left[\hat{B}^{j-1}_{\alpha\beta\gamma\omega} - z_{L(j\text{-}2)}\hat{A}^{j-1}_{\alpha\beta\gamma\omega}\right] - \frac{1}{H^{j}}\left[\hat{B}^{j}_{\alpha\beta\gamma\omega} - z_{L(j)}\hat{A}^{j}_{\alpha\beta\gamma\omega}\right] \quad j > \max(i,s)+1$$

$$F^{isj}_{\alpha\beta\gamma\omega} = -\frac{1}{H^{j}}\left[\hat{B}^{j}_{\alpha\beta\gamma\omega} - z_{L(j)}\hat{A}^{j}_{\alpha\beta\gamma\omega}\right] \quad j = \max(i,s)+1$$

$$F^{irsj}_{\alpha\beta\gamma\omega} = \frac{1}{H^{j-1}}\left[\hat{B}^{j-1}_{\alpha\beta\gamma\omega} - z_{L(j-2)}\hat{A}^{j-1}_{\alpha\beta\gamma\omega}\right] - \frac{1}{H^{j}}\left[\hat{B}^{j}_{\alpha\beta\gamma\omega} - z_{L(j)}\hat{A}^{j}_{\alpha\beta\gamma\omega}\right] \quad j > \max(i,r,s) + 1$$

$$F^{irsj}_{\alpha\beta\gamma\omega} = -\frac{1}{H^{j}}\left[\hat{B}^{j}_{\alpha\beta\gamma\omega} - z_{L(j)}\hat{A}^{j}_{\alpha\beta\gamma\omega}\right] \quad j = \max(i,r,s) + 1$$

where

$$H^{p} = \sum_{k=L(p-1)}^{L(p)-1} (z_{k+1} - z_k)$$

$$\hat{A}^{p}_{ijkl} = \sum_{k=L(p-1)}^{L(p)-1} Q^{k}_{ijkl}(z_{k+1} - z_k)$$

$$\hat{B}^{p}_{ijkl} = \frac{1}{2}\sum_{k=L(p-1)}^{L(p)-1} Q^{k}_{ijkl}\left(z^2_{k+1} - z^2_k\right) \qquad (i,j,k,l = 1,2,3)$$

$$\hat{D}^{p}_{ijkl} = \frac{1}{3}\sum_{k=L(p-1)}^{L(p)-1} Q^{k}_{ijkl}\left(z^3_{k+1} - z^3_k\right)$$

Appendix B

STIFFNESS, GEOMETRIC STIFFNESS AND MASS MATRICES

The element stiffness matrix $[K]$ and geometric stiffness and mass matrices $[G]$ for the axisymmetric model are calculated to be

$$^{11}K_{ij} = \int_r \left[rA_{1111}\psi_{i,r}\psi_{j,r} + A_{1122}(\psi_{i,r}\psi_j + \psi_i\psi_{j,r}) + \frac{1}{r} A_{2222}\psi_i\psi_j \right] dr$$

$$^{13}K_{ij}^k = \int_r \left[rB_{1111}^k\psi_{i,r}\psi_{j,r} + B_{1122}^k(\psi_{i,r}\psi_j + \psi_i\psi_{j,r}) + \frac{1}{r} B_{2222}^k\psi_i\psi_j \right] dr$$

$$^{14}K_{ij}^s = \int_r \left[rE_{1111}^s\psi_{i,r}\psi_{j,r} + E_{1122}^s(\psi_{i,r}\psi_j + \psi_i\psi_{j,r}) + \frac{1}{r} E_{2222}^s\psi_i\psi_j \right] dr$$

$$^{22}K_{ij} = \int_r rA_{1313}\psi_{i,r}\psi_{j,r}dr$$

$$^{23}K_{ij}^k = \int_r rB_{1313}^k\psi_{i,r}\psi_{j,r}dr$$

$$^{25}K_{ij}^{s} = \int_r rE_{1313}^{s}\psi_{i,r}\psi_{j,r}dr$$

$$^{33}K_{ij}^{lk} = \int_r \left[rD_{1111}^{lk}\psi_{i,r}\psi_{j,r} + D_{1122}^{lk}(\psi_{i,r}\psi_j + \psi_i\psi_{j,r}) + \frac{1}{r} D_{2222}^{lk}\psi_i\psi_j + rD_{1313}^{lk}\psi_i\psi_j \right] dr$$

$$^{34}K_{ij}^{ls} = \int_r \left[rF_{1111}^{sk}\psi_{i,r}\psi_{j,r} + F_{1122}^{sk}(\psi_{i,r}\psi_j + \psi_i\psi_{j,r}) + \frac{1}{r} F_{2222}^{sk}\psi_i\psi_j \right] dr$$

$$^{35}K_{ij}^{ls} = \int_r rF_{1313}^{sk}\psi_i\psi_{j,r}dr$$

$$^{44}K_{ij}^{ns} = \int_r \left[rE_{1111}^{ns}\psi_{i,r}\psi_{j,r} + E_{1122}^{ns}(\psi_{i,r}\psi_j + \psi_i\psi_{j,r}) + \frac{1}{r} E_{2222}^{ns}\psi_i\psi_j \right] dr$$

$$^{55}K_{ij}^{ns} = \int_r rE_{1313}^{ns}\psi_{i,r}\psi_{j,r}dr$$

The geometric stiffness matrix

$$^{22}G_{ij} = \int_r n\psi_{i,r}\psi_{j,r}dr$$

$$^{25}G_{ij}^{s} = \int_r n^s\psi_{i,r}\psi_{j,r}dr$$

$$^{55}G_{ij}^{ns} = \int_r n^{ns}\psi_{i,r}\psi_{j,r}dr$$

The mass matrix

$$^{11}G_{ij} = {}^{22}G_{ij} = \int_r rI^o\psi_i\psi_j dr$$

$$^{13}G_{ij}^{k} = \int_r rI^k\psi_i\psi_j dr$$

$$^{14}G_{ij}^{s} = {}^{25}G_{ij}^{s} = \int_{r} r\bar{I}^{s}\psi_i\psi_j dr$$

$$^{33}G_{ij}^{lk} = \int_{r} rI^{lk}\psi_i\psi_j dr$$

$$^{34}G_{ij}^{ls} = \int_{r} r\tilde{I}^{sl}\psi_i\psi_j dr$$

$$^{44}G_{ij}^{ns} = {}^{55}G_{ij}^{ns} = \int_{r} r\bar{I}^{ns}\psi_i\psi_j dr$$

The element stiffness matrix $[K]$ and geometric stiffness and mass matrices $[G]$ for the two-dimensional model are calculated to be

$$^{\alpha\gamma}K_{ij} = \int_{\Omega^e} A_{\alpha\beta\gamma\omega}\psi_{i,\beta}\psi_{j,\omega}dx_1dx_2$$

$$^{\alpha(\gamma+3)}K_{ij}^{k} = \int_{\Omega^e} B_{\alpha\beta\gamma\omega}^{k}\psi_{i,\beta}\psi_{j,\omega}dx_1dx_2$$

$$^{\alpha(\gamma+5)}K_{ij}^{s} = \int_{\Omega^e} E_{\alpha\beta\gamma\omega}^{s}\psi_{i,\beta}\psi_{j,\omega}dx_1dx_2$$

$$^{33}K_{ij} = \int_{\Omega^e} A_{\alpha3\gamma3}\psi_{i,\alpha}\psi_{j,\gamma}dx_1dx_2$$

$$^{3(\gamma+3)}K_{ij}^{k} = \int_{\Omega^e} B_{\alpha3\gamma3}^{k}\psi_{i,\alpha}\psi_j dx_1dx_2$$

$$^{38}K_{ij}^{s} = \int_{\Omega^e} E_{\alpha3\gamma3}^{s}\psi_{i,\alpha}\psi_{j,\gamma}dx_1dx_2$$

$$^{(\alpha+3)(\gamma+3)}K_{ij}^{lk} = \int_{\Omega^e} \left(D_{\alpha\beta\gamma\omega}^{lk}\psi_{i,\beta}\psi_{j,\omega} + D_{\alpha3\gamma3}^{lk}\psi_i\psi_j\right)dx_1dx_2$$

$$^{(\alpha+3)(\beta+5)}K^{ls} = \int_{\Omega^e} F^{sl}_{\alpha\beta\gamma\omega}\psi_{i,\beta}\psi_{j,\omega}dx_1dx_2$$

$$^{(\alpha+3)8}K^{ls}_{ij} = \int_{\Omega^e} F^{sl}_{\alpha3\gamma3}\psi_i\psi_{j,\gamma}dx_1dx_2$$

$$^{(\alpha+5)(\gamma+5)}K^{ns}_{ij} = \int_{\Omega^e} E^{ns}_{\alpha\beta\gamma\omega}\psi_{i,\beta}\psi_{j,\omega}dx_1dx_2$$

$$^{88}K^{ns}_{ij} = \int_{\Omega^e} E^{ns}_{\alpha3\gamma3}\psi_{i,\alpha}\psi_{j,\gamma}dx_1dx_2$$

The geometric stiffness matrix

$$^{33}G_{ij} = \int_{\Omega^e} n_{\alpha\beta}\psi_{i,\alpha}\psi_{j,\beta}dx_1dx_2$$

$$^{38}G^s_{ij} = \int_{\Omega^e} n^s_{\alpha\beta}\psi_{i,\alpha}\psi_{j,\beta}dx_1dx_2$$

$$^{88}G^{ns}_{ij} = \int_{\Omega^e} n^{ns}_{\alpha\beta}\psi_{i,\alpha}\psi_{j,\beta}dx_1dx_2$$

The mass matrix

$$^{\alpha\beta}G_{ij} = {}^{33}G_{ij} = \int_{\Omega^e} I^o\psi_i\psi_j dx_1dx_2$$

$$^{\alpha(\beta+3)}G^k_{ij} = \int_{\Omega^e} I^k\psi_i\psi_j dx_1dx_2$$

$$^{\alpha(\beta+5)}G^s_{ij} = {}^{3(\beta+5)}G^s_{ij} = \int_{\Omega} \bar{I}^s\psi_i\psi_j dx_1dx_2$$

$$^{(\alpha+3)(\beta+3)}G_{ij}^{lk} = \int_{\Omega^e} I^{lk}\psi_i\psi_j dx_1 dx_2$$

$$^{(\alpha+3)(\beta+5)}G_{ij}^{ls} = \int_{\Omega^e} \tilde{I}^{sl}\psi_i\psi_j dx_1 dx_2$$

$$^{(\alpha+5)(\beta+5)}G_{ij}^{ns} = {}^{88}G_{ij}^{ns} = \int_{\Omega^e} \bar{I}^{ns}\psi_i\psi_j dx_1 dx_2$$

Appendix C

DIRECT AND TANGENT STIFFNESS MATRICES

The direct and tangent stiffness matrices and the force vector for the axisymmetric model are given as:

$$({}^{12}K_{ij})_L = \int_r \left[r(A_{1111}\xi_{,r} + E^s_{1111}\bar{\xi}^s_{,r})\psi_{i,r}\psi_{j,r} + (A_{1122}\xi_{,r} + E^s_{1122}\bar{\xi}^s_{,r})\psi_i\psi_{j,r} \right] dr$$

$$({}^{15}K^s_{ij})_L = \int_r \left[r(E^s_{1111}\xi_{,r} + E^{su}_{1111}\bar{\xi}^u_{,r})\psi_{i,r}\psi_{j,r} + (E^s_{1122}\xi_{,r} + E^{su}_{1122}\bar{\xi}^u_{,r})\psi_i\psi_{j,r} \right] dr$$

$$({}^{22}K_{ij})_L = \int_r r\left[A_{1111}(\xi_{,r})^2 + 2E^s_{1111}\xi_{,r}\bar{\xi}^s_{,r} + E^{su}_{1111}\bar{\xi}^s_{,r}\bar{\xi}^u_{,r} + A_{1313} \right]\psi_{i,r}\psi_{j,r}dr$$

$$({}^{23}K^k_{ij})_L = \int_r \left[r\left(B^k_{1111}\xi_{,r} + F^{sk}_{1111}\bar{\xi}^s_{,r}\right)\psi_{i,r}\psi_{j,r} + \left(B^k_{1122}\xi_{,r} + F^{sk}_{1122}\bar{\xi}^s_{,r} + rB^k_{1313}\right)\psi_{i,r}\psi_j \right] dr$$

$$({}^{24}K^s_{ij})_L = \int_r \left[r(E^s_{1111}\xi_{,r} + E^{su}_{1111}\bar{\xi}^u_{,r})\psi_{i,r}\psi_{j,r} + (E^s_{1122}\xi_{,r} + E^{su}_{1122}\bar{\xi}^u_{,r})\psi_{i,r}\psi_j \right] dr$$

$$({}^{25}K^s_{ij})_L = \int_r r\left[E^s_{1111}(\xi_{,r})^2 + 2E^{su}_{1111}\xi_{,r}\bar{\xi}^u_{,r} + E^{rsu}_{1111}\bar{\xi}^r_{,r}\bar{\xi}^u_{,r} + E^s_{1313} \right]\psi_{i,r}\psi_{j,r}dr$$

$$({}^{35}K_{ij}^{ls})_L = \int_r \left[r\left(F_{1111}^{sl}\xi_{,r} + F_{1111}^{rsl}\bar{\xi}_{,r}^{r}\right)\psi_{i,r}\psi_{j,r} + \left(F_{1122}^{sl}\xi_{,r} + F_{1122}^{rsl}\bar{\xi}_{,r}^{r} + rF_{1313}^{sl}\right)\psi_i\psi_{j,r}\right]dr$$

$$({}^{45}K_{ij}^{ns})_L = \int_r \left[r(E_{1111}^{ns}\xi_{,r} + E_{1111}^{nsu}\bar{\xi}_{,r}^{u})\psi_{i,r}\psi_{j,r} + (E_{1122}^{ns}\xi_{,r} + E_{1122}^{nsu}\bar{\xi}_{,r}^{u})\psi_i\psi_{j,r}\right]dr$$

$$({}^{55}K_{ij}^{ns})_L = \int_r r\left[E_{1111}^{ns}(\xi_{,r})^2 + 2E_{1111}^{nsu}\xi_{,r}\bar{\xi}_{,r}^{u} + E_{1111}^{nsuv}\bar{\xi}_{,r}^{u}\bar{\xi}_{,r}^{v} + E_{1313}^{ns}\right]\psi_{i,r}\psi_{j,r}dr$$

The other components of $[K]_L$ are the same as the ones given in Appendix B.

$$({}^{12}K_{ij})_{NL} = \int_r \frac{1}{2}\left[r(A_{1111}u_{z,r} + E_{1111}^{s}\bar{u}_{z,r}^{s})\psi_{i,r}\psi_{j,r} + (A_{1122}u_{z,r} + E_{1122}^{s}\bar{u}_{z,r}^{s})\psi_i\psi_{j,r}\right]dr$$

$$({}^{15}K_{ij}^{s})_{NL} = \int_r \frac{1}{2}\left[r(E_{1111}^{s}u_{z,r} + E_{1111}^{su}\bar{u}_{z,r}^{u})\psi_{i,r}\psi_{j,r} + (E_{1122}^{s}u_{z,r} + E_{1122}^{su}\bar{u}_{z,r}^{u})\psi_i\psi_{j,r}\right]dr$$

$$\begin{aligned}({}^{22}K_{ij})_{NL} = \int_r \frac{1}{2} r\,\Big[\; & A_{1111}u_{z,r}(u_{z,r} + 3\xi_{,r}) + E_{1111}^{s}u_{z,r}(\bar{u}_{z,r}^{s} + 3\bar{\xi}_{,r}^{s}) \\ & + E_{1111}^{s}\bar{u}_{z,r}^{s}(u_{z,r} + 3\xi_{,r}) + E_{1111}^{su}\bar{u}_{z,r}^{u}(\bar{u}_{z,r}^{s} + 3\bar{\xi}_{,r}^{s})\Big]\psi_{i,r}\psi_{j,r}dr\end{aligned}$$

$$({}^{23}K_{ij}^{k})_{NL} = \int_r \left[r\left(B_{1111}^{k}u_{z,r} + F_{1111}^{sk}\bar{u}_{z,r}^{s}\right)\psi_{i,r}\psi_{j,r} + \left(B_{1122}^{k}u_{z,r} + F_{1122}^{sk}\bar{u}_{z,r}^{s}\right)\psi_{i,r}\psi_j\right]dr$$

$$({}^{24}K_{ij}^{s})_{NL} = \int_r \left[r(E_{1111}^{s}u_{z,r} + E_{1111}^{su}\bar{u}_{z,r}^{u})\psi_{i,r}\psi_{j,r} + (E_{1122}^{s}u_{z,r} + E_{1122}^{su}\bar{u}_{z,r}^{u})\psi_{i,r}\psi_j\right]dr$$

$$\begin{aligned}({}^{25}K_{ij}^{s})_{NL} = \int_r \frac{1}{2} r\,\Big[\; & E_{1111}^{s}u_{z,r}(u_{z,r} + 3\xi_{,r}) + E_{1111}^{su}u_{z,r}(\bar{u}_{z,r}^{u} + 3\bar{\xi}_{,r}^{u}) \\ & + E_{1111}^{su}\bar{u}_{z,r}^{u}(u_{z,r} + 3\xi_{,r}) + E_{1111}^{rsu}\bar{u}_{z,r}^{r}(\bar{u}_{z,r}^{u} + 3\bar{\xi}_{,r}^{u})\Big]\psi_{i,r}\psi_{j,r}dr\end{aligned}$$

$$({}^{35}K_{ij}^{ls})_{NL} = \int_r \frac{1}{2}\left[r\left(F_{1111}^{sl}u_{z,r} + F_{1111}^{rsl}\bar{u}_{z,r}^{r}\right)\psi_{i,r}\psi_{j,r} + \left(F_{1122}^{sl}u_{z,r} + F_{1122}^{rsl}\bar{u}_{z,r}^{r}\right)\psi_i\psi_{j,r}\right]dr$$

$$({}^{45}K_{ij}^{ns})_{NL} = \int_r \frac{1}{2}\left[r(E_{1111}^{ns}u_{z,r} + E_{1111}^{nsu}\bar{u}_{z,r}^{u})\psi_{i,r}\psi_{j,r} + (E_{1122}^{ns}u_{z,r} + E_{1122}^{nsu}\bar{u}_{z,r}^{u})\psi_i\psi_{j,r}\right]dr$$

$$({}^{55}K_{ij}^{ns})_{NL} = \int_r \frac{1}{2} r\left[\, E_{1111}^{ns}u_{z,r}(u_{z,r} + 3\xi_{,r}) + E_{1111}^{nsu}u_{z,r}(\bar{u}_{z,r}^{u} + 3\bar{\xi}_{,r}^{u}) \right.$$
$$\left. + E_{1111}^{nsu}\bar{u}_{z,r}^{u}(u_{z,r} + 3\xi_{,r}) + E_{1111}^{nsuv}\bar{u}_{z,r}^{u}(\bar{u}_{z,r}^{v} + 3\bar{\xi}_{,r}^{v})\right]\psi_{i,r}\psi_{j,r}dr$$

$$({}^{21}K_{ji})_{NL} = 2({}^{12}K_{ij})_{NL} \quad , \quad ({}^{32}K_{ji}^{k})_{NL} = \frac{1}{2}({}^{23}K_{ij}^{k})_{NL} \quad , \quad ({}^{42}K_{ji}^{s})_{NL} = \frac{1}{2}({}^{24}K_{ij}^{s})_{NL}$$

$$({}^{51}K_{ji}^{s})_{NL} = 2({}^{15}K_{ij}^{s})_{NL} \quad , \quad ({}^{52}K_{ji}^{s})_{NL} = ({}^{25}K_{ij}^{s})_{NL} \quad , \quad ({}^{53}K_{ji}^{sl})_{NL} = 2({}^{35}K_{ij}^{ls})_{NL} \quad , \quad ({}^{54}K_{ji}^{sn})_{NL} = 2({}^{45}K_{ij}^{ns})_{NL}$$

The tangent stiffness matrix

$$({}^{22}K_{ij})_T = ({}^{22}K_{ij})_L + ({}^{22}K_{ij})_{NL} + \int_r r\left[N_{rr} + \frac{1}{2}(A_{1111}u_{z,r} + E_{1111}^{s}\bar{u}_{z,r}^{s})(u_{z,r} + \xi_{,r})\right.$$
$$\left. + \frac{1}{2}(E_{1111}^{s}u_{z,r} + E_{1111}^{su}\bar{u}_{z,r}^{u})(\bar{u}_{z,r}^{s} + \bar{\xi}_{,r}^{s})\right]dr$$

$$({}^{25}K_{ij}^{s})_T = ({}^{25}K_{ij}^{s})_L + ({}^{25}K_{ij}^{s})_{NL} + \int_r r\left[\bar{N}_{rr}^{s} + \frac{1}{2}(E_{1111}^{s}u_{z,r} + E_{1111}^{su}\bar{u}_{z,r}^{u})(u_{z,r} + \xi_{,r})\right.$$
$$\left. + \frac{1}{2}(E_{1111}^{su}u_{z,r} + E_{1111}^{suv}\bar{u}_{z,r}^{v})(\bar{u}_{z,r}^{u} + \bar{\xi}_{,r}^{u})\right]dr$$

$$({}^{55}K_{ij}^{ns})_T = ({}^{55}K_{ij}^{ns})_L + ({}^{55}K_{ij}^{ns})_{NL} + \int_r r\left[\bar{N}_{rr}^{ns} + \frac{1}{2}(E_{1111}^{ns}u_{z,r} + E_{1111}^{nsu}\bar{u}_{z,r}^{u})(u_{z,r} + \xi_{,r})\right.$$
$$\left. + \frac{1}{2}(E_{1111}^{nsu}u_{z,r} + E_{1111}^{nsuv}\bar{u}_{z,r}^{v})(\bar{u}_{z,r}^{u} + \bar{\xi}_{,r}^{u})\right]dr$$

$$({}^{12}K_{ij})_T = ({}^{12}K_{ij})_L + 2({}^{12}K_{ij})_{NL} \quad , \quad ({}^{15}K_{ij}^{s})_T = ({}^{15}K_{ij}^{s})_L + 2({}^{15}K_{ij}^{s})_{NL}$$

$$({}^{32}K_{ij}^{l})_T = ({}^{32}K_{ij}^{l})_L + ({}^{32}K_{ij}^{l})_{NL} \quad , \quad ({}^{35}K_{ij}^{ls})_T = ({}^{35}K_{ij}^{ls})_L + 2({}^{35}K_{ij}^{ls})_{NL}$$

$$({}^{42}K_{ij}^{n})_T = ({}^{42}K_{ij}^{n})_L + ({}^{42}K_{ij}^{n})_{NL} \quad , \quad ({}^{45}K_{ij}^{ns})_T = ({}^{45}K_{ij}^{ns})_L + 2({}^{45}K_{ij}^{ns})_{NL}$$

All the other components of tangent stiffness matrix are given as

$$[K]_T = [K]_L + [K]_{NL}$$

$$^{1}F_i = N_r \psi_i r$$

$$^{2}F_i = Q_z \psi_i r + \int_r p \psi_i r dr$$

$$^{3}F_i^k = N_r^k \psi_i r$$

$$^{4}F_i^s = \overline{N}_r^s \psi_i r$$

$$^{5}F_i^s = \overline{Q}_z^s \psi_i r$$

The direct and tangent stiffness matrices and the force vector for the two-dimensional model are given as:

$$({}^{\alpha 3}K_{ij})_L = \int_{\Omega^e} (A_{\alpha\beta\gamma\omega}\xi_{,\gamma} + E^s_{\alpha\beta\gamma\omega}\overline{\xi}^s_{,\gamma})\psi_{i,\beta}\psi_{j,\omega} dx_1 dx_2$$

$$({}^{\alpha 8}K^s_{ij})_L = \int_{\Omega^e} [E^s_{\alpha\beta\gamma\omega}\xi_{,\gamma} + E^{su}_{\alpha\beta\gamma\omega}\overline{\xi}^u_{,\gamma}]\psi_{i,\beta}\psi_{j,\omega} dx_1 dx_2$$

$$({}^{33}K_{ij})_L = \int_{\Omega^e} [A_{\alpha\beta\gamma\omega}\xi_{,\alpha}\xi_{,\gamma} + E^s_{\alpha\beta\gamma\omega}(\xi_{,\alpha}\overline{\xi}^s_{,\gamma} + \overline{\xi}^s_{,\alpha}\xi_{,\gamma}) + E^{su}_{\alpha\beta\gamma\omega}\overline{\xi}^s_{,\alpha}\overline{\xi}^u_{,\gamma} + A_{\beta 3\omega 3}]\psi_{i,\beta}\psi_{j,\omega} dx_1 dx_2$$

$$({}^{3(\gamma+3)}K^k_{ij})_L = \int_{\Omega^e} [(B^k_{\alpha\beta\gamma\omega}\xi_{,\alpha} + F^{sk}_{\alpha\beta\gamma\omega}\overline{\xi}^s_{,\alpha})\psi_{i,\beta}\psi_{j,\omega} + B^k_{\alpha 3\gamma 3}\psi_{i,\alpha}\psi_j] dx_1 dx_2$$

$$({}^{3(\gamma+5)}K^s_{ij})_L = \int_{\Omega^e} (E^s_{\alpha\beta\gamma\omega}\xi_{,\alpha} + E^{su}_{\alpha\beta\gamma\omega}\overline{\xi}^u_{,\alpha})\psi_{i,\beta}\psi_{j,\omega} dx_1 dx_2$$

$$({}^{38}K^s_{ij})_L = \int_{\Omega^e} [E^s_{\alpha\beta\gamma\omega}\xi_{,\alpha}\xi_{,\gamma} + E^{su}_{\alpha\beta\gamma\omega}(\xi_{,\alpha}\overline{\xi}^u_{,\gamma} + \overline{\xi}^u_{,\alpha}\xi_{,\gamma}) + E^{rsu}_{\alpha\beta\gamma\omega}\overline{\xi}^r_{,\alpha}\overline{\xi}^u_{,\gamma} + E^s_{\beta 3\omega 3}]\psi_{i,\beta}\psi_{j,\omega} dx_1 dx_2$$

$$({}^{(\alpha+3)8}K^{ls}_{ij})_L = \int_{\Omega^e} [(F^{sl}_{\alpha\beta\gamma\omega}\xi_{,\gamma} + F^{rsl}_{\alpha\beta\gamma\omega}\overline{\xi}^r_{,\gamma})\psi_{i,\beta}\psi_{j,\omega} + F^{sl}_{\alpha 3\gamma 3}\psi_i\psi_{j,\gamma}] dx_1 dx_2$$

$$({}^{(\alpha+5)8}K_{ij}^{ns})_L = \int_{\Omega^e} (E_{\alpha\beta\gamma\omega}^{ns}\xi_{,\gamma} + E_{\alpha\beta\gamma\omega}^{nsu}\bar{\xi}_{,\gamma}^{u})\psi_{i,\beta}\psi_{j,\omega}dx_1dx_2$$

$$({}^{88}K_{ij}^{ns})_L = \int_{\Omega^e} [E_{\alpha\beta\gamma\omega}^{ns}\xi_{,\alpha}\xi_{,\gamma} + E_{\alpha\beta\gamma\omega}^{nsu}(\xi_{,\alpha}\bar{\xi}_{,\gamma}^{u} + \bar{\xi}_{,\alpha}^{u}\xi_{,\gamma}) + E_{\alpha\beta\gamma\omega}^{nsuv}\bar{\xi}_{,\alpha}^{u}\bar{\xi}_{,\gamma}^{v} + E_{\beta 3\omega 3}^{ns}]\psi_{i,\beta}\psi_{j,\omega}dx_1dx_2$$

The other components of $[K]_L$ are the same as the ones given in Appendix B.

$$({}^{\alpha 3}K_{ij})_{NL} = \int_{\Omega^e} \frac{1}{2}(A_{\alpha\beta\gamma\omega}u_{3,\gamma} + E_{\alpha\beta\gamma\omega}^{s}\bar{u}_{3,\gamma}^{s})\psi_{i,\beta}\psi_{j,\omega}dx_1dx_2$$

$$({}^{\alpha 8}K_{ij}^{s})_{NL} = \int_{\Omega^e} \frac{1}{2}(E_{\alpha\beta\gamma\omega}^{s}u_{3,\gamma} + E_{\alpha\beta\gamma\omega}^{su}\bar{u}_{3,\gamma}^{u})\psi_{i,\beta}\psi_{j,\omega}dx_1dx_2$$

$$\begin{aligned}({}^{33}K_{ij})_{NL} = \int_{\Omega^e} \frac{1}{4} \; \{ & A_{\alpha\beta\gamma\omega}[u_{3,\alpha}(u_{3,\gamma} + 3\xi_{,\gamma}) + u_{3,\gamma}(u_{3,\alpha} + 3\xi_{,\alpha})] \\ & + E_{\alpha\beta\gamma\omega}^{s}[u_{3,\alpha}(\bar{u}_{3,\gamma}^{s} + 3\bar{\xi}_{,\gamma}^{s}) + u_{3,\gamma}(\bar{u}_{3,\alpha}^{s} + 3\bar{\xi}_{,\alpha}^{s})] \\ & + E_{\alpha\beta\gamma\omega}^{s}[\bar{u}_{3,\alpha}^{s}(u_{3,\gamma} + 3\xi_{,\gamma}) + \bar{u}_{3,\gamma}^{s}(u_{3,\alpha} + 3\xi_{,\alpha})] \\ & + E_{\alpha\beta\gamma\omega}^{su}[\bar{u}_{3,\alpha}^{s}(\bar{u}_{3,\gamma}^{u} + 3\bar{\xi}_{,\gamma}^{u}) + \bar{u}_{3,\gamma}^{s}(\bar{u}_{3,\alpha}^{u} + 3\bar{\xi}_{,\alpha}^{u})]\}\psi_{i,\beta}\psi_{j,\omega}dx_1dx_2\end{aligned}$$

$$({}^{3(\gamma+3)}K_{ij}^{k})_{NL} = \int_{\Omega^e} (B_{\alpha\beta\gamma\omega}^{k}u_{3,\alpha} + F_{\alpha\beta\gamma\omega}^{sk}\bar{u}_{3,\alpha}^{s})\psi_{i,\beta}\psi_{j,\omega}dx_1dx_2$$

$$({}^{3(\gamma+5)}K_{ij}^{s})_{NL} = \int_{\Omega^e} (E_{\alpha\beta\gamma\omega}^{s}u_{3,\alpha} + E_{\alpha\beta\gamma\omega}^{su}\bar{u}_{3,\alpha}^{u})\psi_{i,\beta}\psi_{j,\omega}dx_1dx_2$$

$$\begin{aligned}({}^{38}K_{ij}^{s})_{NL} = \int_{\Omega^e} \frac{1}{4} \; \{ & E_{\alpha\beta\gamma\omega}^{s}[u_{3,\alpha}(u_{3,\gamma} + 3\xi_{,\gamma}) + u_{3,\gamma}(u_{3,\alpha} + 3\xi_{,\alpha})] \\ & + E_{\alpha\beta\gamma\omega}^{su}[u_{3,\alpha}(\bar{u}_{3,\gamma}^{u} + 3\bar{\xi}_{,\gamma}^{u}) + u_{3,\gamma}(\bar{u}_{3,\alpha}^{u} + 3\bar{\xi}_{,\alpha}^{u})] \\ & + E_{\alpha\beta\gamma\omega}^{su}[\bar{u}_{3,\alpha}^{u}(u_{3,\gamma} + 3\xi_{,\gamma}) + \bar{u}_{3,\gamma}^{u}(u_{3,\alpha} + 3\xi_{,\alpha})] \\ & + E_{\alpha\beta\gamma\omega}^{suv}[\bar{u}_{3,\alpha}^{v}(\bar{u}_{3,\gamma}^{u} + 3\bar{\xi}_{,\gamma}^{u}) + \bar{u}_{3,\gamma}^{v}(\bar{u}_{3,\alpha}^{u} + 3\bar{\xi}_{,\alpha}^{u})]\}\psi_{i,\beta}\psi_{j,\omega}dx_1dx_2\end{aligned}$$

$$({}^{(\alpha+3)8}K_{ij}^{ls})_{NL} = \int_{\Omega^e} \frac{1}{2}(F_{\alpha\beta\gamma\omega}^{sl}u_{3,\gamma} + F_{\alpha\beta\gamma\omega}^{rsl}\bar{u}_{3,\gamma}^{r})\psi_{i,\beta}\psi_{j,\omega}dx_1dx_2$$

$$({}^{(\alpha+5)8}K_{ij}^{ns})_{NL} = \int_{\Omega^e} \frac{1}{2}\,(E_{\alpha\beta\gamma\omega}^{ns} u_{3,\gamma} + E_{\alpha\beta\gamma\omega}^{nsu} \bar{u}_{3,\gamma}^{u})\psi_{i,\beta}\psi_{j,\omega} dx_1 dx_2$$

$$\begin{aligned}({}^{88}K_{ij}^{ns})_{NL} = \int_{\Omega^e} \frac{1}{4}\ \Big\{ & E_{\alpha\beta\gamma\omega}^{ns}[u_{3,\alpha}(u_{3,\gamma} + 3\xi_{,\gamma}) + u_{3,\gamma}(u_{3,\alpha} + 3\xi_{,\alpha})] \\ & + E_{\alpha\beta\gamma\omega}^{nsu}[u_{3,\alpha}(\bar{u}_{3,\gamma}^{u} + 3\bar{\xi}_{,\gamma}^{u}) + u_{3,\gamma}(\bar{u}_{3,\alpha}^{u} + 3\bar{\xi}_{,\alpha}^{u})] \\ & + E_{\alpha\beta\gamma\omega}^{nsu}[\bar{u}_{3,\alpha}^{u}(u_{3,\gamma} + 3\xi_{,\gamma}) + \bar{u}_{3,\gamma}^{u}(u_{3,\alpha} + 3\xi_{,\alpha})] \\ & + E_{\alpha\beta\gamma\omega}^{nsuv}[\bar{u}_{3,\alpha}^{v}(\bar{u}_{3,\gamma}^{u} + 3\bar{\xi}_{,\gamma}^{u}) + \bar{u}_{3,\gamma}^{v}(\bar{u}_{3,\alpha}^{u} + 3\bar{\xi}_{,\alpha}^{u})]\Big\}\psi_{i,\beta}\psi_{j,\omega} dx_1 dx_2\end{aligned}$$

$$({}^{3\beta}K_{ij})_{NL} = 2({}^{\alpha 3}K_{ij})_{NL}\ ,\quad ({}^{(\alpha+3)3}K_{ij}^{l})_{NL} = \frac{1}{2}\,({}^{3(\gamma+3)}K_{ij}^{k})_{NL}\ ,\quad ({}^{(\alpha+5)3}K_{ij}^{n})_{NL} = \frac{1}{2}\,({}^{3(\gamma+5)}K_{ij}^{s})_{NL}$$

$$({}^{8\beta}K_{ij}^{n})_{NL} = 2({}^{\alpha 8}K_{ij}^{s})_{NL}\ ,\quad ({}^{83}K_{ij}^{n})_{NL} = ({}^{38}K_{ij}^{s})_{NL}$$

$$({}^{8(\beta+3)}K_{ij}^{nk})_{NL} = 2({}^{(\alpha+3)8}K_{ij}^{ls})_{NL}\ ,\quad ({}^{8(\beta+5)}K_{ij}^{ns})_{NL} = 2({}^{(\alpha+5)8}K_{ij}^{ns})_{NL}$$

The tangent stiffness matrix is given

$$\begin{aligned}({}^{33}K_{ij})_T = ({}^{33}K_{ij})_L + ({}^{33}K_{ij})_{NL} + \int_{\Omega^e}\Big[& N_{\beta\omega} + \frac{1}{2}\,(A_{\alpha\beta\gamma\omega}u_{3,\alpha} + E_{\alpha\beta\gamma\omega}^{s}\bar{u}_{3,\alpha}^{s})(u_{3,\gamma} + \xi_{,\gamma}) \\ & + \frac{1}{2}\,(E_{\alpha\beta\gamma\omega}^{u}u_{3,\alpha} + E_{\alpha\beta\gamma\omega}^{su}\bar{u}_{3,\alpha}^{s})(\bar{u}_{3,\gamma}^{u} + \bar{\xi}_{,\gamma}^{u})\Big]\psi_{i,\beta}\psi_{j,\omega} dx_1 dx_2\end{aligned}$$

$$\begin{aligned}({}^{38}K_{ij}^{s})_T = ({}^{38}K_{ij}^{s})_L + ({}^{38}K_{ij}^{s})_{NL} + \int_{\Omega^e}\Big[& \bar{N}_{\beta\omega}^{s} + \frac{1}{2}\,(E_{\alpha\beta\gamma\omega}^{s}u_{3,\alpha} + E_{\alpha\beta\gamma\omega}^{su}\bar{u}_{3,\alpha}^{s})(u_{3,\gamma} + \xi_{,\gamma}) \\ & + \frac{1}{2}\,(E_{\alpha\beta\gamma\omega}^{su}u_{3,\alpha} + E_{\alpha\beta\gamma\omega}^{suv}\bar{u}_{3,\alpha}^{v})(\bar{u}_{3,\gamma}^{u} + \bar{\xi}_{,\gamma}^{u})\Big]\psi_{i,\beta}\psi_{j,\omega} dx_1 dx_2\end{aligned}$$

$$\begin{aligned}({}^{88}K_{ij}^{ns})_T = ({}^{88}K_{ij}^{ns})_L + ({}^{88}K_{ij}^{ns})_{NL} + \int_{\Omega^e}\Big[& \bar{N}_{\beta\omega}^{ns} + \frac{1}{2}\,(E_{\alpha\beta\gamma\omega}^{ns}u_{3,\alpha} + E_{\alpha\beta\gamma\omega}^{nsu}\bar{u}_{3,\alpha}^{u})(u_{3,\gamma} + \xi_{,\gamma}) \\ & + \frac{1}{2}\,(E_{\alpha\beta\gamma\omega}^{nsu}u_{3,\alpha} + E_{\alpha\beta\gamma\omega}^{nsuv}\bar{u}_{3,\alpha}^{v})(\bar{u}_{3,\gamma}^{u} + \bar{\xi}_{,\gamma}^{u})\Big]\psi_{i,\beta}\psi_{j,\omega} dx_1 dx_2\end{aligned}$$

$$({}^{(\alpha+3)3}K_{ij}^{l})_T = \big({}^{(\alpha+3)3}K_{ij}^{l}\big)_L + \big({}^{(\alpha+3)3}K_{ij}^{l}\big)_{NL}\ ,\qquad ({}^{(\alpha+3)8}K_{ij}^{ls})_T = ({}^{(\alpha+3)8}K_{ij}^{ls})_L + 2({}^{(\alpha+3)8}K_{ij}^{ls})_{NL}$$

$$({}^{(\alpha+5)3}K_{ij}^{n})_T = \big({}^{(\alpha+5)3}K_{ij}^{n}\big)_L + \big({}^{(\alpha+5)3}K_{ij}^{n}\big)_{NL}\ ,\qquad ({}^{(\alpha+5)8}K_{ij}^{ns})_T = ({}^{(\alpha+5)8}K_{ij}^{ns})_L + 2({}^{(\alpha+5)8}K_{ij}^{ns})_{NL}$$

All the other components of tangent stiffness matrix are given as

$$[K]_T = [K]_L + [K]_{NL}$$

$$^{\alpha}F_i = \int_{\Gamma^e} N_\alpha \psi_i dS$$

$$^{3}F_i = \int_{\Gamma^e} Q_3 \psi_i dS + \int_{\Omega^e} p \psi_i dx_1 dx_2$$

$$^{(\alpha+3)}F_i^k = \int_{\Gamma^e} N_\alpha^k \psi_i dS$$

$$^{(\alpha+5)}F_i^s = \int_{\Gamma^e} \overline{N}_\alpha^s \psi_i dS$$

$$^{8}F_i^s = \int_{\Gamma^e} \overline{Q}_3^s \psi_i dS$$

Vita

The author was born on September 20, 1963 in Seoul, Korea. After graduating from Daesung Senior High School in 1982, he entered Yonsei University in Seoul, Korea. Upon completion of Bachelor of Science in Architectural Engineering in the spring of 1986, he started his graduate studies at the same institution. In the spring of 1988, he was awarded the degree of Master of Science in the Structural Mechanics Division of the Architectural Engineering. Right after getting married to the former Myoungwha Choi in December 1988, he came to the United States and joined the Department of Engineering Science and Mechanics at Virginia Polytechnic Institute and State University to continue his graduate studies for the degree of Doctor of Philosophy in Engineering Mechanics. He is currently a member of the American Society of Mechanical Engineers (ASME), American Institute of Aeronautics and Astronautics (AIAA), Virginia Tech Center for Composite Materials and Structures (CCMS), Center for Intelligent Material Systems and Structures (CIMSS), and the Korean Scientists and Engineers Association in America (KSEA). After graduation, he will work on smart structures as a research scientist.